ZANCO Journal of Pure and Applied Sciences
The official scientific journal of Salahaddin University-Erbil
https://zancojournals.su.edu.krd/index.php/JPAS

ISSN (print):2218-0230**, ISSN (online):** 2412-3986**, DOI: http://dx.doi.org/10.21271/zjpas**

RESEARCH PAPER

An Investigation into the Factors Influencing the Reduction of Construction Materials Wastage in Erbil City- KRG-Iraq

Khalil Ismail Wali*

Department of Civil Engineering, College of Engineering, Salahaddin University-Erbil, Kurdistan Region, Iraq. Email:

A B S T R A C T:
The aim of this study is to identify the factors affecting the construction material waste generation and to determine the magnitude of construction waste material in Erbil city. To achieve this study, a form of a questionnaire was prepared comprised of the factors influencing the waste generation of construction material, and assessment of seventeen different construction materials was selected to examine the approximate magnitude of their waste. The survey data was analyzed by adopting the relative important index (RII) method. The result of the analysis revealed that the top significant causes of wastage of materials on construction projects were due to the lack of on-site waste management plans; frequent changes to design, lack of supervision, improper storing of materials; lack of possibilities to order small quantities; lack of skilled workers. Also the study found that the waste percentage of materials used ranged from 3.3% to 8.5%., and the waste percentage of fine aggregate, coarse aggregate, and timber were in a range of 6% to 7% while the waste of cement, steel reinforcement, concrete, concrete block and brick in a range of 5% to 6%, whereas the waste in gypsum reached 8.5%. Furthermore, the study found that poor planning and rework contributing as a significant aspect of waste generation in Erbil city.

KEY WORDS: Wastage Reduction; Factors Influencing; Construction Materials; Waste Management.
DOI: http://dx.doi.org/10.21271/ZJPAS.32.4.1
ZJPAS (2020) , 32(4);1-11 .

1. INTRODUCTION

Waste reduction of construction materials in the construction industry is essential aspect not only from the view of efficiency of project management related to the financial return, since, the environmental impact is also growing in recent years in the sense of the adverse impact of the waste generation of building materials on the society and environment. The waste of construction materials accounts for between 15 and 30% of urban waste, and building materials wastage is difficult to recycle due to high levels of pollution and contamination due to the availability of insufficient space and lands for its disposal in large cities (Bossink and Brouwers, 1996). For the production of building materials require of using large amounts of nonrenewable resources of energy, since the resources that are in danger and risk of depletion, including timber, sand, and crushed stone (Wyatt, 1978). Although construction waste occurs and accumulates during the actual construction process, there is an understanding that it is caused by events and actions at the design stage, materials procurement handling, and during the construction stages of project and delivery processes (Kavithra et al., 2017). According to modern production philosophy, waste should be understood as any inefficiency that results in the use of equipment, materials, labor (Koskela, 1992).

The construction waste was defined as “quality costs, rework, unnecessary transportation trips,

* **Corresponding Author:**
Khalil Ismail Wali
E-mail: khalil.wali@su.edu.krd
Article History:
Received: 22/09/2019
Accepted: 25/11/2019
Published: 00/09 /2020

long distances, improper choice of management methods and poor constructability" (Alarcón et al., 2002). The physical wastage is included loss of construction materials and damages whereas, cost and time overrun refer to non-physical waste. Hence, the waste can be defined as the difference between the total quantity of material brought to the project site and the actual amount used (Enshassi, 1996).

Furthermore, waste is defined as "any losses that generate a direct or indirect cost but do not add any value to the product." Moreover, the construction waste can be defined as any inefficiency activities that result in the use of equipment, labor, materials, or capital in larger quantities other than those considered in the production of a building (Formoso et al., 1999).

A study focused on waste management stated that the production of waste could be displaced and reused. Materials like glass, plastic, and PVC, and paper products are collected and recycled into new materials and products (Davis et al., 2006).

A study identified two case studies of construction projects to reduce construction waste generation in the UAE construction sites by a literature review of research, and concluded that people are lack of awareness, less importance towards the waste management on sites and showed that contractors consider that waste management is an extra cost of the project (Al-Hajj and Iskandarani, 2012).

Another study focused on the economic aspects of waste minimization of construction waste materials in terms of cost savings of construction projects in India. In addition, they found that due to lack of site waste management systems, lack awareness of waste minimization in the Indian construction industry cause of generation of large quantities of material waste (Jain, 2012).

It is necessary to reduce waste generation and increase the reuse and recycling process to overcome the shortage of aggregate from natural sources being discovered in many parts of the country, so now recycled aggregate can use in construction processes. The government Municipal waste laws are required to modify and prepare effective plans, and strict rules and regulations are essential to forget out of this problem (Bansal and Singh, 2014). The mechanism of handling the construction materials will contribute to improving the efficiency and cost-effectiveness on the construction site. The study revealed that minimization of the amount of wastage of construction materials during the construction phases helps reduce the cost of the project (Singh, 2015).

A research study indicated that the management of construction materials waste plays an essential factor in the reduction of project costs(Sawant Surendra et al., 2016).

A study suggested that waste planning and management practices could be important for reducing waste generation like strict construction waste management, project drawings, no design changes during the construction process. Moreover, concluded poor knowledge, poor design documentation, and lack of awareness towards waste minimization would increase construction waste generation. Site supervisors should be with the understanding of waste minimization, which could reduce waste generation on sites (Ajayi et al., 2017).

The main aims of this study are to assess the perception of construction professionals, towards the efficient performance of construction activities related to the reduction of construction material wastes and as follows:

To identify the most critical factors that influence the construction material waste produced during construction activities, and to determine the magnitude of waste generated in construction projects in Erbil city.

2. MATERIALS AND METHODS

2.1 Preparation of questionnaire

The questionnaire designed to be self-administered and to facilitate conducting on-site interviewed survey conducted. The primary form

of the questionnaire subjected to correction and revisions by the feedback received during the pilot study conducted to review and assess the feasibility of the survey. The final form of the questionnaire comprises three parts as follows:
The first part investigated the necessary personal information of the respondent profiles and working category and the type of construction projects. The second part of the questionnaire devoted to studying the factors effect on a waste generation was distributed on seven significant groups, such as factors related to design, worker, management process, site condition, procurement, and factors related to external conditions. The third part of the questionnaire focused on the investigation of the respondent's perception of the waste percentage generated on construction site for seventeen types of materials. The respondents were requested to reply to require enquires based on their previous professional experience and skills in the execution of construction projects to score their perception related to the magnitude of construction materials waste. Various types of construction materials selected, such as; cement, fine sand, coarse aggregate, steel reinforcements, concrete, concrete blocks, brick, gypsum, glass, roofing materials, paint, PVC water pipes, mosaic tile, ceramic tiles, marble tiles, and electrical items. A total of 110 questionnaires were distributed for this survey, of which 43 were completed with a valid response, and this indicated a response rate of 40%.

2.2 Study Area

The current study involved surveying the construction materials waste generation in twelve project sites under construction in Erbil city, as presented in Table 1.

Table 1: The Study Area in Erbil City

No.	Project Name and location
1.	Cristal Hotel 2-100m Road Near Empire
2.	Runaky Towers- Runaky Neighborhood
3.	Zanyari Apartments-60m Road Near Stadium
4.	Majdi Mall 2- Masif Salahaddin Road
5.	Empire Wings Apartments-100m Road
6.	4 Towers – Bahirka Road- Bahrka Road
7.	Justice Tower- Opposite Sami Abdurahman Park
8.	Majdi Hospital- Masif Salahaddin Road
9.	Erbil International Hospital-100m Road Near Hogr Fuel Station
10.	Construction of 7 Multi-Stories Apartment In Erbil (280 Units)- Near Majdi Mall 120m road
11.	Mnw Tower-40m Road Opposite Dream City
12.	Department of Construction of Schools-Erbil Governorate

2.3 Statistical Analysis Techniques

The collected data were statistically analyzed by calculation of Relative Important Index (RII) conducted in terms of quantitative and qualitative analysis of data collection in this study using questionnaires, interviews, field observation, and documentary sources. To calculated and the RII by using equation (1) (Fadiya et al., 2013).

$$RII = \sum_{i=1}^{5} \frac{i}{5} \, x \, \frac{n_i}{N} \qquad (1)$$

Where; $\mathbf{n_i}$ is referred to the number of respondents that chose **i** for the frequency.
While **N** is the total number of responses, and **i** is the weight of category **i**.
To demonstrate the procedure for calculation RII by using Equation (1) as an example for the first factor (frequent design change) which listed in Table. 4, and as follows:

$$\boldsymbol{RII}(_{\boldsymbol{Frequent\ design\ change}}) = \frac{(1*1+2*8+3*16*4*11+5*7)}{(5*43)} = 0.6698$$

2.4 Reliability Test

The Cronbach's alpha results give value ranged from 0 to 1, and it was calculated to estimate the internal consistency of reliability of measurement scale, and the closer to 1 indicate the high degree of reliability range, thus Cronbach's alpha coefficient should fall within a range of 0.7 to 1.0 (Yockey, 2018). The Cronbach's alpha was estimated by using the SPSS package; the result of calculating the Cronbach's alpha was 0.91; this value indicates that the collected data is very reliable, as shown in Table2.

Table 2: Cronbach's Alpha Value

Cronbach's Alpha	No. of Items
0.910	38

3. RESULTS and DISCUSSIONS

3.1 Respondents Profile

The questionnaires distributed to various professionals, engineering, and technical staff involved in construction projects in Erbil city, to investigate the respondent's profiles. Table 3. shows that among the respondents working in building construction accounting for 49% and 49% in other types of projects such as dams, water supply, sewage, etc. and only 2% in road construction.

Table 3: Summary of Respondents Personal Information and Background

CHARACTERISTICS		Frequency	Percent (%)
Type of construction	Building Construction	21	49
	Road Construction	1	2
	other construction types	21	49
Total		43	100
Type of Project	Public	28	65
	Private	15	35
Total		43	100
Respondent's Qualification	Primary Education	1	2
	Diploma Degree	3	7
	Bachelor's Degree	33	77
	Master Degree	4	9
	Ph.D. Degree	2	5
Total		43	100
Specialization	Civil	36	84
	Architect	4	9
	Other	3	7
Total		43	100.0
Category	Consultant	4	9
	Project Manager	19	44
	Site Engineer	18	42
	Contractor	2	5
Total		43	100.0

3.2 Identification the Factors Influencing the Materials Waste Generation

From the results presented in Table 4, showed that the factors influencing the materials waste generation analyzed in terms of relative importance index (RII) for seven aspects in terms of groups (design, handling, worker, management, site condition, procurement, and external factors), and each group divided to sub-items. The analysis of RII indicates that the in design aspect the highest RII of 0.6698 related to frequent design change, while in handling issue a poor quality of materials comes in highest RII of 0.6047. Whereas, in worker the shortage of skilled worker reached to 0.6372, and in management aspect the poor planning and in the procurement aspect the ignorance of specifications are both recorded the RII at rate of 0.6279.

Table 4: RII for Significance Causes of Waste in Construction Projects

GROUP	No.	CAUSE OF CONSTRUCTION WASTE	Weight					RII Of Causes
			1	2	3	4	5	
DESIGN	1	Frequent design changes	1	8	16	11	7	0.6698
	2	Design errors	8	5	12	10	8	0.6233
	3	Lack of design information	2	12	16	7	6	0.6140
	4	Complicated design	6	8	15	7	7	0.6047
	5	Inexperience designer	6	10	12	8	7	0.6000
	6	Conflect between design and other contract documents.	7	10	13	7	6	0.5767
HANDLING	1	Wrong material storage	2	13	17	8	3	0.5860
	2	Poor material handling	4	15	12	9	3	0.5628
	3	Damage during transportation	6	10	14	11	2	0.5674
	4	Poor quality of materials	5	8	16	9	5	0.6047
	5	Delay during delivery	4	7	20	9	3	0.6000
WORKER	1	Workers mistakes	2	16	17	7	1	0.5488
	2	Incompetent worker	3	15	17	6	2	0.5488
	3	Damage caused by workers	2	8	21	9	3	0.6140
	4	Lack of experience	2	6	18	15	2	0.6419
	5	Shortage of skilled workers	2	7	18	13	3	0.6372
	6	Inappropriate use of materials	3	9	16	13	2	0.6093
MANAGEMENT	1	Poor planning	3	11	14	7	8	0.6279
	2	Poor site management	6	9	10	10	8	0.6233
	3	Poor supervision	7	9	11	7	9	0.6093
	4	Inappropriate construction methods	4	9	17	11	2	0.5907
	5	Lack of coordination among parties	1	12	15	12	3	0.6186
	6	Poor information quality	3	16	11	8	5	0.5814
	7	Rework	2	7	16	12	6	0.6605
SITE CONDITION	1	Leftover materials on site	3	15	12	5	8	0.6000
	2	Poor site condition	2	9	17	12	3	0.6233
	3	Waste resulting from packaging	2	12	20	7	2	0.5767
	4	Crews interference	6	12	17	6	2	0.5349
	5	Change order Occurrence.	6	11	14	9	3	0.5628
PROCUREMENT	1	Ordering errors	5	13	15	7	3	0.5535
	2	Error in shipping	7	12	17	7	0	0.5116
	3	Mistakes in quantity surveys	9	5	14	11	4	0.5814
	4	Ignorance of specifications	3	12	9	14	5	0.6279
	5	Difficulties of ordering small quantities.	3	14	11	7	8	0.6140
EXTERNAL	1	Effect of weather	5	11	7	11	9	0.6372
	2	Theft	14	12	10	5	2	0.4558
	3	Vandalism	13	9	11	8	2	0.4930
	4	Lack of legatitive enforcement	14	8	14	6	1	0.4698

Further analysis conducted to evaluate the effects of overall causes contributed to the waste generation on a group basis as illustrated in Fig.1. Which shows that the management and design aspects had the most significant impact on waste

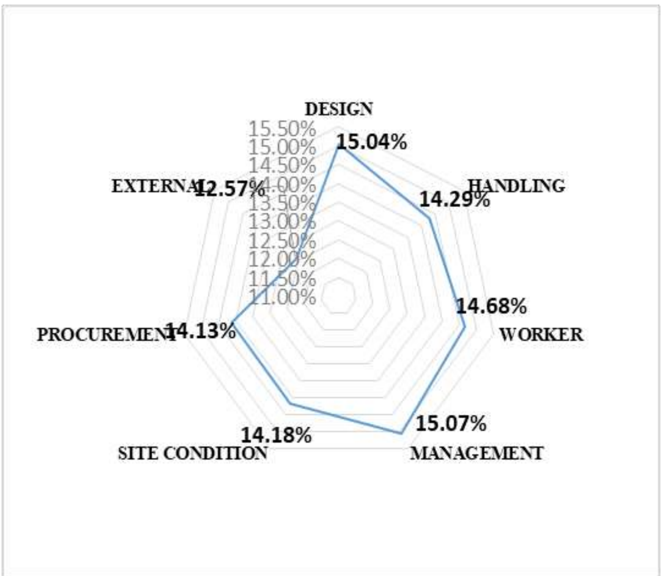

generation in a rate of 15.07% and 15.04% respectively, while the external factors received minimum rate of 12.57%.

Figure 1. Factors Contribution to Wastage as groups

3.2.1 Factors related to Design

Analysis of the causes related to the design aspect

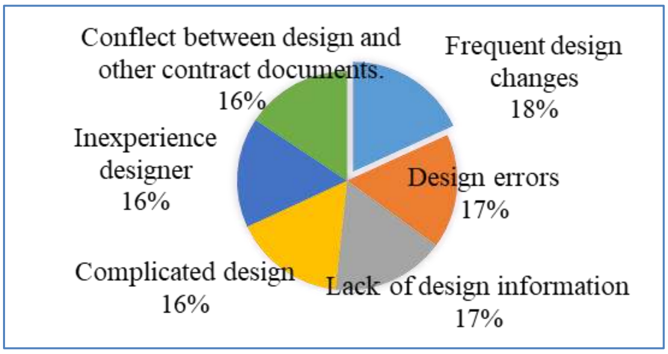

showed that the frequent design changes in the design process contributes to highest rate of 18% in construction waste, as shown in Figure 2**.**

Figure 2: Factors affecting wastage in the design

3.2.2 Factors related to Handling of Materials

Handling factors are one of the essential elements, which affect construction waste generation. Figure 3 shows the most effective source was the poor quality of the material and delay during delivery at a rate of 21 %.

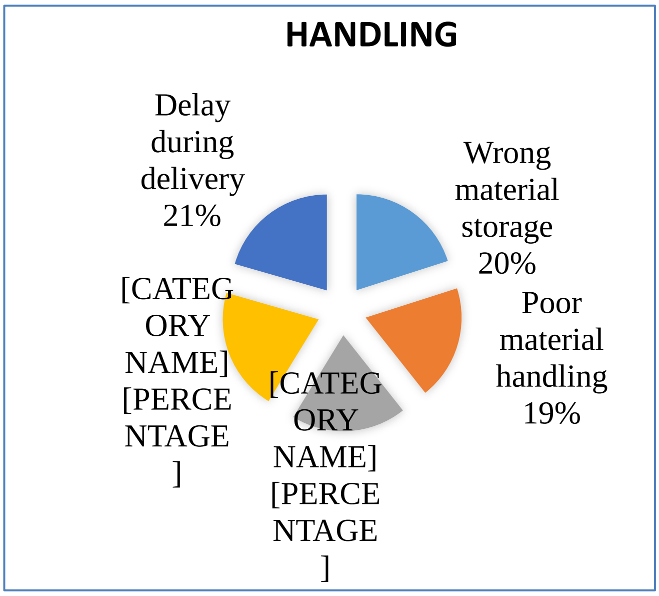

Figure 3: Factors affecting wastage in handling group

3.2.3 Factors related to Workers

The factors related to workers group, which produce wastes indicating that the significant sources of debris in this group are lack of experience of workers and shortage of skilled workers at a rate of 18% as be observed in Figure 4.

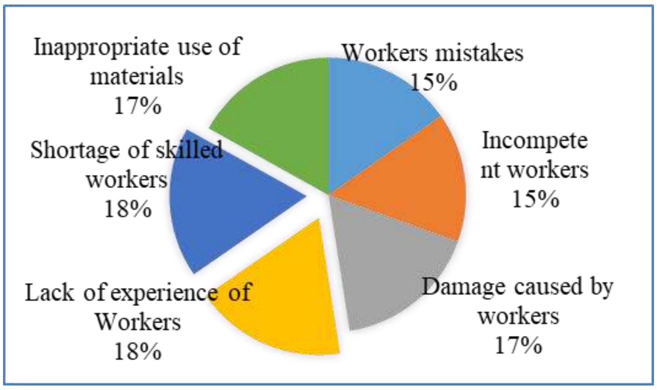

Figure 4: Factors affecting construction materials waste in workers group

3.2.4 Factors related to Management

Figure 5 illustrates the factors related to management have a crucial role in reducing construction waste. Seven causes devoted to management studied in this study showed that poor planning and rework were the most effective source of waste at a rate of 15%.

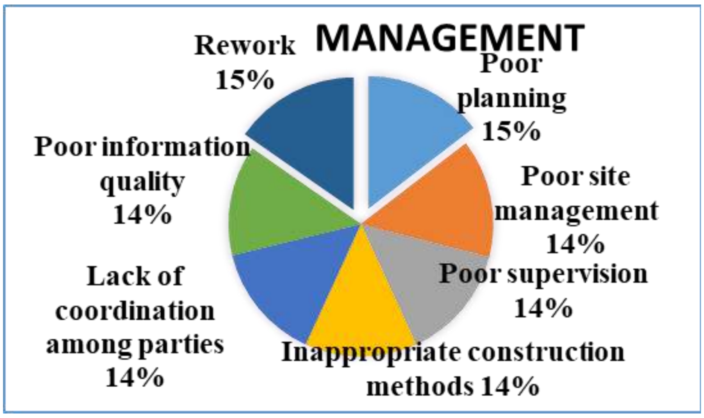

Figure 5: Factors affecting wastage in management.

3.2.5 Factors related to Site Condition

The condition of the site has a direct effect on construction waste because the construction materials generally packaged and stored on the project site the study showed that the most effective cause was the poor site condition, leftover materials and packaging at a rate of 22%, 21%, and 20% respectively as shown in Figure 6**.**

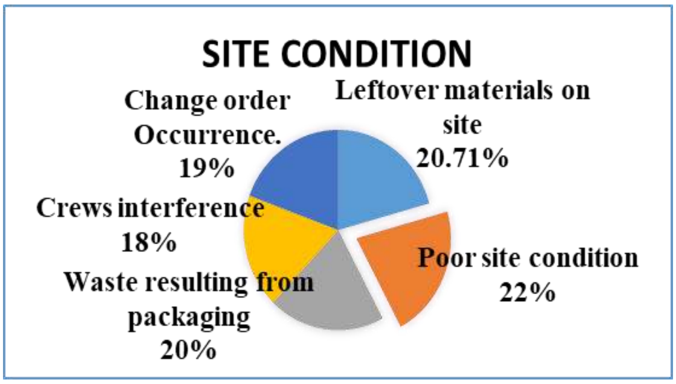

Figure 6: Factors affecting wastage in site conditions.

3.2.6 Factors related to Procurement

The procurement process of the delivery of the material to the site also examined and showed that the most effective source was the ignorance of Specifications at a rate of 22%, as seen from Figure7.

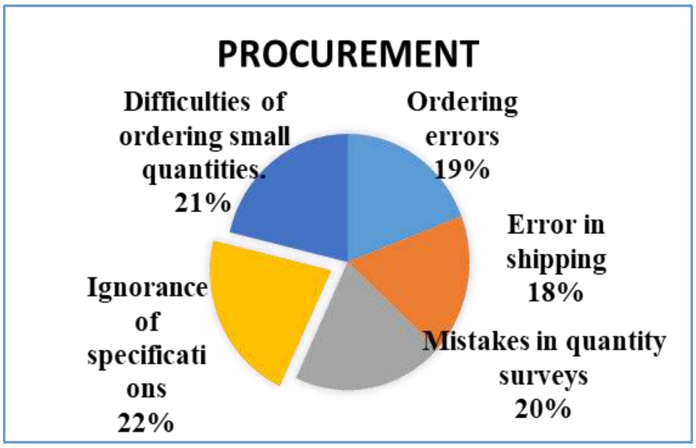

Figure 7: Factors affecting waste in procurement.

3.2.7Factors related to External

Figure 8 shows the most significant source in external factors that contribute to the waste generated during construction was the effect of weather at a rate of 31%.

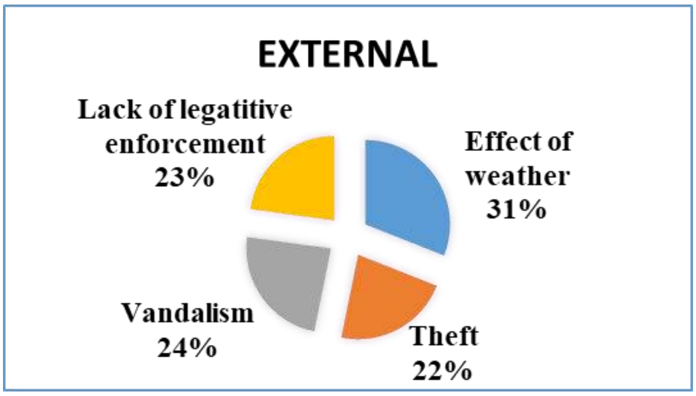

Figure 8: External factors affecting waste generation.

4.3 The Magnitude of Construction Materials Waste Generation

In the third part of the questionnaire examined the magnitude of construction materials waste generation where seventeen materials selected as detailed in Figure 9, which showed that the highest percentage of waste generated in Gypsum at a rate of 8.5%, while the waste in gravel and sand at a rate of 7.7% and 7.2% respectively. Whereas 7.4% in ceramic tiles.

4.4 Identification of factors influencing on the magnitude of waste generation

Concerning the causes of waste generation related to the quantity of waste of selected materials that the top significant factors influencing the waste generation due to lack of experience and improper operation in the project site in dealing with the following construction materials summarized in Table 5.

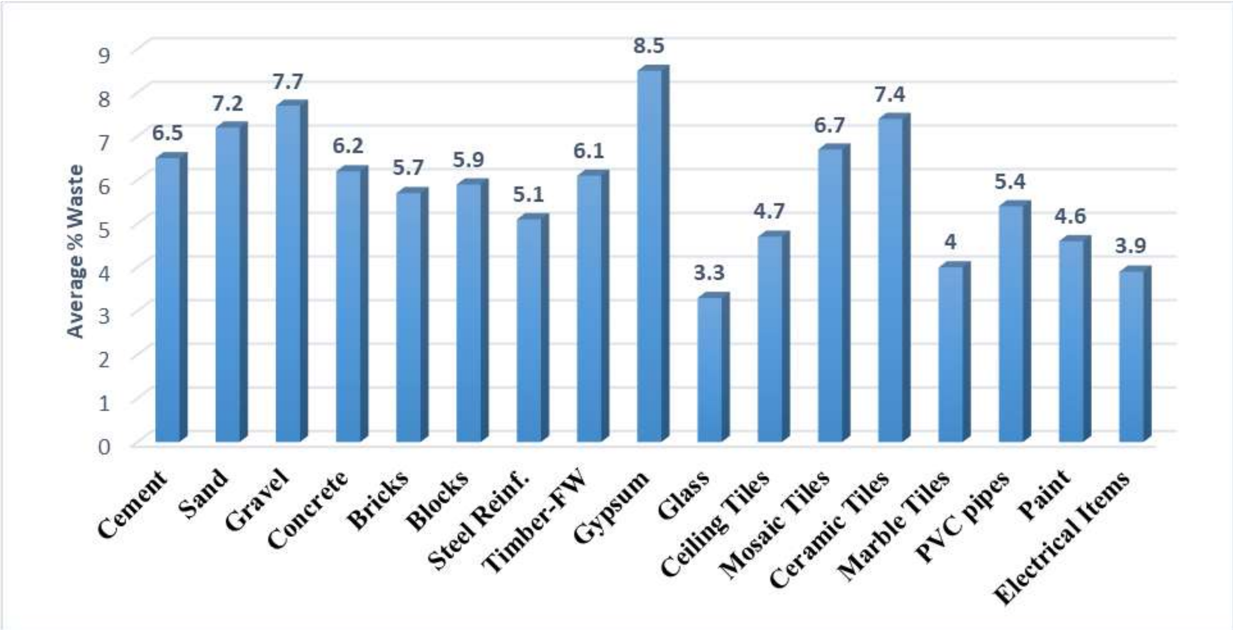

Figure 9: Average percentage of construction waste materials

Table 5. The Causes of Construction Materials waste generation

No.	Material	Top significance causes of wastages
1.	Cement	❖ Excessive or unnecessary consumption of mortar ❖ Improper storage method ❖ Mixing in unsuitable places ❖ Mixing of amounts more than the required ❖ Inappropriate way of transportation
2.	Sand	▪ Excessive or unnecessary consumption of sand ▪ Damaging the remained quantities in the workplace ▪ Improper storage method
3.	Gravel	✓ Mixing excessive amounts greater than required ✓ Far distance between the place of mixing and casting ✓ Wrong handling ✓ Losing the aggregate while passing the equipment on it
4.	Concrete	➢ Insufficient estimation of the amount of concrete required

		➢ Requiring an extra allowance of concrete ➢ Flaws in the framework assembling process ➢ Inadequate use of vibration which causes problems in concrete ➢ Use of insufficient equipment's and tools ➢ Far distance between the place of mixing and casting
5.	Blocks& Bricks	• Defects from the manufacturing of block • Lack of halves and quarters of blocks • Excessive cutting of blocks • Damaging of blocks during the process of cutting • Damaging of blocks during unloading and transportation
6.	Steel bars	✚ Improper cutting of bars ✚ Using lengthier bars than required ✚ Type of reinforcement method (bend bar, cut bar) ✚ Overlapping because of incorrect the length of bars ✚ Lack of skilled workers ✚ Damage during storage and rusting
7.	Timber	✓ No optimized cutting of timber boards ✓ low durability and reusability of formwork ✓ Cutting for interior fittings and finishing ✓ Wrong storage ✓ Use of low-quality wood ✓ Breaking of timber boards during the removal of the frames
8.	Gypsum	❖ Mixing amounts more than the required ❖ Ordering excessive quantities of gypsum ❖ The damaging result from severe weather conditions ❖ Poor storage method ❖ The excessive thickness of gypsum plastering
9.	Ceiling Tiles	○ Wastages from the necessary cutting process ○ Ordering additional quantities more than required ○ Unsuitable storage leading to deterioration or damage ○ Damage from handling or transportation
10.	Ceramic, Marble& Mosaic Tiles	✚ Damaging the tile during the process if necessary cutting ✚ Damage during transportation ✚ Excessive quantities of tiles, over-ordering ✚ Damage during finishing ✚ Inadequate skill workers
11.	PVC Pipes	➢ Ordering additional quantities more than required ➢ Cutting the pipes inappropriately ➢ Poor storage method ➢ Theft and vandalism
12.	Paint	▪ Paint damage under weather conditions ▪ Directly exposing the paint area to dust ▪ Inappropriate cleaning of walls and slabs prior painting process ▪ The damaging result from the addition of other materials to paint ▪ Wrong storage
13.	Electrical Items	✓ Excessive quantities required, over-ordering ✓ Excessive cutting of wires at ends ✓ Using additional amount more than required

5.CONCLUSION and RECOMMENDATIONS

This study has identified the primary sources and causes of construction materials wastages in construction projects in Erbil city from the perspective and views of construction practitioners. The analysis of survey data showed that the most effective source of waste generation was in the management aspect comes in the first rank in contributing to the waste generation, particularly poor planning and rework at a rate of 15% among seven factors tested in the area of management. While the design aspect comes in the second rank comes, particularly the cause of frequent design change that was contributing to the waste generation at a rate of 18%. The analysis extended to determine the magnitude of construction materials waste generation of sixteen types of materials. It was found that top highest percentage of waste generation was in gypsum at a rate of 8.5%, 7.7% in gravel, 7.4% in ceramic tiles, whereas in the sand, mosaic tiles, cement and concrete were 7.2%, 6.7%, 6.5%, 6.2% respectively.

Therefore, it is recommended to focus on the following issues to reduce the waste generation in construction projects:

- To adopt lean construction principles to minimize waste generation and maximize the value of project.
- To adopt a precise mechanism in management area to detect waste generation, by setting up clear waste management procedures and guidelines on identifying waste and that adopting a system to determine waste is essential since this will help in minimizing waste as well as discouraging the generation of waste by employs involved in construction development.
- Establishing a waste minimization plan is to encourage operators to be aware of the threat and negative impact of waste on society, environment.
- Encouraging recycling and reuse policies
- Diffusing the culture of understanding of the concept of waste generation management system and its implication to overrun the project cost and profitability among the workers and professionals in the construction sector in Erbil city.

REFERENCES

AJAYI, S. O., OYEDELE, L. O., BILAL, M., AKINADE, O. O., ALASKA, H. A. & OWOLABI, H. A., 2017. Critical management practices influencing on-site waste minimization in construction projects. *Waste management,* 59**,** 330-339.

AL-HAJJ, A. & ISKANDARANI, T. Reducing waste generation on the UAE construction sites. 7th International Conference on Innovation in Architecture, Engineering and Construction, 2012.

ALARCÓN, L. F., DIETHELM, S. & ROJO, O. Collaborative implementation of lean planning systems in Chilean construction companies. Tenth Annual Conference of the International Group for Lean Construction (IGLC-10), August, Brazil, 2002. 1-11.

BANSAL, S. & SINGH, S., 2014. A sustainable approach towards the construction and demolition waste. *International Journal of Innovative Research in Science, Engineering and Technology,* 3**,** 1262-1269.

BOSSINK, B. & BROUWERS, H., 1996. Construction waste: quantification and source evaluation. *Journal of construction engineering and management,* 122**,** 55-60.

DAVIS, G., PHILLIPS, P. S., READ, A. D. & IIDA, Y. 2006. Demonstrating the need for the development of internal research capacity: Understanding recycling participation using the Theory of Planned Behaviour in West Oxfordshire, UK. *Resources, Conservation and Recycling,* 46**,** 115-127.

ENSHASSI, A. 1996. Materials control and waste on building sites: Data in the study was obtained from 86 housing projects in several locations in the Gaza Strip. *Building Research and Information,* 24**,** 31-34.

FADIYA, O. O., GEORGAKIS, P., CHINYIO, E. & AKADIRI, P. 2013. Analyzing the perceptions of UK building contractors on the contributors to the cost of construction plant theft. *Journal of Financial Management of Property and Construction,* 18**,** 128-141.

FORMOSO, C. T., ISATTO, E. L. & HIROTA, E. H. Method for waste control in the building industry. Proceedings IGLC, 1999. 325.

HINTON, P., BROWNLOW, C., MCMURRAY, I. & COZENS, B. 2004. Using SPSS to analyze questionnaires: Reliability. *SPSS explained***,** 356-366.

JAIN, M. 2012. Economic Aspects of Construction Waste Materials in terms of cost savings–A case of Indian Construction Industry. *International Journal of Scientific and Research Publications,* 2**,** 1-7.

KAVITHRA, S., AMBIKA, D. & SHANKARI, R. S. 2017. A REVIEW ON QUANTIFIED IMPACTS OF CONSTRUCTION LABOUR PRODUCTIVITY TOWARDS PROJECT PERFORMANCE.

KOSKELA, L. 1992. *Application of the new production philosophy to construction*, Stanford University Stanford, CA.

SAWANT SURENDRA, B., MANOJ, H. & MADHAV, K. 2016. Impact of the Construction Waste on the Cost of the Project. *International Journal of Engineering Research Volume*, 126-128.

SINGH, T. S., 2015. Management of Construction Waste Materials: A Review. *International Journal of Geology, Agriculture and Environmental Sciences*, 3.

WYATT, D., 1978. Material management, Part I. *Occasional Paper: The Chartered Institute of Building*.

YOCKEY, R. D., 2018. *SPSS Demystified: A simple guide and reference*, Routledge.

ZANCO Journal of Pure and Applied Sciences
The official scientific journal of Salahaddin University-Erbil
https://zancojournals.su.edu.krd/index.php/JPAS

ISSN (print):2218-0230**, ISSN (online):** 2412-3986**, DOI: http://dx.doi.org/10.21271/zjpas**

RESEARCH PAPER

GENERATING MODELS OF SOFTWARE SYSTEMS DURING EXPLORATORY

Akreen M. Saleh[1], Moayad Y. Potrus[2]

[1]Department of Software and Informatics, College of Engineering, Salahaddin University-Erbil, Kurdistan Region, Iraq
[2]Department of Software and Informatics, College of Engineering, Salahaddin University-Erbil, Kurdistan Region, Iraq

A B S T R A C T:
One of the major parts of the software testing is event-driven software (EDS), all actions of the software come from events. Interaction of the user to the graphic user interface (GUI) of the web and desktop applications will generate events, or for the embedded systems events and signals received from equipment, these are examples of Event-Driven Software. using EDS for software testing gives to the software tester a great result to test software because it generates a large number of events that could be cover most of the EDS's area. In this paper, an automated full-model and sub-model generation have been introduced during the system under testing, it produces test cases of websites to overcome faults and long time-consuming. The stage of the testing procedure includes generating full-model of the websites then extracting sub-model from the full-model in the next stages, test cases generated with path coverage. The proposed testing procedure has been analyzed with the four case studies consisting of Fault Detection and Fault Detection Effectiveness. Has been testing with a manual testing method and it proved its efficiency regarding test generation and time. Further, the sub-model test generation provides more accurate test case suite generation than full-model testing.

KEY WORDS: MBT, Graph theory, Software testing, full-model automation, Sub-model extraction
DOI: http://dx.doi.org/10.21271/ZJPAS.32.4.2
ZJPAS (2020) , 32(4);12-21 .

1.INTRODUCTION

The recent software development market is characterized by the increasing complexity of implemented systems, a decline in the time to market, and a demand for real-time operation of these systems on various platforms. One of the most important software development applications is a website, Websites are client-side software applications and accessed through browsers, mostly consists of (HTML) HyperText Markup Language pages it might be static and simple (Utting and Legeard, 2007).

* **Corresponding Author:**
Akreen M. Saleh
E-mail: akreen.muhialdeen@su.edu.krd or agrin.muhyeadin@gmail.com
Article History:
Received: 15/10/2019
Accepted: 15/02/2020
Published: 08/09 /2020

Testing techniques are usually classified as black-box and white-box. Black-box (functional testing) depends on knowledge requirements and the client needs to determine the test cases. White box testing means structural test or interior testing, based on internal code structure and depends on the programmer's skill, this testing is usually done at the unit level. One of the best techniques that can be applied for testing efficiency and software quality is Model-Based Testing (MBT). According to Mark Utting and Bruno Legeard (Utting and Legeard, 2007), MBT allows the automatic generation of test cases through a model built based on the expected behaviour of the software under test (SUT).

MBT is an approach that has several advantages reported in the literature, such as the automatic test case generation, fault detection effectiveness, and reduction in time and cost for testing (Utting and Legeard, 2007).

In this research, an algorithm proposed to generate automatically full-model of the website under testing and sub-model extraction, that helps the tester to generate automatic test case suite. The test case suite generated from the smaller models extracted from the full-model. In the empirical evaluation find out that the proposed algorithms generated better test cases suite and less time-consuming against manually exploration strategy and full-model compared with sub-model of the proposed algorithm, it is clearly seen that the testers easily can be managed sub-models for generating .a set of test cases and more accurate test cases suite will be generated.

There are several sources for problems in the website testing area. The main problem is manually generating test cases, it causes a decline in system release time in the system under testing (SUT). Change a requirement from the website tester must be re-generate test cases manually.

This paper proposes to evaluate the use of the model-based testing MBT concepts in the design and execution of automated tests in websites and using mutation testing to evaluate the efficiency of automated test.

2. BACKGROUND

To face faults in software testing in development, there are a large number of techniques that can be applied (Myers et al., 2012). Among them techniques defined for the automated test case generation using behavioral or structural model, also called a test model of the system under testing (SUT). This approach is known as Model-Based Testing (MBT) (De Cleva Farto and Endo, 2015). Model-based testing depends on three key technologies: 1. notation used for the data model, 2. test-generation algorithm, 3. tools to generate tests. Unlike the generation of test infrastructure, model notations and test-generation algorithms are portable across(Dalal et al.). MBT divided into four main steps: 1. modeling, 2. test generation, 2. Concretization 4. test execution (El-Far and Whittaker, 2002).

In modelling, the tester uses her/his knowledge to build a test model of the system under testing. the requirements are source of the information for the functionality of software being tested. An operating system, competing solutions, libraries and other specifications are factors that software product in an environment presented. The tester should be learning and understand the system under testing and test execution. It is advised to build test models based on the requirements, to maximize the independence between the model and the system under testing (Utting et al., 2012), to know and building a test model software analysis and design can be used. The test case generation algorithm based on the technique used to define the test model.

Modelling techniques must own features to create test case generation cheaper and easy automation (El-Far and Whittaker, 2002). For the automatic test case generation, a tool has been used. The test model has submitted as input then a set of test cases generated from test selection criterion and tool. during the system under testing, generated test cases not executable and at the abstract level. Finally to convert test cases from abstract level to the executable level in the system under testing concretization will involve. Execution of the test cases in the system under testing comes after conversion from the abstract level into the executable test cases. After the execution process, the results are analyzed and corrective actions are taken. If the test model defines both input and output values an automatic check may be performed.

Event Sequence Graph "ESG", can be used to show precisely the requirements and functionality of the system under testing to build the test model, some modelling techniques. ESG used to build a test model and modelling techniques. It is assumed that the modelling technique adopted for the model-based testing "MBT" is formal (Hierons et al., 2009). In MBT there are several modelling techniques used, like Finite State Machines (Lee and Yannakakis, 1996), Labeled Transition Systems(Tretmans, 1996), and UML(Hierons et al., 2009).

In this paper, the ESG technique has been adopted because of its ease to express communications between events and the simplicity to learn the requirements and functionality of the system under testing. An ESG is a directed graph, *used to model interactions between the software events and consists of nodes that represent events while the edges are valid sequences of these events (Belli et al., 2006, Yuan et al., 2011).*

3. Related Work

In this section, several existing works have presented a categorized survey of generating models during the testing process. These related works are categorized according to the different strategies they have chosen for ways to create their own test cases.

An event-flow graph consists of nodes which represent events and edges that connect two events. In EDS can show each event changes, e.g. changing the colour of an input on a page in a website (Memon, 2007).

Memon (Memon, 2007) has introduced a technique based on the event-flow graph. In this paper, a tool used named GUIRipper for dividing the application and then event flow graph generated this solution categorized as a semi-automatic method. Event flow graph compared with another graph such as Finite State Machine (FSM), Complete Interaction Sequence (CIS) (Li et al., 2007) and Genetic Model(Pargas et al., 1999). After dividing the application overlapped sections created (Li et al., 2007) and by using the GUIRipper enabled features on the page will detect between the problems.

Belli et al. (Belli et al., 2006) have proposed an Event Sequence Graph (ESG) to model the behaviour of GUI. A tool has been created named GATE tool used to create and run test cases. The tool can be work with the ESG matrix and user input.

Herbold et al. (Herbold et al.) have suggested usage-based testing for EDS. This approach has three layers, that used to find which functionality of the application is used by the user. In the first layer users, actions are registered. Then in the next layer, registered actions are converted. Finally, in the last layer, the usage profile is generated from the events.

Herbold (Herbold and Steffen, 2012) for test case generation has proposed three new strategies based on usage-based testing. The first strategy, test paths are picked with a high probability. However, the number of valid sequences will increase exponentially. The second strategy, to reduce the sequences number of event, the first strategy and the random walk technique is used. The third strategy is to provide more gain in selecting test paths, a heuristic greedy strategy uses. Besides, AutoQUEST platform has developed by Herbold and Harms (Herbold and Harms) for EDS testing. on the AutoQUEST platform, usage-based testing is implemented and many testing techniques have been implemented. AutoQUEST is to present a testing technique independent from platforms and this was one of the main goals

Tonella et al. (Tonella and Ricca, 2004) have introduced an extraction of the website model in dynamic analysis. On the website, HTML code generated by the server-side and user actions on input values is required. In this paper, ReWeb tool created the model, is presented as a Markov Chain with expectation values on the edges. The method is known as semi-automatic because of using a tool named TestWeb tool which is including a test generator and test executer.

In the test section test, the criterion can be selected by the tester. In this method, like (Herbold et al.), the model does not cover all functionalities of the website if the input values are not selected entirely by the user.

(Ahmed and Bures, 2019) present an automated approach for generating models of smart TV applications based on black-box reverse engineering. The approach explored the user interface of the TV apps by using a remote control device and a model constructed cumulatively. The approach is used as a black-box technique, a tool has been implemented called EvoCreeper. the model generated in runtime mode by exploring the state of the user interface, this step is done without any information of the internal structure of the app.

4. Methodology

In this section proposed algorithm will be explained for the automated full-model generation and the strategy of extracting a sub-models from the full-model explained that the extraction process is done by selecting a node as a first node and another node as a last node of the sub-model then the algorithm extracted the sub-model from full-model automatically and then the sub-models ready and node-event coverage testing applied to generated a set test cases for the website under testing.

4.1 . Model Generation and Sub-model Exclusion

In this section, new strategy has been presented of automatically generating models of websites during testing. The technologies used in the strategy was google chrome extension and javascript for model creation. Figure 1,2 and 3 example of the developed google chrome extension. The method rely on the black-box technique for graph generation and does not need information about the code part of the website. The website is modelled as a directed graph G=(N, E), where N is a set of nodes at least one node exist, $N \neq 0$, and E is a set of edges. E is a subset of N x N possibilities.

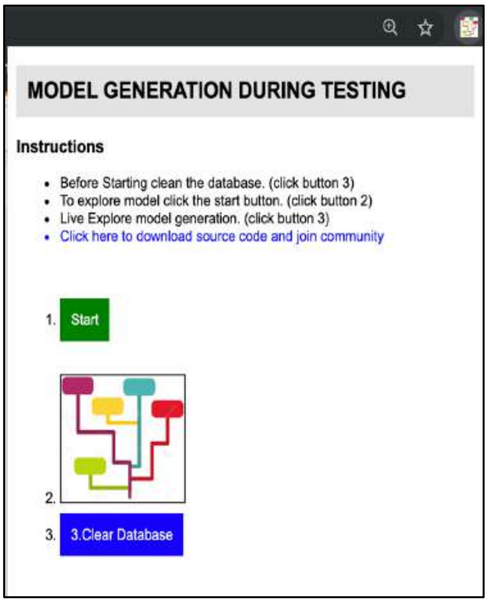

Figure 1: Proposed algorithm browser extension main view.

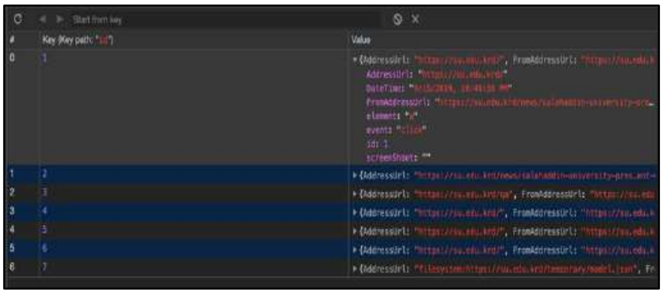

Figure 2: Proposed algorithm (node and event) database.

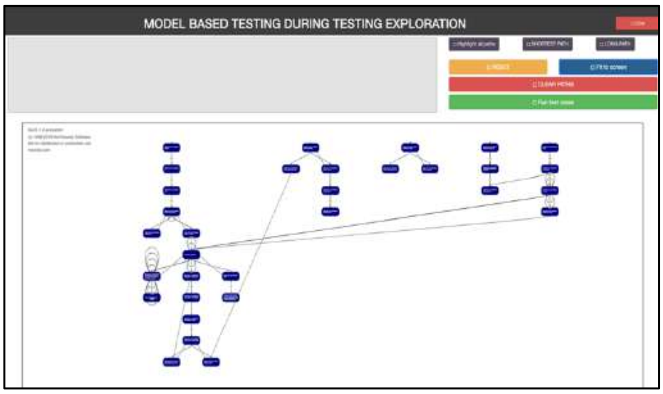

Figure 3: Extension Full-Model and Sub-Model Generator.

In the graph, one starting node defined, ns $\in$ N. The set Ne $\subseteq$ N contains the end nodes of the graph, where Ne $\neq$ 0. Each node corresponds to a UI element (state) of the website. Every edge communicates to possible events of the website. These events can be triggered by google chrome extension,

In this study, e $\in$ {key up, key down, keypress, blur, focus, click, double click, mouse hover, mouse down, navigation} for each e $\in$ E. To identify all the important states in the website user interface for exhibition in the graph, an algorithm developed to detect all events and navigations of the website, the algorithms called GUIRipper used to detect GUI elements that rip over the website that developed by HTML.

Algorithm 1 presents the levels of the Model Generator Algorithm. The algorithm detects testers all evens over GUI elements of the website to be tested, the events are edge E and the web page address converted to nodes of the model N. Start node Ns is that page the algorithm started, the algorithm first checks element type of the HTML tags of the web page and then detect events of each elements for instance form elements such as 'input, radio button, checkbox and select' for navigation checks anchor URL, when event detected the algorithm will add to the list of events e $\in$ E and page address add to the nodes N, the process will continue until the tester stops the algorithm by clicking the stop button in extension and end node of the model N algorithm stopped and there was nothing to test.

Algorithm 1 Model Generator Algorithm

```
node ←[]
link ←[]
referreAddress ←""
elementType ←getTagType
if elementType =anchor then
    referreAddress = anchorURL;
  if elementType = "input,radio,check box,select" then
    referreAddress = mainURL;
      for each event E do
          node ←[key: E.fromAddress, title: E.fromAddress]
          link ← [from : E.fromAddress, to : E.referreAddress]
      end for
```

4.2. An Automated Framework

According to the problems and challenges so far, an automated framework would propose to test websites. This framework shows our image for a strategy to automate the testing process. The framework working on the web browser which the nowadays browsers include an extension for developers and the framework developed for google chrome extension. Figure(4) reveals a summary of this framework and explains the fundamental components and their relationship to each other. The frameworks support only black-box testing the tester install the extension on google chrome web browser by clicking the start button in the extension, the testing algorithm started on the opened tab of the browser then algorithm detects testers event on the website, the events used in algorithm such as input events "key up, key down, keypress, blur, change, focus, on select, on submit, on reset", mouse events " mouse over, mouse out, mouse down, mouse up, mouse move" and click events "click, double click" detail of the algorithm will present in section 4.2.1.

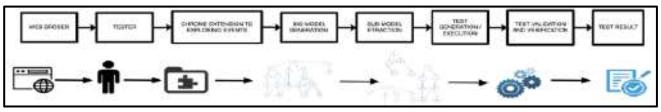

Figure 4: An automated framework of the proposed algorithm.

The algorithm uses a browser database to store logs, figure(3) shows a part of the full-model data in the browsers local database. then the testing process done tester stops the algorithm, then full-model will generate that contains nodes and edges. The tester will generate a sub-model from a full-model to generate test cases and validate test cases finally test results will be presented to the user.

4.2.1 Proposed Algorithm

To catch all the important events in the website to present in the model for test generation, an algorithm has been developed, that algorithm can be able to detect all web events during user tests the website.

Algorithm 1 shows the steps of the model generator algorithm. when tester hits the start button algorithm will be start and the current web page address is the main node of the model, the algorithm checks the type of the elements and it detects events to know at which element this event happens, another ability to detect navigation from the anchor tag. The address of the page will be adding to the list of the nodes and during detecting an event algorithm checks the address URL from and to the page then add to the link list to be model. Stopping condition by tester side after clicking the stop button of the algorithm stops. Full-model will be generated and ready to extract the sub-model then generate test cases.

4.2.2 Proof of Concept

In this section, the proposed algorithm will be illustrated as shown in algorithm 1. in this case a website developed that contains 10 nodes(pages) and 26 events(interactions) to implement the proposed algorithm. the algorithm implemented in google chrome extension, at first the tester must be installed on the browser and then the exploration process starts by clicking the start button in the program.

The website under testing will ready then tester start the exploration process and the proposed strategy will generate the full-model(graph) automatically during the exploration process, then the exploration process continued until all nodes explored.

in this stage the automated full-model ready to break into smaller parts called sub-model. sub-model is a part of full-model, the extraction process of sub-model from full-model will be done by selecting the first node as a start node Ns and another node as a last node of Nl and then the sub-model will be ready. Sub-model that will help the tester to be more accurate and less time losing during generating a set of test cases against full-model.

5. Experiential Evaluation

For evaluating the power of the model generation and test case generation strategy. Four case study of the website online chosen, during the evaluation process we address the following research questions.

- Research question 1(RESQ1): Is the proposed strategy able to explore and detect nodes(pages) and events(interactions) of the website under testing?
- Research question 2(RESQ2): Is an automated full-model and sub-models are valid, and it complete model(graph) in term of number of nodes(pages) and events(interactions)?
- Research question 3(RESQ3): What is the performance of the algorithm to detect events of manual exploration for chosen websites?

Research in the area of exploration test cases on the websites is very difficult. A long-time process may be needed for the testers to generate models and extract test cases, as it is new in software testing. As a result, not many websites and repositories are available for benchmarking. Most developers develop websites in different techniques and it is hard for the tester to test the website during development. However, there are some tools for generating models after completing the system.

Four different websites chosen of different sizes online, to illustrate the effectiveness of our approach. These websites are from different areas and have differing numbers of functionalities. Table 1 reveals the title and address of websites.

A set of experiments has been handled to address RESQ1 and RESQ3. The purpose was to differentiate the models and test cases of the websites created through manual exploration. To test our strategy against manual testing, We guided students from software engineering study program, we divided students into four groups of 30 participants.

Table (1) Case Studies for the implementing proposed algorithm.

#	Title	Link
1	Test Case study website	github.com/agreensaleh/mbt.git
2	Salahaddin university website	https://su.edu.krd
3	Webmail Horde	http://demo.horde.org
4	CPanel for web hosting	https://cpanel.net

The extension installed on laptop or desktop computers on google chrome browser, algorithm stores the target events, states and timestamps of the exploration. Every student in each group of the website testing has been assigned to explore and export the database of exploration logs. The finishing of the testing was the student decides all parts of the website to have been explored. Then the algorithm prepared events to generate models during testing then automatically full-model generated. Several attributes have been analyzed for each model, like as the time required to build the model, the number of nodes in the model and the unique nodes in the model. The proposed modelling, for generating test cases it will extract sub-model from full-model then it will be easy to generate test cases.

To address RESQ2, the proposed model generation was compared against other existed model generating algorithm such as (Ahmed and Bures, 2019). The requirements of the generated model at least have one node and the model must not be empty, should have its starting node, and all nodes of the model must have at least one incoming edge and except the starting node. additionally, in the model, at least one end node must be presented. the generated model must be able to reach from any node to the end node, finally, every node must be reachable from the main node

Figure 5 shows the produced directed full-model graph and sub-model of the test case study website. The nodes represent the pages and the arrows(edges) represent the events. The website consists of 10 nodes and derives by 87 Events as shown partially in figure 5. Figure 8 and 9 show the box plot of the results for the comparison between the algorithm and manual generation. Due to the personal and nondeterministic nature of the outcomes gotten by each student, and to ensure reasonable comparisons with more details, box plots used to compare the result.

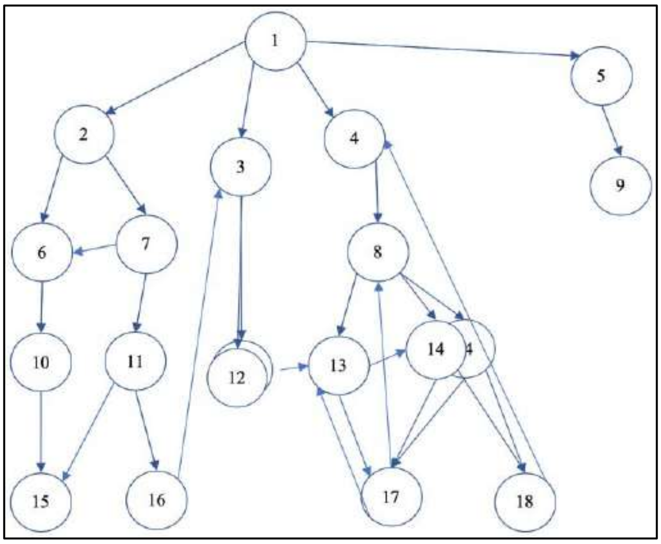

Figure 5: Full-model a part of test case study.

Figure 6 and 7 show the process of applying the proposed sub-modeling technique on the main website. As it can be seen from figure 7, the full-model has been divided into three sub-models in which each consist of 8,5 and 6 nodes respectively. Moreover, these graphs consist of 4,4 and 3 events shown in table 2.

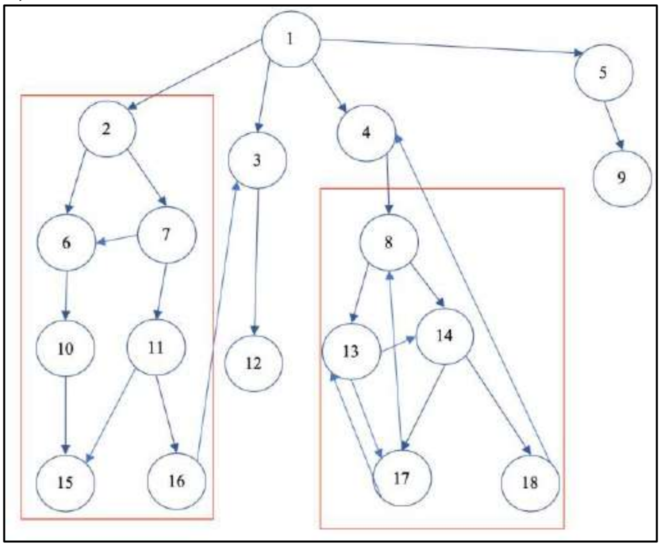

Figure 6: Extracting sub-models from full-model.

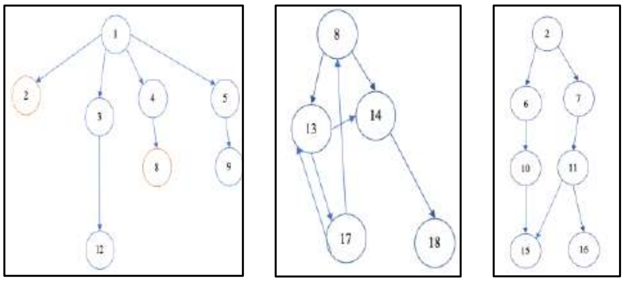

a) sub-model 1 b) Sub-Model 2 c) Sub-Model 3

Figure 7: Sub-models extracted from the automated full-model(graph).

Table (2) Test case generation result.

Model	No. Nodes	Test Cases
Full-Model	18	468
	TOTAL	468
Sub-Model-1	8	30
Sub-Model-2	5	35
Sub-Model-3	7	49
	TOTAL	114

Figure 8a shows the box plot of algorithm exploration versus manual exploration of the graph of the website, the blue color operate as manual exploration and the orange color identified for the algorithm exploitation. It is clear seen that both exploration for detecting nodes of the website are the same, due to the small number of pages in website. Figure 9a and table 2 show the difference between exploring time for manual and algorithm exploration, the exploring time for the manual exploration may vary from each participant's, generating the full graph of the website, exploring time will change from 15-20 minutes, algorithm generate the full graph during website exploration no need time to generating full graph. The completion of manual exploration depends on the participant's understanding and experience with the website. While the strategy explored graph without need to write pages and derive events of the website, the participant's had to write pages and events then generate graphs.

Figure 8b shows the result of the su website, all pages detect by the both exploration is less than 50 pages, manual exploring vary from each participant's, exactly half of the participant's detect pages between 32 and 46 pages, at least 25% of the participant's between 21 and 31 pages. Exploring time shown in figure 9b and table 3, most of the participant's generate *the full graph between 52 and 58 minutes, while the rest of them more than 58 and less than 110 minutes.*

Figure 8c and 8c shows the manual exploration result of the webmail and CPanel websites. It can be seen that in table 5 shows page comparison of the webmail, participant's explore pages between 44 and 80 pages and the time exploration time exploration between 60 and 146 minutes, table 6 shows CPanel page exploration that 90 and 140 pages explored and the time exploration time exploration between 130 and 170 minute.

Table (3) No of pages and time exploration of the manual against proposed algorithm.

Case study	Time explored (Manual)	No. of pages explored (Manual)	Time explored (Algorithm)	No. of pages explored (Algorithm)
Case study website	15-20 minutes	10 pages	0 minutes	10 pages
Su website	33-110 minutes	12-50 pages	0 minutes	50 pages
Webmail website	55-150 minutes	44-80 pages	0 minutes	80 pages
CPanel website	130-170 minutes	90-140 pages	0 minutes	140 pages

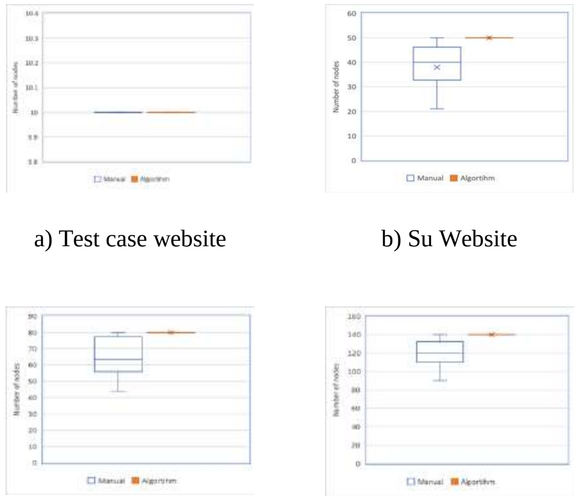

a) Test case website b) Su Website

c) Webmail web application d) CPanel web application

Figure 8: Comparing the number of unique nodes detected by algorithm exploration with the manual exploration.

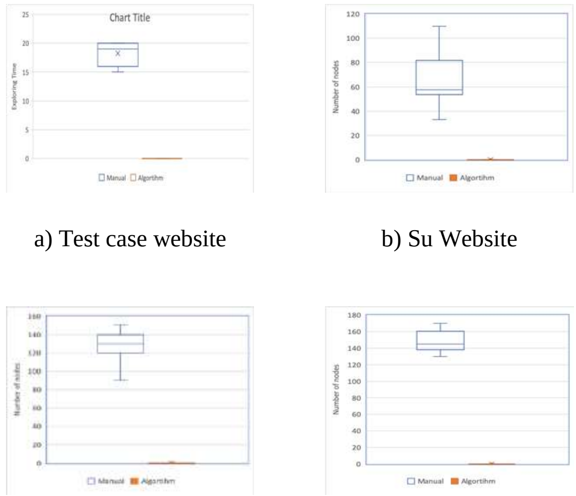

a) Test case website b) Su Website

c) Webmail web application d) CPanel web application

Figure 9: Exploration Time comparisons between Algorithm and Manual exploration.

One of the main features of the website is that it can grow dynamically. This means pages can be add or links can be increased. This will make the regression testing more time consuming when a node is added. the subgraph (model) will help generate test cases that are only relayed to the affected graphs(models) instead of the full model. This is one of the advantages of using this technique.

5. CONCLUSIONS

In this paper, the strategy for automatically reverse engineering websites presented by using the chrome extension. Events explored from websites by involving navigation in GUI, this happens without knowing the internal structure of the website “it is an example of the black-box”. The directed graph model generated after extensively exploring events and states in a given website. The strategy implemented in the google chrome extension that works in a web browser or laptop and personal computers.

To evaluate the strategy, two medium-sized and two large websites used. The effectiveness and performance of our strategy demonstrated from the evaluation results. It can be seen that the proposed strategy generated test cases less than automated full-model and less-time losing during generating set test cases.

To generate test cases node-event coverage testing strategy was implemented and in this strategy nodes(pages) N and events(interactions) E will be multiplied which is N X E, as a result, the number of test cases generated for the full-model was 18 X 26 = 468 test cases and for all sub-models is 114 test cases, the number of test cases of the sub-model is less than full-model and the test cases is more accurate and more efficient.

The strategy can be used to detect events during testing and models automatically generated tester easily can be tracked generated model. The generated models have an advantage in stages of developing a website in term of quality enhancement, software testing, finding disappeared requirements, evaluating the user experience and provided virtualization of the website for an understanding the events and states.

There are several possibilities for future research. A quick step forward is to use the strategy-generated models to test numerous applications and identify new errors. as well, for automatically traverse on all website events and stated we are planning to use this strategy.

Acknowledgements

First and above all, I would like to thank God Almighty for providing me with this opportunity and granting me strength, knowledge, and capability to undertake this research study and to proceed successfully. Without his blessings, this achievement would not have been possible.

I would like to express my deep gratitude to my supervisor Asst. Prof. Dr. Moayad Yousif Potrus for his patience, enthusiasm, insightful comments, and immense knowledge. His guidance helped me in all the time of research and writing of this paper.

References

AHMED, B. S. & BURES, M. 2019. EvoCreeper: Automated Black-Box Model Generation for Smart TV Applications. IEEE Transactions on Consumer Electronics, 65, 160-169.

BELLI, F., BUDNIK, C. J. & WHITE, L. 2006. Event-based modelling, analysis and testing of user interactions: approach and case study. Software Testing, Verification and Reliability, 16, 3-32.

DALAL, S. R., JAIN, A., KARUNANITHI, N., LEATON, J. M., LOTT, C. M., PATTON, G. C. & HOROWITZ, B. M. Model-based testing in practice. ACM, 285-294.

DE CLEVA FARTO, G. & ENDO, A. T. 2015. Evaluating the model-based testing approach in the context of mobile applications. Electronic Notes in Theoretical Computer Science, 314, 3-21.

DEMILLO, R. A., LIPTON, R. J. & SAYWARD, F. G. 1978. Hints on Test Data Selection: Help for the Practicing Programmer. Computer, 11, 34-41.

EL-FAR, I. K. & WHITTAKER, J. A. 2002. Model-Based Software Testing. Hoboken, NJ, USA: John Wiley & Sons, Inc.

HERBOLD, S., GRABOWSKI, J. & WAACK, S. A Model for Usage-Based Testing of Event-Driven Software. 2011/06//. IEEE, 172-178.

HERBOLD, S. & HARMS, P. AutoQUEST -- Automated Quality Engineering of Event-Driven Software. 2013/03//. IEEE, 134-139.

HERBOLD, S. & STEFFEN. 2012. Usage-based Testing of Event-driven Software.

HIERONS, R. M., KRAUSE, P., LÜTTGEN, G., SIMONS, A. J. H., VILKOMIR, S., WOODWARD, M. R., ZEDAN, H., BOGDANOV, K., BOWEN, J. P., CLEAVELAND, R., DERRICK, J., DICK, J., GHEORGHE, M., HARMAN, M. & KAPOOR, K. 2009. Using formal specifications to support testing. ACM Computing Surveys, 41, 1-76.

LEE, D. & YANNAKAKIS, M. 1996. Principles and methods of testing finite state machines-a survey. Proceedings of the IEEE, 84, 1090-1123.

LI, P., HUYNH, T., REFORMAT, M. & MILLER, J. 2007. A practical approach to testing GUI systems. Empirical Software Engineering, 12, 331-357.

MA, Y. S., KWON, Y. R. & OFFUTT, J. 2002. Inter-class mutation operators for Java. Proceedings - International Symposium on Software Reliability Engineering, ISSRE, 2002-Janua, 352-363.

MEMON, A. M. 2007. An event-flow model of GUI-based applications for testing. Software Testing, Verification and Reliability, 17, 137-157.

MYERS, G. J., SANDLER, C. & BADGETT, T. 2012. The art of software testing, John Wiley & Sons.

PARGAS, R. P., PARGAS, R. P., HARROLD, M. J. & PECK, R. R. 1999. Test-Data Generation Using Genetic Algorithms. SOFTWARE TESTING, VERIFICATION AND RELIABILITY, 9, 263--282.

TONELLA, P. & RICCA, F. 2004. Statistical testing of Web applications. Journal of Software Maintenance and Evolution: Research and Practice, 16, 103-127.

TRETMANS, J. 1996. Conformance testing with labelled transition systems: Implementation relations and test generation. 29, 49-79.

UTTING, M. & LEGEARD, B. 2007. Practical Model-Based Testing.

UTTING, M., PRETSCHNER, A. & LEGEARD, B. 2012. A taxonomy of model-based testing approaches. Software Testing, Verification and Reliability, 22, 297-312.

VOAS, J. M. & M, J. 1992. PIE: a dynamic failure-based technique. IEEE Transactions on Software Engineering, 18, 717-727.

YUAN, X., COHEN, M. B. & MEMON, A. M. 2011. GUI Interaction Testing: Incorporating Event Context. IEEE Transactions on Software Engineering, 37, 559-574.

POTRUS, M. Y. 2016. Maintenance Scheduling Optimization for Electrical Grid Using Binary Gray Wolf Optimization Technique. ZANCO Journal of Pure and Applied Sciences.

KANAR SHUKR MOHAMMED, M. Y. P. B. F. A. D. 2018. Effect of Hybrid Teaching Methodology and Student Group Policy on Object Oriented Problem Solving. ZANCO JOURNAL OF PURE AND APPLIED SCIENCES, 30.

ZANCO Journal of Pure and Applied Sciences
The official scientific journal of Salahaddin University-Erbil
https://zancojournals.su.edu.krd/index.php/JPAS

ISSN (print):2218-0230**, ISSN (online):** 2412-3986**, DOI: http://dx.doi.org/10.21271/zjpas**

RESEARCH PAPER

Adaptive-Sliding Mode Trajectory Control of Robot Manipulators with Uncertainties

Mustafa M. Mustafa[1], Ibrahim Hamarash[1,2], Carl D. Crane[3]

[1]Department of Electrical Engineering, College of Engineering, Salahaddin University-Erbil, Kurdistan Region, Iraq
[2]Department of Computer Science and Engineering, University of Kurdistan Hewler, Iraq
[3]Department of Mechanical and Aerospace Engineering, University of Florida, FL, USA

A B S T R A C T:

In this paper, we propose and demonstrate an adaptive-sliding mode control for trajectory tracking control of robot manipulators subjected to uncertain dynamics, vibration disturbance, and payload variation disturbance. Throughout this work we seek a controller that is, robust to the uncertainty and disturbance, accurate, and implementable. To perform these requirements, we use a nonlinear Lyapunov-based approach for designing the controller and guaranteeing its stability. MATLAB-SIMULINK software is used to validate the approach and demonstrate the performance of the controller. Simulation results show that the derived controller is stable, robust to the disturbance and uncertainties, accurate, and implementable.

KEY WORDS: Nonlinear Control, Uncertainty, Robot Manipulator.
DOI: http://dx.doi.org/10.21271/ZJPAS.32.4.3
ZJPAS (2020) , 32(4);22-29 .

1. INTRODUCTION

Many robot manipulators in the modern world are required to work in high speed and high accuracy. For many applications, such as in the medical area, manufacturing printed circuit boards, robot manipulators are required to be manipulated accurately with high speed despite the uncertainty in the dynamics. Such a disturbance, that is caused by a vibration and/or a payload variation, causes a major uncertainty in the dynamics of robot manipulators. Without an efficient controller, that can reject this disturbance and deal with the uncertainty, the robot manipulator will perform poorly in terms of stability and accuracy. Therefore, the methods of robot manipulators control need to be developed to damp the disturbance torques while trajectory tracking control, specially the disturbance that is caused by vibration and payload variation.

Some position tracking control methods consider the disturbance as an uncertainty in the dynamics. While there are other methods consider this disturbance as exogenous torques to be damped separately. Therefore, many linear and nonlinear control approaches are used for trajectory tracking control. In (Economou *et al.*, 2000), the authors utilize finite impulse response filters to design a controller that suppress residual vibrations in flexible payloads carried by robot manipulators. However, the controller is restricted due to the limitations of these filters with nonlinear systems and the natural frequencies' knowledge requirements about the payload. In

* **Corresponding Author:**
Mustafa M. Mustafa
E-mail: mustafa.atrushi@su.edu.krd
Article History:
Received: 22/12/2019
Accepted: 19/02/2020
Published: 08/09 /2020

(Mamani, Becedas and Feliu, 2012), a sliding mode control (SMC) is used to control the position of a single link flexible robot arm. The controller rejects the disturbances that are caused by actuator friction and payload; however, the actuator bandwidth of this controller is beyond the classical limits. In (Feliu *et al.*, 2013), an innovative algorithm is designed to control a three degree of freedom flexible robot arm in the presence of vibrations. The control algorithm cancels the vibration and shows an accurate trajectory tracking control with acceptable control effort; however, the kinematics and the compliance matrix of the robot need to be known. In (Slotine and Li, 1987), another control algorithm is derived, based on the adaptive control theory, to solve the problem of trajectory tracking when the payload is unknown. The same theory is utilized by (Craig, Hsu and Sastry, 1987) to reject the exogenous disturbances while trajectory tracking, where the dynamics is assumed to be known. In (Hsia and Gao, 1990), the payload variation is treated within the dynamics of the robot by the proportional derivative (PD) control law. The authors of (Dawson *et al.*, 1990), use a PD controller with proper gains and initial conditions after bounding the disturbances, where they show uniformly bounded (UB) results of the tracking error. The input torques in (Craig, Hsu and Sastry, 1987; Slotine and Li, 1987) are better to that in (Dawson *et al.*, 1990; Hsia, Lasky and Guo, 1991; Spong, 1992) in term of implementation; however, these controllers are not robust to vibration and payload variation. Other works consider the fact that the disturbance cannot be linear parameterized, therefore, neural network and fuzzy logic methods are called through the control design (Dixon, Zergeroglu and Dawson, 2004; Gao *et al.*, 2018; Nafia *et al.*, 2018). However, there are many limitations with these controllers; therefore, the integral of the sign of the error (RISE) is utilized in (Cai, de Queiroz and Dawson, 2006; Patre *et al.*, 2006; Pedroza, MacKunis and Golubev, 2014; Shao *et al.*, 2018; Su, Xie and Li, 2019) to dominate the limitations and yield asymptotic tracking errors.

The authors of (Mustafa, Hamarash and Crane, 2020), propose two nonlinear control approaches to control the position/displacement of robot manipulators in the presence of disturbance torques due to vibration and payload variation. In both proposed approaches the tracking error approaches zero or a region around zero. However, the estimation of the parameters is not considered while control design which decreases the control effort at the cost of accuracy. In this paper, we present an adaptive-sliding mode approach for trajectory tracking control of robot manipulators. The approach deals with the uncertainty in the dynamics and reject the disturbance of vibration and payload variation. The unknown parameters in the dynamics are estimated by using the adaptation law of the known parameters. Then, the disturbances are rejected separately by sliding mode control. The same disturbances that are formed for the first approach in (Mustafa, Hamarash and Crane, 2020) are called in this work to test the designed controller.

The paper is organized as follows: Section 2 introduces the dedicated dynamic model of the robot and preliminaries. In Section 3, the problem is formulated, and the controller is analyzed and designed. Simulation results are presented and analyzed is Section 4. The conclusions are given in Section 5.

2. THE DEDICATED DYNAMIC MODEL AND PRELIMINARIES

By considering uncertain disturbance torques caused by external vibration and payload variation, the dedicated dynamics for an n-degree-of-freedom, revolute-joints robot arm in joint-space coordinates is expressed as follows:

$$M(q)\ddot{q} + V_m(q,\dot{q})\dot{q} + G(q) = \tau - \tau_v - \tau_l \qquad (1)$$

where q, $\dot{q}$, and $\ddot{q} \in \mathfrak{R}^n$ denote the angular displacement, angular velocity, and angular acceleration vectors, respectively; $M(q) \in \mathfrak{R}^{n\times n}$ represents the inertia matrix; $V_m \in \mathfrak{R}^{n\times n}$ represents the Coriolis-centripetal matrix; $G(q) \in \mathfrak{R}^n$ represents the gravity vector; $\tau \in \mathfrak{R}^n$ represents the torque input of the joints; $\tau_v \in \mathfrak{R}^n$ represents the disturbance due to external vibration; and $\tau_l \in \mathfrak{R}^n$ represents the payload variation torque.

For the subsequent controller design and analysis, we list the following property and assumption for the dynamics in Eq. (1) (Dixon *et al.*, 2013):

Property 1. The Coriolis and centrifugal matrix $V_m(q,\dot{q})$ can be appropriately determined such that

$$\chi^T \left(\dot{M}(q) - 2V_m(q,\dot{q})\right)\chi = 0\,, \quad \forall \chi \in \mathfrak{R}^{\mathrm{n}} \tag{2}$$

where $\dot{M}(q)$ is the derivative of the inertia matrix.

Assumption 1. Effects of the friction in the robot dynamics are neglected because it is out of the scope of this work.

3. PROBLEM FORMULATION AND CONTROL DESIGN

In this section the tracking control problem of robot manipulator is formulated in the presence of external vibration and payload variation. An auxiliary term is defined, and two assumptions are introduced regarding the properties of the position, velocity, and acceleration of the robot links. The auxiliary term and the assumptions are considered in the analysis and control design.

3.1. Problem Formulation

Robot manipulators are required to perform their tasks regardless the uncertainty in the dynamics and external disturbance, such as vibration and payload variation. Since the robot manipulator performs tasks by its end effector, we need to command the end-effector to a target point or following a desired trajectory within the workspace. An inverse kinematics process can be computed to obtain the joint-space trajectories (Crane III and Duffy, 2008; Hasan and Hamarash, 2017; Hasan, Crane III and Hamarash, 2019). For this manner, we need to design the input torque τ in Eq. (1), which drives the robot's links. In other words, the objective is to design the joint's input torque τ that the angular position q follows the desired position q_d accurately (i.e., $(q_d - q) \to 0$ as $t \to \infty$, where t denotes the time) even if there are uncertainty in the dynamics, vibration disturbance τ_v, and payload variation τ_l.

In order to design the controller by following Lyapunov analysis, we define the term (Slotine, Li and others, 1991):

$$\eta =: \Delta\dot{q} + \sigma\Delta q \tag{3}$$

where $\eta \in \mathfrak{R}^{\mathrm{n}}$ is a filtered signal of Δq; $\sigma \in \mathfrak{R}^{\mathrm{n}\times\mathrm{n}}$ is a positive definite diagonal gain matrix; Δq is the position error.

Assumption 2. The desired link position q_d is known; the current position and velocity q and $\dot{q}$ are measurable due using of an encoder. This also makes η, Δq, and $\Delta\dot{q}$ measurable.

Assumption 3. The acceleration $\ddot{q}$ is not measurable, because measuring the acceleration requires differentiating the velocity which produces noise.

3.2. Analysis and Control Design

For the design purpose that fulfills our objective, we define the following Lyapunov function candidate

$$V := \frac{1}{2}\eta^T M(q)\eta + \frac{1}{2}\tilde{\phi}^T \Lambda^{-1}\tilde{\phi} \tag{4}$$

where $V \in \mathfrak{R}$; $\tilde{\phi}$ is subsequent term that will be defined later; $\Lambda \in \mathfrak{R}^{n\times n}$ is a diagonal matrix. Taking the time derivative of Eq. (4) gives

$$\dot{V} = \frac{1}{2}\dot{\eta}^T M(q)\eta + \frac{1}{2}\eta^T \dot{M}(q)\eta + \frac{1}{2}\eta^T M(q)\dot{\eta} + \frac{1}{2}\dot{\tilde{\phi}}^T\Lambda^{-1}\tilde{\phi} + \frac{1}{2}\tilde{\phi}^T\Lambda^{-1}\dot{\tilde{\phi}}. \tag{5}$$

Since all parts in the above equation are scalar quantities, we can take the transpose of $\frac{1}{2}\dot{\eta}^T M(q)\eta$ and $\frac{1}{2}\dot{\tilde{\phi}}^T\Lambda^{-1}\tilde{\phi}$ which simplifies Eq. (5) to be

$$\dot{V} = \frac{1}{2}\eta^T\dot{M}(q)\eta + \eta^T M(q)\dot{\eta} + \tilde{\phi}^T\Lambda^{-1}\dot{\tilde{\phi}}. \tag{6}$$

Utilizing the term $M(q)\dot{\eta}$ in Eq. (6), we take the derivative of (3) and multiply it by $M(q)$ to obtain

$$M(q)\dot{\eta} = M(q)\Delta\ddot{q} + \sigma M(q)\Delta\dot{q}. \tag{7}$$

Equation (7) can be extended by substituting $\Delta\ddot{q} = \ddot{q}_d - \ddot{q}$ to obtain

$$M(q)\dot{\eta} = M(q)\ddot{q}_d - M(q)\ddot{q} + \sigma M(q)\Delta\dot{q}. \tag{8}$$

Using $M(q)\ddot{q} = \tau - \tau_v - \tau_l - V_m(q,\dot{q})\dot{q} - G(q)$ from Eq. (1), we can write Eq. (8) as

$$M(q)\dot{\eta} = M(q)\ddot{q}_d - \tau + \tau_v + \tau_l + V_m(q,\dot{q})\dot{q} + G(q) + \sigma M(q)\Delta\dot{q}. \tag{9}$$

Since $\dot{q} = \dot{q}_d - \Delta\dot{q}$ and $\Delta\dot{q} = \eta - \sigma\Delta q$, we will replace $\dot{q}$ so we rewrite Eq. (9) as

$$M(q)\dot{\eta} = M(q)\ddot{q}_d - \tau + \tau_v + \tau_l + V_m(q,\dot{q})[\dot{q}_d - \eta + \sigma\Delta q] + G(q) + \sigma M(q)\Delta\dot{q}. \quad (10)$$

We define

$$Y\phi := V_m(q,\dot{q})\dot{q}_d + V_m(q,\dot{q})\sigma\Delta q + \sigma M(q)\Delta\dot{q} + G(q) + M(q)\ddot{q}_d \quad (11)$$

where $Y \in \mathfrak{R}^{n\times m}$ is the regression matrix that has the states of the system which are linear in the parameters; $\phi \in \mathfrak{R}^{n}$ is the parameters vector which has unknown positive constants. Substituting (11) into (10) yields

$$M(q)\dot{\eta} = Y\phi - V_m(q,\dot{q})\eta - \tau + \tau_v + \tau_l. \quad (12)$$

To design the control input τ we utilize Eq. (12) which is the open loop error system. First, we use the certainty equivalence approach to deal with the term $Y\phi$. Second, we use two gain matrices to deal with both error in the system and the disturbance torques. Since it is possible to inject measurable terms in the input torque, input torque τ is designed as following

$$\tau = Y\hat{\phi} + K_1\eta + K_2 sgn(\eta) \quad (13)$$

where $\hat{\phi}$ is the estimate of the unknown parameter in the system; K_1, and K_2 are positive diagonal gain matrices; $sgn(\eta)$ is the signum function that is defined as

$$sgn(\eta) := \begin{cases} -1, & \eta < 0 \\ 0, & \eta = 0 \\ 1, & \eta > 0. \end{cases}$$

The estimate of the unknown parameters $\hat{\phi}$ means that we do not exactly know ϕ, we just know an approximation of it. By substituting (13) into (12) we get

$$M(q)\dot{\eta} = Y\tilde{\phi} - V_m(q,\dot{q})\eta - K_1 - K_2 sgn(\eta) + \tau_v + \tau_l \quad (14)$$

where $\tilde{\phi} = \phi - \hat{\phi}$ is the mismatch between the actual and the estimated parameters.

Now in order to investigate the validity of the designed input torque τ in (13), we substitute (14) into (6) that gives

$$\dot{V} = \frac{1}{2}\eta^T\dot{M}(q)\eta - \eta^T V_m(q,\dot{q})\eta + \eta^T[Y\tilde{\phi} - K_1\eta - K_2 sgn(\eta) + \tau_v + \tau_l] + \tilde{\phi}^T\Lambda^{-1}\dot{\tilde{\phi}}. \quad (15)$$

By calling Property 1, we can write Eq. (15) as

$$\dot{V} = \eta^T[Y\tilde{\phi} - K_1\eta - K_2 sgn(\eta) + \tau_v + \tau_l] + \tilde{\phi}^T\Lambda^{-1}\dot{\tilde{\phi}}. \quad (16)$$

Since $\tilde{\phi} = \phi - \hat{\phi}$ and ϕ is constant, $\dot{\tilde{\phi}} = -\dot{\hat{\phi}}$. Therefore, we replace $\dot{\tilde{\phi}}$ with $-\dot{\hat{\phi}}$ in Eq. (16) so it is written as

$$\dot{V} = \eta^T\left[Y\tilde{\phi} - K_1\eta - K_2 sgn(\eta) + \tau_v + \tau_l\right] - \tilde{\phi}^T\Lambda^{-1}\dot{\hat{\phi}}. \quad (17)$$

Now, we design the estimate parameter $\dot{\hat{\phi}} = \Lambda Y^T\eta$. By taking the transpose of the term $Y\eta^T\tilde{\phi}$ in (17) and substituting the designed $\dot{\hat{\phi}}$ in the same equation, it gives

$$\dot{V} = -\eta^T K_1\eta - \eta^T K_2 sgn(\eta) + \eta^T(\tau_v + \tau_l). \quad (18)$$

If we upper bound the norm of the disturbances $||\tau_v + \tau_l||$ by a constant c, and we pick the elements of K_2 to be bigger than the constant c so it can dominant it, the derivative of the Lyapunov function $\dot{V}$ in (18) can be upper bounded as follows

$$\dot{V} \le -K_1||\eta||^2. \quad (19)$$

The above result makes the derivative of the Lyapunov function a negative semi-definite function. Therefore, we apply theorem 8.4 in (Khalil, 2002) and conclude that $\eta \to 0$ as $t \to \infty$. Additionally, since the error Δq is a low pass filter of η, this means that what happens to η happens to the error Δq. Eventually, we conclude that the error Δq approaches zero as time goes to infinity.

4. ROBOT MODEL FORMULATION AND SIMULATION RESULTS

In this section, the results of the simulation verification and validation of the proposed control approach are reported. Therefore, a two-link robot manipulator is formulated, two disturbance signals are generated to represent the vibration and payload variation torques, and the proposed controller is applied. The robot model, disturbances, and the proposed controller are simulated in MATLAB-SIMULINK as shown in Figure 1.

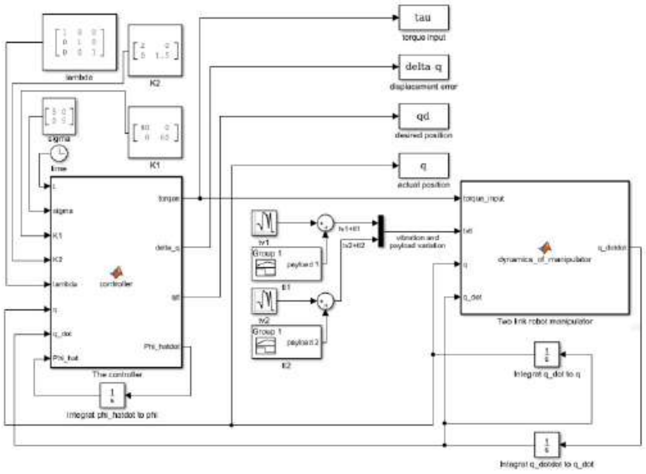

Figure 1: Simulation diagram of the control design and the robot dynamics

Each block contains a function that is built according to the mathematical analysis in the previous section. Table 1 presents the physical parameters of the two-link robot manipulator.

Table (1) Physical parameters of the two-link manipulator

Symbol	Description	Value	Unit
$\boldsymbol{m_1}$	Mass of link 1	0.5	kg
$\boldsymbol{m_2}$	Mass of link 2	0.4	kg
$\boldsymbol{l_1}$	Length of link 1	0.6	M
$\boldsymbol{l_2}$	Length of link 2	0.5	M

Each link is modelled as a uniform rectangular bar. We use Eq. (1) to represent the dynamics of the robot as follows:

$$\begin{bmatrix} M_{11} & M_{12} \\ M_{21} & M_{22} \end{bmatrix}\begin{bmatrix} \ddot{q}_1 \\ \ddot{q}_2 \end{bmatrix} + \begin{bmatrix} V_1 \\ V_2 \end{bmatrix} + \begin{bmatrix} G_1 \\ G_2 \end{bmatrix} = \begin{bmatrix} \tau_1 \\ \tau_2 \end{bmatrix} - \begin{bmatrix} \tau_{v1} \\ \tau_{v2} \end{bmatrix} - \begin{bmatrix} \tau_{l1} \\ \tau_{l2} \end{bmatrix} \tag{20}$$

Where

$$M_{11} = (m_1 + m_2)l_1^2 + m_2 l_2^2 + 2m_2 l_1 l_2 \cos(q_1)$$

$$M_{12} = m_2 l_2^2 + m_2 l_1 l_2 \cos(q_2)$$

$$M_{21} = m_2 l_2^2 + 2m_2 l_1 l_2 \cos(q_2)$$

$$M_{22} = m_2 l_2^2$$

$$V_1 = -m_2 l_1 l_2 (2\dot{q}_1 \dot{q}_2 + \dot{q}_2^2)\sin(q_2)$$

$$V_2 = m_2 l_1 l_2 \dot{q}_1^2 \sin(q_2)$$

$$G_1 = (m_1 + m_2) g l_1 \cos(q_1) + m_2 g l_2 \cos(q_1 + q_2)$$

$$G_2 = m_2 g l_2 \cos(q_1 + q_2)$$

and the Earth gravity constant $g = 9.807\, m/s^2$. The disturbance torques τ_v and τ_l will be presented subsequently. All of the above equations are written in the block that is representing the dynamics of the manipulator in Figure 1.

The desired positions for both links are set as follows:

$$\begin{bmatrix} q_{d1} \\ q_{d2} \end{bmatrix} = \begin{bmatrix} 114.95^{\circ}\sin(1.5t)e^{-0.03} \\ 85.94^{\circ}\cos(2t)e^{-0.03} \end{bmatrix} \tag{21}$$

and their initial conditions are:

$$\begin{bmatrix} q_{d1}(0) \\ q_{d2}(0) \end{bmatrix} = \begin{bmatrix} 0 \\ 85.94^{\circ} \end{bmatrix}. \tag{22}$$

The disturbance signals are formed to match the mentioned assumptions. Therefore, the disturbance torque of vibration $[\tau_{v1} \quad \tau_{v2}]^T$ is composed by a bounded Gaussian noise. Therefore, we set a mean value = $[0 \quad 0]^T$, a variance = $[0.01 \quad 0.015]^T$, and a sampling time $0.01s$.

The disturbance torques of the payload variation for both links are represented respectively as follows:

$$\tau_{l1} = \begin{cases} 0.65\text{ Nm}, & 4\,s \le t \le 8\,s \\ 0.15\text{ Nm}, & 8\,s \le t \le 10\,s \\ 0, & \text{otherwise} \end{cases}$$

$$\tau_{l2} = \begin{cases} 0.75\text{ Nm}, & 4\,s \le t \le 8\,s \\ 0.25\text{ Nm}, & 8\,s \le t \le 10\,s \\ 0, & \text{otherwise.} \end{cases}$$

These signals are represented separately as shown in block diagram in Figure 2.

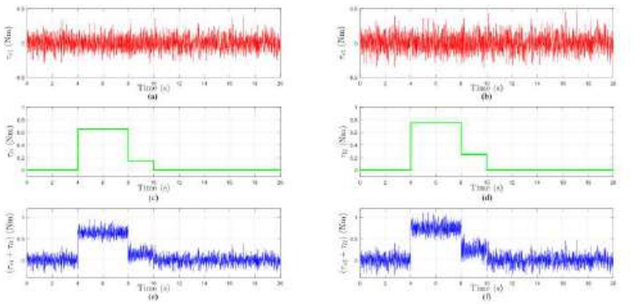

Figure 2: Disturbance torques due to vibration and payload variation: (a) and (b) vibration effect; (c) and (d) payload variation effect; (e) and (f) effect of combination on link 1 and link 2, respectively.

Also, the disturbances' effect on the first and second links is shown in the same figure. The bounds of these disturbances are:

$$\begin{bmatrix}-0.2873\\-0.3518\end{bmatrix} \leq \begin{bmatrix}\tau_{v1}+\tau_{l1}\\\tau_{v2}+\tau_{l2}\end{bmatrix} \leq \begin{bmatrix}0.9446\\1.1108\end{bmatrix}$$

The controller, that is derived analytically, and the desired trajectories are written in the controller block in Figure 1. All control gains are chosen to yield the best performance using trial and error method. Therefore, the control gains for the proposed control design are selected as $K_1 = diag[80 \quad 60]$, $K_2 = diag[2 \quad 1.5]$, $\sigma = diag[5 \quad 5]$, and $\Lambda = diag[1 \ 1 \ 1\,]$. The input torques of the proposed controller is shown in Figure 3.

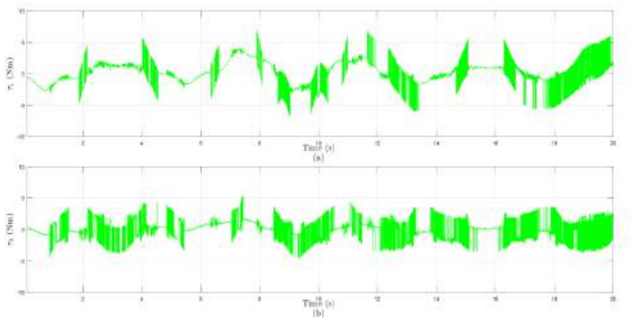

Figure 3: Torque inputs of the proposed controller: (a) joint 1 (b) joint 2.

The input torque values for both joints have high oscillations with respect to time, however, these oscillations are not beyond the classical bandwidth limit of the actuators which are driving the robot links. However, the law values of input torque are relatively law compared with other approaches from the literature. Therefore, these input torque can be implemented at low cost and they do not saturate the actuators which are driving the robot links.

The proposed controller performance is shown in Figure 4.

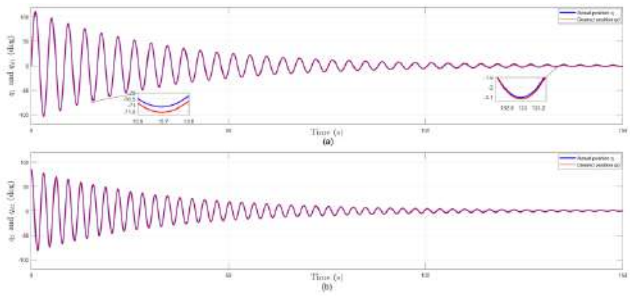

Figure 4: Tracking performance of the proposed control approach: (a) and (b) desired and actual position of link 1 and link 2, respectively;

This figure depicts the robot actual angular displacements q_1 and q_2 with respect to time, and their desired references q_{d1} and q_{d2}, respectively. We notice that the errors Δq_1 and Δq_2 approach zero as time passes as shown in Figure 5.

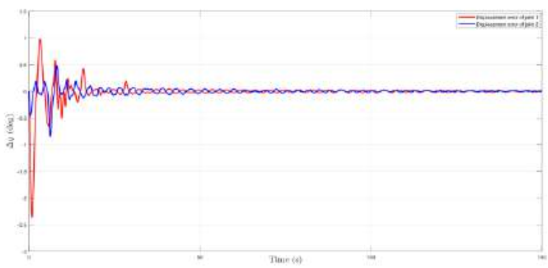

Figure 5: Angular displacement error of link 1 and link 2.

To provide further explanation and validate the performance of the proposed controller, we use the following statistical indices for the angular displacement error and the input torque:

1. Maximum absolute values of the displacement error for each link.

$$\Delta q_{imax} = \max_{j=1,..,M}(|\Delta q_i(j)|) \qquad (23)$$

2. Root mean square rms values of the displacement error and input torque for each link and joint, respectively.

$$\Delta q_{irms} = \sqrt{\frac{1}{M}\sum_{j=1}^{M}||\Delta q_i(j)||^2} \qquad (24)$$

$$\tau_{irms} = \sqrt{\frac{1}{M}\sum_{j=1}^{M} ||\tau_i(j)||^2} \qquad (25)$$

where i is the link/joint number and M is the number of sampling steps of the simulation. Table 2 presents the indices in (23), (24), and (25) for both links/joints obtained from Figure 3 and Figure 4.

Table (2) Performance summary for the proposed controller

Indexes	First link/joint	Second link/joint
$\boldsymbol{\Delta q_{max}}$**(deg)**	0.9756	0.4804
$\boldsymbol{\Delta q_{irms}}$**(deg)**	0.1199	0.0385
$\boldsymbol{\tau_{irms}}$**(Nm)**	1.8105	1.6727

According to the physical parameters of the robot in Table 1, the external disturbances, and the obtained results in Table 2, we see that the proposed controller is implementable, efficient, and accurate. Moreover, the time for evaluating control actions of the proposed controller is presented in Table 3.

Table (3) Performance of the proposed controller in terms of computation time

No. of calls	Time/Call (ms)	Total time (s)
344013	0.0062	2.14

The oscillation of the input torques with settling time for both links are presented in Table 4.

Table (4) Oscillation and settling time of the input torques

Link/joint order	Maximum oscillation ($\mathbf{kH_z}$)	Settling time (s)
First	1.01	15.2
Second	0.98	13.5

As presented, the settling time is high; however, the amplitude of the error is not significant; therefore, it does not affect the performance and stability of the system. Furthermore, the input torques oscillation are not beyond the classical bandwidth limits of the actuators.

5. Conclusion

In this paper, we present an adaptive-sliding mode approach for position control of robot manipulators, in joint space, in the presence of uncertain torques due to vibration and payload variation. Firstly, the problem of tracking control for an n-degree-of-freedom, revolute-joints, serial robot arm is formulated. Secondly, the controller is designed based on the Lyapunov analysis and following the adaptive and sliding mode control approach. The rms values of the error are 0.119 deg and 0.03 deg for link 1 and link 2, respectively. Which means, despite the uncertainty that is caused by the uncertain dynamics, vibration, and payload variation, the controller is shown to guarantee asymptotic tracking displacement errors. Additionally, the input torque rms values are 1.81 Nm and 1.67 Nm for joint 1 and joint 2, respectively. These values are relatively law compared with other approaches from the literature despite the high oscillation. This makes the controller implementable at low cost and reasonable control effort.

Acknowledgements

This study was supported by Salahaddin University-Erbil, Iraq, and the University of Florida, FL, USA, in the Framework of a split-side Ph.D. program.

Conflict of Interest

The authors declare no conflict of interest.

References

Cai, Z., de Queiroz, M. S. and Dawson, D. M. (2006) ‘Robust adaptive asymptotic tracking of nonlinear systems with additive disturbance’, IEEE Transactions on Automatic Control. IEEE, 51(3), pp. 524–529.

Craig, J. J., Hsu, P. and Sastry, S. S. (1987) ‘Adaptive control of mechanical manipulators’, The International Journal of Robotics Research. Sage Publications Sage UK: London, England, 6(2), pp. 16–28.

Crane III, C. D. and Duffy, J. (2008) Kinematic analysis of robot manipulators. Cambridge University Press.

Dawson, D. M. et al. (1990) ‘Robust control for the tracking of robot motion’, International Journal of Control. Taylor & Francis, 52(3), pp. 581–595.

Dixon, W. E. et al. (2013) Nonlinear control of engineering systems: a Lyapunov-based approach. Springer Science & Business Media.

Dixon, W. E., Zergeroglu, E. and Dawson, D. M. (2004) 'Global robust output feedback tracking control of robot manipulators', Robotica. Cambridge University Press, 22(4), pp. 351–357.

Economou, D. et al. (2000) 'Robust vibration suppression in flexible payloads carried by robot manipulators using digital filtering of joint trajectories', in Intl. Symposium on Robotics and Automation, pp. 244–249.

Feliu, V. et al. (2013) 'A Robust Controller for A 3-DOF Flexible Robot with a Time Variant Payload', Asian Journal of Control. Wiley Online Library, 15(4), pp. 971–987.

Gao, H. et al. (2018) 'Neural network control of a two-link flexible robotic manipulator using assumed mode method', IEEE Transactions on Industrial Informatics. IEEE, 15(2), pp. 755–765.

Hasan, D. S., Crane III, C. and Hamarash, I. I. (2019) 'Using Inertia Sensors for Orientation Estimation of Robot Manipulators', ZANCO Journal of Pure and Applied Sciences, 31(s3), pp. 318–323.

Hasan, D. S. and Hamarash, I. (2017) 'Real time data acquire from multiple Accelerometers and IMU to calculate 3-direction angles and relative orientation', ZANCO Journal of Pure and Applied Sciences, 29(2).

Hsia, T. C. and Gao, L. S. (1990) 'Robot manipulator control using decentralized linear time-invariant time-delayed joint controllers', in Proceedings., IEEE International Conference on Robotics and Automation, pp. 2070–2075.

Hsia, T. C. S., Lasky, T. A. and Guo, Z. (1991) 'Robust independent joint controller design for industrial robot manipulators', IEEE transactions on industrial electronics. IEEE, 38(1), pp. 21–25.

Khalil, H. K. (2002) Nonlinear Systems. Prentice Hall.

Mamani, G., Becedas, J. and Feliu, V. (2012) 'Sliding mode tracking control of a very lightweight single-link flexible robot robust to payload changes and motor friction', Journal of Vibration and Control. Sage Publications Sage UK: London, England, 18(8), pp. 1141–1155.

Mustafa, M. M., Hamarash, I. and Crane, C. D. (2020) 'Dedicated Nonlinear Control of Robot Manipulators in the Presence of External Vibration and Uncertain Payload', Robotics, 9(1). doi: 10.3390/robotics9010002.

Nafia, N. et al. (2018) 'Robust interval type-2 fuzzy sliding mode control design for robot manipulators', Robotics. Multidisciplinary Digital Publishing Institute, 7(3), p. 40.

Patre, P. M. et al. (2006) 'Asymptotic tracking for systems with structured and unstructured uncertainties', in Proceedings of the 45th IEEE Conference on Decision and Control, pp. 441–446.

Pedroza, N., MacKunis, W. and Golubev, V. (2014) 'Robust nonlinear regulation of limit cycle oscillations in uavs using synthetic jet actuators', Robotics. Multidisciplinary Digital Publishing Institute, 3(4), pp. 330–348.

Shao, X. et al. (2018) 'RISE and disturbance compensation based trajectory tracking control for a quadrotor UAV without velocity measurements', Aerospace Science and Technology. Elsevier, 74, pp. 145–159.

Slotine, J.-J. E. and Li, W. (1987) 'On the adaptive control of robot manipulators', The international journal of robotics research. Sage Publications Sage CA: Thousand Oaks, CA, 6(3), pp. 49–59.

Slotine, J.-J. E., Li, W. and others (1991) Applied nonlinear control. Prentice hall Englewood Cliffs, NJ.

Spong, M. W. (1992) 'On the robust control of robot manipulators', IEEE Transactions on automatic control. IEEE, 37(11), pp. 1782–1786.

Su, Z., Xie, M. and Li, C. (2019) 'RISE based active vibration control for the flexible refueling hose', Aerospace Science and Technology. Elsevier.

ZANCO Journal of Pure and Applied Sciences
The official scientific journal of Salahaddin University-Erbil
https://zancojournals.su.edu.krd/index.php/JPAS

ISSN (print):2218-0230**, ISSN (online):** 2412-3986**, DOI: http://dx.doi.org/10.21271/zjpas**

RESEARCH PAPER

Structural Response of AISC- composite concrete filled circular steel Columns under Lateral Load

Sinan Abdulkhaleq Yaseen[1], Muhammed Ali Ihsan Saber[2] and Bayan Salim Al-Numan[3]

[1,2] Department of Civil Engineering, College of Engineering, Salahaddin University-Erbil, Kurdistan Region, Iraq
[3] Civil Engineering Department, Tishk International University

A B S T R A C T:

In this article, there is a theoretical behavior research of composite frames consist of American Institute of Steel Construction (AISC)-composite pipes-filled with concrete to act as circular steel columns joined with steel beams subjected to unchanged axial loads and a lateral increasing load. The effects of column height and skin thickness, based on those available in the AISC manual, on the load-deformation reaction of composite frames, including steel tubes filled with concrete STFC, loaded by maximum vertical load allowed by AISC manual, were studied. A ANSYS program was used to develop a finite element (FE) model. This simulation considers linear and non-linear response of the composite materials. The obtained outcomes from the FE analysis were presented and discussed. Over the range of column heights (from 3048 mm to 6096 mm), no buckling has been reached and failure modes were observed after formation of plastic hinges at the connection of beam-column. For skin thicknesses (from 14.76 mm to 5.92 mm), varied load-deformation responses have been obtained. Stiffer Responses were obtained for skin thickness 14.76 mm. Lateral load range at failure was from 9.2 to 20.8 % of the maximum AISC vertical load, and displacement ductility was ranged from 1.71 to 3.08 for circular-STFC frames.

KEY WORDS: Composite frames; steel tubes filled with concrete; finite element modelling
DOI: http://dx.doi.org/10.21271/ZJPAS.32.4.4
ZJPAS (2020) , 32(4);30-37 .

1. INTRODUCTION:

Due to high strength, stiffness and ductility of steel tubes filled with concrete STFC, they are used in buildings to carry lateral static/dynamic forces. Many research works were published for the analysis of STFC investigating the most effective parameters on their structural behavior. Shams (Shams & Saadeghvaziri ,1997) published on safety factors for short tubular STFC. Zhao et al (Zhao & Grzebieta, 1999) published a research on SHS filled beams under cyclic loading. Schneider (Schneider, 1998) developed a nonlinear 3D finite element models for STFC elements by ABAQUS program.

* **Corresponding Author:**
Sinan Abdulkhaleq Yaseen
E-mail: sinan.yaseen@su.edu.krd
Article History:
Received:19/12/2019
Accepted: 19/02/2020
Published: 08/09 /2020

Hu et al [Hu et al., 2003) used ABAQUS for circular section, square section, and square section stiffened by reinforcing ties to develop FE nonlinear model to investigate the behavior of STFC. Numerical trial-and-error method was used to capture concrete properties to fit the analysis to experimental results. Han et al (Han et al., 2007) used ABAQUS for modelling STFC that loaded by uniaxial compression for confined core concrete of STFC. Lin-Hai et al (Lin-Hai et al., 2008) used ABAQUS to model STFC framed to steel beams. FE modelling was developed to analyze the frame under cyclic loading. Analysis was verified by 6 tested frames. Lin-Hai et al (Lin-Hai et al.2011) studied on the behavior of composite frames with steel tubes filled with concrete (STFC) columns joined with steel beam under unchanged axial load on the

STFC columns with laterally subjected cyclic load. From the analysis, a simplified lateral hysteretic load versus lateral deformation model. Fa-xing et al. studied composite frame consists of STFC circular column joined with steel- concrete beam under subjected to cyclic lateral loading (Fa-xing et al., 2018). The obtained outcomes from the modeling of FE were in shows very close agreement while comparing with experimental data in terms of modes of failure, load-displacement response curves, and skeleton curves.

The behavior investigation is the main objective of this work to see the behavior of STFC framed to steel sectioned beam and loaded to maximum load allowed by AISC steel manual (AISC, 2005), and subjected to an increasing lateral load. A FE modelling using ANSYS program (ANSYS, 2016) was developed to analyze the frame. The AISC design parameters, namely height-to-size L/D with size-to-thickness of the section skin D/t ratios of STFC, are investigated. The aim of the research is to study the effects of column height and skin thickness, based on those available in the AISC manual, on the load-deformation reaction of composite frames, including steel tubes filled with concrete STFC, loaded by maximum vertical load allowed by AISC manual

2. Composite Frames Used in the FE Analysis

Table (1) shows details of nine STFC connected to steel beam. The used material properties were the strength of concrete (28 MPa) and the yield strength of steel (290 MPa). Fig. (1) Shows views of the composite frame with a close view of the connection of beam with columns, and column with base plate connection. The beam has total span of (4775 mm) with standard section specification of (W12x106), (AISC, 2005).

Table (1) Details of the STFC Frame.

Frame	fc MPa	Fy MPa	Outer Dia.(mm)	Skin Thick. (mm)	D/t	Effective Height (mm)	L/D	Vertical load per (ASD) (No) kN
L10-t1	28	290	254	14.76	17.21	3048	12	1939
L10-t2	28	290	254	8.86	28.65	3048	12	1428
L10-t3	28	290	254	5.92	42.92	3048	12	1152
L15-t1	28	290	254	14.76	17.21	4572	18	1753
L15-t2	28	290	254	8.86	28.65	4572	18	1272
L15-t3	28	290	254	5.92	42.92	4572	18	1023
L20-t1	28	290	254	14.76	17.21	6096	24	1481
L20-t2	28	290	254	8.86	28.65	6096	24	1085
L20-t3	28	290	254	5.92	42.92	6096	24	863

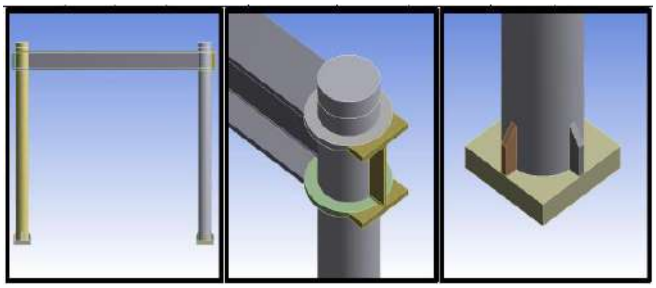

Figure 1: Typical composite frame.

3. Modelling

FE modelling using ANSYS was carried out. The element modeling of circular steel shell, stiffening ribs and steel beams were constructed according to solid 186 element. While solid 185 element was used for modeling A (50.0) mm thick steel base plate, which was added at the fixed support locations for the STFC in order to prevent any problems caused by stress concentration. This plate more range in stress distribution that applied on supports. Each finite element has eight nodes, the number of degree of freedom are three for three main directions in each node. To represent concrete material for in the FE simulation, soild 65 element was used. Like the previous element definition, each finite element has eight nodes, the number of degree of freedom are three for three main directions in each node. The mentioned elements have of plastic deformation, cracking, and crushing ability in three directions. The mesh sizes were changed to reach to the full fit one in terms of results stability and consuming elapsed time. The chosen meshes that used for composite simulated frames are shown in Fig. (2) (Yaseen, 2020). The friction coefficient between the interface of steel shell and core concrete was taken to be 0.35 (Lin-Hai, 2011). while the elastic modulus and Poisson’s ratio for concrete material were 25.0 GPa and 0.2, respectively, for all studied models. The ANSYS program allow a bilinear or multi linear steel stress-strain curves, the modulus of elasticity and Poisson’s ratio for elastic stage up to proportional limit were 210 GPa, and Poisson’s ratio of 0.3.

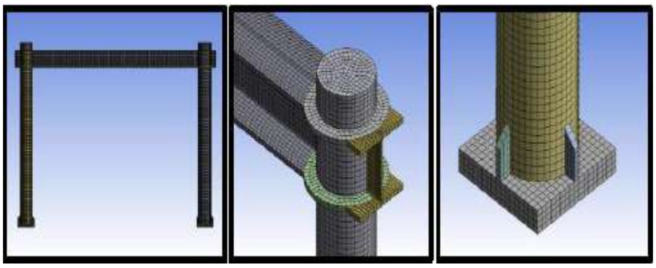

Figure 2: Mesh distribution for the composite frame.

3.1. Material Properties

The properties of the STFC frame material are defined as follows:

3.1.1. Concrete

The construction of these types of element is obstacle to make a real represented member in behavior point of view, by having a quasi-brittle property and changing behavior by concrete in both compression and tension. Normal weight Concrete obeys atypical stress-strain relation curve (Bangash, 1989) when as the strength range defined to be 28 MPa as shown in Fig. (3). The load deformation response in compression for concrete from linearly elastic range up to 40% when exceed the stress of maximum limits. A gradual increase incrememnt it seen in the merge of maximum limit point σ_{cu} , starting to descend into a softening region, and eventually crushing failure modes occurs when reaching the ultimate strain limits ε_{cu}. The material load deflection response behave to be linear elastic to maximum limits in tensile strength in tension, occurring cracks start after that to decrease the carrying capacity gradually to zero (Bangash, 1989). However, using this ideal relation curve work as a negative slope portion was not preferred in defining finite element materials which lead to convergence problems.

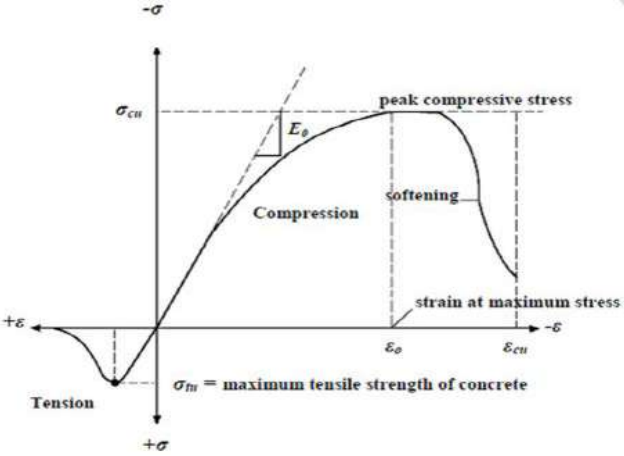

Figure 3: Typical Uniaxial Compressive and Tensile Stress-Strain Curve for Concrete (Bangash , 1989).

The uniaxial stress-strain relationship is required in defining concrete material in ANSYS program in compression. To consider a uniaxial compressive stress-strain in construction the concrete response curve, some numerical equations that used by (Desayi & Krishnan, 1964), Equations (1) and (2), were used that work with all strength range along with Equation (3) (Bangash, 1989).

$$f = \frac{E_c\,\varepsilon}{1+\left(\frac{\varepsilon}{\varepsilon_o}\right)^2} \qquad (1)$$

$$\varepsilon_o = \frac{2f_c'}{E_c} \qquad (2)$$

$$E_c = \frac{f}{\varepsilon} \qquad (3)$$

$f = Stress\ at\ any\ strain\ \varepsilon$
$\varepsilon = Strain\ at\ stress\ f$
$\varepsilon_o = Strain\ at\ the\ ultimate\ compressive\ strength\ f_c'$

A compressive uniaxial stress-strain relationship is simplified and shown as in Fig. (4), which is for each STFC model to constructed well consist six points connected by straight lines. The linear stage was up (0.30*f'*c) of the curve that starts from at zero stress and strain to be point No.1engaging equation (3). While equation (1) employing modulus of elasticity, initial strain, and strains for stress evaluation in all points No. 2, 3, and 4, the initial strain ε_0 is calculated from Equation (2) by using concrete compressive strength and the modulus of elasticity. In the fifth point an assumption was made of perfectly plastic behavior at ε_0 and *f'*c to be point 5.

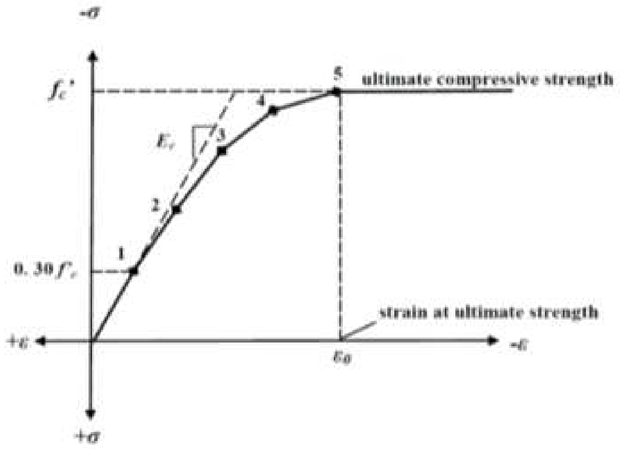

Figure 4: Simplified compressive uniaxial stress-stain curve for concrete (Desayi and Krishnan, 1964).

3.1.2. Steel Tube Column and Base Plates

An actual stress strain response curve is the outcome from tensile tests, which used to be a tensile stress-strain curve in defining steel properties in the finite element model. However, to removing the negative slope portion of the curve from this stress-strain curve, the response was modified to gain the more convergence in finite element model, and a modification performed in zero slop part after yield to a mild positive slope.

3.2. Verification of the FE Model

The experimental data results used for comparison with the FE model as a validity verification. The element column beam connection STFC in composite frames tested by Lin-Hai Hana et al. are used in this paper to verify the proposed FE model using ANSYS program. For frame (CF-13) (Lin-Hai, 2011), with circular STFC columns, the basic information is;

1.45m was clear frame column height with 2.5m beam span. The used column tube size was 140mm in diameter and 2mm thickness. The beam's section dimensions are; 140mm depth, 65mm flange width, 3.44mm flange thickness, and 3.44 web thickness. The mechanical properties are presented in table (2) for the beam and STFC column element. The result data of verification analysis are given in table (3), Fig. (5) Shows the deflected shape of the frame under FE model analysis using ANSYS program. Figs (6) to (8) show the maximum principal stresses at the regions of frame connections.

The comparison shows that high accuracy has been achieved for the FE model using ANSYS program in predicting the load-displacement relationship of the composite frames.

Table 2. the material properties of the steel STFC frame [7].

Element	Yielding Strength f_y (N/mm²)	Ultimate Strength f_u (N/mm²)	Modulus of Elasticity E_s (N/mm²)	Poisson`s Ratio *v*
STFC Column	327.7	397.9	2.063×10^5	0.266
Steel Beam	303.0	440.9	2.061×10^5	0.262

Table 3. the verified theoretical and the experimental results.

Item	The experimental[7]	The theoretical FE model results	Theor./Exp. %
Axial Load of STFC Column (kN)(Constant)	410	410	100
Ultimate Lateral Load (kN)(Ultimate Frame Capacity)	55.25	55.6	101
Lateral Displacement of the frame at yield (mm)	12.5	12.46	101

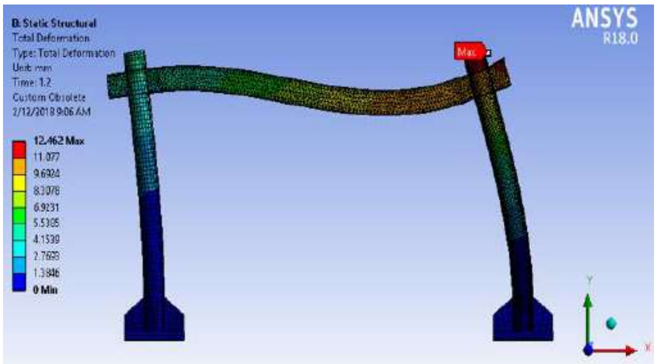

Figure 5: The deflected shape of the Lin-Hai Hana et al. frame under FE model analysis for verification using ANSYS program(Lin-Hai et al., 2008).

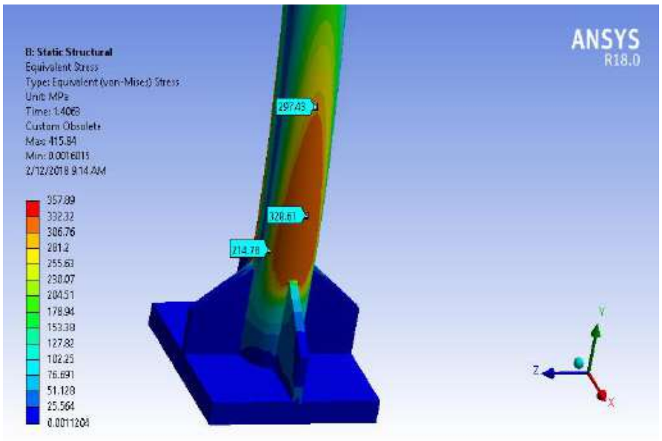

Figure 6: Maximum principal stresses at the region of the right column-base connection of Lin-Hai Hana et al. frame for verification purposes(Lin-Hai et al., 2008).

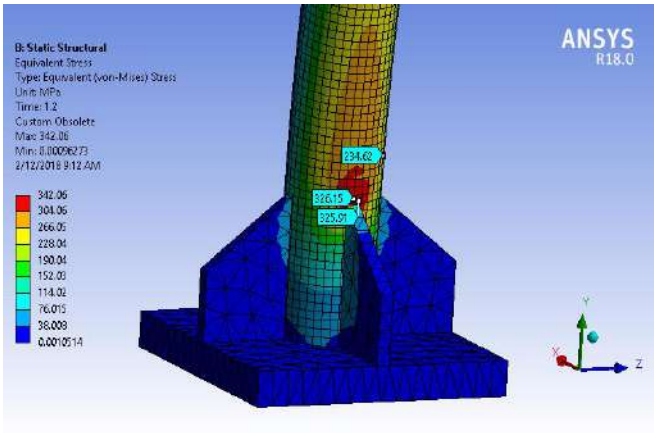

Figure 7: Maximum principal stresses at the region of the left column-base connection of Lin-Hai Hana et al. frame for verification purposes (Lin-Hai et al., 2008).

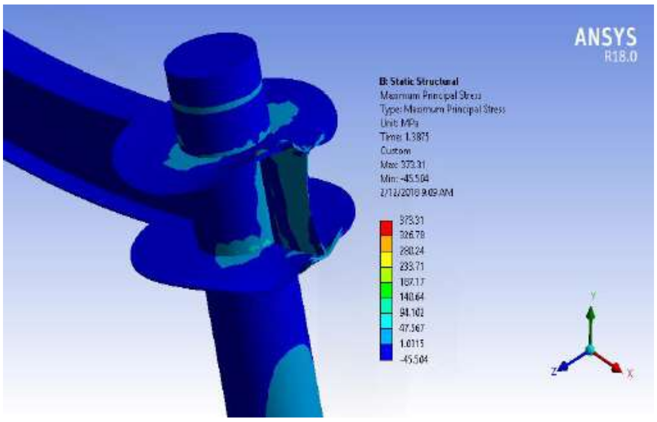

Figure 8: Maximum principal stresses at the region of the beam-column connection of Lin-Hai Hana et al. frame for verification purposes(Lin-Hai et al., 2008).

3.3. Analysis Type and Boundary Conditions

The static analysis type is utilized for the finite element model. In nonlinear analysis, the total load applied to a finite element model is divided into a series of load increments called load steps. At the completion of each incremental solution, the stiffness matrix of the model is adjusted to reflect nonlinear changes in structural stiffness before proceeding to the next load increment. The ANSYS program (ANSYS 18) (ANSYS, 2016) uses Newton-Raphson equilibrium iterations for updating the model stiffness. Newton-Raphson equilibrium iterations provide convergence at the end of each load increment within a tolerance limit.

4. Result and discussion
4.1. Failure Modes

Figs. (9) and (10) show failure modes and maximum stresses resulted from FE analysis. All the composite frames exhibited similar failure mode. Plastic hinges were formed at the top and the bottom of the STFC. No concrete core crush was observed. Thus, composite action was maintained throughout.

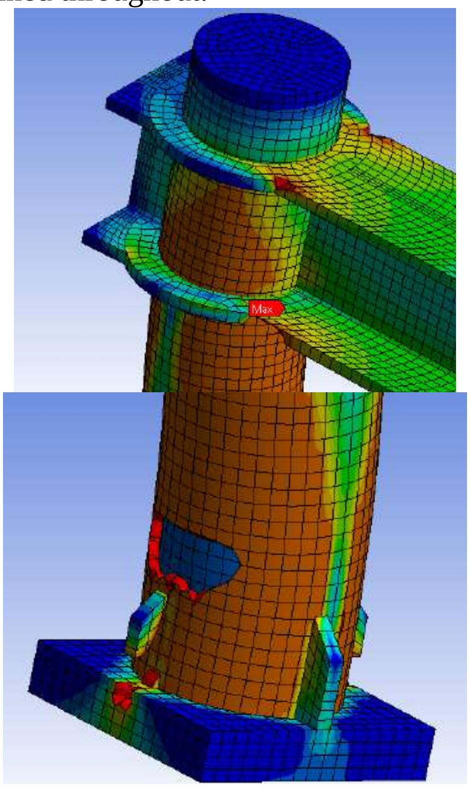

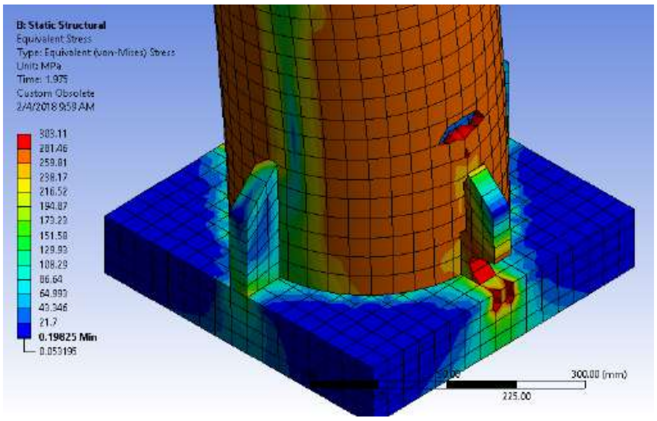

Figure 9: Failure mode and maximum stresses column-base connections.

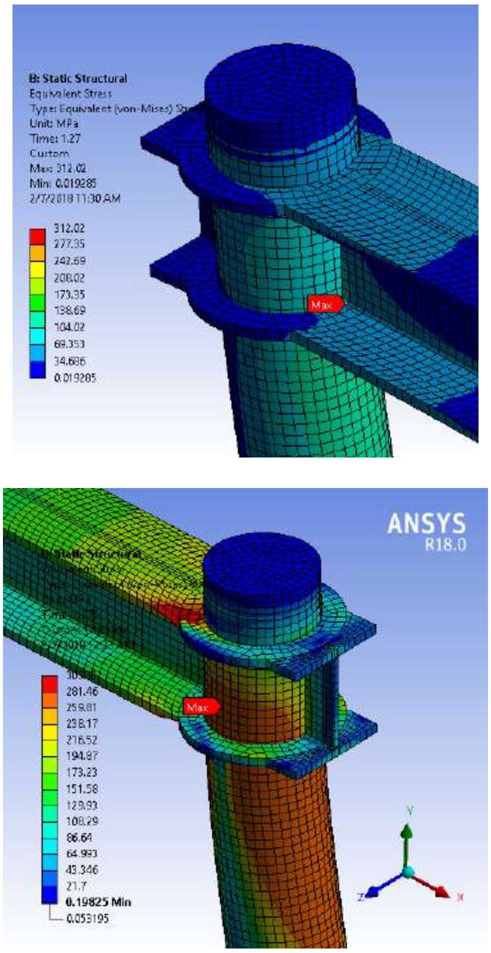

Figure 10: Maximum stresses at beam-column connection.

4.2. Maximum Stresses

Maximum stresses maps are shown in Figs. (9) and (10). Maximum stress occurred at the connection with the steel beam which was 312MPa. These figures show the stress distribution at the steel shell. The greater values are shown at the beam-column connection and at the top and bottom regions of the STFC. The maximum value 312 MPa (> 290 MPa) indicates a plastic hinge formation at the connection of the steel beam and the top of the STFC, showing the connection fixing ability that allow the hinge to occur close to the connection point.

4.3. Load Displacement Response

Figs. (11-13), show the lateral load – lateral displacement curves for STFC length, L = (3048 mm,4572mm, and 6096mm), for steel shell thicknesses, t = (14.76 mm), (8.86 mm), and (5.92 mm), respectively. The load-strain curve for a composite frame at top connection is shown in Fig. (14).

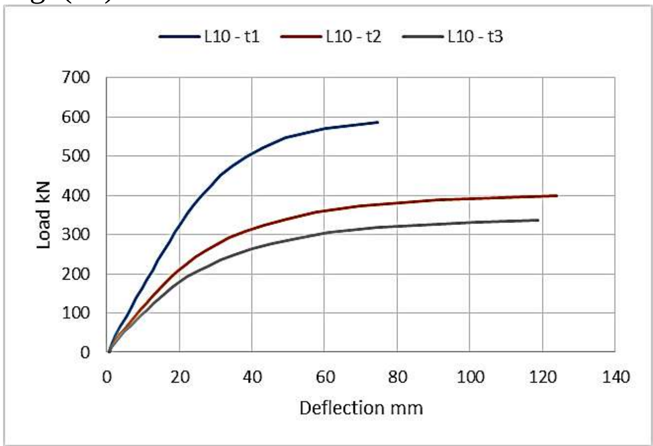

Figure 11: Lateral load – lateral displacement curves for STFC length, L = (3048 mm), for various steel shell thicknesses t = 14.76mm.

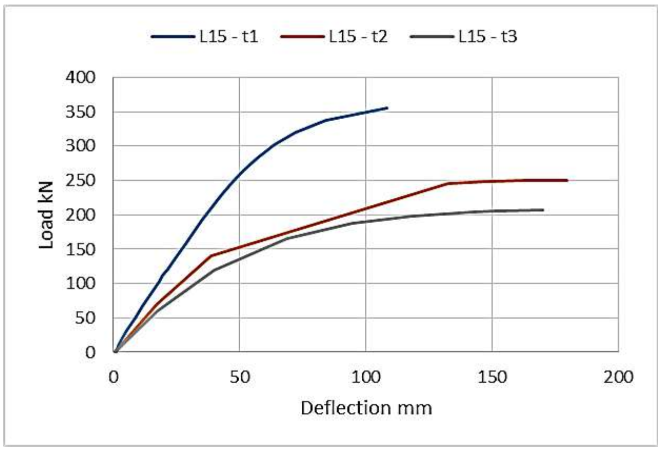

Figure 12: Lateral load – lateral displacement curves for STFC length, L = (4572 mm), for various steel shell thicknesses t = 8.86mm.

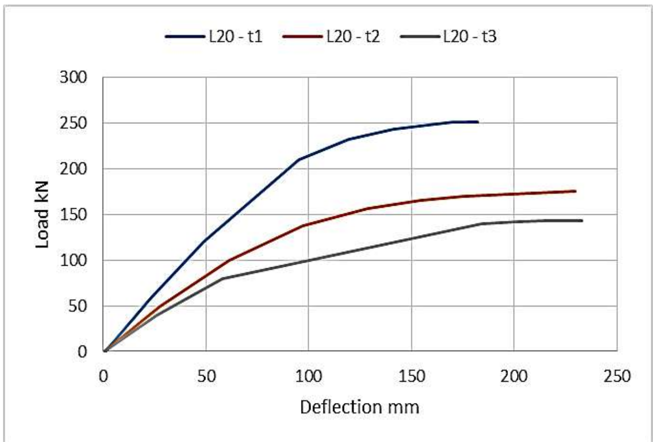

Figure 13: Lateral load – lateral displacement curves for STFC length, L = (6096 mm), for various steel shell thicknesses t = 5.92mm.

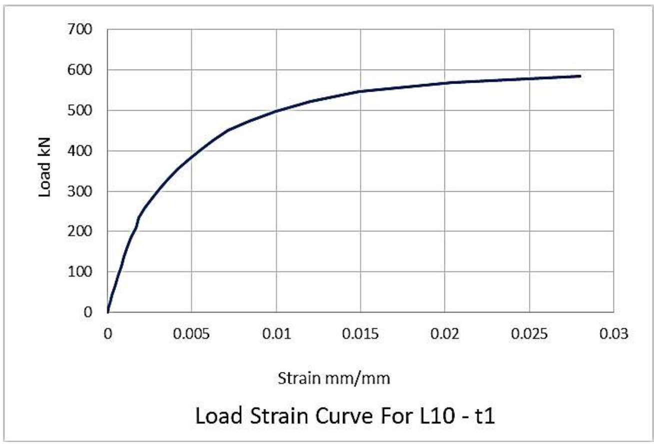

Figure 14: Load-strain curve for Frame L10-t1 at top connection.

From the figures it can be seen that STFC with steel shells of t = 14.76 mm shows the stronger and stiffer response over the other thicknesses which generally yielded close results to each other. At length L = 3048 mm, ratios of STFC of steel shell thickness t = 14.76 mm strength to those STFC of t = 8.86 mm. and of t = 5.92 mm. at ultimate stage were 402.6 kN /180.22 kN = 2.24, and 402.6 kN / 150.12 kN = 2.68.

Effect of column height can be also evaluated. It can be shown that STFC with steel shell of t = 14.76 mm. ratios of STFC of height L = 3048 mm. strength to those STFC of L = 4572 mm. and of L = 6096 mm. at ultimate stage were 402.6 kN /284.42 kN = 1.42, and 402.6 kN / 210.10 kN = 1.92.

Table (4) shows the lateral loads at yield and at failure, and the corresponding lateral displacements, for the studied AISC-STFC composite frames.

Table (4) Lateral loads at yield and at failure, and the corresponding lateral displacements, for the composite frames.

Frame	Hight (mm)	Skin thickness (mm)	Δ_y (mm)	P_y (kN)	Δ_u (mm)	P_u (kN)
L10 - t1	3048	14.76	9.66	162	26.1	402.6
L10 - t2	3048	8.86	9.5	94	19.88	180.22
L10 - t3	3048	5.92	9.4	80.5	16.1	150.12
L15 - t1	4572	14.76	19.4	125.8	53.4	284.42
L15 - t2	4572	8.86	13.5	79.4	35.8	139.5
L15 - t3	4572	5.92	11.8	65.4	36.34	120.25
L20 - t1	6096	14.76	40.5	100.45	95.01	210.1
L20 - t2	6096	8.86	29.4	52.95	61.15	100.95
L20 - t3	6096	5.92	25.9	40.18	57.93	80.45

4.4. Lateral to Vertical Load Ratio

The composite frames of this study were loaded by the maximum value allowed by the AISC (AISC, 2005). Table (5) gives the percentage of lateral load (P) to the maximum allowed vertical load (No), at yield and at failure. The range of lateral load to maximum vertical load, at yield was (4.6 – 8.4%), and at failure was (9.2 – 20.8%). Greatest percentage of lateral loads are obtained for L =3048 mm. height and lower but similar percentages for L = 4572 mm. and L =6096 mm. height frames. The lower percentage in general may be due to the fact that the STFCs are loaded with max allowed load by the AISC.

Table (5) Percentages of lateral load (P) to maximum vertical load (No), at yield and at ultimate.

Frame	P_y/N_o %	P_u/No %
L10 - t1	8.4	20.8
L10 - t2	6.6	12.6
L10 - t3	7	13
L15 - t1	7.3	16.4
L15 - t2	6.2	11
L15 - t3	6.4	11.8
L20 - t1	6.8	14.2
L20 - t2	4.9	9.3
L20 - t3	4.7	9.3

4.5. Displacement Ductility

Table (6) shows the displacement ductility (Δu / Δy) ratios for the composite frames of this work. The range of ductility ratios is 1.71 to 3.06 with an average of 2.43 indicates good ductility of the composite frames (Lin-Hai, 2011). No indication is found on the effect of slenderness on the ductility. It should be reminded that the STFCs are loaded with maximum load allowed by AISC which affects the lateral load value and hence the lateral displacement at failure will be lower.

Table (6) Displacement ductility (Δu / Δy) ratios for the composite frames.

Frame	D_u/D_y
L10 - t1	2.7
L10 - t2	2.09
L10 - t3	1.71
L15 - t1	2.75
L15 - t2	2.65
L15 - t3	3.08
L20 - t1	2.35
L20 - t2	2.08
L20 - t3	2.24
Average	**2.41**

5. Conclusions

The structural response of composite frames consisted of STFC columns connected to steel beam was investigated. The FE modeling was used to analyze the frames using ANSYS. The STFC columns were those listed in AISC steel manual. Lateral load was applied to failure. The following conclusions can be drawn:

1.All the composite frames exhibited similar failure mode. Plastic hinges were formed at the top and at the bottom of the STFC. No concrete core crush was observed. Thus, composite action was maintained throughout.

2.Maximum stress occurred at the connection with the steel beam was 312 MPa indicating a plastic hinge formation.

3.Load-displacement response shows significant stiffness and strength of AISC-STFC column of thickness t = 0.581 in. (14.7 mm). This column with length L = 10 ft. has a strength 2.24 times that of the column with t = 0.349 in., and 2.68 times that of t = 0.233 in.

4.Effect of column height was evaluated. For STFC with steel shells of t = 14.76 mm., ratios of STFC of height L = 3048 mm. strength to those STFC of L = 4572 mm. and of L = 6096 mm. at ultimate stage were 1.42 and 1.92, respectively.

5.The range of lateral load to maximum vertical load, at yield was (4.6 – 8.4%), and at failure was (9.2 – 20.8%). Greatest percentages of lateral loads are obtained for L =3048 mm. height.

6.The range of ductility ratios was 1.71 to 3.06 with an average of 2.43. Greater ductility ratio may be obtained should the vertical loads of the AISC STFC columns were reduced.

References

AISC, (2005). American Institute of Steel Construction, Manual of Steel Construction, 13th Edition. Chicago.

AHMED G.H. (2015). Mechanical Properties for Splices of Welded Reinforcing Steel Bars, ZANCO Journal of Pure and Applied Sciences, 27(6), 99-112.

ANSYS, (2016). ANSYS User's Manual Revision 5.5. ANSYS, Inc., Canonsburg, Pennsylvania.

BANGASH, M. Y. H. (1989). Concrete and Concrete Structures: Numerical Modeling and Applications. London: Elsevier Science Publishers Ltd.

DESAYI, P. AND KRISHNAN, S., (1964). Equation for the Stress-Strain Curve of Concrete. Journal of the American Concrete Institute, 61(3), 345-350.

FA-XING DING, GUO-AN YIN, LI-ZHONG JIANG, YU BAI (2018). Composite frame of circular STFC column to steel-concrete composite beam under lateral cyclic loading. Thin-walled Structures, (122), 137-146.

HU H.T., HUANG C.S., WU M.H., WU Y.M. (2003). Nonlinear analysis of axially loaded concrete-filled tube columns with confinement effect. Journal of Structural Engineering, ASCE 2003;129(10), 1322–9.

HAN L.H., YAO G.H., TAO Z. (2007). Performance of concrete-filled thin-walled steel tubes under pure torsion. Thin-Walled Structures, 45(1), 24–36.

LIN-HAI HAN, WEN-DA WANG, XIAO-LING ZHAO (2008). Behavior of steel beam to concrete-filled SHS column frames: Finite element model and verifications, Engineering Structures, 30(6), 1647–1658.

LIN-HAI HAN, WEN-DA WANG, ZHONG TAO (2011). Performance of circular STFC column to steel beam frames under lateral cyclic loading. Journal of Constructional Steel Research, 67(5), 876–890

SCHNEIDER S.P. (1998). Axially concrete-filled steel tubes. Journal of Structural Engineering, ASCE 1998;124(10), 1125.

SHAMS M, SAADEGHVAZIRI MA (1997). State of the art of concrete-filled steel tubular columns. ACI Structural Journal, 94(5), 558–571.

YASEEN, S.A. (2020). Flexural Behavior of Self Compacting Concrete T-Beams Reinforced With ARFP. *ZANCO Journal of Pure and Applied Sciences*, 32(3).

ZHAO X.L., GRZEBIETA R.H. (1999). Void-Filled SHS beams subjected to large deformation cyclic bending. Journal of Structural Engineering, ASCE, 125(9), 1020.

ZANCO Journal of Pure and Applied Sciences
The official scientific journal of Salahaddin University-Erbil
https://zancojournals.su.edu.krd/index.php/JPAS

ISSN (print):2218-0230, **ISSN (online):** 2412-3986, **DOI: http://dx.doi.org/10.21271/zjpas**

RESEARCH PAPER

Optimized frame detection technique in vehicle accident using deep learning

Mardin A. Anwer[1], Shareef M. Shareef[1], Abbas M. Ali[1]

[1]Department of Software and Informatics, College of Engineering, Salahaddin University-Erbil, Kurdistan Region, Iraq

A B S T R A C T:

Video processing becomes one of the most popular and needed steps in machine leering. Todays, Cameras are installed in many places for many reasons including government services. One of the most applications for this concern is traffic police services. One of the main problems of using videos in machine learning application is the duration of the video; which is consuming time, paperwork and space in processing. This leads to increase the computation cost through a high number of frames. This paper proposes an algorithm to optimize videos duration using a Gaussian mixture model (GMM) method for real accident video. The Histogram of Gradient (HoG) has been used to extract the features of the video frames, a scratch CNN has been designed and conducted on two common datasets; Stanford Dogs Dataset (SDD) and Vehicle Make and Model Recognition Dataset (VMMRdb) in addition to a local dataset that created for this research. The experimental work is done in two ways, the first is after applying GMM, the finding revealed that the number of frames in the dataset was decreased by nearly 51%. The second is comparing the accuracy and complexity of these datasets has been done. Whereas the experimental results of accuracy illustrated for the proposed CNN, 85% on the local dataset, 85% on SDD Dataset and 86% on VMMRdb Dataset. However, applying GoogleNet and AlexNet on the same datasets achieved 82%, 79%, 80%, 83%, 81%, 83% respectively.

KEY WORDS: Intelligent transportation system, Object detection, video processing technique, video segmentation, Gaussian mixture model, transfer learning, deep learning, GoogleNet, AlexNet.
DOI: http://dx.doi.org/10.21271/ZJPAS.32.4.5
ZJPAS (2020) , 32(4);38-47 .

1.INTRODUCTION:

Many applications on Intelligent Transport Systems (ITS) focus on three missions which are detecting (Minaee et al., 2015), tracking and recognizing vehicles in image sequences. Most of these applications apply their proposed algorithms and techniques on common datasets such as SUN2012 (Clady et al., 2008), 101_Object Categories (Ranganatha and Gowramma, 2018) and CIFAR-10 (Hasanpour et al., 2018) and COLD and IDOL (Salih and Ali, 2019)

* **Corresponding Author:**
Mardin A. Anwer
E-mail: mardin.anwer@su.edu.krd
Article History:
Received: 30/12/2019
Accepted: 22/02/2020
Published: 08/09 /2020

Deep learning algorithms perform well when the dataset is large because these algorithms are data dependencies to understand it perfectly (Anwer et al., 2019). However, minimizing the number of frames in each video will increase the number of videos in the dataset. CNN replaces the standard methods of video classification which consist of three stages with a single neural network that is trained end to end from raw pixel values to classifier outputs (Niebles et al.,2010). Currently, there are no video classification benchmarks that coordinate the scale and variety of existing picture datasets since recordings are essentially more troublesome to gather, clarify and store. Converting video to frames is a fundamental step when dealing with video processing. In this research, MATLAB Deep learning tool has been used to accomplish the proposed CNN. Deep and transfer learning algorithms depend heavily on high-end machines, contrary to traditional machine learning algorithms, which can work on low-end machines. This is as a result of the necessities of deep learning formula embrace GPUs that are associate degree integral part of its operating. Deep learning algorithms inherently do an oversized quantity of matrix operations. These operations are with efficiency optimized employing a GPU. Hence, GPU is made for working in machine learning. We had many alternatives such as using cloud computing for deep learning or on-premises. However, in this research the implantation environment was a computer with 8 GB RAM, CPU @2.40GH and MATLAB Simulink with deep learning toolbox are used to conclude the results. The paper is organized as follows: section on is an introduction, section two is about the related studies and literature review. Methodology explained in section three. Section four clarify results and discussion. We finish with conclusions and future work.

1.1. Gaussian mixture model

A Gaussian mixture (GM) is characterized as a raised combination of Gaussian densities (Jakob et al. ,2003). A Gaussian mixture model (GMM) is valuable for modelling data that comes from one of several groups: the groups could be diverse from each other, but data points within the same group can be well-modelled by a Gaussian distribution (Kolekar, 2010). Image is divided up into a mixture of pixel cells. The esteem of the pixel may be a number that appears the intensity or color of the picture. Let X be a irregular variable that takes these values. For a probability model determination, we assumed to have a mixture of Gaussian distribution as the following:

$$f\,(x) = \sum_{i=1}^{k} p_i \;\; N(x|\, \mu_i, \sigma_i^2) \qquad (1)$$

Where k is the number of components or regions and $p_i>0$

weight such that $\sum_{i=1}^{k} p_i \,= 1,$

$$N(\mu_i, \sigma_i^2) = \frac{1}{\sigma\sqrt{2\pi}} \exp\left(\frac{-(x-\mu_i)^2}{2\sigma_i^2}\right) \qquad (2)$$

where μ_i, σ_i^2 are mean and standard deviation of class i. For a given image X, the lattice data are the values of pixels and MoG is our pixel-based model. However, the parameters are $\theta = (p_1, \dots, p_k, \dots, \mu_1, \dots, \mu_k, \dots, \sigma_1^2, \dots, \sigma_k^2)$ and we can guess the number of regions in MoG by the histogram of lattice data.

1.2 The Histogram of Gradient

HOG features provide a concise but powerful image representation for general object classification. They have found significant application in the field of pedestrian identification (Navneet and Bill, 2005), where they have continued to provide one of the more robust feature extraction techniques even in recent analyses. HOG features are based on gradient angle and magnitude distributions, and in visual data, they are robust due to the gradient's natural invariance to slight changes in ambient lighting and colour variations. Equation number 3 is used to find the magnitude and direction of the gradient.

$$g = \sqrt{g_x^2 + g_y^2} \qquad (3)$$

$$\theta = arctan\,\frac{g_y}{g_x} \qquad (4)$$

1.3 Google net Framework

GoogleNet described as a Networks with Parallel Concatenations. It proposed an architecture that associates the strengths of the NiN and repeated blocks paradigms [9]. Their architecture involved twenty-two deep CNN layers with fifty-six million parameters less than AlexNet (Christian et al.,2015). Figure 1 shows the construction of the GoogleNet.

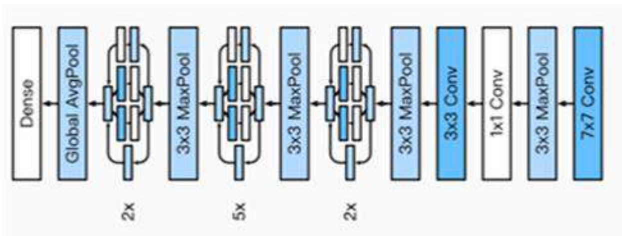

Figure 1: Full GoogLeNet Model (Das., 2017)

1.4 AlexNet framework

AlexNet is one of the most widely-used architecture as CNN models (Krizhevsky et al.,2012). It consists of eight layers which are: convolution, max pooling and fully connected. AlexNet used non-linearity (Relu) activation function because of better training performance than tanh and sigmoid. Figure 2 shows the construction of AlexNet. It is important to highlight that AlexNet needed six days to be trained using two Nvidia Geforce GTX 580 GPUs which is the reason for why their network is split into two pipelines (Siddharth ,2017).

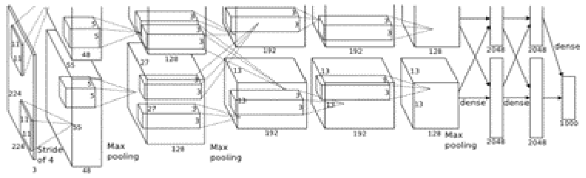

Figure 2: An illustration of the architecture of AlexNet (Alex et al,2012)

2. LITURETURE REVIEW

Video indexing ended up one of the foremost critical domains in video applications since 1990, specifically change of videos into a format appropriate for retrieval frameworks. In such scenery, the approach is repeatedly as follows: to begin with videos are fragmented into shots, at that point keyframes are extracted from each shot. At this point, the issue of looking through videos can be performed through picture recovery, i.e. by recovering keyframes comparable to a picture submitted as inquiry (Zhang et al.,1997)(Chang et al.,1999)(Pickering and Ru¨ger,2003)(Sze et al.,2005). Alternately nowadays the same applications are substantial but utilizing speech processing (Dey et al. ,2018), signal processing (Sreenu et al.,2019), deep learning (Padalkar, 2010) and neural network. Figure 3 illuminates the classified construction of video. (Karpathy et al.,2014) run a wide empirical evaluation of CNNs on large-scale video classification using a new dataset of one million YouTube videos belonging to 487 classes. They retain the top layers on the UCF-101 Action Recognition dataset and observe significant performance improvements compared to the UCF-101 baseline model (63.3% up from 43.9%). (Sochor et al.,2016) used images from video frames and CNN to boost the recognition performance using 3D vehicle bounding box. Some researchers created car accident dataset from scratch and develop custom software to process on it (Mustaffa and HOKAO, 2013). In their investigation (Xinchen et al., 2017) classified the sorts of vehicles utilizing Faster R-CNN (Region-Convolutional Neural Networks). They demonstrated that utilizing deep learning is more strength and higher precision than conventional machine learning strategies. Thus, (Sun et al.,2019) improved Faster R-CNN algorithm by adding Regional Proposal Network (RPN) to the convolution layer 5 in Faster R-CNN. Recently, academics are attentive on pre-trained and fine-grained CNN in their research. (Yang et al.,2015) distributed a huge dataset for fine-grained vehicle sort recognition they proposed a CNN-based strategy for fine-grained vehicle model recognition which accomplished of recognizing vehicles from diverse perspectives. Extra fine-grained vehicle type recognition technique was done by (Fang et al., 2017) based on a combination of local and global features extracted from the CNN model which is afterwards named pre-trained AlexNet. More details about Alexnet will be discussed in section 3.3.2.

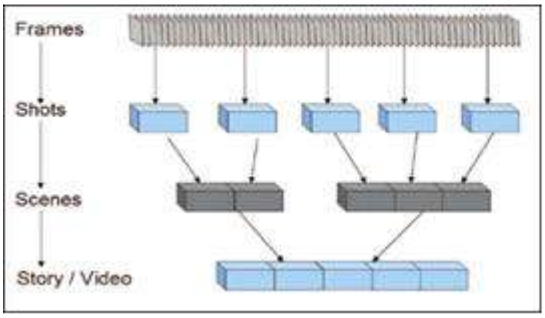

Figure 3: Hierarchical Structure of Video (Milind,2010)

3. THE PROPOSED METHOD

This research consists of three stages which are building a raw dataset, building new dataset and complexity comparison. Figure 4 demonstrates the main methodology of this research. Each stage will be detailed in separate sections.

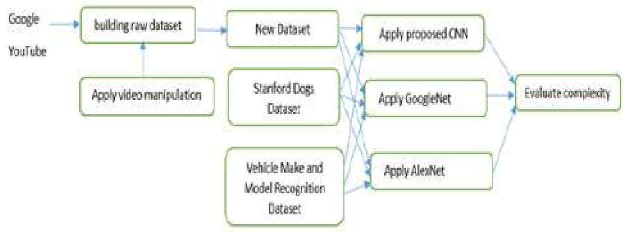

Figure 4: The main methodology of the research

3.1 Building new dataset

The first stage toward executing this research is to build a dataset. This considered as a changeling issue. YouTube and Google were the main sources of these videos. Some sources were from some countries official sites that publish vehicle crash accident in their country and no copyright need it for using them. The dataset that we built contained 10 videos. These videos are recorded at different traffic light positions in different countries. Also, two of the videos were taken from animation website.

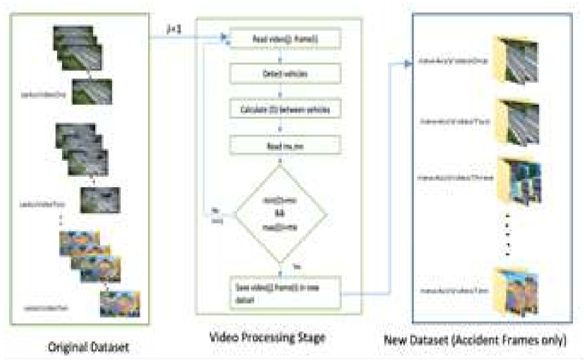

Figure 5: Methodology of creating a new dataset

3.2 Optimized dataset

By using video manipulation process only accident frames will be saved to create a new dataset. The process is applied for all videos in the raw dataset. This means the new dataset will contain 10 new folders with fewer frames number. The number of frames in each folder is different than the other because the time length of each video is different and the accident frames in some videos are more than the other. In some videos, the accident starts in the second 50 and last to minute 2. While other videos start in minute 1 and last until minute 7. The number of frames compromised depending on specific parameters. Table 1 shows the number of frames before and after stage one. The end of this process is a new data set that contains ten folders.

3.2.1 Detecting accident Frames

This section presents the main techniques for accident frames detection in videos. Each video consists of sequence of frames f, f= {f1, f2, f3, …., fn}. The function G, computer Gaussian mixture model to calculate centroids (C). Distance (D) measures the difference between frames fi and fi+1 in the sequence at each time (t). Calculating maximum and minimum distance is an adjustment calculation between the frames. When the vehicles are very far from each other than max(distance) will be saved. The opposed is true when the vehicles are very close. While applying this algorithm on different videos we discovered that the main problem of this approach is calculating min and max. However, even if they were not calculated properly, it will increase 5-8 frames which do not increase the number of frames in the new dataset. The algorithm is written below. For vehicles detection Gaussian mixture model is used. Figure 5 shows the methodology used in the proposed work. The algorithm explains how frames inside the video analyzed to be processed for recognizing the accident. The following is a segment of pseudo-code for the proposed algorithm used in this research.

Algorithm one: Accident frames detection

```
Procedure Video handling (vcarAccVideoTwo,
C,d)

Repeat for video file

for each f in carAccVideoTwo  do

  if(size(C,1)>1) then

       if(size(C,1)==2) then

            call find the distance(d)

         elseif(size(C,1)==3) then

            call find the distance(d)

         elseif(size(C,1)==4)  then

            call find the distance(d)

            elseif(size(C,1)==5)  then

            call find the distance(d)

       end if

   mx <-- max(d)
```

mn <-- min(d)

end for

until no frame in the video

end procedure

Figure 6: The original frame number 49 from carAccVideoOne (b) binary image of frame number 49 (c) detecting the car object from carAccVideoTwo (d) foreground segmentation of image frame number 254. (e) consider the vehicles as accidents cars for reporting. (f) label the vehicles that are close to making accidents.

3.3 Network Configuration

The last stage is the process of CNN configuration. It involves 3 phases; design, train and checking the accuracy. Figure 7 shows the steps needed for this stage. Network configuration.

3.3.1 Features Extraction and classification

Extracting salient features is the major critical phase in most research in object recognition and computer vision tasks. Hence, some works have concentrated on extracting strong features for a variety of image classification tasks [1]. Bag-of-words model is a common method used for image classification due it gave a promise results for a huge of research works. However, BoW is containing some drawbacks like leads a high dimensional feature vector and in-order visual words for the represented images; this leads to giving similarity of images with different content (Liu et al.,2015).

Table (1) Number of frames in each video before and after applying a video optimization step.

Folder Name	Number of frame (original videos)	Duration	Number of frames after manipulating videos
carAccVideoOne	238	00:03:07	150
carAccVideoTwo	240	00:04:08	198
carAccVideoThree	302	00:03:30	169
carAccVideoFour	304	00:03:50	115
carAccVideoFive	345	00:04:15	146
carAccVideoSix	302	00:04:10	175
carAccVideoSeven	398	00:05:14	111
arAccVideoEight	398	00:05:14	130
carAccVideoNine	238	00:03:20	180
carAccVideoTen	402	00:10:01	200

Figure 7: Network outline phases

In CNN, convolution layers, max-pooling layers and activation function are responsible for extracting features while the fully connected layer is used for classification. It collects the final convoluted feature and returns a column vector where each row focuses towards a class. More accurately, components of the output vector each represent the likelihood estimation of each class and the sum of the components is one as shown in figure 8. The extracted features of each video have been used for SVM (Support Vector Machine) classifier.

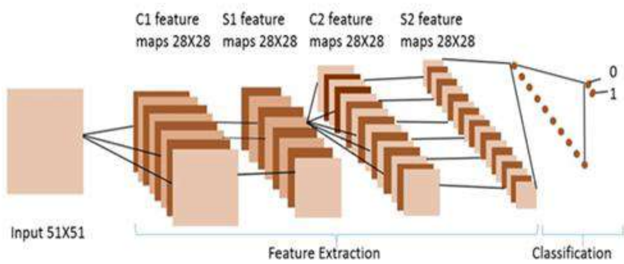

Figure 8: CNN layers for feature extraction and classification [28]

3.3.2 The proposed architecture of CNN

The proposed construction of the CNN contains input layer, numerous convolutional layers (C), max-pooling layers (M), and fully connected layers (F). Pooling layer is mostly used immediately after the convolutional layer to decrease the spatial size. As a result, the number of parameters and computation will be decreased to avoid overfitting. The experimental work has been started with twelve basic layers of architecture, then the number of layers has been tuned increasingly to match the planed accuracy. Table 2 illustrates one of the configurations of structured CNN. However, the results were not as expected, and the accuracy was 0.1619 which is 16.19%. After adding additional layers, the accuracy increased and became 27.26% then 49% as shown in figure 9. More experiments have been done by adding more layers, led to increasing the accuracy to be more than 98%. The final architecture of the proposed CNN demonstrates in table 3.

Table (2) One of the intended CNN structure in our research

Layer No.	Layer Type
1	Input layer
2	Convolutional
3	Relu
4	Max pooling
5	Cross Chanel
6	Convolutional
7	Relu
8	Max pooling
9	Fully connected
10	Fully connected
11	Soft max
12	Classification

In each design, Different parameters have been applied for the entire layers regularly until match the accuracy needed. Figure ten illustrates the required accuracy that we were seeking.

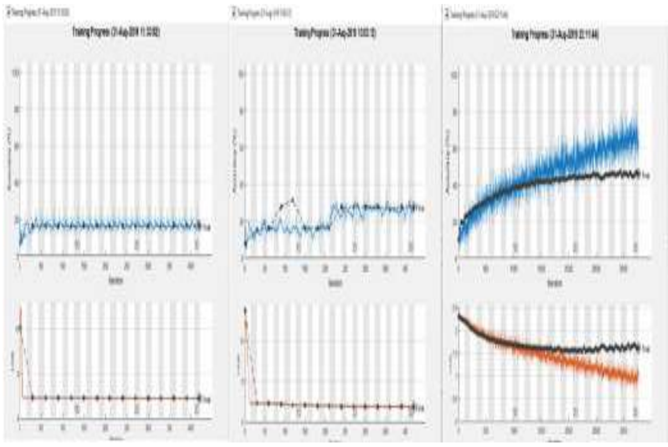

(a) (b) (c)

Figure 9: Validation accuracy, training and loss cycles. (a) for proposed CNN in table 3. (b),(c) after adding more layers.

Table (3) The final version of the CNN structure in our research

Layer No.	Layer Type
1	Input layer
2	Convolutional
3	Relu
4	Cross Chanel
5	Max pooling
6	Convolutional
7	Relu
8	Cross Chanel
9	Convolutional
10	Relu
11	Convolutional
12	Relu
13	Max pooling
14	Fully connected
15	Relu
16	Drop out
17	Fully connected
18	Relu
19	Drop out
20	Fully connected
21	Soft max
22	Classification

4. RESULTS AND DISCUSSION

In order to evaluate the proposed CNN, raw, Stanford Dogs and Vehicle Make and Model Recognition Datasets have been used. Ten videos from Google and YouTube have been collected for constructing a raw dataset. In order to apply 10 folders that contain the video's frames in the experimental work. After detecting accident vehicles in the frames, the proposed technique will save the accident frames in a new folder to become a new dataset, the frames will be selected based on Gaussien mixture model. The proposed work decreased the number of frames from 2,769 to 1,300. This, in turn, reducing the consumed time for further analyzing the videos for E-government purpose due to fewer frames within each folder

The first dataset has been collected from open sources website. While the duration and the size of the videos were different, the optimization technique using Gaussian mixture model has been used to detect the vehicle accidents frames and save it in another folder. Table 4 shows the dataset used in this research and the number of frames in each dataset. The total number of images used in this research was 10765 with .jpg extension but variance dimensions in each dataset. For the input layer, we started training the proposed CNN with the original dimensions of the frames which were 219X415X3 coloured images. While training, we discover that it took long times and the structure needed extra layers for feature computation. We also test 38X38X3 dimensions and check the differences in computation cost. Because the datasets will be tested in AlexNet and GoogleNet, the input images should be close to the input layer dimension images of these networks which are 227X227X3 and 224X224X3 respectively. Consequently, we changed the dimensions of all frames patch to be 227X227X3. Figure 11 shows a random image of each folder in a raw dataset with 227x227x3 dimension. Recording feature extraction stage, we enhance the features produced by CNN by feeding them to SVM.

Table (4) Dataset used for testing the proposed CNN

Data set	No. of images
Optimized	1564
Stanford Dogs	4560
Vehicle Make and Model Recognition	4300

We have multiple fully connected layers in our recommended structure. This is because it learns higher-level features and the result assistance the final layer especially when a sigmoid function is used as an activation function. Table 5 indicates the accuracy outcomes of the CNNs applied to the datasets. Our proposed model involves 22 layers. It reduces the complexity and number of parameters to be used in a laptop with 8GB RAM. Figure 12 shows the probability accuracy when applying our suggested CNN model on different datasets.

Table (5) The recognition accuracy when adopting different datasets

Dataset / **Accuracy**	**The proposed CNN**	**GoogleNet**	**AlexNet**
optimized dataset	85%	82%	83%
Stanford Dogs dataset	85%	79%	81%
Vehicle Make and Model Recognition Dataset (VMMRdb)	86%	80%	83%

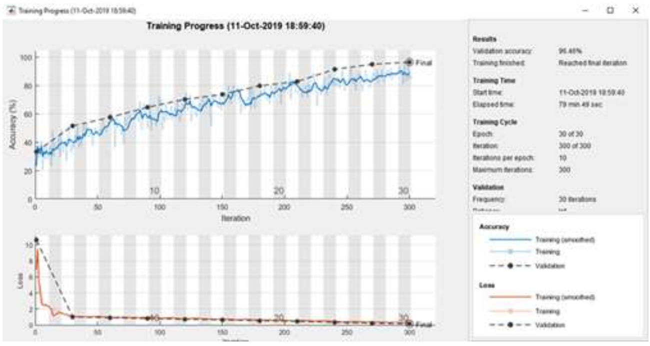

Figure 10: Training process for CNN structure in the table 4.

Figure 11: Images of car accident videos with 227X227X3 dimension**.**

5. CONCLUSIONS AND FUTURE WORK

In this research, an optimized technique for accidents vehicles dataset images reduction has been used and a CNN is designed from scratch to train and do the classification process for a self-generation report. Optimizing the dataset in video manipulation increases the accuracy. Since reducing frames rate per each video focusing only on accidental frames, leads to processing fewer features during the reduced video duration. This dataset along with the other two datasets were trained using the proposed CNN. The architectures and parameters for the GoogleNet and AlexNet have been modified to build the proposed net.

In future work, we hope to corporate with traffic police to obtain a high number of accident vehicle videos to create a dataset with 100 videos and generate detailed report about the accidents. Besides, using cloud computing to easily manipulate large datasets to be easily ingested and managed to train algorithms.

Figure 12. The score of each image using the proposed CNN.

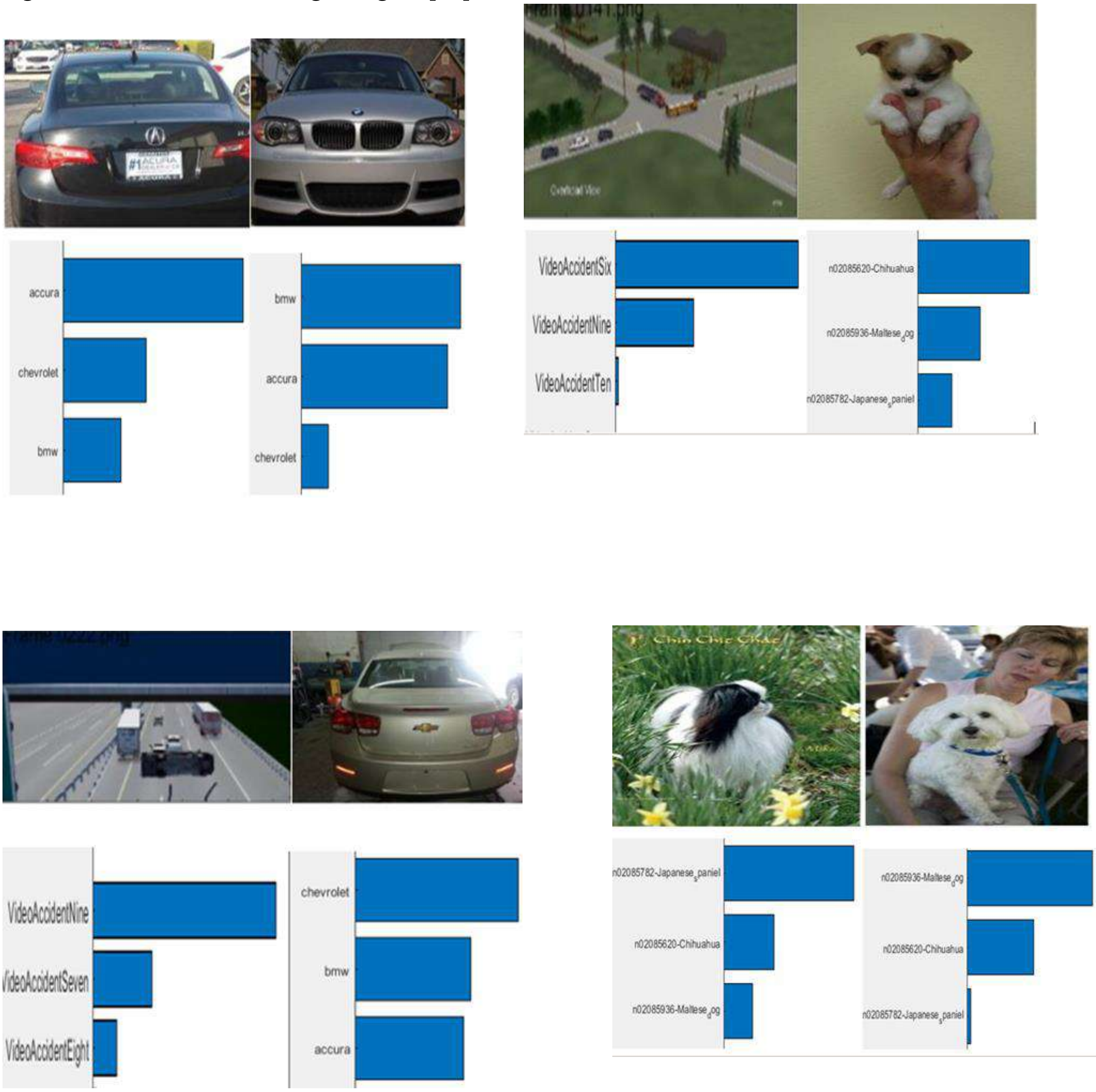

Acknowledgements

I would like to thank the supervisors that help to enrich the research.

References

Anwer M., Shareef M, Ali A. (2019)' Smart Traffic Incident Reporting System in e-Government' ECIAIR conference, UK DOI: 10.34190/ECIAIR.19.061

Chang H.S., S. Sull, and S.U. Lee (1999) 'Efficient video indexing scheme for content- based retrieval'. IEEE Transactions on Circuits and Systems for Video Technol- ogy, 98:1269–1279.

Christian Szegedy, Wei Liu, Yangqing Jia, Pierre Sermanet, Scott Reed, Dragomir Anguelov, Dumitru Erhan, Vincent Vanhoucke, and Andrew Rabinovich (2015) ' Going deeper with convolutions'. In Proceedings of the IEEE conference on computer vision and pattern recognition, 1–9.

Clady, Xavier & Negri, Pablo & Milgram, Maurice & Poulenard, Raphael (2008)' Multi-class Vehicle Type Recognition System'. 5064. 228-239. 10.1007/978-3-540-69939-2_22.

Dey N., Ashour A.S (2018) 'Applied Examples and Applications of Localization and Tracking Problem of Multiple Speech Sources'. In: Direction of Arrival Estimation and Localization of Multi-Speech Sources. Springer Briefs in Electrical and Computer Engineering. Springer, Cham.

Fang J., Y. Zhou, Y. Yu, and S. Du(2017) 'Fine-grained vehicle model recognition using a coarse-to-fine convolutional neural network architecture' IEEE Trans. Intell. Transp. Syst., vol. 18, no. 7, pp. 1782–1792, Jul.

Hasanpour, S., Rouhani M., Fayyaz, M., Sabokrou, M., (2018). 'Let's keep it simple,using simple architectures to out perform deeper and more complex architectures'. arXiv:1608.06037v7.

Huang YL (2018) 'Video Signal Processing'. In: Dolecek G. eds Advances in Multirate Systems. Springer, Cham.

Jakob Verbeek, Nikos Vlassis, Ben Krose (2003) 'Efficient greedy learning of Gaussian mixture models '.Neural Computation, Massachusetts Institute of Technology Press MIT Press, 2003, 15 2, pp.469-485. 10.1162/089976603762553004.

Karpathy A., G. Toderici, S. Shetty (2014) 'Large-scale Video Classification with Convolutional Neural Networks.'

Kolekar M., (2018)' Intelligent video surveillance system: An algorithm Approach'. CRC Press, Tayor & Francis Group.

Krizhevsky, Alex , Sutskever, Ilya , Hinton, Geoffrey (2012) 'ImageNet Classification with Deep Convolutional Neural Networks'. Neural Information Processing Systems. 25. 10.1145/3065386.

Liu H., Tang H.,Xiao W.,Guo Z., Tian L., Gao Y. (2016) 'Sequential Bag-of-Words model for human action classification'. CAAI Transactions on Intelligence Technology, Volume 1, Issue 2, Pages 125-136

Minaee S., Abdolrashidi A., and Y. Wang (2015) 'Iris recognition using scattering transform and textural features', in Signal Processing and Signal Processing Education Workshop SP/SPE, 2015 IEEE, 2015, pp. 37-42.

Mustaffa A., K. HOKAO (2013) 'Database development of road traffic accident case study Johor Bahru, Malaysia' Journal of Society for Transportation and Traffic Studies JSTS Vol.3 No.1.

Navneet Dalal, Bill Triggs (2005) 'Histograms of Oriented Gradients for Human Detection. International Conference on Computer Vision & Pattern Recognition' (CVPR '05), San Diego, United States. pp.886—893.

Niebles J. C., C.-W. Chen, and L. Fei-Fei (2010) 'Modeling temporal structure of decomposable motion segments for activity classification'. In ECCV, pages 392–405. Springer.

Padalkar, Milind (2010) 'Histogram Based Efficient Video Shot Detection Algorithms'. 10.13140/RG.2.1.1590.3847.

Pickering M.J. and S. Ru¨ger (2003) 'Evaluation of key-frame based retrieval techniques for video'. Computer Vision and Image Understanding, 922-3:217–235.

Ranganatha S., Gowramma, Y. (2018) 'Image Training and LBPH Based Algorithm for Face Tracking in Different Background Video Sequence'. International Journal of Computer Sciences and Engineering. 6. 349-354. 10.26438/ijcse/v6i9.349354.

Salih. D., Ali .A (2019)' Appearance-based indoor place recognition for localization of the visually impaired person' ZJPAS (2019) , 31(4);70-81. DOI: http://dx.doi.org/10.21271/ZJPAS.31.4.8

Siddharth Das., (2017) 'CNN Architectures: LeNet, AlexNet, VGG, GoogLeNet, ResNet and more'. online at [https://medium.com/@sidereal/cnns-architectures-lenet-alexnet-vgg-googlenet-resnet-and-more-666091488df5]

Sochor J., A. Herout, and J. Havel (2016) ‘Box Cars: 3D boxes as CNN input for improved fine-grained vehicle recognition’ in Proc. Comput. Vis. Pattern Recognit., Jun., pp. 3006–3015.

Sreenu, G., Saleem Durai, M.A (2019) ‘Intelligent video surveillance: a review through deep learning techniques for crowd analysis’. J Big Data 6, 48 doi:10.1186/s40537-019-0212-5.

Sun X., Gu J., Huang R.,Zou R.,Giron B. (2019) ‘Surface Defects Recognition of Wheel Hub Based on Improved Faster R-CNN’. Electronics 2019, 8, 481; doi:10.3390/electronics8050481.

Sze K.W., K.M. Lam, and G. Qiu. (2005) ‘A new key frame representation for video segment retrieval’. IEEE Transactions on Circuits and Systems for Video Technology, 159:1148–1155.

Xinchen Wang X., Zhang W.,Wu X., Xiao L., Qian Y.,Fang Z. (2017) ‘Real-time vehicle type classification with deep convolutional neural networks’. J Real-Time Image Proc DOI 10.1007/s11554-017-0712-5, Springer.

Yang L., P. Luo, C. C. Loy, and X. Tang (2015) ‘A large-scale car dataset for fine-grained categorization and verification’. in Proc. Comput. Vis. Pattern Recognit., Jun., pp. 3973–3981.

Zhang H.J., J. Wu, D. Zhong, and S.W. Smoliar (1997) ‘An integrated system for content-based video retrieval and browsing’. Pattern Recognition, 304:643–658.

ZANCO Journal of Pure and Applied Sciences
The official scientific journal of Salahaddin University-Erbil
https://zancojournals.su.edu.krd/index.php/JPAS

ISSN (print):2218-0230**, ISSN (online):** 2412-3986**, DOI: http://dx.doi.org/10.21271/zjpas**

RESEARCH PAPER

Challenges Facing the Implementation of Building Information Modeling (BIM) Techniques in Iraq.

Mahmood Maad Mahdi[1]* Dana Khider Mawlood[2]

[1]Department of Civil Engineering, College of Engineering, Salahaddin University-Erbil, Kurdistan Region, Iraq
[2]Department of Civil Engineering, College of Engineering, Salahaddin University-Erbil, Kurdistan Region, Iraq

A B S T R A C T:

Building Information Modeling (BIM) technology is a modern technology in the construction industry that has seen widespread and implementation in construction projects around the world in recent years. Developing countries trying to follow up on the newly developed methods and technologies in terms of the architecture, engineering and construction (AEC) industry. Iraq is one of these countries that depends on the traditional methods for design and managing construction projects. This paper aims to review and analyze the most important constraints and challenges (barriers) that stand against the implementation of BIM technology in the AEC industry of Iraq. This paper is part of an ongoing master thesis that in dedicated to the application of BIM technology in the Iraqi AEC industry. A comprehensive literature review has been made beside a face-to-face interview with specialists in the AEC industry along with a questionnaire survey directed to the specialists involved in the process of building and construction and some expert academic parties. The reliability has been approved statically, and the analysis showed that the most influential barriers are lack of demand, lack of authority's support, absence of a national standard for BIM, lack of experts, and the social and habitual resistance to change. The results gained were discussed and compared to the previous studies. More effort must be taken by authorities to overcome these barriers to improve the AEC industry and to take BIM techniques into implementation in Iraq.

KEY WORDS: BIM Barriers, building information modeling, construction project, Iraq.
DOI: http://dx.doi.org/10.21271/ZJPAS.32.4.6
ZJPAS (2020) , 32(4);48-57 .

1.INTRODUCTION:

For the last two decades, the Iraqi construction industry is known for being at the end of the track in terms of the management and modern techniques in the architecture, engineering and construction (AEC) industry. This is due to several factors which take time to discuss, in addition to the circumstances experienced by Iraq, the most important factor is the lack of professionals and experts in terms of modern technologies. It is worth mentioning that the process of construction and project management in Iraq is still done in the old traditional method which depending on two-dimensional drawings, paper documents, and hand calculations especially in preparing bill of quantity (BOQ) and cost estimations besides the total absence of using software tools (rare use) in this term, as well as the process of collaboration and communication, is very weak between the project's stakeholders. These old methods can no longer accommodate large, modern megaprojects, as they have proved low efficiency in dealing with complex buildings and overlapped events (Penttilä, 2006). Therefore, the method of implementing and managing Iraqi

* **Corresponding Author:**
Mahmood Maad Mahdi
E-mail: mahmood.mahdi@su.edu.krd or mahmoodm.mahdi@gmail.com
Article History:
Received: 16/12/2019
Accepted: 25/02/2020
Published: 08/09/2020

architecture, engineering and construction (AEC) industry should be developed through the adoption and the use of modern techniques that can reduce problems and mistakes, and risks in the AEC industry, like reducing time and cost overrun, improve the quality, reducing wastes in materials, etc. Mahdi and Ali (2019) as well as Wali and Othman (2019) highly recommended the use of advanced technologies such as BIM technique to reduce problems like reducing wastage of construction materials and reducing risks in the Iraqi AEC industry. it can be said that the most important and advanced technology is the building information modeling (BIM) techniques. BIM technique has proven high efficiency in providing solutions to most of the AEC industry's problems. It must be mentioned that Iraq is the only Middle Eastern country that did not take BIM technique into consideration yet (Egyptian, 2017).

In the BIM handbook, Eastman et al. (2011) describe BIM as one of the most promising developments in the architecture, engineering, and construction (AEC) industries; as beginning to change the way buildings look, the way they operate and the way they are built. Also mentioned that BIM is not only software but a human activity that basically involves broad changes in the construction process. Eastman continued that BIM is a computer-aided technology used for generating and modeling building information, as well as the related processes of procurements, production, communicating and collaboration.

Due to the approved benefits, sustainability and the solutions provided by BIM techniques around the globe, it is important to take serious steps to adopted this technique in the country. This paper is part the ongoing master thesis that is dedicated to the application of BIM technology in the Iraqi AEC industry, and it aims to review, study and analyze the most effective constraints and challenges (barriers) that stand against the implementation of technology in the AEC industry of Iraq.

2. LITERATURE REVIEW

There are many issues facing building information modeling (BIM) implementing, and there are many challenges and opportunities for architectural, engineering and construction (AEC) industry exists in the term of (BIM). Apparently, some of these issues have been solved over time by the advancement of related technologies; yet, various problems are arising when dealing with the implementation of BIM. In his research, Chan et al. (2019) aimed to identify and evaluate the possible benefits of and barriers to the implementation of BIM in the construction industry of Hong Kong. The significant barriers were related to habitual resistance to change by AEC stakeholders, lack of organizational support, and lack of BIM standards. On the other hand, Ullah et al. (2019) from Estonia presented a paper as part of doctoral research that aims to define the barriers to the adoption of BIM and to develop a framework for effective implementation of this technique. Lack of awareness about BIM benefits, Lack of BIM experts, Lack of demand on BIM were the highest barriers determined. One of their objectives, Hasan and Rasheed (2019), was to investigate the challenges facing 5D-BIM implementation. The main barriers that facing BIM were culture resistance to change, believing that current software and the traditional methods are fare enough and no need for new technologies.

In his research, Sardroud et al. (2018a), studied the barriers facing (BIM) implementation in the construction industry. The researcher aimed in his study to summarize the available information related to (BIM) application in the construction industry and to focus on the most repetitive challenges and barriers. The most critical challenges facing the implementation of this technology found in this study were the contract and legal barriers, management system, cultural problems, and economic and security issues. On the other hand, Hatem et al. (2018) adopted a quantitative approach by conducting a questionnaire directed to professionals to investigate BIM barriers. Their results showed the weakness of the government's efforts, shortage of specialists in (BIM) field, resistance to change and Poor knowledge about the benefits of (BIM) are the highest potential barriers of using (BIM).

In his study, Ahmed (2018) from Bangladesh aimed to identify the most crucial barriers to the implementation of Building Information Modeling (BIM) and to develop a relative rank with their relative impact on these issues. The results of this study showed that the five most crucial barriers to the implementation of BIM are social and habitual resistance to change, Traditional methods of contracting, Training expenses, High cost of software purchasing, Lack of awareness about (BIM). The researcher highlighted the importance of government support to adopt this technology.

Both (2012) from Germany studied the potentials and the barriers for Implementing (BIM) in the AEC industry. He aimed to analyze the existence of (BIM) practices and the difficulties facing its implementation in his country. The researcher determined the potentials, barriers, and constraints of the application of (BIM) in the different processes as well as the target groups. The Assessment showed that the highest barriers facing BIM were technological, educational, economic, and normative barriers. The conspicuous differences in the assessment of the BIM barriers between BIM-users and Non-BIM users show the high necessity of education and information by AEC associations and chambers.

3. QUESTIONNAIRE FORMING AND DESIGN

Through the process of reviewing previous researches and studies, it is likely to find a large number of obstacles to the application of BIM technique. These obstacles differ from one author to another, from one country to another as time progresses, but the main factor in their diversity and multiplicity is the degree of development of the construction industry in each country.

Thus, to achieve the objectives of this paper, a questionnaire form will be adopted as the main source of data. Eleven important barriers have been selected in this research. The selection was made through a deep comprehensive literature review, published articles, and other resources, as well as face-to-face interviews with engineers, experts involved in the process of building and construction and some expert academic parties. Table 1 below shows the selected BIM barriers according to previous researchers.

Regarding the design of the questionnaire, all information that could help in achieving the study objectives was collected, reviewed and formalized to be appropriate for the survey study. The first part of the questionnaire inquires the respondent's general information like experience, knowledge, and positions in the AEC industry. While the second part, which is the core of the survey, investigates the impact of each of the selected barriers on BIM implementation in Iraq. The importance of these barriers depends on the three points scale, where (3 = high), (2 = moderate) and (1 = low). After collecting of data, they will be analyzed using the statistical packaging for social science (SPSS) software version 25 Microsoft Excel.

The questionnaire was distributed personally and by email to 75 members of the top and middle management in different construction companies, and different other specialists in the field of the construction industry. Only 63 valid questionnaires were received and analyzed with a response ratio of 84%.

Table (1) The selected BIM barriers according to previous researchers.

	References \ Barriers	B1	B2	B3	B4	B5	B6	B7	B8	B9	B10	B11
1	(Chan et al., 2019)	*	*	*				*		*	*	*
2	(Hamada et al., 2016)	*	*								*	*
3	(Hamada et al., 2016a)		*	*	*	*	*		*		*	*
4	(AWAD, 2017)			*		*		*		*		*
5	(Babatunde et al., 2019)		*	*			*	*		*	*	*
6	(Banawi, 2017)			*			*	*	*			
7	(Sardroud et al., 2018)		*	*	*	*		*	*	*		
8	(Saleh, 2015)	*	*	*	*	*	*	*			*	*
9	(Kiani et al., 2015)	*	*			*					*	*
10	(Hosseini et al., 2015)		*	*			*			*	*	*
11	(ALHUMAYN et al., 2017)	*				*			*	*	*	*
12	(BEKR, 2017)	*	*						*	*	*	
13	(Shaban and Elhendawi, 2018)			*	*	*			*	*	*	
14	(Beitelmal et al., 2017)				*		*		*	*	*	
15	(Al-Zwainy et al., 2017)		*	*	*	*		*	*		*	
16	(Matarneh and Hamed, 2017)		*	*	*	*	*			*		*
17	(Yan and Demian, 2008)	*	*	*	*	*						
18	(Newton and Chileshe, 2011)			*	*	*						
19	(Kassem et al., 2012)	*	*	*		*		*			*	
20	(Ku et al., 2011)					*		*	*	*	*	
21	(Kjartansdóttir, 2011)	*		*	*	*						*
22	(Hamidimonazam et al., 2016)	*	*			*			*			*
23	(Thurairajah and Goucher, 2013)			*	*	*	*			*	*	
24	(Ahmed et al., 2014)		*	*	*	*	*		*	*	*	
25	(Kushwaha, 2016)			*		*	*				*	*
26	(Crowley, 2013)			*			*			*		*
27	(Abubakar et al., 2014)		*	*	*	*	*	*	*		*	
28	(Liu et al., 2015)				*	*	*				*	*
29	(Hosseini et al., 2016)	*		*				*		*	*	*
30	(Hamidimonazam et al., 2016)	*	*				*			*		*
	Frequency	**12**	**17**	**21**	**14**	**20**	**14**	**11**	**12**	**17**	**20**	**17**

***B1**: Believing the current used technology is enough. **B2**: People refuse to learn / Social and habitual resistance to change. **B3**: The high cost of training for BIM software. **B4**; The cost of hiring BIM specialists and additional staff. **B5**: The cost of BIM software and the cost of its updates. **B6**: Lack of support / Lack of BIM related investments. **B7**: Uncertainty of the benefits of BIM implementation. **B8**: Traditional methods of contracting (BIM need special contracting conditions). **B9**: Absence or incomplete national standard for BIM. **B10**: Lack of BIM experts. **B11**: Lack of demand from customers or other companies for projects implemented using BIM technologies.*

4. STATISTICAL RELIABILITY

One of the basic requirements in any research paper is maintaining accurate measurements and acceptable results. So, a pilot survey was conducted to check the validity and reliability of the questionnaire form. the researcher performed internal consistency measuring and used Cronbach's alpha as it is one of the most important common methods for testing reliability (Yockey, 2017). the results of internal consistency giving the values of the Spearman's rho correlation and p-values are shown in Table 2. It shows that p-values were less than 0.05 which means that all the items are consistent and valid.

Table (2) Questionnaire's Internal Consistency.

Factor	Correlation Coefficient	P-Value
B1	.650**	0.00
B2	.749**	0.00
B3	.700**	0.00
B4	.731**	0.00
B5	.703**	0.00
B6	.822**	0.00
B7	.722**	0.00
B8	.587**	0.01
B9	.773**	0.00
B10	.777**	0.00
B11	.738**	0.00

**Correlation is significant at the 0.01 level (2-tailed).
*Correlation is significant at the 0.05 level (2-tailed).

Table 3 shows the classifications of reliability according to Cronbach's alpha value. By conducting these methods to test the questionnaire reliability, the result gained by using SPSS 25 showed that the value of Cronbach's alpha is on the good scale, as shown in Table 4 and Table 5 below, which confirm the questionnaires' reliability.

Table (3) Cronbach's alpha Reliability Classifications (Yockey, 2017).

Cronbach's alpha	Degree of reliability
α≥0.9	Excellent
0.9>α≥0.8	Good
0.8>α≥0.7	Acceptable
0.7>α≥0.6	Questionable (Moderate)
0.6>α≥0.5	Poor
0.5>α	Unacceptable

Table (4) Cronbach's alpha Reliability.

Case Processing Summary

		N	%
Cases	Valid	63	100.0
	Excluded[a]	0	.0
	Total	63	100.0

a. Listwise deletion based on all variables in the procedure.

Table (5) Cronbach's alpha Reliability.

Reliability Statistics

Cronbach's Alpha	N of Items
.907	11

5. DATA ANALYSIS METHOD

In terms of data analysis, the analyzed data including the descriptive analysis shows (frequencies, means,) and relativity importance index (RII) will be used to rank (R) each selected factor questionnaire. The effectiveness index will be calculated for the data collected using the below formula (Saleh, 2015).

$$\boldsymbol{RII = \frac{\Sigma W}{A * N}} \ldots\ldots\ldots\ldots\ldots\ldots\ldots\ldots\ldots\ldots\ldots .(\mathbf{1})$$

where

W: The weight given by respondents for each component (ranging from 1 to 3);

A: Represents the highest weight (which equals 3);

N: Represents the total number of respondents.

6. RESULTS AND DISCUSSION

6.1. RESPONDENTS' PROFILE

The characteristics of target respondents are presented in Table 6 gives the percentage of each category, while Figure 1 shows the percentage of respondent's knowledge about BIM.

Table (6) Cronbach's alpha Reliability Classifications (Yockey, 2017)

Information	Categories	Percentage (%)	Information	Categories	Percentage (%)
Sector	Public	49.2	Group (Job)	Designer	19.0
	Private	19.0		Consultant	30.2
	both sectors	31.7		Project manager	7.9
Gender	Male	76.2		Site engineer	39.7
	Female	23.8		Other	3.2
Age (years)	21 – 30	11.1	Use of BIM	Yes	9.5
	31 – 40	39.7		No	90.5
	41 – 50	17.5	Use of CAD	Don't use the CAD	9.5
	More than 51	31.7		Use only 2D CAD	63.5
Academic qualification	Diploma	3.2		Use only 3D CAD	1.6
	Bachelor	69.8		Use both 2D & 3D	25.4
	Master	6.3	Software	Autodesk AutoCAD	40.6%
	Ph.D.	19.0		SKETCH UP	9.8%
	Other	1.6		MS EXCEL	24.1%
Specialization	Architect	27.0		MS PROJECT	4.5%
	Civil	66.7		PRIMAVERA	1.5%
	Electrical	1.6		REVIT structural	3.8%
	Mechanical	4.8		REVIT architecture	6.8%
Practical experience	≤ 5	7.9		ARCHICAD	2.3%
	6 – 15	42.9			
	16 – 25	28.6		3D MAX	6.8%
	More than 26	20.6			

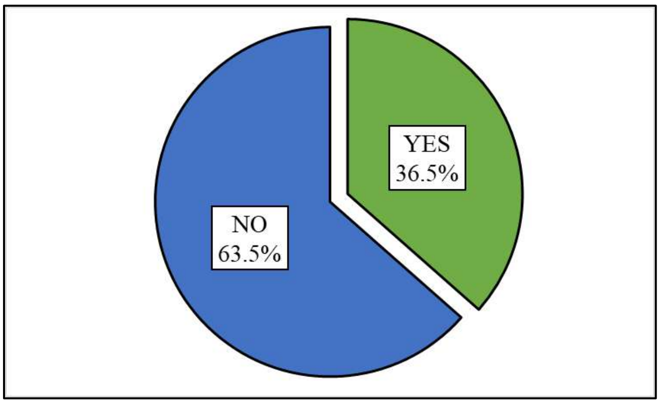

Figure 1: Respondent's Knowledge about BIM Technique

Table 6 shows the description of the participants in this study. The results obtained from the questionnaire show that, 49.2% of respondents working in the public sector, 19.0% work in private sector while the rest of them work in both sectors. Males represent 76.2% of the respondents, 39.7% of the participants were aged (31 – 40) years old, 69.8% has a bachelor's degree, 66.7% were civil engineers, 30.2% were consultants and 42.9% have a (6 – 15) years of experience. The survey showed that around 9.5% of participants use BIM technology, in other words, they use only a few parts of the BIM technique like cost estimation. Only 6.8% and 3.8% using REVIT architecture and REVIT structural respectively, and around 2.3% using ARCHICAD which are BIM-based software. By asking the respondent, have you ever heard of the applications and solutions of BIM? the results showed that only 36.5% of them know about BIM, see Figure 1. Moreover, the source of respondent's knowledge about BIM is represented in Table 7 below.

Table (7) Respondents' source of knowledge about BIM.

Source of Respondent's knowledge about BIM	Read researches related to BIM	51.4%
	participated in conferences or meetings related to BIM	17.1%
	part dealt with in my university	11.4%
	I am training on the use of the BIM programs individually	17.1%
	Other	2.9%

6.2. CHALLENGES (BARRIERS) FACING BIM IMPLEMENT IN IRAQ

Table 8 shows the results of the most eleven selected barriers to the implementation of BIM technology in Iraq. it shows the values of the mean, standard deviation, relative importance index RII and the ranking for each Barrier. The values of the relative importance index are ranged from 0.63 to 0.8. B6 and B11, (Lack of BIM related investments and Lack of demand from customers or other companies for projects implemented using BIM technologies) are in the first position and they almost have the same value of RII which equals 0.79 and 0.8 respectively. The last item in the ranking list is for B1(believing the currently used technology is enough) with RII of 0.63. The values of mean were ranger from 1.9 to 2.4, the highest value of mean is for B11 as it ranked first in this part of the survey. In terms of coefficient of variation, the values of standard deviation indicate a good relationship between the data for which it ranges from 0.73 to 0.82.

The absence or incomplete national BIM standard (B9) is another high effected barrier to BIM implementation. Creating and forming such standard needs top support from authorities (i.e. government and engineering union) in Iraq. It is essential to develop such standards to follow up on the development of the AEC industry around the globe including the Middle East region. Egypt for example, as a Middle Eastern country, created its BIM standards and published it in 2018 to control and regulate the implementation of BIM techniques in their AEC industry (EGBIMC, 2019). On the other hand, lack of BIM experts barrier is so related to the social resistance to change with the lack of support and demand as well as the time, cost and effort needed for the training on BIM related software. The uncertainty of the benefits provided by the application of BIM technique has a significant influence on AEC stakeholder refusal to change, this is why most of the respondents are unwilling to spend time and money to train on BIM software. All the barriers reviewed in this paper are related to each other in a way or another.

It is important to inform engineers and authorities in the Iraqi AEC industry by the benefits of the BIM applications to overcome these barriers. It must be noted that BIM benefits cannot be shown by another Questionnaire survey, but it needs to be supported with a real case study. Education is vital to create a new generation of engineers that are willing to operate advance technologies and methods in the AEC industry. The barriers related to costs were ranked 8, 9, and 10 in this survey. This means if authorities are convinced to support and demand the implementation of BIM techniques, the cost factor will not be a serious issue that stops BIM application. If they realize the amount of the benefits gained out of BIM implementation, the number of monies will be willingly spent on the training and implementation.

(2018a) find that the cultural and the financial issues come in as the highest challenges that face BIM implementation. To summarize the comparison with the previous studies mentioned in Table 1 earlier, the data were applying in SPSS software to calculate the percentage of each selected factor over these papers. Figure 2 below expresses the comparison of the chosen barriers between its percentage in the previous studies and RII percentage this paper.

It is clearly noticed that the barrier coded B4 which stands for the cost of hiring BIM specialists and additional staff is high compared with its percentage in analyzed previous studies. Through the literature review, it can be said that the low percentage of this barrier is because all of them have BIM specialists already, so there is no need to hire additional staff (i.e. only a few members if needed) compared with the situation in Iraq.

Table (8) Challenges (Barriers) on BIM Implementation in Iraq.

No.	Items	Mean	SD	RII	Rank
B1	Believing the current used technology is enough	1.94	0.82	0.63	11
B2	People refuse to learn / Social and habitual resistance to change	2.19	0.74	0.73	5
B3	The high cost of training for BIM software	2	0.76	0.67	8
B4	The cost of hiring BIM specialists and additional staff	1.95	0.71	0.65	9
B5	The cost of BIM software and the cost of its updates	1.9	0.78	0.65	10
B6	Lack of support / Lack of BIM related investments	2.38	0.75	0.79	2
B7	Uncertainty of the benefits of BIM implementation	2.03	0.82	0.68	7
B8	Traditional methods of contracting (BIM need special contracting conditions)	2.13	0.83	0.71	6
B9	Absence or incomplete national standard for BIM	2.32	0.78	0.77	3
B10	Lack of BIM experts	2.24	0.80	0.75	4
B11	Lack of demand from customers or other companies for projects implemented using BIM technologies	2.4	0.73	0.80	1

By comparing the results gained by this paper with the results of the previous studies showed earlier, there are consistent with the results of Hatem et al. (2018). Poor efforts by the government on BIM implementation comes in the first position followed by a lack of experts and poor knowledge of BIM. Gerges et al. (2017) showed that resistance of change and the belief in the efficiency of the currently used technology come in the first position among all barriers. Lack of BIM experts and lack of demand comes in the second and third positions while Sardroud et al.

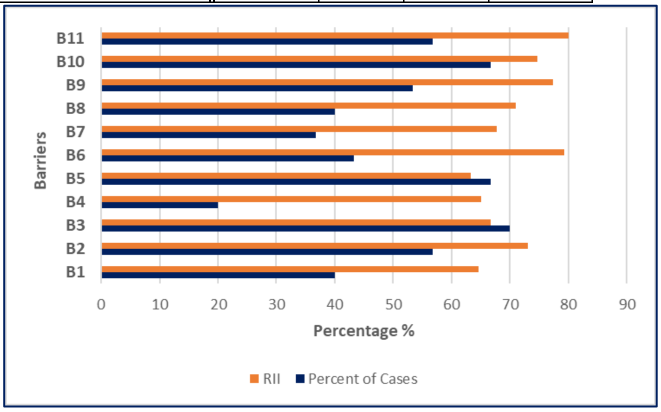

Figure 2: Comparison of Barriers between its Percentage on Previous Studies and this Paper

By comparing this to B10 "lack of BIM experts", it can conclude that more BIM specialists are always needed to improve the application of this technology and use it on a wide range (i.e. including it in all project types in the AEC industry).

7. CONCLUSIONS AND RECOMMENDATIONS

This paper studied the barriers and challenges facing the implementation of BIM techniques. The barriers were discussed through a comprehensive literature review and extended face-to-face interviews with the specialist in the AEC industry. The results of the questionnaire prepared for the study were analyzed, and the results showed that Lack of demand on using BIM technique and Lack of BIM related investments (Lack of support) are the most effective barriers in the Iraqi AEC industry. Regardless of believing that new methods must be adopted in the industry, yet there is no support from authorities towards implementing new techniques, whether financial or any other types of support.

It is essential to develop a national standard for BIM technology to follow up improvements and to reduce the gap between Iraq and at least the Middle Eastern countries in the term of AEC industry. Lack of knowledge about this technique and the benefits of its application plays a vital role in the implementation of BIM in Iraq. More effort must be taken by authorities to overcome these barriers to improve the AEC industry in Iraq.

Based on the previously identified conclusions, the results obtained from this research, and the comments of respondents through interviews and the questionnaire survey, the following points can be recommended:

- Develop systems and laws to meet the highest international standards for the optimal use of modern technology.
- Develop rules and regulations towards the application of BIM techniques.
- The use of (employ) experts and consultants to assist ministries and government departments in preparing the appropriate plan for the implementation of BIM technology.
- Organizing events, conferences, and exhibitions that promote the benefits of BIM technology.
- Include BIM technology in the engineering curriculum.
- Develop a national standard for BIM technology.

Acknowledgment:

I would like to express my genuine thankfulness and gratitude especially to *Prof. Dr. Maad Mahdi* for his support. Appreciation is devoted to *Al-Qatif Engineering Bureau* and its director consultant Engineer *Mr. Ali Salman*, for his guidance, advice, and cooperation who have made the accomplishment of this paper possible.

References

ABUBAKAR, M., IBRAHIM, Y., KADO, D. & BALA, K. (2014). Contractors' perception of the factors affecting Building Information Modelling (BIM) adoption in the Nigerian Construction Industry. Computing in civil and building engineering (2014).

AHMED, S. (2018). Barriers to Implementation of Building Information Modeling (BIM) to the Construction Industry: A Review. Journal of Civil Engineering and Construction, 7, 107-107.

AHMED, S. M., EMAM, H. H. & FARRELL, P. (2014) Barriers to BIM/4D implementation in Qatar. The 1st international conference of cib middle east & north africa conference, 2014. 533-547.

AL-ZWAINY, F., MOHAMMED, I. A. & AL-SHAIKHLI, K. A. (2017). Diagnostic and assessment benefits and barriers of BIM in construction project management. Civil Engineering Journal, 3, 63-77.

ALHUMAYN, S., CHINYIO, E. & NDEKUGRI, I. (2017). The barriers and strategies of implementing BIM in Saudi Arabia. WIT Transactions on The Built Environment, 169, 55-67.

AWAD, I. (2017). BUILDING INFORMATION MODELING (BIM) Principles, Usage, Benefits and Challenges for its application in the Kingdom of Saudi Arabia (KSA. The British University in Dubai (BUiD).

BABATUNDE, S. O. & EKUNDAYO, D. (2019). Barriers to the incorporation of BIM into quantity surveying undergraduate curriculum in the Nigerian universities. Journal of Engineering, Design Technology, 17, 629-648.

BANAWI, A. (2017) Barriers to implement building information modeling (BIM) in public projects in Saudi Arabia. International Conference on Applied Human Factors and Ergonomics, 2017. Springer, 119-125.

BEITELMAL, W., MOLENAAR, K. R., JAVERNICK-WILL, A. & PELLICER, E. (2017). Challenges and barriers to establishing infrastructure asset management: A comparative study between Libya and the USA. Engineering, Construction Architectural Management, 24, 1184-1202.

BEKR, G. A. (2017). EXPLORING BARRIERS IN IMPLEMENTING BUILDING INFORMATION MODELING: A PRELIMINARY STUDY.

BOTH, P. V. (2012). Potentials and barriers for implementing BIM in the German AEC market: results of a current market analysis.

CHAN, D. W., OLAWUMI, T. O. & HO, A. M. (2019). Perceived benefits of and barriers to Building Information Modelling (BIM) implementation in construction: The case of Hong Kong. Journal of Building Engineering, 25, 100764.

CROWLEY, C. (2013). Identifying opportunities for quantity surveyors to enhance and expand the traditional quantity surveying role by adopting building information modelling. CITA BIM Gathering, Dublin, Ireland.

EASTMAN, C., TEICHOLZ, P., SACKS, R. & LISTON, K. (2011). BIM handbook: A guide to building information modeling for owners, managers, designers, engineers and contractors, John Wiley & Sons.

EGBIMC (2019). the Egyptian code for building information modeling (BIM). G01.

EGYPTIAN, R. (2017). Application of BIM in the Middle East [Online]. Available: https://www.egyres.com/تطبيق-الـbim--في-بلدان-الشرق-الأوسط/ [Accessed 20-Dec 2018].

GERGES, M., AUSTIN, S., MAYOUF, M., AHIAKWO, O., JAEGER, M., SAAD, A. & GOHARY, T.-E. (2017). An investigation into the implementation of Building Information Modeling in the Middle East. Journal of Information Technology in Construction (ITcon), 22, 1-15.

HAMADA, H., HARON, A., ZAKIRIA, Z. & HUMADA, A. (2016a). Benefits and Barriers of BIM Adoption in the Iraqi Construction Firms. International Journal of Innovative Research in Advanced Engineering, 3, 76-84.

HAMADA, H. M., HARON, A. T., ZAKARIA, Z. & HUMADA, A. M. (2016b) Challenges and Obstacles of Adoption BIM Technology in the Construction Industry in Iraq. The National Conference for Postgraduate Research, 2016b. 43-8.

HAMIDIMONAZAM, H., HOSSEINI, M. R. & ZAERI, F. (2016). Barriers to adopting building information modelling (BIM) within South Australian small and medium sized enterprizes. Project Management Development—Practice Perspectives, 125-132.

HASAN, A. N. & RASHEED, S. M. (2019). The Benefits of and Challenges to Implement 5D BIM in Construction Industry. Civil Engineering Journal, 5, 412-421.

HATEM, W. A., ABD, A. M. & ABBAS, N. N. (2018). Barriers of Adoption Building Information Modeling (BIM) in Construction Projects of Iraq. Engineering Journal, 22, 59-81.

HOSSEINI, M., NAMZADI, M., RAMEEZDEEN, R., BANIHASHEMI, S. & CHILESHE, N. Barriers to BIM adoption: Perceptions from Australian small and medium-sized enterprises (SMEs). AUBEA (2016): Proceedings of the 40th Australasian Universities Building Education Association Annual Conference, (2016). Central Queensland University, 271-280.

HOSSEINI, M. R., AZARI, E., TIVENDALE, L. & CHILESHE, N. Barriers to adoption of building information modeling (BIM) in Iran: Preliminary results. The 6th International Conference on Engineering, Project, and Production Management (EPPM2015), Gold Coast, Australia, 2015.

KASSEM, M., BROGDEN, T. & DAWOOD, N. (2012). BIM and 4D planning: a holistic study of the barriers and drivers to widespread adoption. Journal of Construction Engineering Project Management, 2, 1-10.

KIANI, I., SADEGHIFAM, A. N., GHOMI, S. K. & MARSONO, A. K. B. (2015). Barriers to implementation of Building Information Modeling in scheduling and planning phase in Iran. Australian Journal of Basic Applied Sciences, 9, 91-97.

KJARTANSDÓTTIR, I. B. (2011). BIM adoption in Iceland and its relation to lean construction.

KU, K. & TAIEBAT, M. (2011). BIM experiences and expectations: the constructors' perspective. International Journal of Construction Education Research, 7, 175-197.

KUSHWAHA, V. (2016). Contribution of building information modeling (BIM) to solve problems in architecture, engineering and construction (AEC) industry and addressing barriers to implementation of BIM. Int. Res. J. Eng. Technol, 3, 100-105.

LIU, S., XIE, B., TIVENDAL, L. & LIU, C. (2015). Critical barriers to BIM implementation in the AEC industry. International Journal of Marketing Studies, 7, 162-171.

MAHDI, M. M. & ALI, N. S. (2019). Reducing Waste of Construction Materials in Civil Engineering Projects In Iraq. J ZANCO Journal of Pure Applied Sciences, 31, 257-263.

MATARNEH, R. & HAMED, S. (2017). Barriers to the adoption of building information modeling in the Jordanian building industry. Open Journal of Civil Engineering, 7, 325.

NEWTON, K. & CHILESHE, N. (2011). Enablers and barriers of building information modelling (BIM) within South Australian construction organisations. University of New South Wales.

PENTTILÄ, H. (2006). Describing the changes in architectural information technology to understand design complexity and free-form architectural expression. Journal of Information Technology in Construction, 11, 395-408.

SALEH, M. A. D. (2015). Barriers and Driving Factors for Implementing Building Information Modelling (BIM) in Libya. Eastern Mediterranean University (EMU)-Doğu Akdeniz Üniversitesi (DAÜ).

SARDROUD, J. M., MEHDIZADEHTAVASANI, M. & AMIN KHORRAMABADI, A. (2018a). Barriers Analysis to Effective Implementation of BIM in the Construction Industry.

SARDROUD, J. M., MEHDIZADEHTAVASANI, M., KHORRAMABADI, A. & RANJBARDAR, A. (2018b) Barriers Analysis to Effective Implementation of BIM in the Construction Industry. ISARC. Proceedings of the International Symposium on Automation and Robotics in Construction, (2018b). IAARC Publications, 1-8.

SHABAN, M. H. & ELHENDAWI, A. (2018). Building Information Modeling in Syria: Obstacles and Requirements for Implementation.

THURAIRAJAH, N. & GOUCHER, D. (2013). Advantages and challenges of using BIM: A cost consultant's perspective.

ULLAH, K., LILL, I. & WITT, E. (2019) An Overview of BIM Adoption in the Construction Industry: Benefits and Barriers. 10th Nordic Conference on Construction Economics and Organization, (2019). Emerald Publishing Limited, 297-303.

WALI, K. I. & OTHMAN, S. A. (2019). Schedule Risk Analysis Using Monte Carlo Simulation for Residential Projects. J ZANCO Journal of Pure Applied Sciences, 31, 90-103.

YAN, H. & DEMIAN, P. (2008). Benefits and barriers of building information modelling.

YOCKEY, R. D., (2017). SPSS Demystified: A Simple Guide and Reference, 2nd ed. 2017, United Kingdom: Taylor & Francis, (2017). https://books.google.iq/books?id=m6Q5DwAAQBAJ

ZANCO Journal of Pure and Applied Sciences
The official scientific journal of Salahaddin University-Erbil
https://zancojournals.su.edu.krd/index.php/JPAS

ISSN (print):2218-0230**, ISSN (online):** 2412-3986**, DOI: http://dx.doi.org/10.21271/zjpas**

RESEARCH PAPER

Investigation of the Microstructure and Wear Properties of AISI 304 Steel Friction Weldments

Jwan Khalil Mohammed[1], Ramadhan H Gardi[2], Dlair O. Ramadan[3]

[1]. Department of Technical Mechanical and Energy Engineering, Erbil Technical Engineering College, Erbil Polytechnic University, Erbil, Iraq
[2] Department of Mechanical and Mechatronics Engineering, College of Engineering, Salahaddin University-Erbil, Kurdistan Region, Iraq
[3] Department of Technical Mechanical and Energy Engineering, Erbil Technical Engineering College, Erbil Polytechnic University, Erbil, Iraq

A B S T R A C T:

In this study, a rotary friction welding technique was used to join austenitic stainless-steel grade AISI 304. The effect of different forging pressure (192.4, 240.5, 288.6 and 384.8 *MPa*) on wear resistance of AISI 304 were examined using a modified pin on disc tester. The microstructure of the AISI 304 was examined as well using an optical microscope. The wear resistance results of the welded specimens were reported better than as received. The variation of increasing wear loss was uniformly changed with sliding distance. Further, it was noted from the experiments that the wear rate increased with increasing forging pressure in which the minimum wear rate was 3 mm^3 at 192.4 *MPa* while a maximum wear rate (25.823 mm^3) occurs at a forging pressure of 384.8 *MPa*. This is due to the microstructure changes which is decreasing grain size and formation of twin grains and also precipitating carbides.

KEY WORDS: Rotary friction welding; Wear rate; Austenitic stainless steel 304; Microstructure; Surface roughness
DOI: http://dx.doi.org/10.21271/ZJPAS.32.4.7
ZJPAS (2020) , 32(4);58-65.

1.INTRODUCTION:

Stainless steels are widely used in various areas in practical applications such as nuclear, chemical and petrochemical industries (Ramirez et al., 2011). Stainless steels which are identified by iron-based alloys containing 8 to 25% nickel and 12 to 30% chromium (Barzinjy, 2016). Generally, there are several types of stainless steels including martensitic, ferritic, austenitic, duplex and precipitation hardening stainless steels (Kirik and Özdemýr, 2015). It is widely utilized in the liquid-handling system and hydraulic machinery due to excellent corrosion resistance, good machinability, low cost and weld-ability (Chiu et al., 2005; Samir A. and Gardi, 2017) and energy-absorption ability (Zhang et al., 2019).

*__Corresponding Author:__
Jwan Khalil Mohammed
E-mail: jwan.eng@hotmail.com
Article History:
Received: 09/01/2020
Accepted: 08/03/2020
Published: 08/09/2020

The AISI-304 is a most common steel among the austenitic stainless steels because of superior corrosion resistance in chemical environments and applicability in various areas, including automotive, food, chemical, nuclear power, energy source, marine transport, petrochemical, military (Hu et al., 2019; Naeem et al., 2019) and liquefied natural gas storage at cryogenic temperatures (Jia et al., 2020). Since, the wear is one of the most common industrial issues which encountered engineering assemblies and components. It diminishes the working efficiency by increasing the fuel usage, material losses and the rate of component replacement (Radhika et al., 2015). In addition, the welding is the other problem for joining materials due to changing the mechanical property of the materials internal strain, slag, pores, and sensitization phenomenon (Almanza-Casas et al., 2011) and tender intermetallic phases (Mercan et al., 2015). However, the 304 austenitic stainless steel (AISI 304 ASS) is a non-ferromagnetic alloy with high toughness and plasticity but owning poor wear resistance (Zhao et al., 2018) when it is welded. Due to formation of intergranular chromium carbides (Park et al., 2004). For the reason that friction welding is a much more preferable rout to join the austenitic stainless steel. Rotary friction welding is a solid-state welding process which used for joining the similar and dissimilar round bar materials. The joint is produced due to the generating heat between two contacted workpieces in which one is fixed and the other rotated with a certain speed. The plastic deformation is produced due to applying the axial force through the stationary side. Thereafter, applying the upset force when the sufficient heat is produced (Akbarimousavi and Goharikia, 2011).

In 2018, Zhao *et al.* examined the wear resistance and corrosion resistance of resistance of the AISI 304 ASS using liquid nitrocarburization technique. Their results showed that both the wear and corrosion resistance of nitrocarburized 304 stainless steel were increased as compare to the non-nitrocarburized one (Zhao et al., 2018). In the same year, Krishna Kumar *et al.* investigated the wear resistance and hardness of AISI 304 by surface alloying process using heat generated gas tungsten arc source. They heated the surface of austenitic stainless samples for 6 *h* in the furnace. The authors revealed that the hardness was increased and wear resistance decreased after the heat treatment process (Krishna Kumar et al., 2018). In addition, Chattrakul and Sornsuwit, (2018) studied the effects of surface appearance, chemical composition and direction of AISI 304, AISI 304L stainless steel and nylon wire on wear resistance of polymer-metal interface. They realized that the sliding direction and surface roughness was more effective than chemical composition of AISI 304 and 304L stainless steel on wear rate. The authors considered that this result is referring to the amount of the contact area and displacement between austenitic stainless steel and nylon wire during the sliding. The authors concluded that the increase in roughness was increased wear rate in parallel direction but decreased it in perpendicular direction. However, in both directions the wear resistance of stainless steel 304 is less than 304L except in case of 1 μm surface roughness (Chattrakul and Sornsuwit, 2018). In 2019, Palanikumar *et al.* evaluated the effect of sliding speed and the temperasture change on the coefficient of friction at the contact interface of AISI 304 austenitic stainless-steel alloys in which subjected to full sliding. Their work was done using a rotatory type pin on disk tribometer. The authors found that the coefficient of friction decreased with increase in sliding speed at full sliding experiments. The sliding experiments results showed that the friction coefficient decreased with increase in sliding speed where the friction coefficient was in the range (0.15–0.28). They observed that during sliding the temperature at the contact interface was increased in the result of increasing in friction at the contact interface (Palanikumar et al., 2019).

During decades ago, a number of studies have been done on wear resistance for different welded methods and materials. However, the majority of attempts have been examined for friction stir welded materials. Unfortunately, there is no study on the literature into the investigation on wear resistance of rotary friction welded joints for the AISI 304 ASS. Therefore, the main aim of the current paper is evaluating the experimental investigation into the wear resistance of austenitic stainless steel AISI 304 with using rotary friction welding.

2.MATERIALS AND METHODS

2.1 Materials

The experiments were conducted on austenitic stainless steel (*AISI 304*) rod. To measure the wear, a duplex stainless steel (SAF 2205) with a hardness of (293 HB), which is higher than the hardness of AISI 304 (123 HB), was used. **Error! Reference source not found.** show the chemical composition. Whereas, **Error! Reference source not found.** provides the mechanical properties of both materials.

Material Type	Elements (wt.%)									
	C	Si	Mn	P	S	Cr	Ni	Mo	N	Fe
AISI 304 Stainless Steel	0.054	0.38	1.67	0.036	0.024	8.2	8	-	0.1	Balance
SAF 2205 Duplex Stainless Steel	0.03	1	2	0.03	0.015	22	5	3.2	0.18	Balance

Table (1) Nominal Chemical Composition

Table (2) Mechanical properties of the both materials

	Yield Strength (MPa)	Ultimate Strength (MPa)	Hardness (HB)	Modulus of Elasticity (GPa)	Melting Range (°C)
AISI 304 Stainless Steel	215	505	123	129	1400-1450
SAF 2205 Duplex Stainless Steel	450	655	293	200	1410-1465

2.2 Experimental Machine Setup and Procedure

The AISI 304 rod was machined to a 15 *mm* diameter using a lathe machine. Then the rod was cut to two different lengths including 60 *mm* and 40 *mm*. The larger workpiece length (60 *mm*) was kept on the stationary chuck of the lathe machine while the smaller length (40 *mm*) was kept on the rotating chuck. To achieve a good welding process, the contact faces of the two mate rods were pre-machined not only to get a smooth surface and to remove the oxide from the surfaces but also to avoid the bending by ensuring a perpendicular contact between the two mated rods.

2.3 Friction Welding Process

The welding process was conducted on a lathe machine. In the rotary friction welding, the most impacting parameters are friction pressure, rotational speed, friction time and forging pressure. In this work, four different forging pressures, (192.4, 240.5, 288.6 and 384.8 *MPa*) were employed to accomplish the welding process. The process was performed by adding a friction pressure of 192.4 *MPa* at the stationary side against the rotational side. Then the forging pressures 192.4 *MPa* was added straight away after stopping the machine. The same procedure was repeated for 240.5, 288.6 and 384.8 *MPa* forging pressures, respectively. It is worth to note that all the welding experiments were conducted at a constant rotation speed of 560 *RPM*, and a constant friction time of 60 *s*. The appearances of the friction welded butt joint of the specimens have been shown in **Error! Reference source not found.**.

Below are some investigations which have been performed to investigate the effects of the welding parameters on the wear, microstructure and the surface roughness of the welded joints.

Figure 1: Friction Welded Specimens at Forging Pressure is (a) 192.4 MPa, (b) 240.5MPa, (c) 288.6 and (d) 384.8 MPa.

2.4 Microstructure

The microstructure of the welded joints was investigated using an optical microscope. The microstructure samples were prepared and flattened using a disc and grinding/polishing machine. The specimens were grinded dry using Al_2O_3 emery papers with a different grades grit including 320, 800 and 1000 grits. The grinded specimens were then polished with a light cloth. Finally, the polished samples were etched, using a solution which prepared according to the ASTM E407 standard, with (HCl +$FeCl_3$+ HNO_3+ distilled water) for 2.5 minutes.

2.5 Measuring Wear

Wear tests were performed using a modified pin-on-disc tester [Model: TE91/1, Pin on Disc Model, Serial No.: U 9259/3, TQ]. The pin was made from the *AISI 304* welded joints in the axial direction of the friction welded joint while the counter face rotating disc was made from the duplex stainless steel (SAF 2205). The wear samples were prepared according to the *ASTM: G99-05* standard. The dimension of the pin is 8 *mm* in diameter and 25 *mm* in length while the dimension of the disc is 65 *mm* in diameter. Figure 2 shows a schematic of the modified pin on disc tester. The pin was attached to the stationary side while the disc to the rotation part. The wear tests were conducted at room temperature in a dry condition. A load of 25 *N* was applied on the pin and the linear velocity was 12.5 *m/min*. Thereafter, different distance including 77, 154 and 232 *m* were considered, and wear rate were calculated. A digital scale, with a least count of 0.001*g*, was used to measure the weight of the samples. Thereafter, the surface roughness of disc has been evaluated using Tyler–Hobson surface roughness tester (Talysur-10) at different points with a 0.8 *mm* sensor sliding distance in which perpendicular on the wear track distance.

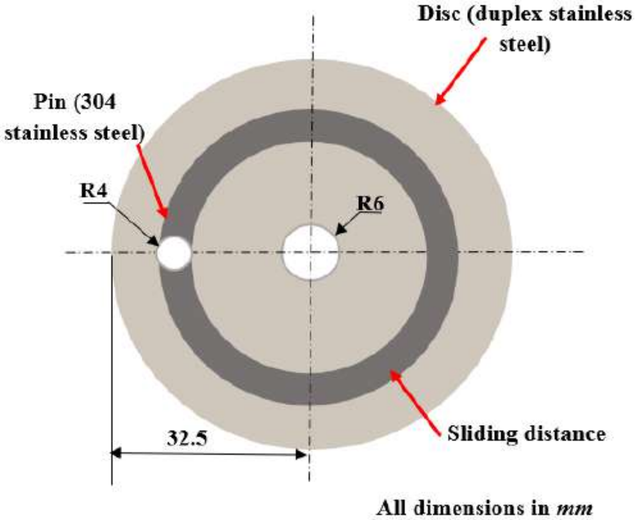

Figure 2: Schematic configuration of the modified pin-on-disk tribometer

1. RESULTS AND DISCUSSIONS

The wear rate of friction welded 304 AISI austenitic stainless steel was conducted for four forging pressure cases (192.4, 240.5, 288.6 and 384.8 *MPa*). The wear rate results were carried out after 2, 4- and 6-min. intervals of time. The wear rate with respect of sliding distance (77, 154 and 232 *m*) for as-received materials is shown in **Error! Reference source not found.**.

In addition, the comparison of wear rate as a function of sliding distance for four pins are shown in the sequence of **Error! Reference source not found.** (a-d), respectively. In addition, the microstructure for welded joints are presented in **Error! Reference source not found.**. Thereafter, the surface roughness of duplex stainless steel SAF 2205 disk for friction welded pins after 6 *min* wear and as-received materials were presented in **Error! Reference source not found.**.

In general, the obtained results revealed that the wear rate are increased with increasing siding distance for both as-received and welded joints. **Error! Reference source not found.** a-d shows the minimum wear rate values (3 mm^3) at 77 *m* sliding distance and maximum was at (25.823 mm^3) 232 *m* sliding distance for all forging pressure cases. This was revealed that the wear rate trends up with increasing sliding distance (from 77 to 154 then 232 *m*). These results are attributed to that at final stage the hard and denies layer of chromium oxide were removed which leads to increasing wear rate. Consistent with this results the previous researcher argued that this was due to the duration of rubbing surface and the reduction of shear strength of the material, which increased the true area of contact between contacting surfaces (Chowdhury et al., 2013) and increasing coefficient of friction (Rana et al., 2016). Furthermore, the study by Naplocha and Kaczmar, (2011) suggested that at dry sliding condition, when the wear rate is changed slowly, the surface layer will produce with changed microstructure and chemical composition. This is due to the formation wear debris from the counterparts, the reinforcing phases, oxides and atmosphere gases.

This study revealed that the wear rate is increased with increasing the forging pressure with constant sliding distance. For instance, the minimum wear rate was recorded (3 mm^3) at a forging pressure of 192.4 *MPa* and a sliding distance of 77 *m* (see **Error! Reference source not found.** a) and this rate increased to its maximum value (9 mm^3) at a forging pressure of 384.8 *MPa* at the same sliding distance. These values were significantly less than the as-received materials which is 23 mm^3 as seen in **Error! Reference**

source not found. at the same sliding distance. This reduction of wear resistance under the effect of forging pressure is attributed to the producing a finer grain size by slicing the grains (twin grains). Further, reducing the hardness in these regions due to the formation carbides in the grain boundaries (**Error! Reference source not found.**). In accordance with this concept the researchers, Thangarasu, Murugan and Dinaharan, in 2014 reported that when the hardness of materials are higher hardness, the lower wear rate will happen, due to increasing the resistance to remove material during sliding.

What is interesting about the data in this study is the friction welding has a significant effect on wear rate. As it can be seen that an excellent improvement of wear resistance was revealed for welded joint compared to as received materials. This improvement is related to microstructure changes at the weld joints such as a great number of twins, the finer grain size at the joints, occurring the two phases (austenitic and ferritic), recrystallizations and large amount of carbides at the grain boundaries as shown in **Error! Reference source not found.** a-d.

The surface roughness of the wear track on the *SAF 2205* duplex stainless steel for as received condition (304 austenitic stainless-steel pin) is measured separately which is 0.9μm. As it can be seen from the graph (**Error! Reference source not found.**), the surface roughness of the disc at a sliding distance of 232 *m*, except the samples at 240.5 *MPa*, are higher as compare to the surface roughness of as-received materials. The surface roughness increased with increasing forging pressure. These results are referring to microstructural changes including creation of different carbides that occurs at joint during welding during heat and plastic deformation. Thus, these results are shows that the correlation between the surface roughness with forging pressure were negatively associated.

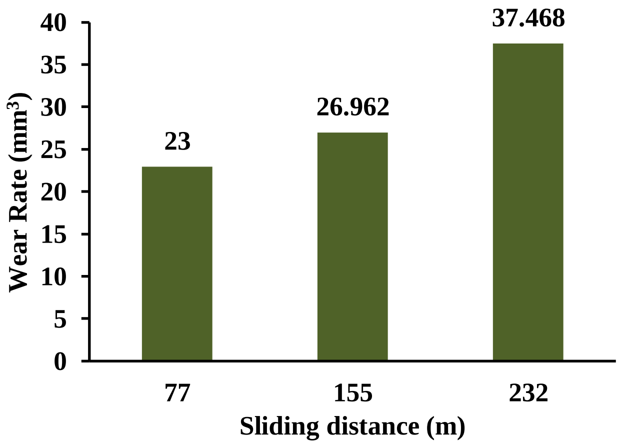

Figure 3: Variation of Wear Rate with Sliding Distance for As-Received Materia

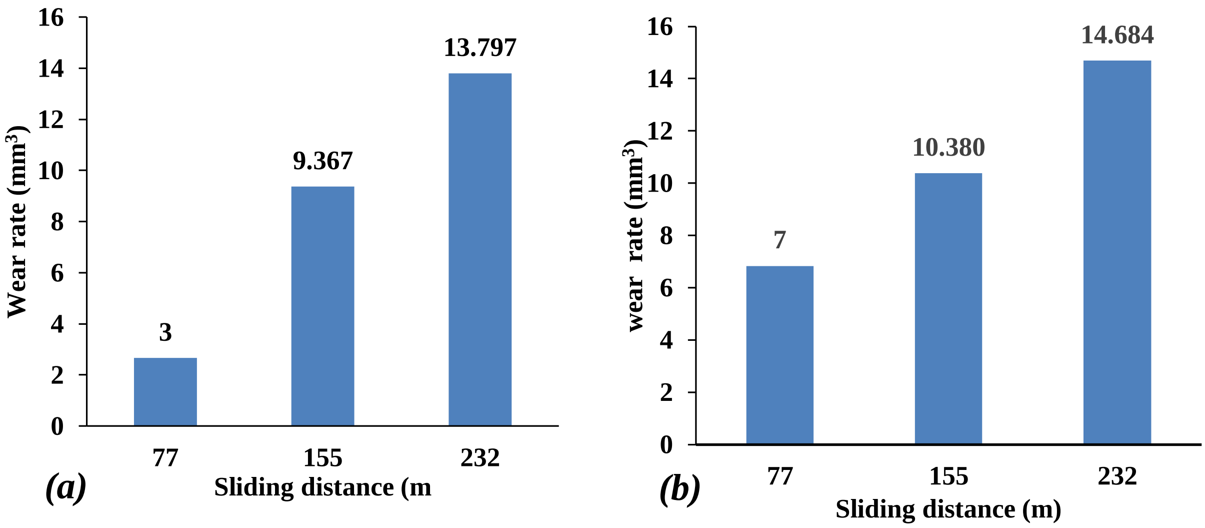

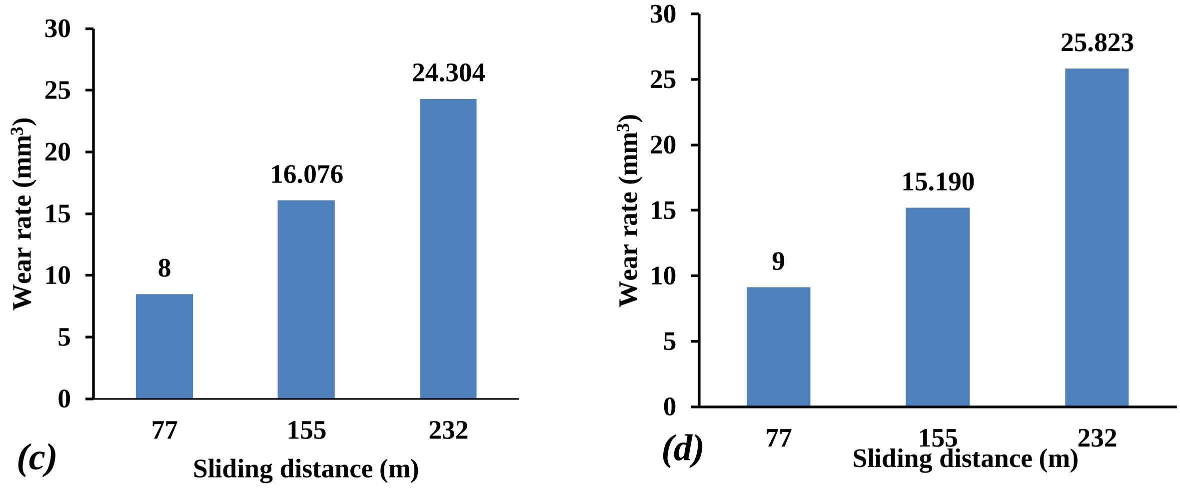

Figure 4: Variation of Wear Rate with Sliding Distance at (a) 192.4 MPa, (b) 240.5 MPa, (c) 288.6 MPa and (d) 384.8 MPa.

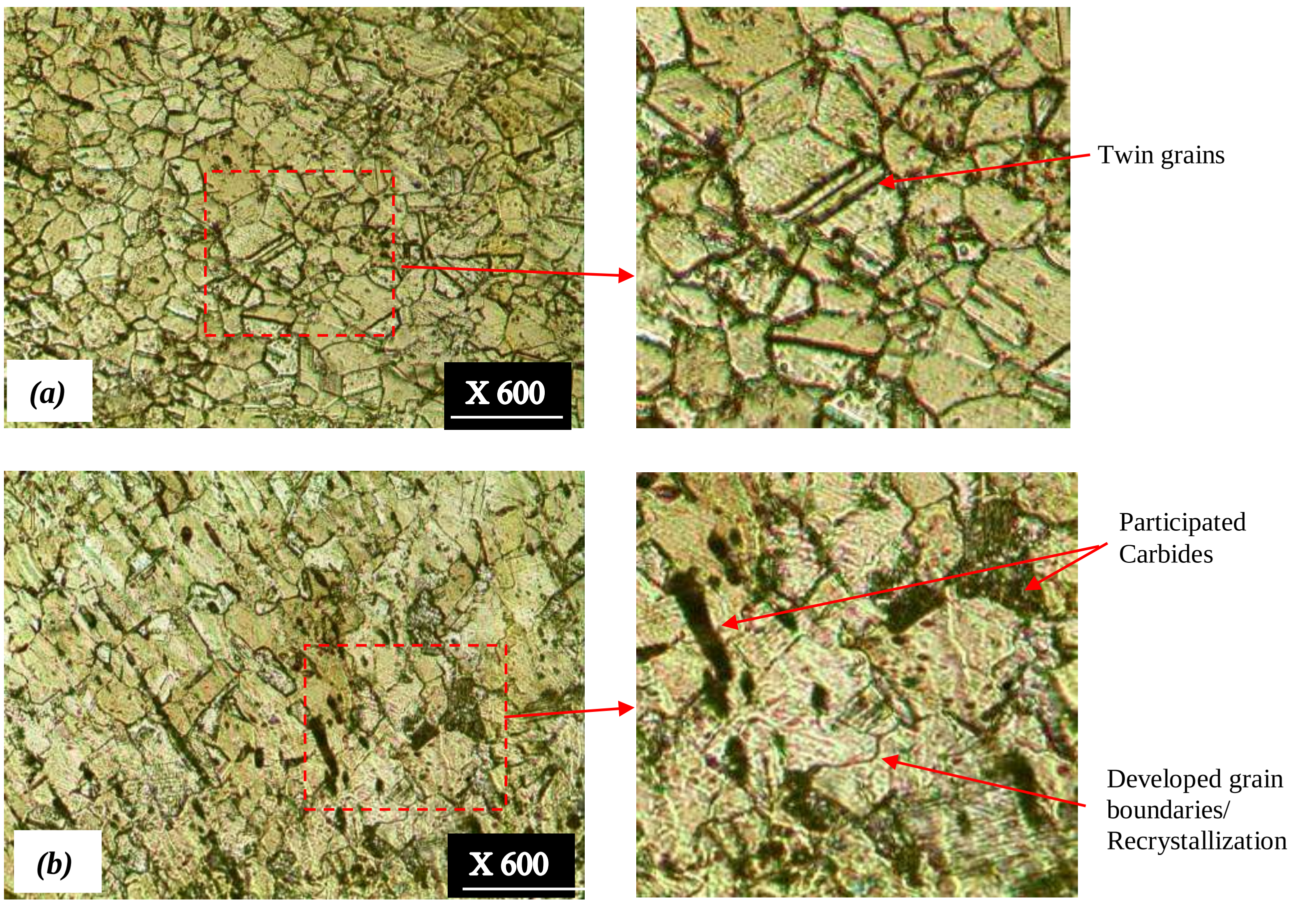

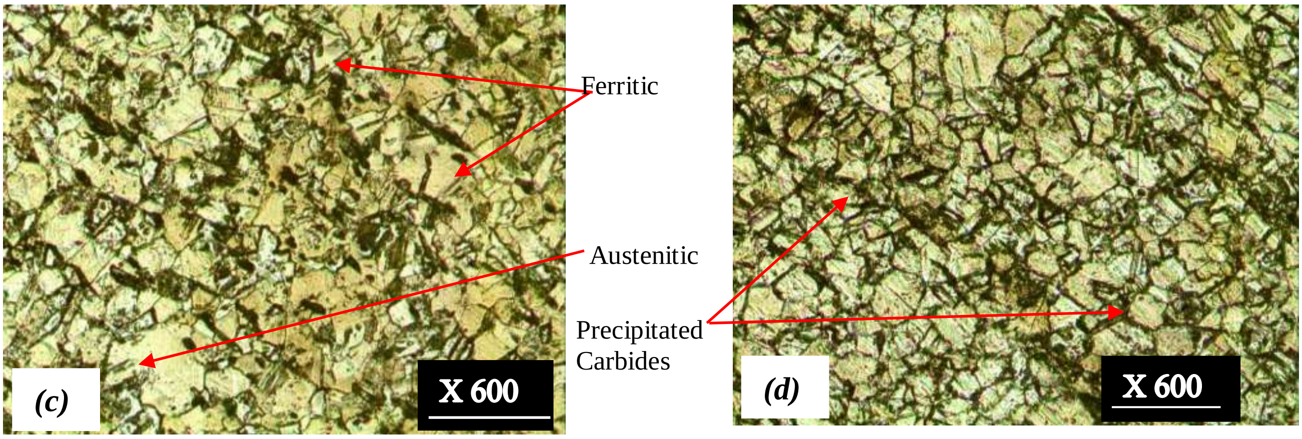

Figure 5: Optical image showing the microstructure of AISI 304 at different forging pressure (a) 192.4 MPa, (b) 240.5 MPa, (c) 288.6 MPa and (d) 384.8 MPa.

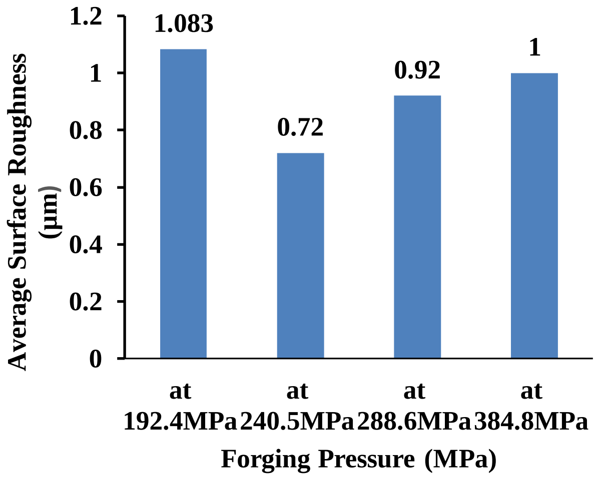

Figure 6: Average Surface Roughness of Disk at Different Forging Pressure Cases.

2. CONCLUSIONS

The aim of the present research was to examine the wear resistance of friction welded joints of AISI 304 ASS. The following conclusions can be drawn from the present study:

1. The friction welding of *AISI 304* austenitic stainless steel improves the wear resistance.
2. The minimum wear rate was 3 mm^3 at 192.4*MPa* forging pressure, while the maximum wear rate was 25.823 mm^3 at 384.8 *MPa* forging pressure.
3. The lowest surface roughness on *SAF 2205 DSS* disc can be obtained when *304 ASS* pin friction welded with 240.5 *MPa* forging pressure.

REFERENCES

Akbarimousavi, S.A.A. and Goharikia, M. (2011), “Investigations on the Mechanical Properties and Microstructure of Dissimilar cp-Titanium and AISI 316L Austenitic Stainless Steel Continuous Friction Welds”, *Materials and Design*, Elsevier Ltd, Vol. 32, pp. 3066–3075.

Almanza-Casas, E., Perez-López, M.J., Steel, R. and Packer, S. (2011), “Evaluation of Mechanical Properties of 304L and 316L Stainless Steels Friction Stir Welded”, *International Offshore and Polar Engineering Conference*, Vol. 8, pp. 530–533.

Barzinjy, A.A.A. (2016), “Electrodeposition of Ni-Cr Alloy from Ethaline Deep Eutectic Solvent”, *ZANCO Journal of Pure and Applied Sciences*, Vol. 28 No. 2, pp. 47–55.

Chattrakul, K. and Sornsuwit, N. (2018), “Study of surface appearance and composition effect on AISI 304 and 304L stainless steel wear against nylon wire”, *Materials Today: Proceedings*, Elsevier Ltd, Vol. 5 No. 3, pp. 9319–9325.

Chiu, K.Y., Cheng, F.T. and Man, H.C. (2005), “Laser Cladding of Austenitic Stainless Steel using NiTi Strips for Resisting Cavitation Erosion”, *Materials Science and Engineering A*, Vol. 402 No. 1–2, pp. 126–134.

Chowdhury, M.A., Nuruzzaman, D.M., Roy, B.K., Dey, P.K., Mostafa, M.G., Islam, M.S. and Mia, M.R. (2013), “Experimental Investigation on Friction and Wear of Stainless Steel 304 Sliding Against Different Pin Materials”, *World Applied Sciences Journal*, Vol. 22 No. 12, pp. 1702–1710.

Hu, B., Liu, Y. and Yu, R. (2019), “Numerical Simulation on Magnetic–Mechanical Behaviors of 304 Austenite Stainless Steel”, *Measurement*, Vol. xxx No. xxxx, p. 107185.

Jia, B., Rusinek, A., Pesci, R., Bahi, S. and Bernier, R. (2020), “Thermo-viscoplastic behavior of 304 austenitic stainless steel at various strain rates and temperatures: Testing, modeling and validation”, *International Journal of Mechanical Sciences*, Elsevier Ltd, Vol. 170, p. 105356.

Kirik, Ý. and Özdemýr, N. (2015), “Effect of Process Parameters on the Microstructure and Mechanical Properties of Friction-Welded Joints of AISI 1040/AISI 3041 Steels”, *Materials and Technology*, Vol. 49 No. 5, pp. 825–832.

Krishna Kumar, M., Saravanan, R., Sellamuthu, R. and Narayanan, V. (2018), “Microstructure, hardness and wear rate of heat treated Titanium surface alloyed

AISI 304 stainless steel", *Materials Today: Proceedings*, Elsevier Ltd, Vol. 5 No. 2, pp. 7571–7576.

Mercan, S., Aydin, S. and Özdemir, N. (2015), "Effect of Welding Parameters on the Fatigue Properties of Dissimilar AISI 2205-AISI 1020 Joined by Friction Welding", *International Journal of Fatigue*, Elsevier Ltd, Vol. 81, pp. 78–90.

Naeem, M., Iqbal, J., Zakaullah, M., Shafiq, M., Mujahid, Z.I., Díaz-Guillén, J.C., Lopez-Badillo, C.M., et al. (2019), "Enhanced wear and corrosion resistance of AISI-304 steel by duplex cathodic cage plasma treatment", *Surface and Coatings Technology*, Vol. 375 No. July, pp. 34–45.

Naplocha, K. and Kaczmar, J.W. (2011), "Wear Mechanisms of Fibre Reinforced Composite Materials based on 2024 and 7075 Aluminum Alloys", *Journal of Achievements in Materials and Manufacturing Engineering*, Vol. 49 No. 2, pp. 180–187.

Palanikumar, P., Gnanasekaran, N., Subrahmanya, K. and Kaliveeran, V. (2019), "Effect of sliding speed and rise in temperature at the contact interface on coefficient of friction during full sliding of SS304", *Materials Today: Proceedings*, Elsevier Ltd, No. xxxx, pp. 2–5.

Park, S.H.C., Sato, Y.S., Kokawa, H., Okamoto, K., Hirano, S. and Inagaki, M. (2004), "Corrosion resistance of friction stir welded 304 stainless steel", *Scripta Materialia*, Vol. 51 No. 2, pp. 101–105.

Radhika, N., Balajit, V. and Palaniappan, S. (2015), "Studies on Mechanical Properties and Tribological Behavior of LM25/Sic/Al2O3 Composites", *Journal of Engineering Science and Technology*, Vol. 10 No. 2, pp. 134–144.

Ramirez, A.J., Benati, D.M. and Fals, H.C. (2011), "Effect of Tool Offset on Dissimilar Cu-AISI 316 Stainless Steel Friction Stir Welding", *Proceedings of the 21th International Offshore and Polar Engineering Conference*, Vol. 8, pp. 548–551.

Rana, H.G., Badheka, V.J. and Kumar, A. (2016), "Fabrication of Al7075 / B4C Surface Composite by Novel Friction Stir Processing (FSP) and Investigation on Wear Properties", *Procedia Technology*, Elsevier B.V., Vol. 23, pp. 519–528.

Samir A., A. and Gardi, R.H. (2017), "Effect of Roller Burnishing Tool Pass on Surface Roughness of Austenitic Stainless Steel AISI 316L", *Zanco Journal of Pure and Applied Sciences*, Vol. 29 No. 6, pp. 75–81.

Thangarasu, A., Murugan, N. and Dinaharan, I. (2014), "Production and wear characterization of AA6082-TiC surface composites by friction stir processing", *Procedia Engineering*, Elsevier B.V., Vol. 97, pp. 590–597.

Zhang, Y., Guo, J., Li, Y., Luo, Z. and Zhang, X. (2019), "A comparative study between the mechanical and microstructural properties of resistance spot welding joints among ferritic AISI 430 and austenitic AISI 304 stainless steel", *Journal of Materials Research and Technology*, Korea Institute of Oriental Medicine, No. x x, pp. 1–10.

Zhao, H., Duan, L., Chen, G., Fan, H., Wang, J. and Zhou, C. (2018), "High corrosion resistance performance of 304 stainless steel after liquid nitrocarburization", *Composites Part B: Engineering*, Elsevier Ltd, Vol. 155, pp. 173–177.

ZANCO Journal of Pure and Applied Sciences
The official scientific journal of Salahaddin University-Erbil
https://zancojournals.su.edu.krd/index.php/JPAS

ISSN (print):2218-0230, **ISSN (online):** 2412-3986, **DOI:** **http://dx.doi.org/10.21271/zjpas**

RESEARCH PAPER

Study of Saving Thermal Energy Using Local Mixed Phase Change Materials.

Hawzheen Abdulrahman Ibrahim[1], Ziyad JamilTalabany[2], Mohammed Jawdat barzanjy[3]

[1,3]Department of Chemical and Petrochemical Engineering, College of Engineering, Salahaddin University-Erbil Kurdistan Region, Iraq
[2]Department of Petroleum Engineering, Engineering College, Knowledge University, Erbil Kurdistan Region, Iraq

A B S T R A C T:

Latent heat storage systems were reported to possess a very slow thermal response, mainly those using organic materials. This is primarily due to the relatively low thermal conductivity organic PCM (phase change material). In this study the paraffin –Al composite phase change material was prepared by mixing Aluminum powder into paraffin, in which paraffin wax was selected as organic phase change material, for the purpose of comparison pure paraffin and paraffin/aluminum composite with (0.1, 0.5, 0.8, 1, 2) mass fraction of aluminum samples were tested. To point out the effect of PCM thickness, four different thickness modules were used. It was found that increasing the thickness of PCM could decrease the heat transfer, which means more heat energy can be saved. The Thermal conductivity value changed from (0.263 W m^{-1} K^{-1}) to (0.918 W m^{-1} K^{-1}) by adding the mass fraction of aluminum powder from (0.1% to 2%) correspondingly. The experiment results concluded that increasing Al mass fractions result in decreased charging time. Adding aluminum powder increases heat transfer, therefore this heat gain is proportional to increasing aluminum mass fraction in paraffin wax.

KEYWORDS: Thermal energy storage, paraffin, Phase change materials, Aluminum powder, Thermal conductivity enhancement
DOI: http://dx.doi.org/10.21271/ZJPAS.32.4.8
ZJPAS (2020) , 32(4);66-74 .

1 INTRODUCTION

Thermal energy storage plays as significant technologies in an effective use of thermal energy and has applications in various areas, such as building heating/cooling systems(Wasmi, Jaffal et al. 2019), solar energy collectors, insulation (Hamad, Talabani et al. 2016), power and industrial waste heat recovery(Zelba, Marin et al. 2003).

* **Corresponding Author:**
Hawzheen Abdulrahman Ibrahim
E-mail: hawzheen.ibrahim@su.edu.krd
Article History:
Received: 22/11/2019
Accepted: 09/03/2020
Published: 08/09 /2020

Thermal energy storage techniques can be classified as sensible heat storage and latent heat storage, Latent thermal energy storage is a particularly attractive technique that provides a high energy storage density and has the property of storing latent heat like the heat of fusion at a constant temperature, i.e. the phase change temperature. Phase change materials (PCMs) that are used as storage media in latent thermal energy storage generally can be classified into two main categories: inorganic compounds and organic compounds. Inorganic PCMs include salt hydrates; salts, metals, and alloys, as well as organic PCMs are comprised of paraffin, fatty acids/esters and polyalcohol (Zelba, Marin et al. 2003).

Among the variety of PCMs proposed paraffin is taken as the most promising phase change material because it has many desirable characteristics such as significant latent heat of fusion, desirable phase change temperature range, non-supercooling, low cost, commercial availability, nontoxic and not corrosive (Kaygusuz and Sari 2005). However, paraffin waxes suffer from a low thermal conductivity (0.23Wm^{-1} K^{-1}) which reduces the rate of heat storage and extraction during the melting and solidification cycles(Zhang and Fang 2006). In order to improve the thermal conductivity of paraffin, extensive investigations have been carried out to enhance the thermal response of paraffin through the addition of different high thermal conductivity materials. These have included the use of graphite foam and graphite nanofibers with paraffin (Chintakrinda, Weinstein et al. 2011); the results showed that significant improvement can be achieved.

(Zhou, Wang et al. 2018) used the foam aluminum/paraffin composite PCM in the wall structure, and investigated that this composite material has a good thermal conductivity for the wall thermal insulation. Some investigators studied the graphite matrix embedded within paraffin, and significant improvement in thermal conductivity was achieved(Nayak, Saha et al. 2006) (Mills, Farid et al. 2006) (Mettawee and Assassa 2007), The paraffin/expanded graphite composites with the mass fraction of 2%, 4%, 7% and 10% EG were prepared by absorbing liquid paraffin into the expanded graphite, It was concluded that the composite PCM with the mass fraction of 10% EG was the most promising one for latent heat thermal energy storages (LHTES) applications due to its form-stable property, high thermal conductivity, good melting temperature (Sarı and Karaipekli 2007)

Using carbon nanotubes (CNTs) as one of the best materials to increase the thermal conductivity of paraffin has been studied by some investigators the results showed that the use of (CNTs) has apparent improving effect for the thermal conductivity without affecting the compatibility of components and thermal energy storage properties (Karaipekli, Biçer et al. 2017, Luo, Wei et al. 2018, Sarı, Biçer et al. 2018). Another technique to increase thermal conductivity of paraffin is emulsifying high thermal conductive nanoparticles in paraffin(e.g. Al2O3, TiO3) (Ho and Gao 2009, Chaichan, Kamel et al. 2015, Farsani, Raisi et al. 2019), the results indicated that the paraffin thermal conductivity increased the risen in the nanoparticles mass fraction.

In the present study, the addition of aluminum powder to paraffin wax (n-hexacosane) to improve the thermal conductivity was investigated experimentally. This study was done using a thermal energy storage test device; the heat transfer characteristics of the charging process were discussed. A comparative study between the results using pure paraffin and that using a composite of paraffin with different aluminum powder mass fraction is presented.

2 MATERIALS AND METHODS

2.1. MATERIALS

Paraffin wax (n-Hexacosane) used as organic phase change material in this study, obtained from scharlau company with a melting point (54^{o}C) according to a manufacturing database. Pure Copper and the aluminum powder obtained commercially. Pure copper rode prepared by lathe machine as a reference material for making four different size modules due to its known thermal conductivity (386 W/m.K)(Holman 1986), and aluminum powder selected because it has high thermal conductivity (204W/m.K) (Holman 1986), also due to its economical price, other significant property advantages associated with aluminum powder is excellent corrosion resistance.

2.2. PREPARATION OF COMPOSITE PCMS

Aluminum powder in paraffin composite was formulated with five mass fractions of Al powder ranging 0.1wt.%, 0.5 wt.%, 0.8 wt.%, 1 wt.% and 2 wt.%, the weights measured using an electronic balance. The thermal conductivity of the composite is defined as:

$$k_c = k_p v_p + k_{Al} v_{Al} \quad (Mettawee, 2007\,)$$

Where $v_p = V_p/V_c$ is the volume fraction of paraffin wax;

$v_{Al} = V_{Al}/V_c$ is the volume fraction of aluminum powder

Then each composite placed in four different thickness samples 4mm, 6mm, 8mm, and 10mm.

2.3. Experimental setup and Procedure

The thermal energy storage of paraffin and paraffin/Al composite PCM in thermal energy storage (TES) system were investigated respectively. The experimental setup is shown in figure (1). The setup mainly consisted of; lower part made of lumber (MDF type), electrical parts (current meter, voltage meter, and temperature controller screens) were placed in, upper part is the PCM module place which consists of a circular electric heater (105mm diameter) in the provided space inside the lower mold to create a uniform heat flux boundary condition at the PCM module base, and both heater and thermal control module are thermally insulated to reduce the heat loss. The voltage and Ampere to the heater are controlled and recorded by Digital voltmeter and Digital Ammeter respectively.

Figure (1) Thermal energy storage apparatus

Three K type thermocouples extended into the PCM module and measure the temperature at various locations with the same depth. A detailed view of the test section with the location of the thermocouples indicated is shown in figure (2). Three Thermocouples were arranged such that two are in the top and bottom of the module and one is in the PCM filed. All thermocouples calibrated by comparing their readings with a calibrated mercury thermometer before use then were held securely in place that did not move during the test.

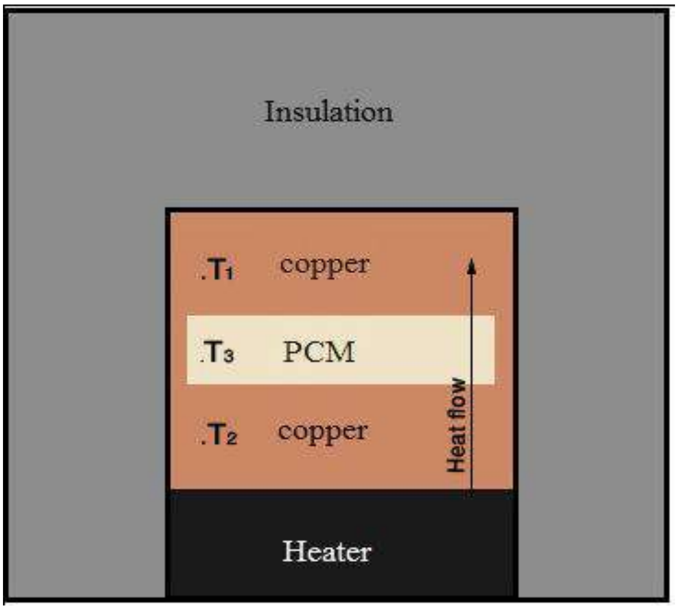

Figure (2) Schematic of the experimental setup with thermocouple points (front view)

The circular test modules are fabricated from pure copper with a dimension (105mm outer diameter and 101mm inner diameter, 15mm thickness) each and have the ring inside module (101mm outer diameter and 95mm inner diameter), with four different thickness 4mm, 6mm, 8mm, and 10mm as shown in figure (3). Each ring in the test module was filled completely with paraffin composite as shown in figure (4) with a known mass fraction of Aluminum and placed in the PCM module base for applying heat flux. Tests were run in all module design for each of five different mass fractions of Al- paraffin composite, for four different applied voltages (4, 6, 8, 10), and the test was repeated for each different thickness, the effect of PCM composite thickness was also examined, the system allowed to heat up while the thermocouples record the temperature of the system, the thermocouple responses recorded with time. In order to know the heat transfer enhancement induced by aluminum powder, the pure paraffin sample was also measured for the purpose of comparison. The temperatures and input voltage would be automatically recorded by a data acquisition system. Thus, the heat transfer rate and the thermal energy storage capacity could be obtained from the analysis of the recorded data.

Figure (3) module sample

Figure (4) module sample 6mm filled with paraffin

3 RESULTS AND DISCUSSION

In The present study, the thermal behavior of pure paraffin and Aluminum-paraffin investigated. The effects of power loading, PCM thickness and Al mass fraction are all examined.

Figure (5) represents the heat transfer of pure copper alone at the different power supply and with pure paraffin. The graph represents four different thickness samples. One is 4mm thick of pure paraffin and others 6mm, 8mm and 10mm thick. As shown in the figure the amount of average heat transfer that passed through the 4mm sample is (3.237 Watt) which is larger than all of the other samples. While the average heat transfer amount of other samples (6mm, 8mm, and 10mm) are (0.945, 0.761, and 0.691 Watt) respectively. Generally, the heat transfer amount decreased with increasing the thickness of pure paraffin, this is due to conduction heat transfer resistance and paraffin thickness. According to the Fourier law of heat conduction, thermal resistance increases with increasing thickness of material so it results in decreasing heat transfer (Holman 1986).

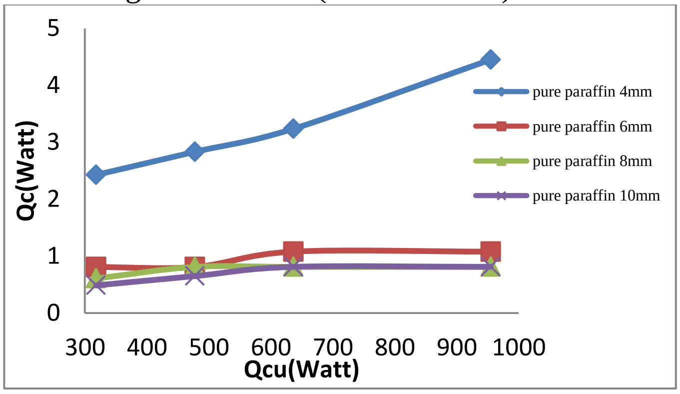

Figure (5) compering heat transfer in pure paraffin between four different thickness module samples

Figure (6) illustrates the heat transfer of copper alone at the different power supply and with paraffin composite used. The graph shows four different thickness samples. One is 4mm thick of paraffin composite material of 0.1 mass fraction of aluminum and others 6mm, 8mm, and 10mm thick. From the figure, one can see that the average heat transfer amount which passed through a 4mm sample is (3.47 Watt) and it is larger than all of the other (6mm, 8mm, and 10mm) are (0.85, 0.81, and 0.74 Watt) heat transfer respectively. However, the change of heat transfer is very small for 6mm, 8mm, and 10mm thickness of composite paraffin, this is due to conduction heat transfer resistance and paraffin composite of 0.1 mass fraction of aluminum thickness. According to the Fourier Law of heat conduction, thermal resistance increases with increasing thickness of material so it results in decreasing heat transfer.

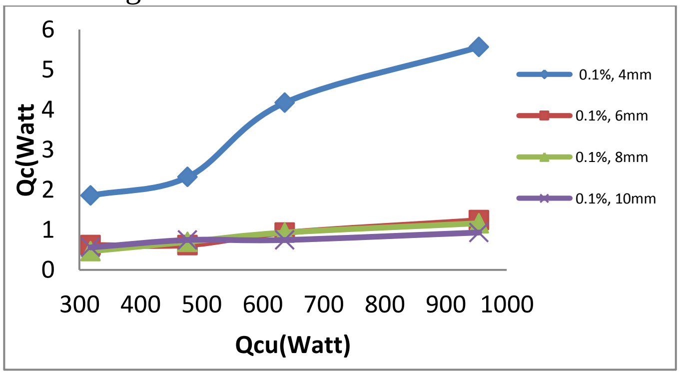

Figure (6) compering heat transfer in 0.1%Al-paraffin between four different thickness module samples

Figure (7) shows the heat transfer of pure copper alone and with paraffin–Al composite for the same power supply and compression of heat transfer for four different samples. One is 4mm thick of paraffin material of 0.5 mass fraction of aluminum and others 6mm, 8mm, and 10mm thick with the same fraction. Figure one shows that the average heat transfer amount which passes through 4mm thick sample is 5.77 Watt and it is greater than all of the other samples(6mm, 8mm, and 10mm) that have an average heat transfer amount (1.402, 0.968, and 0.917 Watt) respectively. Nevertheless, the change of heat transfer is very small among 6mm, 8mm, and 10mm thickness of Al-paraffin; this is due to conduction heat transfer resistance and paraffin composite of 0.5 aluminum mass fraction thickness. According to the Fourier Law of heat conduction, thermal resistance increases with increasing thickness of material so it results in decreasing heat transfer.

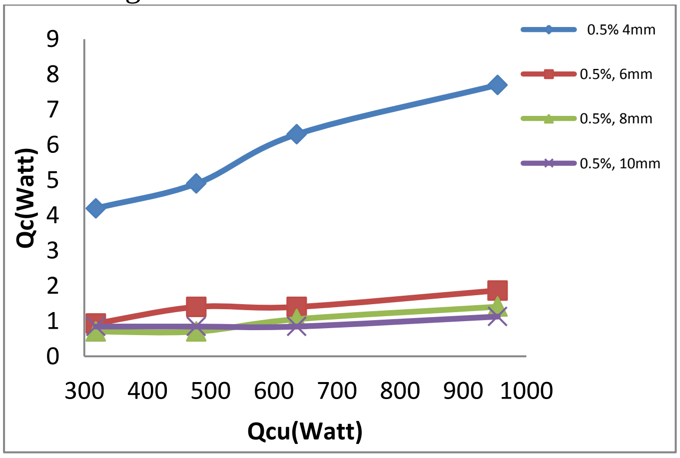

Figure (7) compering heat transfer in 0.5%Al-paraffin between four different thickness module samples

Figure (8) represents the heat transfer of pure copper alone and with paraffin–Al for the same power supply and comparison of heat transfer for four different samples. One is 4mm thick of paraffin material of 0.8 mass fraction of aluminum and others 6mm, 8mm and 10mm thick with the same composition. The figure clearly indicates that the average heat transfer passed through 4mm thick sample is greater than all of the other samples and is about 7.45 Watt while the average heat transfer passed through three other samples 6mm, 8mm and 10mm are (1.42, 0.99 and 0.91 Watt) respectively. However, the change of heat transfer is very small for 6mm, 8mm and 10mm thickness of composite paraffin, this is due to conduction heat transfer resistance and paraffin composite of 0.8 mass fraction of aluminum thickness. According to the Fourier Law of heat conduction, thermal resistance increases with increasing thickness of material so it results in decreasing heat transfer. These results are in agreement with the results of (Shivan and Talabany 2017)

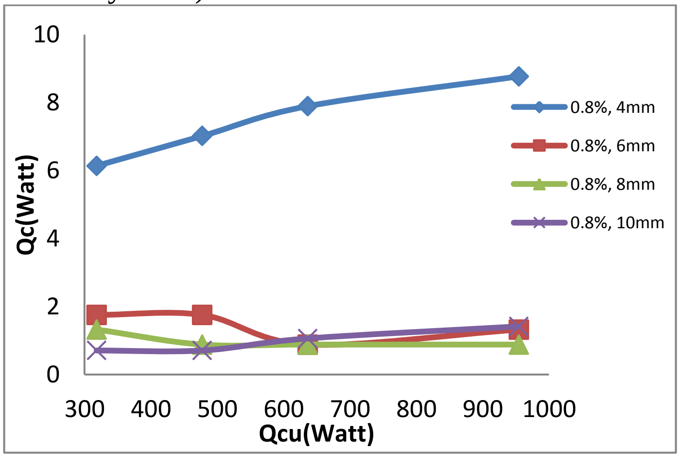

Figure (8) compering heat transfer in 0.8%Al-paraffin between four different thickness module samples

Figure (9) illustrates the heat transfer of copper alone at the different power supply and with Al- paraffin used. The graph shows four different types of samples. One is 4mm thick of paraffin with the material of 1 mass fraction of aluminum and others 6mm, 8mm, and 10mm thick. From the figure, it is found that the average heat transfer which passed through 4mm sample is about (8.207 Watt) and it is larger than all of the other samples that the average heat transfer of other samples (6mm, 8mm, and 10mm) are (2.161, 1.128 and 1.71 Watt) respectively. However, the change of heat transfer is very small for 6mm, 8mm and 10mm thickness of composite paraffin; this is due to conduction heat transfer resistance and thickness of paraffin with 1 mass fraction of aluminum. According to the Fourier Law of heat conduction, thermal resistance increases with increasing thickness of material so it results in decreasing heat transfer.

Figure (10) represents the heat transfer of pure copper alone at the different power supply and with Al-paraffin used. The graph shows four different types of samples. One is 4mm thick of paraffin with the material of 2 mass fraction of aluminum and others 6mm, 8mm, and 10mm thick. As shown in the figure the amount of average heat transfer that passes through the 4mm sample is (14.63 Watt) which is larger than all of the other samples. While the average heat transfer of other samples (6mm, 8mm, and 10mm) are (3.707, 2.08 and 1.933 Watt) respectively. Generally, heat transfer amount decreased with increasing the thickness of Al-paraffin, this is due to conduction heat transfer resistance in paraffin species which has low thermal conductivity. According to the Fourier Law of heat conduction, thermal resistance increases with increasing thickness of material so it results in decreasing heat transfer.

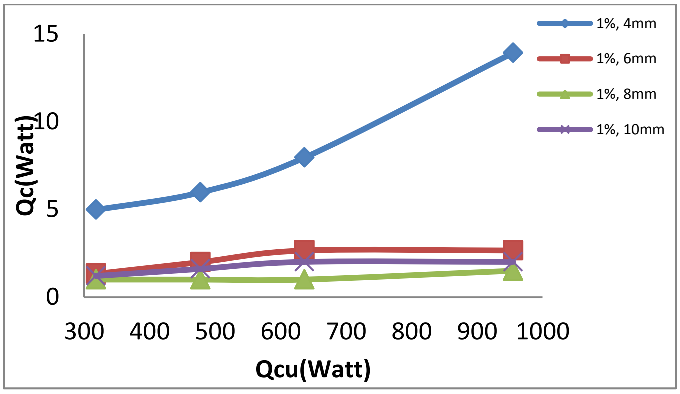

Figure (9) compering heat transfer in 1%Al-paraffin between four different thickness module samples

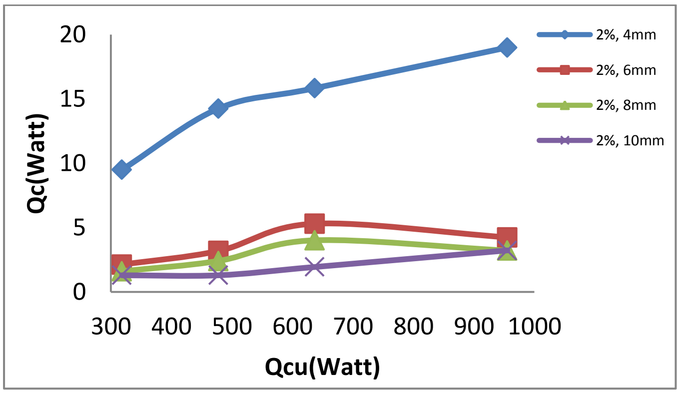

Figure (10) compering heat transfer in 2%Al-paraffin between four different thickness module samples

Figure (11) shows the comparison of heat transfer that passed through a 4mm thick module between pure paraffin sample and five different Al powder mass fraction samples. Generally, the heat transfer is increased by increasing the power supply for each sample. The average heat transfer of pure paraffin is 3.237 Watt and this is slightly increased to 3.478 Watt by adding 0.1% Al powder. Heat transfer improved with adding Al powder in general. As shown in the figure 2% Al –paraffin sample has the largest average heat transfer (14.634 Watt) than the other samples. This is due to thermal conductivity enhancement by adding Al powder, as shown in figure (15) thermal conductivity of the composites increased with increasing mass fraction of aluminum powder.

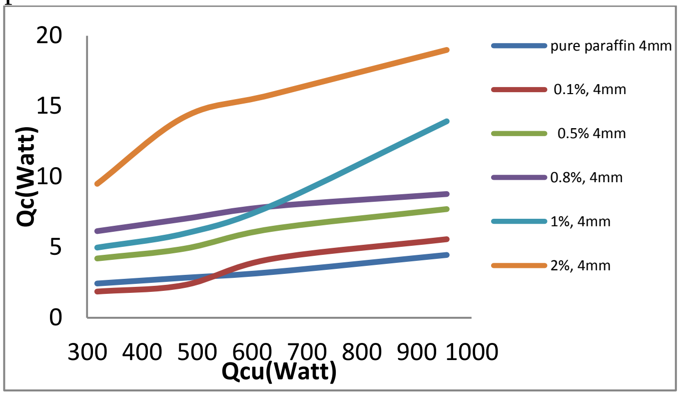

Figure (11) 4mm sample comparison of heat between paraffin and Al mass fractions

Figure (12) shows the comparison of heat transfer that passed through a 6mm thick module between pure paraffin sample and five different Al powder mass fraction samples. Generally, the heat transfer is increased with increasing the power supply for each sample, however, for 2% Al-paraffin composite heat transfer decreased when power supply higher than 6V as a result of different ambient temperatures between tests. The average heat transfer of pure paraffin is 0.945 Watt and this is increased to 1.066, 1.403, 1.699 and 2.161 Watt by adding 0.1, 0.5, 0.8 and 1% Al powder respectively. As shown in the figure 2% Al –paraffin sample has the largest average heat transfer (3.707 Watt) than the other samples. In general, the figure indicated that the Heat transfer improved by adding Al powder. This is due to thermal conductivity enhancement by adding Al powder, as shown in figure (15) thermal conductivity of the composites increased with increasing mass fraction of aluminum powder.

Figure (13) shows the comparison of heat transfer that passed through an 8mm thick module between pure paraffin sample and five different Al powder mass fraction samples. Generally, the heat transfer is increased with increasing the power supply for each sample; however, for 2% Al-paraffin composite heat transfer decreased when power supply higher than 6V as a result of different ambient temperatures between tests. The average heat transfer of pure paraffin is 0.761 Watt and this is slightly increased to 0.814 Watt by adding 0.1% Al powder. In general, the figure indicates that the Heat transfer improved by adding Al powder. As shown in the figure 2% Al –paraffin sample has the largest average heat transfer (2.805 Watt) than the other samples. This is due to thermal conductivity enhancement by adding Al powder, as shown in figure (15) thermal conductivity of the composites increased with increasing mass fraction of aluminum powder. These results are in agreement with results from (Ho and Gao 2009) which used Alumina nanoparticles in paraffin.

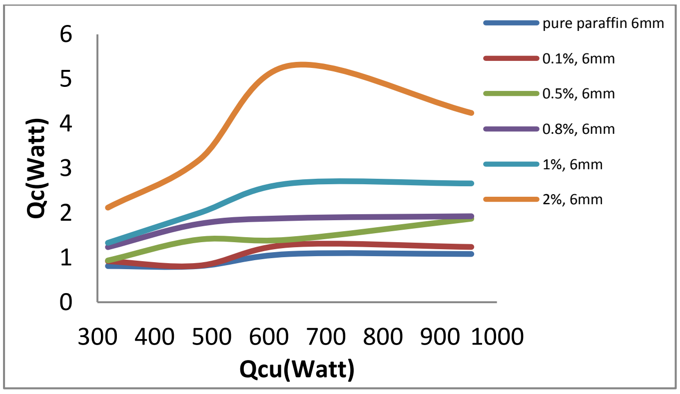

Figure (12) 6mm sample comparison of heat between paraffin and Al mass fractions

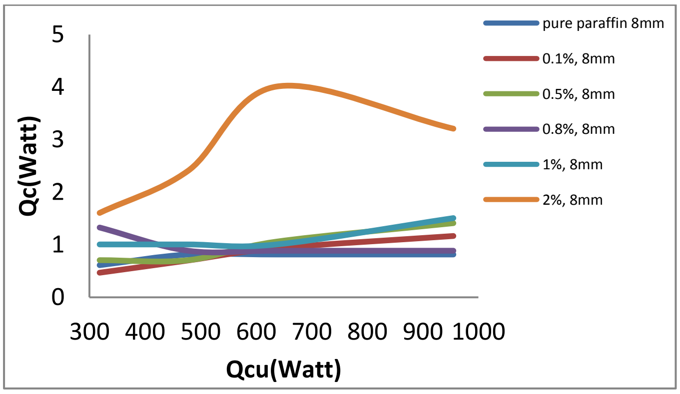

Figure (13) 8mm sample comparison of heat between paraffin and Al mass fractions

Figure (14) shows the comparison of heat transfer that passed through a 10mm thick module between pure paraffin sample and five different Al powder mass fraction samples. Generally, the heat transfer is increased by increasing the power supply for each sample. The average heat transfer of pure paraffin is 0.691 Watt and this is increased to 0.746, 0.917, 0.974 and 1.710 Watt by adding 0.1, 0.5, 0.8 and 1% Al powder respectively. As shown in the figure 2% Al –paraffin sample has the largest average heat transfer (1.933 Watt) than the other samples. In general, the figure indicated that the Heat transfer improved by adding Al powder. This is due to thermal conductivity enhancement by adding Al powder, as shown in figure (15) thermal conductivity of the composites increased with increasing mass fraction of aluminum powder.

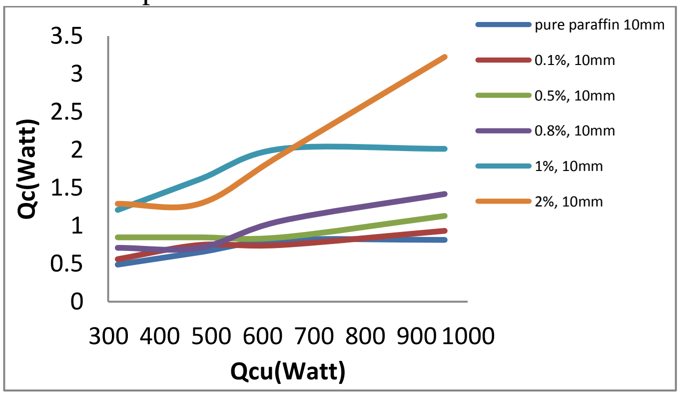

Figure (14) 10mm sample comparison of heat between paraffin and Al mass fractions

Figure (15) shows the comparison of average heat transfer between pure paraffin and five different Al mass fractions for each module sample, as shown in the figure for 4mm think module sample the average heat transfer significantly increase with increasing Aluminum mass fraction it reaches 10.634 Watt for 2% Al –paraffin which is 2.28% higher than average heat transfer of pure paraffin. For 6mm sample the average heat transfer of pure paraffin is 0.945 watt it is increasing by 7.027%, 27.183%, 30.545%, 48.225%, 268.479% by adding 0.1, 0.5, 0.8, 1, 2 Al mass fraction respectively, the thermal conductivity curve in the figure indicates that increasing of average heat transfer with increasing aluminum mass fraction it refers to thermal conductivity enhancement in paraffin by aluminum as it has high thermal conductivity than paraffin. It can be seen that the value of thermal conductivity changed from 0.264 W m^{-1} k^{-1} to 0.919 W m^{-1} k^{-1} with increasing of Aluminum mass ratio, compared with the thermal conductivity of pure paraffin, it is increased from 14.74% to 299.5%.

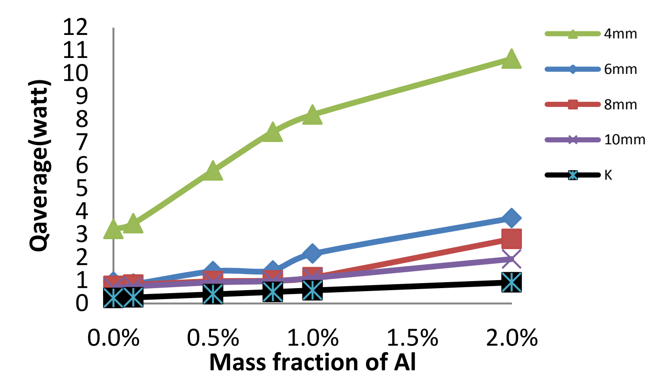

Figure (15) average heat transfer comparison between paraffin and Aluminum mass fraction for each sample

4 CONCLUSIONS

Paraffin wax considered most prospective phase change material for use in thermal energy storage systems because it has a desirable melting temperature range, low cost, commercial availability and good latent heat capability (Zhao, Lu et al. 2010), however, it has low thermal conductivity. Embedding aluminum powder in the paraffin enhances the thermal conductivity of paraffin wax. Based on the presented experimental study following conclusion can be drawn,

1. Thermal conductivity value changed from (0.263 W m-1 K-1) to (0.918 W m-1 K-1) with increasing the mass fraction of aluminum powder from (0.1% to 2%) correspondingly.

2. Adding aluminum powder with mass fraction range (0.1-2%) increases heat transfer and this heat gain is proportional to increasing aluminum mass fraction in paraffin wax.

3. The charging time decreases as the Al mass fraction is increased according to the percent mass fraction used.

4. Heat transfer which passed through the PCM is decreased with increasing thickness of paraffin composite.

An experimental study concerning heat transfer performance of the higher mass fraction of aluminum in paraffin PCM composite shall be presented in the future.

References

Chaichan, M. T., S. H. Kamel and A. Al-Ajeely (2015). "Thermal conductivity enhancement by using nano-material in phase change material for latent heat thermal energy storage Systems." Saussurea 5(6): 48-55.

Chintakrinda, K., R. D. Weinstein and A. S. Fleischer (2011). "A direct comparison of three different material enhancement methods on the transient thermal response of paraffin phase change material exposed to high heat fluxes." International Journal of Thermal Sciences 50(9): 1639-1647.

Farsani, R. Y., A. Raisi and A. Mahmoudi (2019). "Successive melting and solidification of paraffin–alumina nanomaterial in a cavity as a latent heat thermal energy storage." Journal of the Brazilian Society of Mechanical Sciences and Engineering 41(9): 368.

Hamad, N. H., Z. J. Talabani and A. K. Mohammed (2016). "Experimental Study for Selection of Composite Materials Used in Thermal Insulation." ZANCO Journal of Pure and Applied Sciences 28(2).

Ho, C. J. and J. Gao (2009). "Preparation and thermophysical properties of nanoparticle-in-paraffin emulsion as phase change material." International Communications in Heat and Mass Transfer 36(5): 467-470.

Holman, J. P. (1986). Heat transfer, McGraw-hill New York.

Ji, H., D. P. Sellan, M. T. Pettes, X. Kong, J. Ji, L. Shi and R. S. Ruoff (2014). "Enhanced thermal conductivity of phase change materials with ultrathin-graphite foams for thermal energy storage." Energy & Environmental Science 7(3): 1185-1192.

Karaipekli, A., A. Biçer, A. Sarı and V. V. Tyagi (2017). "Thermal characteristics of expanded perlite/paraffin composite phase change material with enhanced thermal conductivity using carbon nanotubes." Energy conversion and management 134: 373-381.

Kaygusuz, K. and A. Sari (2005). "Thermal energy storage system using a technical grade paraffin wax as latent heat energy storage material." Energy Sources 27(16): 1535-1546.

Luo, D., F. Wei, H. Shao, L. Xiang, J. Yang, Z. Cui, S. Qin and J. Yu (2018). "Shape stabilization, thermal energy storage behavior and thermal conductivity enhancement of flexible paraffin/MWCNTs/PP hollow fiber membrane composite phase change materials." Journal of materials science 53(22): 15500-15513.

Mettawee, E.-B. S. and G. M. Assassa (2007). "Thermal conductivity enhancement in a latent heat storage system." Solar Energy 81(7): 839-845.

Mills, A., M. Farid, J. Selman and S. Al-Hallaj (2006). "Thermal conductivity enhancement of phase change materials using a graphite matrix." Applied Thermal Engineering 26(14-15): 1652-1661.

Nayak, K., S. Saha, K. Srinivasan and P. Dutta (2006). "A numerical model for heat sinks with phase change materials and thermal conductivity enhancers." International Journal of Heat and Mass Transfer 49(11-12): 1833-1844.

Sarı, A., A. Biçer and G. Hekimoğlu (2018). "Effects of carbon nanotubes additive on thermal conductivity and thermal energy storage properties of a novel composite phase change material." Journal of Composite Materials: 0021998318808357.

Sarı, A. and A. Karaipekli (2007). "Thermal conductivity and latent heat thermal energy storage characteristics of paraffin/expanded graphite composite as phase change material." Applied Thermal Engineering 27(8-9): 1271-1277.

Shivan and Z. J. Talabany (2017). Study of Thermal Energy Storage with Local Phase Change Materials Master, Salahaddin University

Wasmi, M. H., H. M. Jaffal and T. W. Mohammed (2019). "The Behavior of Glauber's Salt as a Heat Storage Material for Residential Iraqi Buildings." ZANCO Journal of Pure and Applied Sciences 31(s3): 26-33.

Zelba, B., J. Marin, L. Cabeza and H. Mehling (2003). "Review on thermal energy storage with phase change; materials, heat transfer analysis and application." Applied Thermal Engineering 23: 251-183.

Zhang, Z. and X. Fang (2006). "Study on paraffin/expanded graphite composite phase change thermal energy storage material." Energy Conversion and Management 47(3): 303-310.

Zhao, C., W. Lu and Y. Tian (2010). "Heat transfer enhancement for thermal energy storage using metal foams embedded within phase change materials (PCMs)." Solar energy 84(8): 1402-1412.

Zhou, Y., Z. Wang, C. Yang, L. Zhang and K. Hao (2018). "RESEARCH ON THERMAL ENERGY STORAGE AND RELEASE CHARACTERISTICS OF FOAM ALUMINUM PARAFFIN COMPOSITE PHASE CHANGE MATERIALS." Journal of Ovonic Research Vol 14(1): 35-47.

ZANCO Journal of Pure and Applied Sciences
The official scientific journal of Salahaddin University-Erbil
https://zancojournals.su.edu.krd/index.php/JPAS

ISSN (print):2218-0230**, ISSN (online):** 2412-3986**, DOI:** **http://dx.doi.org/10.21271/zjpas**

RESEARCH PAPER

Power and Thermal Management Issues for Portable Processors

Diary R. Sulaiman

Department of Electrical Engineering, College of Engineering, Salahaddin University-Erbil, Kurdistan Region, Iraq

A B S T R A C T:

The advancement of modern CMOS technology scaling causes an exponential rise of system's power dissipation and temperatures in submicron technology node, which growth production and operating costs. Thermal energy and generated heat are becoming a prominent major issue in the context of portable applications (telephony, PDAs, digital cameras ...) and must be considered at each design level. The performance of portable processors is critically affected by dissipated power and operational temperature. The designers are forced to design a proper cooling system, especially heatsinks which consistently allows a low power and low temperature regulation of high-speed processors .

In this article, several different heatsinks are modeled, tested, and designed to optimize the microprocessor's cooling system while ensuring proper thermal operation and lowest power dissipation. The proposed adopted heatsink and their selected design configurable parameters are analyzed theoretically for different validations conditions and operation modes in various real-time thermal conditions. Thermal Analysis Package is used for simulation the proposed heatsinks model. Results shows the specification improvements of the design model for ensuring power required to cool in time of 0.851 W, time to cool by 15s, and heat to remove is 12.77J which confirms theoretical fundamentals and sufficient improvement of temperature minimization and better performance of the cooling system was achieved.

KEY WORDS: Portable Systems, Microprocessors; Thermal management; Heatsink Design; Power Dissipation minimization.
DOI: http://dx.doi.org/10.21271/ZJPAS.32.4.9
ZJPAS (2020) , 32(4);75-81 .

1. INTRODUCTION

Current trends of portable processors have experienced a massive sustained growth in performance, platform's features, functionality, and complexity. This advanced technology translates into higher power dissipation and bringing forth-extra high temperatures, creates a massive demand for a novel cooling system design. The overall objective of thermal minimization in portable processors is to weaken the system operating cost while providing long-term device reliability.

* **Corresponding Author:**
Diary R. Sulaiman
E-mail: diary.sulaiman@su.edu.krd or diariy@gmail.com
Article History:
Received: 08/04/2020
Accepted: 01/05/2020
Published: 08/09 /2020

The evolution of power density in Intel processors is shown in Figure 1, and 40 years of microprocessors trend data is shown in Figure 2 (Smelt, 2018, Rupp, 2018, SULAIMAN et al., 2019).

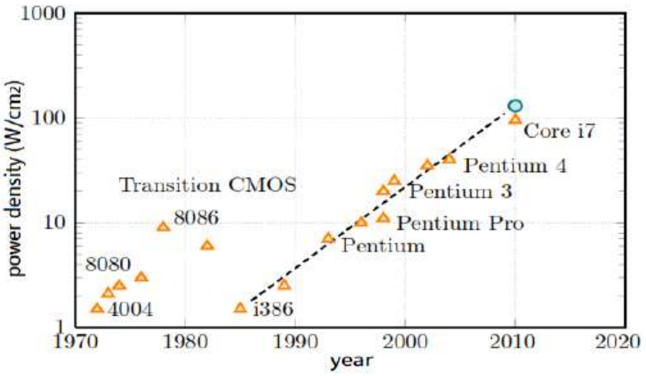

Figure 1: Evolution of power density in Intel processors

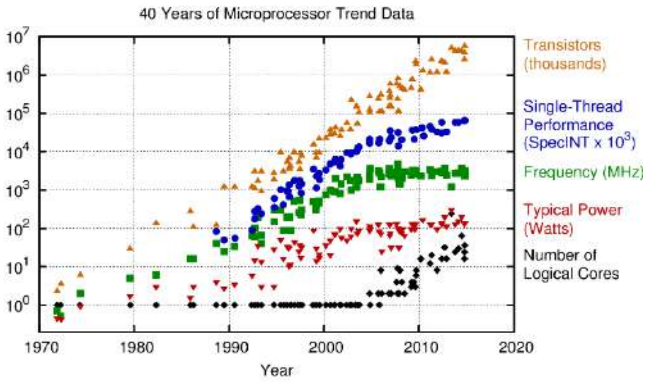

Figure 2: 40 years of microprocessors trend data

There are several techniques for power and thermal challenges in microprocessors for portable systems; a proper design of the chip heatsink has a vital role in the system. The heatsink design methodology generally takes design margins to prevent the uncertainty of the processors and guarantee operational functions and performance to ensure correct operation at the lowest cost (R. Sulaiman et al., 2017). The general structure of a heatsink and heat flow is shown in Figure 3. For advanced technological nodes, performance no longer means high frequency only, but also a lower power and temperature. Thus, to estimate the overall power and thermal energy efficiency, it is necessary to guarantee that for a certain frequency, the dissipated power and temperature consumed will be minimum. Nano technologies introducing the gains in speed and higher power consumption of microprocessors and digital circuits, hence, the design of heatsinks is no longer been negligible that affecting performance as well as robustness of the cooling system (HamaAli et al., 2019).

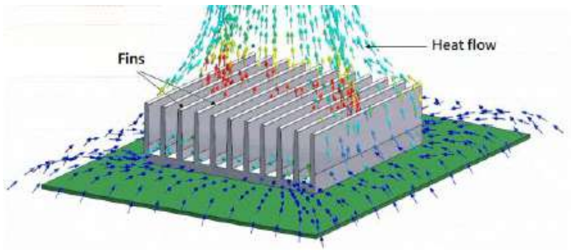

Figure 3: Heatsink general structure and heat flow

From microprocessors rigorous survey of power and thermal reduction in portable systems, it is observed that, there have been numerous articles, and published studies on the heatsink design and processor's power and thermal minimization techniques. To this end, number of new works published recently has been pointed out.

(Hanafi et al., 2015) proposed radial plate fin heatsink with a new dimension for optimal design that maximizes heat dissipation and reduce the size of heatsink on CPU chip. The multi objective particle swarm optimization are investigated for finding optimal dimensions of heatsink radial plate fin design. The comparison of the model and fitness optimal value of fitness functions for radial heatsink are explained that confirms an increment of heat dissipation and area reduction. (Gierczak et al., 2016) presented analysis, modeling, and simulation of distributing temperatures in a heat-sink. The realization was carried out in the laboratory model of processor and source of heat was designed. Four different heaters were fabricated as thick-film resistors screen-printed on alumina substrate, and useful information in optimization heatsink process was collected. (Todmal and Mukherjee, 2017) Are comparing various design of heatsinks for different fin numbers, fin thickness, copper core height and rotation speed of the fan for CPU cooling which dissipating 130W heat, furthermore an optimized heatsink design is presented to dissipate a lower heat level. (Ahmed et al., 2018) performs a comprehensive survey on the optimization methods for hydrothermal design of heatsinks, and investigations were carried out for active and passive methods for improving heat removing in heatsinks by modifying fluid and solid domain. (Fornaciari and Soudris, 2019) presented the digital controller for microprocessors thermal management and designed as part of a project (HARPA) the goal of this proposal was the inclusion into a unified design of controlling temperature, performance /power trade-off, and stability analysis, was carried out. They were assessed and verified that using as a solid benchmark, and free to multi-physics configurations. The experimental results were carried out on a modern processor architecture and compared to previous studies which shows improvements that is easy to set up, calibrate and maintain. (Dede et al., 2019) presented design and optimization of a 3D heat flow scheme applicable for power electronics thermal management. This optimization method focused on temperature minimization simultaneously of multiple gate drive IC devices. The design, fabrication prototype, and development of an experimental test bench were applied for thermal performance characterization, experimental results show highest temperature reduction for the gate drive IC devices in a laboratory environment. (Singh et al., 2020) proposed three individual mini-channels with differently configured interconnecting secondary channels heatsink geometry, based on finite volume method, they solved mathematical model in ANSYS to study the issue numerically. The results findings proved that, lowest base plate temperature of mini-channel heatsink is noticed at 10° secondary channel angle, and performance of electronic device will be analyzed at 10° secondary channel angle.

This article presented many different heatsinks, study, model, and the design were explored in order to optimize the microprocessor's cooling system while ensuring proper thermal operation. The proposed adopted heatsink design model was analyzed theoretically for different validations conditions and operation modes in various real-time temperatures and environmental conditions. The simulation and results are confirmed through Thermal Analysis Package which shows sufficient improvements of the design model for ensuring power required to cool in time of 0.851W, time to cool by 15s, and heat to remove is 12.77J which confirms theoretical fundamentals and sufficient improvement of temperature minimization and ensures better performance of the cooling system.

2 HEATSINK DESIGN PARAMETERS AND CONSTRAINTS

A heatsink is a heat exchanger which transfers thermal energy/heat generated from a higher temperature microprocessor chip to a lower temperature environment. It reduces the chip temperature or hotspot by air convection and improves efficient energy consumption. Therefore, design a specific heatsink need to consider number of constraints and parameters. The constraints are primarily out of designer's control (Neyestani et al., 2019). The most significant constraint is the rate of removed heat, and is mainly has a fixed value that need to be adequate for processor's heat dissipation rate. highest operating temperature is another constraint, and is defined by properties of the used material, it has to be higher than maximum operating temperature of the chip, and ambient average temperature must be taken into consideration for thermal resistance calculations (Markowski et al., 2019).

The heatsink design parameters contain the heatsink material, number and dimension of fins, fin alignments, and the base plate thickness as shown in Figure 4.

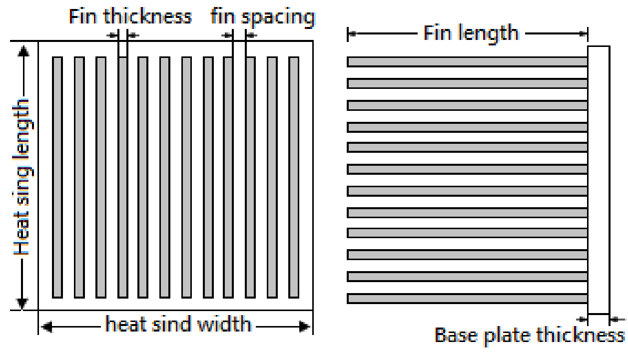

Figure 4: The design parameters of a heatsink

High thermal conductivity metal and relatively low cost are preferred, like Aluminum and Copper. More specifically, Copper is the most used effective material, because it has many desirable thermally efficient properties, durable heat exchangers, and thermal conductivity. However, in portable systems weight is a big concern, this is motivated designers to use Aluminum instead, and especially for microprocessor's heatsinks. It has also a good thermal conductivity, less expensive, lighter weight, and easier to work, making it a better choice for portable processors (Ilsche et al., 2019).

Shape and number of the fins are additional most important factors for heatsink performance, the heat spread area is enhanced by number and shape of fins. Alignment of fins on the base plate acts a vital role particularly for heatsinks which are cooled by. The thickness of base plate provides uniform distribution of heat through the base of heatsink, since the processor chip is mainly smaller than the heatsinks. The heat flow between the semiconductor chip and ambient air is modeled as a series of resistances to the heat flow, the sum of these resistances is the total thermal resistance of the chip die to ambient air (Mjallal et al., 2018). In order to obtain maximum heat distribution and minimum thermal resistance, each of these parameters and constraints must be considered well as explained in the design procedure.

To ensure that the microprocessor does not overheat, finding an efficient heat transfer path from the chip to the environment is crucial. The heat transfer path can be from the chip /printed circuit board, to a heatsink, to the air flow supplied by a fan. Microprocessors are essentially having a maximum operating temperature which is called maximum junction temperature. The designer is necessarily having to prevent exceeding this temperature to prevent the chip damage. The component will produce heat during normal operation when operating in an environmental condition for a specified ambient temperature. The maximum power dissipation reduction amount is given by (SULAIMAN, 2016),

$$P_{D-\max} = \frac{T_j - T_A}{R_{total}} \qquad (1)$$

$$R_{total} = \theta_{sc} + \theta_{cs} + \theta_{jc} \qquad (2)$$

Where, PD_{-max} is maximum power dissipation, T_j is the maximum operating or junction temperature, T_A is ambient temperature, R_{total} is total thermal resistance to surroundings, θ_{sc} is the heatsink thermal resistance, θ_{cs} is the case thermal resistance, and θ_{jc} is the junction thermal resistance, this is explained in Figure 5.

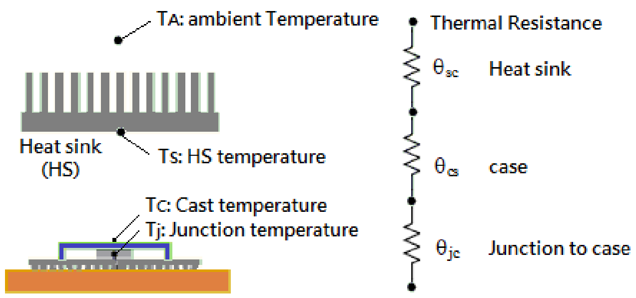

Figure 5: The heatsink thermal resistance

The heatsink thermal resistance (θ_{sc}) consists of two resistors, the resistance of base (R_b), and the resistance of fins (R_f), it can be given by,

$$\theta_{cs} = \frac{t_b}{k\,A_b} \qquad (3)$$

Where t_b is the thickness of the heatsink base, k is the thermal conductivity of the heatsink material, and A_b is the area of the of the heatsink base.

Thermal resistance is used to describe the relative resistance of heat transfer that is present in a chip and is varied that could be found in data sheets (Rotem et al., 2013). And principally, the average ambient temperature will be minimized with time as illustrated in the following equation,

$$T_{A-av} = \frac{T_{air-in} + T_{air-out}}{2} \qquad (4)$$

Where, $T_{A\text{-}av}$ is average ambient heat temperature, $T_{air\text{-}in}$ is temperature of input air to the heatsink, and $T_{air\text{-}out}$ is temperature of output air from the heatsink.

The heatsink size calculation is basically depending on an established equation for estimating heatsink volume during the early stages of heatsink design, it generally estimates the overall heatsink volume within +/- 15% of the final design.

$$V = \frac{Q\ R_v}{\Delta T} \qquad (5)$$

Where, V is the estimated heatsink volume, Q is the heat source power, ΔT is the thermal budget, and R_v is the volume thermal resistance.

The required heatsink surface area for U shaped aluminum fins that are generally preferred because of its high-performance characteristics. The design contribution principles are to increase the heatsink surface area, and to reduce its weight and the mean distance of heatsink from the processor in to be cooled.

3 THE DESIGN PROCEDURE

The design of high-performance thermal suppression heatsinks of portable microprocessors is the core of this article goal. In order to achieve this goal, and better heatsink design to suit most current high-speed processors, the constraint and design factors of a specific heatsink were chosen as shown in Table 1. The designs of heatsinks with rectangular fins, the fin height, space, and thickness are varied to obtain the specification of; Power required to cool in time: 0.851 W, Time to cool:15s, and heat to remove;12.77 J. Table 2 shows the heatsink under test for the purpose of finding an appropriate heatsink that has the required specifications that are listed.

Table (1) The heatsink design parameters

Dimensions: Width, Height, Thickness (mm)	50,35,1
Material type	Aluminum Ex alloy, 6063 TS
Fin shape	Rectangular
Temperature range (^{o}C)	35-75
T_A: Ambient Temperature ((^{o}C)	35
Ts: Surface Temperature ((^{o}C)	75
T_{A-avr}: Ambient Temperature (^{o}C)	55
Heat to remove (J)	12.77
Total surface area (Cm^2)	38.40
Surface temperature constraint	<85°C
Total Volume (mm3)	341.0
Passive cooling load (W)	0.731
Active cooling load (W)	50.00
Total cooling load (W)	50.731
Time to cool (s)	15
Power required to cool in Time (W)	0.851
Fin Thickness (mm)	1
Heat transfer coefficient W/m^2 K	4
Dry air Density (ρ) at 35 ^{o}C (kg/m^3)	1.0755
Dry air Thermal conductivity (k) at 35 ^{o}C W/mK	0.28625
Dry air Prandtl number (P_r) at 35 ^{o}C	0.7215
Dry air (β) at 35 ^{o}C	0.0030
Material type	Aluminum Ex alloy, 6063 TS

Table (2) Heatsinks undertest

Heatsink Base Dimension (50, 35, 1) mm			
#	**Fin Dimensions (mm)**	**Heat Reduction in 15s (J)**	**Power Reduction in 15s (W)**
1	2, 2, 1	10.23	0.732
2	2, 3, 1	7.58	0.495
3	2, 4, 1	5.24	0.322
4	3, 2, 1	12.77	0.851
5	3, 3, 1	9.36	0.659
6	3, 4, 1	7.24	0..442
7	4, 2, 1	11.35	0.782
8	4, 3, 1	8.52	0.527
9	4, 4, 1	6.16	0.380
12	2, 2, 2	6.75	0.645
13	2, 3, 2	5.23	0.410
14	2, 4, 2	4.93	0.286
15	3, 2, 2	6.12	0.536
16	3, 3, 2	4.85	0.375
17	3, 4, 2	4.31	0.213
18	4, 2, 2	5.42	0.472

The fin dimensions is calculated as shown in the following steps:

Fin spacing:
to find optimum fin spacing, it is first necessary to find out Rayleigh number (R_a).
$R_a=0.00788*10^7*T_{A-av} = 0.00788*40*10^7$
$= 0.4334*10^7$
Fin Spacing (centre-to-centre)$=2.714*L/R_a^{0.25}$
$= \{2.714*0.05/(0.4334*10^7)^{0.25}\}-0.001$
$= 0.00322-0.001$
$=3$ mm
Exact Fin Spaceing:3mm-0.5mm-0.5mm=2mm

Number of fins:
Base Width/(fin Thickness*Fin space)
=0.035/(0.001*0.002) *15%
=17.5+2.625
=20 fins

Total cooling load (TCL):
TCL=heat transfer coefficient*A* T_{A-av}
50.731=4*A*55
A=0.2305 m^2 =Total Fin Area + Base area
$A=4*N_F*L_F*H_f)+ (L*H)$

Heatsink Height (H_f):
$H_f=A-(L*H)/(4*N_F*L_F)$
=(0.2305-0.00175)/(4*20*0.001)
= 3 mm

Therefore the Fin Dimensions (Heigh, Space,Thickness) is (3, 2, 1)mm.

A typical design includes thermal reduction as well as power dissipation reduction that representing the heatsink performance. Therefore, the heatsink of the base dimension (height, width, thickness) of 50mm, 35mm, 1mm, and the fin dimensions (height, space, thickness): 3mm, 2mm, 1mm are selected which it meets the factors and requirements mentioned that fits the qualifications of portable processors.

4 SIMULATION RESULTS & DISCUSSION

This study concerns a simulation via the Thermal Analysis Package software for the proposed heatsink design which is suitable for most of portable processors. The base plate dimension is (50mm, 35mm, 1mm), as shown in Figure 6, the heat source is applied to the specified location based upon the hottest spot of the processors that is validated in previous studies.

The rectangular fins are designed (3, 2, 1) mm, this is shown in Figure 7, the number of fins that are covered the base plate is 20 fins.

The effect of ambient temperature is tested, this is shown in Figure 8, and the temperature contours is shown in Figure 9.

The rate of temperature reduction vs time is shown in Figure 10.

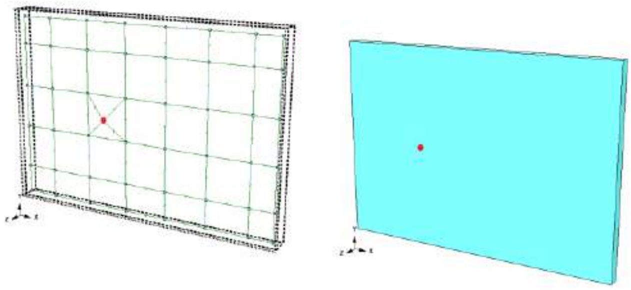

Figure 6: The base plate (50, 35, 1) mm with heat source

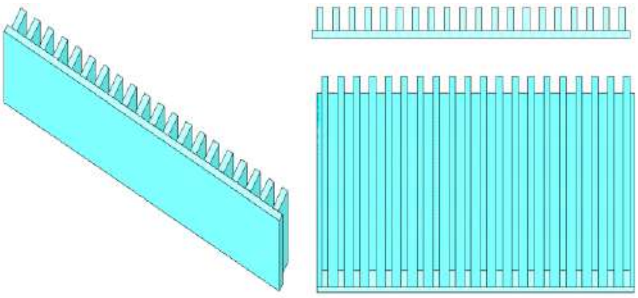

Figure 7: The heatsink fins (3, 2, 1)mm

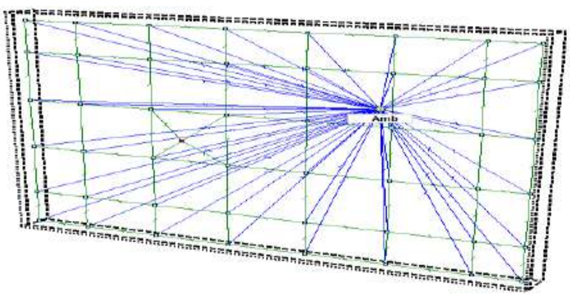

Figure 8: The effect of ambient temperature

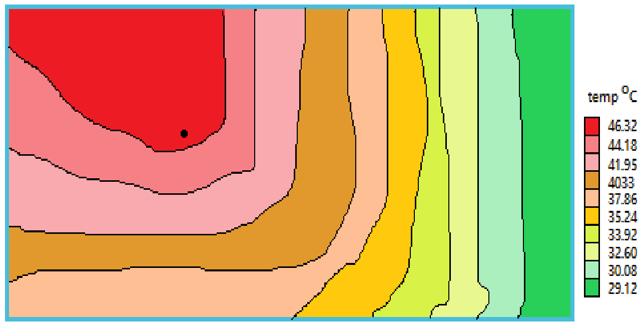

Figure 9: The temperature contours

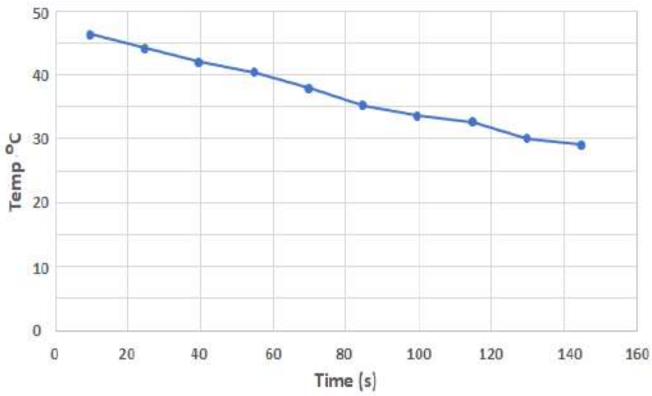

Figure 10: The temperature reduction Vs time

These results verifying that, the proposed heatsink can reduce 0.851 W and 12.77J at 15s, and it suitable for power and temperature limits of portable processors, the processor have a minimum average safe temperature bound and power consumption using the proposed heatsink to a high-performance estimation. It is verifying power as well as temperature aware to the processor designers in their verification efforts, all results are obtained in a real-time simulation setup. Therefore, the proposed design will help to the design corner requirements rather than power and thermal improvements as well as space reduction and material savings were attained.

5 CONCLUSIONS

The design and simulation of many different heatsinks are performed in order to achieve a low temperature, low power, and active operation of portable processors. The computer simulation and thermal analysis of different base dimensions as well as shape and dimensions of fins are used. From simulation results, the heatsink of the base dimension (height, width, thickness) of 50mm, 35mm, 1mm, and the fin dimensions (height, space, thickness): 3mm, 2mm, 1mm are identified

and selected which it meets the factors and design parameters. Results shows the specification improvements of the design model for ensuring power required to cool in time of 0.851 W, time to cool by 15s, and heat to remove is 12.77J which confirms theoretical fundamentals, sufficient improvement of power and temperature minimization, and better performance of the cooling system was achieved.
The maximum temperature reduction values are different for all heatsink profiles, it is clear that, the fin height and spacing has higher effects than the other parameters for obtaining maximum temperature reduction, it is mainly was 2^{o}C at 15s. The followed procedure in this article is significantly reducing time required for heatsink design and simulation model. Therefore, the presented design can be considered as a proper design constraint for portable processors

References

AHMED, H. E., SALMAN, B., KHERBEET, A. S. & AHMED, M. 2018. Optimization of thermal design of heatsinks: A review. *International Journal of Heat and Mass Transfer,* 118**,** 129-153.

DEDE, E. M., LIU, Y., JOSHI, S. N., ZHOU, F., LOHAN, D. J. & SHIN, J.-W. 2019. Optimal design of three-dimensional heat flow structures for power electronics applications. *Journal of Thermal Science and Engineering Applications,* 11.

FORNACIARI, W. & SOUDRIS, D. 2019. *Harnessing Performance Variability in Embedded and High-performance Many/Multi-core Platforms,* Springer.

GIERCZAK, M., MARKOWSKI, P. & DZIEDZIC, A. Modeling, simulation and analysis of temperature distribution in a heatsink. 2016 39th International Spring Seminar on Electronics Technology (ISSE), 2016. IEEE, 122-127.

HAMAALI, G., R. SULAIMAN, D. & IBRAHIM, M. 2019. Power and thermal management in SRAM and DRAM using adaptive body biasing technique. *IEICE Electronics Express***,** 16.20190432.

HANAFI, M. Z. M., ISMAIL, F. S. & ROSLI, R. Radial plate fins heatsink model design and optimization. 2015 10th Asian control conference (ASCC), 2015. IEEE, 1-5.

ILSCHE, T., SCHÖNE, R., SCHUCHART, J., HACKENBERG, D., SIMON, M., GEORGIOU, Y. & NAGEL, W. E. 2019. Power measurement techniques for energy-efficient computing: reconciling scalability, resolution, and accuracy. *SICS Software-Intensive Cyber-Physical Systems,* 34**,** 45-52.

MARKOWSKI, P. M., GIERCZAK, M. & DZIEDZIC, A. 2019. Modelling of the Temperature Difference Sensors to Control the Temperature Distribution in Processor Heatsink. *Micromachines,* 10**,** 556.

MJALLAL, I., FARHAT, H., HAMMOUD, M., ALI, S. & ASSI, I. 2018. Improving the cooling efficiency of heatsinks through the use of different types of phase change materials. *Technologies,* 6**,** 5.

NEYESTANI, M., NAZARI, M., SHAHMARDAN, M., SHARIFPUR, M., ASHOURI, M. & MEYER, J. 2019. Thermal characteristics of CPU cooling by using a novel porous heatsink and nanofluids. *Journal of Thermal Analysis and Calorimetry,* 138**,** 805-817.

R. SULAIMAN, D., HAMARASH, I. & IBRAHIM, M. 2017. Adaptive supply and body voltage control for ultra-low power microprocessors. *IEICE Electronics Express,* 14**,** 20170306-20170306.

ROTEM, E., GINOSAR, R., MENDELSON, A. & WEISER, U. C. Power and thermal constraints of modern system-on-a-chip computer. 19th International Workshop on Thermal Investigations of ICs and Systems (THERMINIC), 2013. IEEE, 141-146.

RUPP, K. 40 years of microprocessor trend data. GitHub, 2018.

SINGH, V., DAS, H. C. & NEMALIPURI, P. 2020. Numerical Analysis of Heat Transfer and Fluid Flow in Mini-channel Heatsink with Interconnecting Channels. *Advances in Mechanical Engineering.* Springer.

SMELT, D. 2018. Modeling many-core processor interconnect scalability for the evolving performance, power and area relation.

SULAIMAN, D. R. 2016. The DVS Controller: Analysis and Design. *ZANCO Journal of Pure and Applied Sciences,* 28.

SULAIMAN, D. R., HAMARASH, I. I. & IBRAHIM, M. A. 2019. The Complete Switching Circuit Design for CPU Joint Body Biasing and Supply Voltage Scaling. *ZANCO Journal of Pure and Applied Sciences,* 31**,** 20-25.

TODMAL, A. S. & MUKHERJEE, K. 2017. Design Of An Active Cpu Cooler Design Incoprating Heat Spreader. *ASEE Northeast Section Conference.* University of Massachusetts Lowell, MA, USA.

ZANCO Journal of Pure and Applied Sciences
The official scientific journal of Salahaddin University-Erbil
https://zancojournals.su.edu.krd/index.php/JPAS

ISSN (print):2218-0230**, ISSN (online):** 2412-3986**, DOI: http://dx.doi.org/10.21271/zjpas**

RESEARCH PAPER

Comparative Investigation of the Spherical Acoustic Microbubble Models in an Unbounded Liquid.

Narmeen N. Nadir[1], Kawa M.A. MANMI[2]

[1]Department of Petroleum Equipment, Erbil Technology Institute, Erbil Polytechnic University
[2] Department of Mathematics, College of Science, Salahaddin University-Erbil, Kurdistan Region, Iraq

A B S T R A C T:
Microbubble oscillating associated with many applications in biomedical and engineering sectors. The spherical oscillations of a single microbubble submerged in a quiescent liquid exerted by an acoustic force can be governed either by the Rayleigh-Plesset (RP) equation or by the Keller-Miksis (KM) equation under different physical assumptions. In this paper, both models were numerically and analytically analyzed, and the systematic parametric study was performed. The viscosity and compressibility effects and linearization in both models were investigated with the aids of MATLAB and Maple tools. In KM, the effects of the linear and nonlinear equations of states (EOS) compared for updating density with time. At the minimum bubble radius, the liquid viscosity surrounding bubble surface expected to be decreased due to rising in temperature. This leads to effects the maximum bubble radius for upcoming cycles.

KEY WORDS: Cavitation, Bubble Oscillation, Rayleigh-Plesset equation, Keller-Miksis, numerical methods for ODEs.
DOI: http://dx.doi.org/10.21271/ZJPAS.32.4.10
ZJPAS (2020) , 32(4);82-88 .

1. INTRODUCTION

Cavitation phenomena can be defined as the formation, rapid expansion and shrink of gas or vapor bubbles in a liquid due to reduction in liquid pressure locally to below the statured vapor pressure (Franc and Michel, 2006). This often occurs in many engineering processes induced by rapid changes in liquid situations. For instance, when a liquid moves in a pipe with sudden decrease in the pipe's cross-section. Classically, cavitation is undesirable as it leads to surface erosion, increase noise, reduction of efficiency and damage in mechanical engines.

* **Corresponding Author:**
Kawa M. A. MANMI
E-mail: kawa.aziz@su.edu.krd
Article History:
Received: 19/03/2020
Accepted: 10/05/2020
Published: 08/09 /2020

industry, semiconductor cleaning, targeted drug delivery, biomedical treatments like kidney stones (Kerabchi et al., 2018) disintegration, promoting chemical processes and the removal of bacterial biofilm in medical and dental applications (Vyas et al., 2019, Manmi et al., 2020). Acoustic waves might be used in majority of these applications, to generate and enhance the cavitation in the fluid, hence this kind of cavitation is called acoustic cavitation.

The bubble and droplet usually take a spherical shape due to surface tension force without interaction with any neighbouring particles or structures. Therefore, understanding spherical bubble oscillation is crucial, as in many situations the bubble's shape during oscillation, can be approximated as spherical. On the other hand, the microbubble surface is stabilized in biomedical applications, to remain spherical and prevent dissolution. This can usually be done by coating the bubble's surface with a shell typically made from lipid, protein, or polymer, commonly known as ultrasound contrast agent (Wang et al., 2015).

The oscillations of a single bubble have been widely studied theoretically, experimentally, and numerically for about one century. The first formal attempt in 1917 was done by Rayleigh who described the growth and contraction of a spherical or approximately spherical bubble in an incompressible and Newtonian liquid without considering the surface tension force and liquid viscosity effects at infinite container. The pressure difference between pressure inside the bubble and the external atmospheric pressure of the surrounding liquid is driving the bubble motion. His works was motivated to investigate cavitation damage and erosion on a ship propeller (Plesset and Prosperetti, 1977).

In 1949, Plesset (Plesset and Prosperetti, 1977) modified his equation to include surface tension and viscous effects under the same assumptions. This leads to introduce the famous and basic Rayleigh-Plesset equation for radial bubble motion. The main weakness of the RPE, is the lack of consideration for the compressibility effects for the surrounding liquid, which means lack of ability to consider damping amplitude of oscillation from acoustic radiation. The shockwaves might be formed due to this acoustic radiation particularly when the bubble is under violent oscillation. Eventually, it might have a large impact on the bubble dynamics.

In 1956, Keller and Kolodner (Keller and Kolodner, 1956) rederived the equation to consider the compressibility (small density variation). In 1980 their equation was developed by Keller and Miksis (Keller and Miksis, 1980) to include the standing acoustic wave. This essential equation for spherical bubble oscillations in a compressible fluid with or without an external acoustic force, is called the Keller-Miksis equation (Keller and Miksis, 1980).

In this study, viscosity and compressibility effects have been investigated in the RP and KM equations. The initial viscosity is increased from μ=0.001 to 0.004 and 0.008 kg (m s)-1. Also, at the end of the first cycle of oscillation the viscosity is increased from μ=0.001 to 0.004 and 0.008 kg (m s)-1 because during bubble collapse, the inertia of the surrounding water causes high pressure and high temperature, reaching around 10,000 kelvins in and surrounding the bubble's surface. Hence, we investigated this viscous change and compared it with constant viscosity during the whole simulation. In the KM model the density is not constant, as it is based on the weakly compressible theory. Therefore, linear and nonlinear equations of state have been used to update the density at each time step and compare the results. Furthermore, for a small amplitude of bubble oscillations the RP and KM are approximated to the linear second order differential equation so we're able to find the analytical solution and compare them with each other.

2. MATHEMATICAL MODELLING

Here we introduce the governing equation of spherical bubble dynamics in an incompressible fluid. For a Newtonian fluid, the governing equation reduces to the Rayleigh–Plesset equation (RPE) (Plesset and Prosperetti, 1977), which represents a second order non-linear ordinary differential equation with dependent variable R (bubble radius) and independent variable t (time).

$$\ddot{R}R + \frac{3}{2}\dot{R}^2 = \frac{1}{\rho}\left(p_b(t) + p_v - p_\infty(t) - \frac{4\mu}{R}\dot{R} - \frac{2\sigma}{R}\right), \qquad (1)$$

where $\dot{R}$ and $\ddot{R}$ are velocity and acceleration of the bubble which are function of time (t), ρ and μ are the density and viscosity of the liquid, σ is surface tension coefficient and p_v is vapour pressure. All parameters were considered as constant throughout this paper, unless otherwise stated. For oscillating bubble without acoustic field, $p_\infty(t)$ is basically a constant p_∞ and is usually considered as ambient pressure. In this paper, we investigate the more interesting case and includes the effects of the pressure $P(t)$ of a planar acoustic standing wave. Thus, the far-field pressure is,

$$p_\infty(t) = p_\infty + P(t) = p_\infty(1 + a\cos(\omega t + \phi)), \qquad (2)$$

where ω is the angular frequency of the acoustic wave, and a << 1 is the pressure perturbation amplitude and ϕ is the wave phase. It can be assuming that the pressure inside bubble p_b follows Dalton's law consist in two parts which are vapour pressure p_v and partial gas pressure. Furthermore, we assume that there is no heat and mass transfer. Therefore, the bubble pressure can be written as (Brennen, 2014, Grieser *et al.*, 2015),

$$p_b = p_{g0}\left(\frac{R_0}{R}\right)^{3k}, \qquad (3)$$

where k is called ratio of specific heat. For adiabatic system, it is real and approximately constant between 1 and 2; and p_{g0} is the gas pressure inside bubble at some bubble size R_0. Using $\Delta p = p_\infty - p_v$ and R_0 to nondimensionalize all variables in Equation (1) (Wang and Manmi, 2014, Wang et al., 2015, Abo *et al.*, 2018) which leads;

$$\ddot{R}_* R_* + \frac{3}{2}\dot{R}_*^2 = \varepsilon R_*^{-3k} + 1 - p_{a*}\cos(\omega_* t_* + \phi) - \frac{4}{Re\, R_*}\dot{R}_* - \frac{2\sigma_*}{R_*}. \qquad (4)$$

Keller-Miksis equation (KM) is a second order nonlinear ordinary differential equation with the dependant variable R_* and independent variable time t_* which describes large amplitude oscillations of bubble in a Newtonian liquid and takes liquid compressibility as a first order approximation into account. It is expressed as,

$$\ddot{R}R\left(1-\frac{\dot{R}}{C}\right) + \frac{3}{2}\dot{R}^2\left(1-\frac{\dot{R}}{3C}\right) = \frac{1}{\rho}\left[\left(1-\frac{\dot{R}}{C}\right)P_L + \frac{R}{C}\dot{P}_L\right], \qquad (5)$$

where C is speed of sound in the liquid and

$$P_L = p_b + p_v - p_\infty(t) - \frac{4\mu}{R}\dot{R} - \frac{2\sigma}{R}. \qquad (6)$$

If C approaches to ∞ equation (5) reduce to equation (1). In order to consider the compressibility; the density must be varying to transfer the wave energy between particles. Equations of states (EOS) are mathematical relationships between the variables of temperature, pressure, volume and moles of pure substance or a mixture (Smith *et al.*, 2013). There are several EOS to formulate this variation, but in adiabatic system density must be only the function of pressure. It can be simply a linear with pressure for ideal gas or it can be nonlinear. A very accurate equation of state for liquids in bubble dynamics is described by Tait (Brennen, 2014, Gilmore, 1952, Koch *et al.*, 2016), and states:

$$\rho = \rho_0\left(\frac{p_L + B}{p_\infty + B}\right)^{\frac{1}{n_T}}, \qquad (7)$$

p_∞ and ρ_∞ are the ambient pressure and the equilibrium density of the liquid respectively, $n_T = 7.15$ and $B = 3046 \times 10^5$ are knows as Tait exponent and Tait pressure respectively.

$$\frac{1}{C^2} = \frac{d\rho}{dp_L} = \frac{\rho_l}{\left(\frac{\rho_l}{\rho_\infty}\right)^{n_T} n_T\,(p_\infty + B)}. \qquad (8)$$

Equations (1) and (5) cannot be solved analytically except for very few special cases (Lauterborn and Kurz, 2010). However, accurate and stable approximate solutions can be obtained by using fourth order Runge-Kutta scheme (RK4). We used Matlab function ode45 here with the options of controlling the relative error and maximum time step to achieve stable numerical solution even for a high frequency microbubble oscillation in a short period time.

3. PARAMETRIC INVESTIGATION

3.1. Numerical investigation of RPE

In this section, parametric studies were performed to investigate the effects of viscosity for the first five cycles on the minimum and maximum bubble radius, time period of each cycle. The parameters in this paper are $R_0 = 4.5\ \mu\text{m}, f = 26.5$ kHz, $p_{a*} = 1.2$ $\sigma = 0.073$ N/m, $\lambda = 1.4$, $\rho = 998\ \text{kg/m}^3$, $p_v = 0.023 p_\infty$, $p_\infty = 1.013$MPa and $\varepsilon = 1 + 2\sigma_*$ (Prosperetti and Hao, 1999, Yuan *et al.*, 1998, Wang, 2016) Figure 1 shows the bubble radius history for three different viscosity μ=0.001, 0.004, 0.008 kg $(\text{m s})^{-1}$, but in Figure 1b, initially in all three cases μ=0.001 and at the end of the first cycle it was changed to 0.004, and 0.05 (dashed red and dotted black lines respectively). Many researchers reported that, in the acoustic cavitation sonoluminescence phenomenon occurs which is releasing thermal energy from the bubble collapse as light emission. The temperature exceeds several thousand Kelvins. On the other hand, the viscosity decreases with increasing temperature. Therefore, based on this we reduced the viscosity at the end of the first collapse in Figure 1b. As can be noted in Figure 1a, b; the maximum bubble radius and time period at each cycle decrease with increasing viscosity and in all cases the bubble radius rapidly damping due to viscosity expect the cases μ=0.001 which is gradually damping.

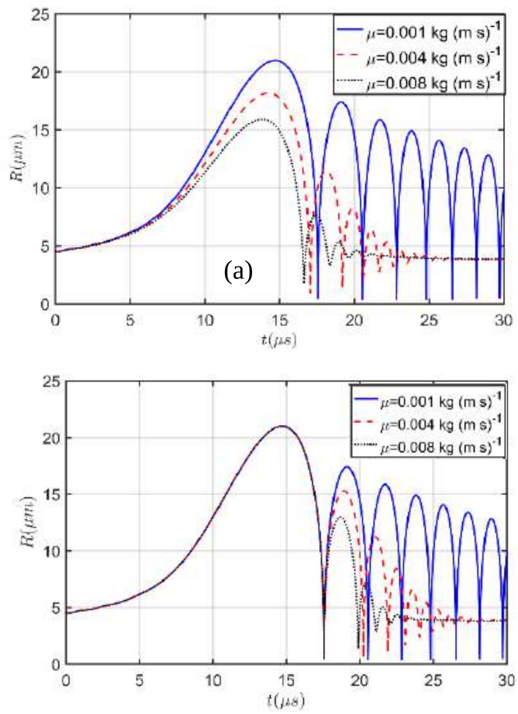

Figure 1: The Bubble radius versus time obtained from numerical solution of RPE with the parameters $R_0 = 4.5$ μm, f =26.5 kHz, $p_{a*} = 1.2$ $\sigma = 0.073$ N/m, $\lambda = 1.4$, $\rho = 998$ kg/m^3, $p_v = 0.023 p_\infty$, $p_\infty = 1.013$ MPa and $\varepsilon = 1 + 2\sigma_*$. (a) Constant viscosity is μ=0.001, 0.004, 0.008 kg (m s)$^{-1}$. (b) Initial viscosity is μ=0.001 kg (m s)$^{-1}$, at the end of first cycle it changed to 0.004 kg (m s)$^{-1}$ (dashed red line) and 0.008 kg (m s)$^{-1}$ (dotted black line).

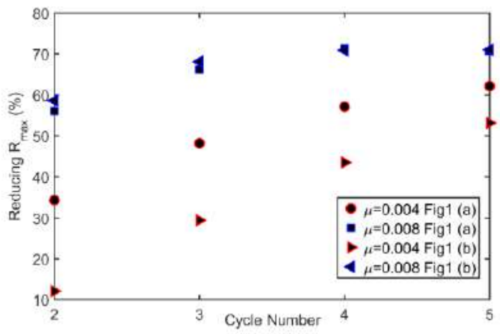

Figure 2: Reducing rate of maximum bubble radius for the cases in Figure 1.

Figure 2 shows that the decreasing rate of maximum bubble radius for the cases μ=0.004 and μ=0.008 to the cases μ=0.001. When the liquid viscosity relatively large as in the case μ=0.008, difference between rate of reductions in the maximum bubble radius is not significant (blue marks) due to dominant the viscose force effects however, in the case μ=0.004 the difference is significant (red marks).

3.2. Numerical investigation of KM

In this section, nonlinear spherical oscillations of microbubble studied for different scenarios. The compressibility of the fluid is usually measured based on Mach number (Ma) which can be expressed by u/C where u is the velocity of the bubble surface in the fluid and C is the speed of sound in that fluid which is about 1465 m/s at 20^{o} Celsius. We used the same parameters in the case of Figure 1 unless otherwise stated.

Firstly, following other researchers in the Literature, we assume that the Ma is constant throughout the whole simulation. Therefore, $u_{\mathrm{ref}} = \sqrt{\frac{p_\infty - p_v}{\rho}} \approx 10$ is used with three different viscosities μ=0.001, 0.004, and 0.008 kg (m s)$^{-1}$. Figure 3a and 3b show the bubble radius history with viscosity either initially or at the end of the first cycle changed respectively. Clearly, the maximum bubble radius R_{max} rapidly decreasing and minimum bubble radius R_{min} increasing with time due to both viscosity and compressibility effects. In Figure 3a the decreasing rate of R_{max} for μ=0.001 in the 2nd, 3rd, 4th and 5th cycle is about 44 %, 21%, 15% and 11%; for μ=0.004 about 45%, 27%, 20% and 11%; and for μ=0.008 50%, 31%, 18% and 9% respectively. For these data we can conclude that in the 2nd and 3rd cycle decreasing rate of R_{max} increase with μ, but in the 4th and 5th do not follow this trend.

Figure 4 shows the changing rate of R_{max} for the cases shown in the Figure 3 with cycle number. We can only observe some discrepancy at the second cycle between cases in Figure 3a and Figure 3b. Further both cases are approached to each other with the cycles number.

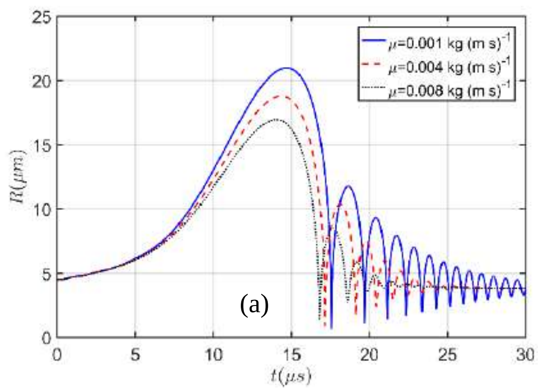

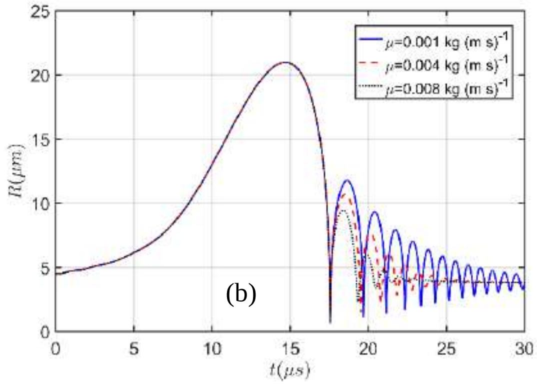

Figure 3: The Bubble radius versus time obtained from numerical solution of KM with speed of sound C=1465 (m s)$^{-1}$ the rest of the parameters are the same as in Figure 1. (a) Constant viscosity is μ=0.001, 0.004, 0.008 kg (m s)$^{-1}$. (b) Initial viscosity is μ=0.001 kg (m s)$^{-1}$, at the end of first cycle it changed to 0.004 kg (m s)$^{-1}$ (dashed red line) and 0.008 kg (m s)$^{-1}$ (dotted black line).

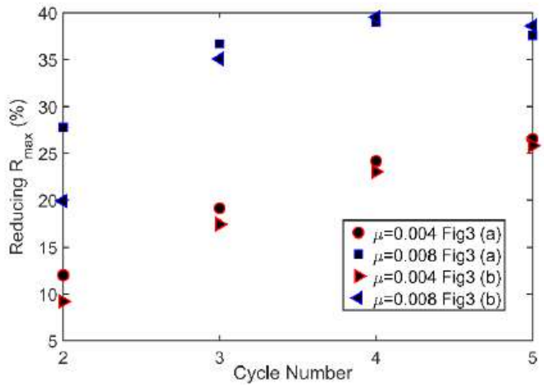

Figure 4: Rate of maximum bubble radius for the cases in Figure 3 versus number of cycles.

Secondly, we use Euler's method to update the density with time as follows:

$$\rho(t+\Delta t)=\rho(t)+\Delta p_L C^2. \qquad (9)$$

Although the liquid (water) is considered as weakly compressible, still small change in the density may has significant effect on the bubble dynamics. Therefore, we used equations (9) and (7) to update the density linearly and nonlinearly respectively at each time steps as can be seen in Figure 5. The compressibility effects more are pronounced when equation (8) is used. The decreasing rate of the maximum bubble radius increase when the equation (8) used instead equation (9).

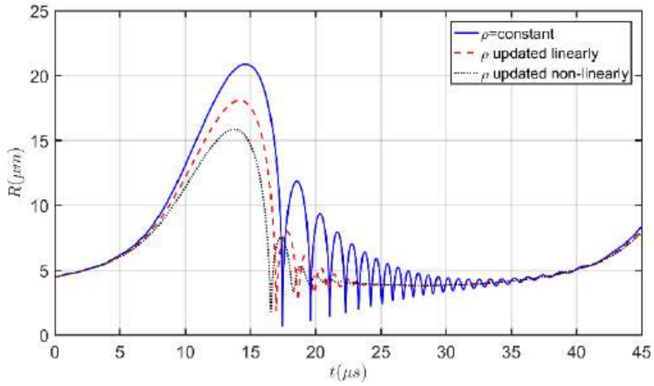

Figure 5: Bubble radius history in compressible liquid by setting ρ=constant=1000 (solid blue line) and using equation (9) (dashed red line) and using equations 7 and 8 (black dotted line).

4. LINEARIZATION OF RPE AND KM

In this section, we assume the oscillation take place around equilibrium radius R_0, so that we can write

$$R(t)=R_0\big(1+x(t)\big), \qquad (10)$$

where $x(t)\ll R_0$. Substituting (10) in (3) and using binomial expansion to give

$$p_b=p_{g0}\left(\frac{1}{1+x(t)}\right)^{3k} = p_{g0}\left[1-3kx(t) + \frac{-3k(-3k-1)}{2!}\big(x(t)\big)^2 + \cdots\right]. \qquad (11)$$

Equations. (10) and (11) allow us to reformulate RPE in equations (1) for x in the form of a linear harmonic-oscillation. Using (10) and (11) in (1) yields,

$$R_0^2[1+x(t)]\,\ddot{x}(t)+\frac{3}{2}R_0^2\dot{x}(t)^2 = \frac{1}{\rho}\begin{bmatrix} p_{g0}(1-3kx(t)+\cdots)-p_v-p_\infty-p_\infty\cos(\omega t+\phi) \\ -4\mu(1-x(t)+\cdots)\dot{x}(t)-\dfrac{2\sigma}{R_0}(1-x(t)+\cdots) \end{bmatrix} \qquad (12)$$

Neglecting the nonlinear terms in (12) and rearrange it to give harmonic-oscillation equation

$$\ddot{x}+2\beta\dot{x}+\omega_0^2x=-a\alpha\cos(\omega t+\phi), \qquad (13)$$

where $\alpha=\frac{p_\infty}{\rho R_0^2}$, $\beta=\frac{2\mu}{\rho R_0^2}$ and $\omega_0^2=\frac{1}{\rho R_0^2}\left(3kp_{g0}-\frac{2\sigma}{R_0}\right)$, which can be solved analytically, subject to initial bubble radius and velocity as initial conditions, to allow us to describe the bubble oscillations over time. The general exact solution of (13) can be expressed as,

$$x(t) = C_1 e^{-t\left(\beta+\sqrt{\beta^2-\omega_0^2}\right)} + C_2 e^{-t\left(\beta-\sqrt{\beta^2-\omega_0^2}\right)} - \frac{a\alpha(\omega_0^2-\omega^2)}{\omega^2-2\omega^2\omega_0^2+4\beta^2\omega^2+\omega_0^4}\cos(\omega t+\phi) - 2\frac{\beta a\alpha\omega}{\omega^2-2\omega^2\omega_0^2+4\beta^2\omega^2+\omega_0^4}\sin(\omega t+\phi). \quad (14)$$

The constants C_1 and C_2 are to be found using the appropriate initial conditions of the bubble. By the same manner with the aid of Maple software (Saeed and Mustafa, 2015), we can simplify the KM equation,

$$\ddot{x} + \beta\dot{x} + \omega_0^2 x = a[\alpha_1 \sin(\omega t+\phi) - \alpha_2\cos(\omega t+\phi)], \quad (15)$$

where

$\alpha_1 = \frac{\omega p_\infty}{\rho R_0 C}, \alpha_2 = \frac{p_\infty}{\rho R_0^2},$

$\beta = \frac{(CR_0^2 p_{g0}(3k-1)+4C^2R_0\mu+R_0^2p_\infty-aR_0^3p_\infty\omega\sin\omega t)}{\rho C^2 R_0^3}$ and

$\omega_0^2 = \frac{1}{\rho R_0^2}\left((3kp_{g0}-2\sigma\right)$. Thus the general exact solution can be expressed as,

$$x(t) = C_1 e^{-t\left(\beta+\sqrt{\beta^2-\omega_0^2}\right)} + C_2 e^{-t\left(\beta-\sqrt{\beta^2-\omega_0^2}\right)} - \frac{a(\omega_0^2-\omega^2)[\alpha_2\sin(\omega t+\phi)-\alpha_1\cos(\omega t+\phi)]}{\omega^2-2\omega^2\omega_0^2+4\beta^2\omega^2+\omega_0^4} - 2\frac{\beta a\omega[\alpha_2\sin(\omega t+\phi)+\alpha_1\cos(\omega t+\phi)]}{\omega^2-2\omega^2\omega_0^2+4\beta^2\omega^2+\omega_0^4}.$$

When *C* approach to ∞ Equation (15) reduce to Equation (13).

5. DISCUSSION

The viscosity and compressibility effects are not always negligible in bubble dynamics, particularly at the end of the bubble collapse phases. Both effects lead to bubble radius damping, as we noticed this in all the figures. In the RP and KM, the maximum and minimum bubble radius and cycle period decrease with viscosity and with time, except in the case of μ=0.001 in RP which the minimum bubble radius doesn't change significantly. In the KM when μ=0.001, the maximum bubble radius decreases rapidly, due to considering compressibility effects while in the RP decreases gradually. Furthermore, the exact solutions of the linearization of both models are similar with more terms in the KM due to considering compressibility effects.

6. CONCLUSION

The RP and KM equations describes the spherical bubble motion at infinite fluid for incompressible and compressible liquid, respectively. In this work, we assume that the pressure inside bubble is uniform and it follows adiabatic process. The viscous and compressibility effects in oscillating spherical microbubbles with and without the presence of the acoustic field were investigated for the RP and KM models. Based on the numerical cases, in the RP model, the maximum bubble radius in each cycle reduces linearly with the increasing viscosity, but in KM this was not occurred in all considered cases. Both models are linearized to the harmonic-oscillator equations with the assumptions of small perturbated oscillation and small amplitude of the excited acoustic wave.

References

ABO, A. A., HUSAIN, S. M. & HUSSEIN, S. A. 2018. Effect of Sudden Rise of Water in Stream on Adjacent Land. *ZANCO Journal of Pure and Applied Sciences,* 30**,** 105-112.

BRENNEN, C. E. 2014. *Cavitation and bubble dynamics*, Cambridge University Press.

FRANC, J.-P. & MICHEL, J.-M. 2006. *Fundamentals of cavitation*, Springer science & Business media.

GILMORE, F. R. 1952. The growth or collapse of a spherical bubble in a viscous compressible liquid. *California Institute of Tech Engineering Report,* No. 26-4.

GRIESER, F., CHOI, P.-K., ENOMOTO, N., HARADA, H., OKITSU, K. & YASUI, K. 2015. *Sonochemistry and the acoustic bubble*, Elsevier.

KELLER, J. B. & KOLODNER, I. I. 1956. Damping of underwater explosion bubble oscillations. *Journal of applied physics,* 27**,** 1152-1161.

KELLER, J. B. & MIKSIS, M. 1980. Bubble oscillations of large amplitude. *The Journal of the Acoustical Society of America,* 68**,** 628-633.

KERABCHI, N., MEROUANI, S. & HAMDAOUI, O. 2018. Depth effect on the inertial collapse of cavitation bubble under ultrasound: Special emphasis on the role of the wave attenuation. *Ultrasonics sonochemistry,* 48**,** 136-150.

KOCH, M., LECHNER, C., REUTER, F., KÖHLER, K., METTIN, R. & LAUTERBORN, W. 2016. Numerical modeling of laser generated cavitation bubbles with the finite volume and volume of fluid method, using OpenFOAM. *Computers & Fluids,* 126**,** 71-90.

LAUTERBORN, W. & KURZ, T. 2010. Physics of bubble oscillations. *Reports on progress in physics,* 73**,** 106501.

MANMI, K., WU, W., VYAS, N., SMITH, W., WANG, Q. & WALMSLEY, A. 2020. Numerical investigation of cavitation generated by an ultrasonic dental scaler tip vibrating in a compressible liquid. *Ultrasonics Sonochemistry*, 104963.

PLESSET, M. S. & PROSPERETTI, A. 1977. Bubble dynamics and cavitation. *Annual review of fluid mechanics*, 9, 145-185.

PROSPERETTI, A. & HAO, Y. 1999. Modelling of spherical gas bubble oscillations and sonoluminescence. *Philosophical Transactions of the Royal Society of London. Series A: Mathematical, Physical and Engineering Sciences*, 357, 203-223.

SAEED, R. K. & MUSTAFA, A. A. 2015. Homotopy Analysis Method to solve Glycolysis system in one dimension. *ZANCO Journal of Pure and Applied Sciences*, 27, 61-70.

SMITH, R., INOMATA, H. & PETERS, C. 2013. *Introduction to supercritical fluids: a spreadsheet-based approach*, Newnes.

VYAS, N., MANMI, K., WANG, Q., JADHAV, A. J., BARIGOU, M., SAMMONS, R. L., KUEHNE, S. A. & WALMSLEY, A. D. 2019. Which parameters affect biofilm removal with acoustic cavitation? A review. *Ultrasound in medicine & biology*.

WANG, Q. 2016. Local energy of a bubble system and its loss due to acoustic radiation. *Journal of Fluid Mechanics*, 797, 201-230.

WANG, Q., MANMI, K. & CALVISI, M. L. 2015. Numerical modeling of the 3D dynamics of ultrasound contrast agent microbubbles using the boundary integral method. *Physics of Fluids*, 27, 022104.

WANG, Q. X. & MANMI, K. 2014. Three dimensional microbubble dynamics near a wall subject to high intensity ultrasound. *Physics of Fluids*, 26, 032104.

YUAN, L., CHENG, H., CHU, M.-C. & LEUNG, P. 1998. Physical parameters affecting sonoluminescence: A self-consistent hydrodynamic study. Physical Review E, 57, 4265.

ZANCO Journal of Pure and Applied Sciences
The official scientific journal of Salahaddin University-Erbil
https://zancojournals.su.edu.krd/index.php/JPAS

ISSN (print):2218-0230, **ISSN (online):** 2412-3986, **DOI: http://dx.doi.org/10.21271/zjpas**

RESEARCH PAPER

First appearance of the cave leech *Erpobdella mestrovi* (Annelida: Erpobdillidae) in Iraq (Morphological and Molecular investigation) from Zalm stream, Sulaimani Province, Kurdistan Region, Iraq

Shayan J. Hamad-Ali Hallaq*, Luay A. Ali[1]

[1]Department of Fish Res. and Aquatic Animals, College of Agricultural Engineering Sciences, Salahaddin University-Erbil, Kurdistan Region, Iraq

[2] Department of Biology, College of Education, Salahaddin University-Erbil, Kurdistan Region, Iraq

A B S T R A C T:

During survey of different water bodies in Kurdistan Region, Iraq for the presence of leeches, only two distinct specimens with special morphological characters were found in the cave mouth of Ahmadawa Water source in February 2019. The morphological (Body size, oral and posterior suckers characters, coloration and body projections were studied) and molecular study (18S rDNA amplifying with a forward primer C1 (ACCCGCTGAATTTAAGCAT at position 25), and reverse primer C3 (CTCTTCAGAGTACTTTTCAAC at position 390) and sequencing of the amplicons) cleared that the present specimens were belonging to the erpobdillid leeches, *Erpobdella mestrovi*, and the present appearance regard as a first in Iraq and all over the Middle-East for this leech.

KEY WORDS: Cave leech, *Erpobdella mestrovi*, Morphology, Molecular, Iraq.
DOI: http://dx.doi.org/10.21271/ZJPAS.32.4.11
ZJPAS (2020) , 32(4);89-97 .

1. INTRODUCTION

Leeches origin and their controversial phylogeny within the Clitellata is a considerable debate subject for annelid systematics. Leeches and branchiobdellidans phylogenetic affinities were proposed before 1823 by Odier who described branchiobdellidans (crayfish worms) under leeches (Borda and Siddall, 2004). In early 1990's, evolutionary hypotheses of leeches were depended on plesiomorphic morphological characters interpretation and identification with corresponding of homologies. The morphological analysis supported leeches as, branchiobdellidans and Acanthobdella peledina have a common and molecular data also supported this hypothesis. However, other explanations for these relationships mentioned ectocommensalistic lifestyle adaptation as a cause of these shared ancestry (Holt, 1989; Brinkhurst, 1999).

DNA identification of leeches so useful since the identifications using standard techniques of taxonomy can sometimes be ambiguous since morphological characteristics are useful when dealing with mature specimens, the larval specimens or cocoon identification is enface lots of problems is identification especially for lower taxa (genus and species), also some taxa share many confused morphological and morphometric characters, whereas DNA characterization is

* **Corresponding Author:**
Shayan Jamal Hamad-Ali Hallaq
E-mail: shayan8992@gmail.com or luay.ali@su.edu.krd
Article History:
Received: 0812/2019
Accepted: 23/01/2020
Published: 08/09 /2020

useful for all taxa and developmental stages (Bely and Weisblat, 2006).

Three genera of erpobdellid leeches, namely *Erpobdella*, *Dina* and *Trocheta* are most species-rich genera. Traditionally can be distinguish by their annulation pattern among them. *Erpobdella* has five un-subdivided annuli per each body somite. Furthermore, the annulation pattern and body coloration patterns has proved to be inappropriate absolutely for the diagnosis of species (Neubert and Nesemann, 1995; Sket and Trontelj, 2008).

Cave leech, *Erpobdella mestrovi* (Kerovec, Kučinić and Jalžić, 1999), first description as a new species were by Kerovec *et al.* (1999) under a synonym *Croatobranchus mestrovi*, from caves in Croatia, Oceguera-Figueroa *et al.* (2005) re-described this species according to their 28S rDNA and changed the genus taxon to *Erpobdella*. This leech species have distinct morphological characters by presence of four oral projections and 12 pairs of body projections but have same basic erpobdillid sexual and digestive properties, some other reports of this leech were done from caves in Slovakia (Sket and Trontelj, 2008). *Erpobdella mestrovi* is a troglobitic leech (A troglobite is a species or population of animals bound to underground habitats (caves and dark wet spaces), living in cold water (4-6°C) (Culver *et al.*, 2009).

All the previous studies were done in Iraq, except that of Bilal *et al.* (2017), were depended only on morphological characters, there for, molecular investigation is a basic need for reviewing of Iraqi Leeches fauna, hence, the present study is the second scientific work deals with this scientific problem.

The present article recorded the first occurrence of *E. mestrovi* in Iraq; the outcome results from morphological examination were confirmed by molecular characterizations of 18S rDNA.

2. MATERIALS AND METHODS

2.1. STUDY AREA AND SAMPLE COLLECTION:

Only two unknown specimens of distinctive leeches were collected from Zalm stream, Sirwan River drainage near Ahmad Awa village (96.1 Km South-East to Sulaimani Province) under the emerged rocks of the cave mouth. Photomicrographs were taken directly for the leeches (as a live with the substratum) for documentation. One captured, leeches were transferred as a live to the laboratory.

2.2 MORPHOLOGICAL INVESTIGATION:

One complete sample and only the anterior and posterior parts of the other were used for morphological study, relaxed in 10% ethanol and put between two glass slides, fixed in 10% formalin, preserved in 70% ethanol. Measurements were taken with ocular micrometers (Kerovec *et al.* (1999; Oceguera-Figueroa *et al.*, 2005).

2.3 MOLECULAR INVESTIGATION were The used sample was the mid-body of one specimen, washed and preserved by deep freeze in ddH2O (-22 C˚). The specimen melted for extraction of the genomic DNA with a DNA extraction kit (GeNet Bio, KOREA). Briefly, macerated in mortar and pestle, transferred into sterile tubes with 200-250 µL tissue lysis buffer, incubated for eight hours. Qualification and quantification of DNA concentration done with Nano Drop (ND- 1000, USA). Samples genomic DNA with (A260–A320) / (A280–A320) ratio was more than 1.7 and outputs more than 30 ng/µL.

Mollaret et al. (2000) methodology was followed for amplification of 18S rDNA region with a polymerase chain reaction (PCR). Universal primers were used, forward primer C1 (ACCCGCTGAATTTAAGCAT at position 25), and reverse primer C3 (CTCTTCAGAGTACTTTTCAAC, position 390) was targeted. PCR reaction and conditions were performed using MJ Research, Applied Biosystem (AB) thermal cycler. The master mix was 50 µL reaction mixture, prepared in PCR tubes containing 2.5 µL DNA templates, 25 µL OnePCRTM master mix (GENEDIREX, KOREA), 1 µL of each primer and 20.5 µL double deionized water (ddH2O). The cycling conditions, 94˚C for 5 min (initial denaturation), 35 cycles of denaturation at 94˚C for 45 sec, annealing temperatures at 51˚C for 45 sec and extension at 72˚C for 45 sec, and 72˚C for 5 min (final extension). Gel electrophoresis was employed to check the validity of PCR products. Five wails with PCR products were prepared and run in 2%

agarose gel, stained with SYBR green that facilitate the DNA visibility with UV light.

The ABI 3130X nucleotide sequence analyzer (SINGAPORE) was used to find the order of nucleotides of 18S rDNA from the specimen. The PCR fragments of the specimens were purified from the agarose and used as a source of DNA template for sequencing.

3. RESULTS AND DISCUSSION

The results of the present study showed the prescience of *Erpobdella mestrovi* (Kerovec, Kučinić & Jalžić, 1999) for first time in Iraq, depending on the following findings:

Only two specimens of *Erpobdella mestrovi* (syname: Croatobarnchus mestrovi) were collected from Zalm stream near Ahmad Awa village under the stones in dark, shadow and cold water sutures.

According to the body length of the two sexually mature collected specimens, is moderately elongated, 28-44 mm long, narrowest body point 3.3-3.6 mm and widest body point 5.4-5.6 mm wide, slight depressed dorso-ventrally, milky to yellow-whitish in color, no visible eyes, the red blood is clearly visible in the ventral side along the lateral coelomic ducts. The total number of annuli 103, five equal annuli comprising the mid-body somite (Fig. 1: A; B; C).

The head region shape is changeable when attach and release, when it free (not attached to the substratum) is slightly expanded, rounded, four pairs of short conical tentacles (0.18-0.21 mm long, 0.11-0.13 mm wide) were extended from anterior and lateral sides, each of them bearing five finger-like papillae (Fig. 1 A; B). These tentacles disappear during sucker adhesion to the substratum. Oral cavity is circular; the mouth have no jaws, is usually widely open (in live and preserved specimens), muscular ridges only visible deep in the pharynx (Fig. 1: A; D).

The body width increases gradually in the caudal direction (very fast in starting of the third body half), clitellar region is slightly swollen (Widest body point without projections) (Fig. 1: A; B).

Gonopores are separated by at least 2.5 annuli, the male gonopore on the annulus anterior to the slightly backward shifted ganglion (probably a2). Studied specimens were having had a typical Erpobdelid male genital atrium with a massive body and conical horns bent distally. The female gonopore starting with somite XVI, (probably b5/b1 = XII/XIII) (Fig. 1: B).

Twelve lateral projections projected from the body, the longest one about 0.5 mm and the shortest 0.04 mm. Two short triangular projections are in the front and behind the longest lateral process. Anal opening is dorsal surrounded by small lips, approximately above the center of the posterior sucker which become a very thin rim when attached (Fig. 1: A; B; C; D).

The sequence from 18S rDNA of *Erpobdella mestrovi* specimens was made of 480 bp (amplified fragment was 521 bp, while after sequencing some miss-nucleotides were excluded, related to quality of sequencing analysis) and put to BLAST then compared with other stored genus of leeches sequences from GenBank database (Fig. 2: A; B; 3).

The blasting of 18S rDNA sequences of the present specimens with that available in Gene Bank showed 98% similarity with the sequences of *Erpobdella mestrovi* (Fig. 2: A; B; 3).

This leech was first described by Kerovec *et al.* (1999) as a new species under the name Croatobranchus mestrovi (Genus name according to the type country Croatia and species name according to the type author Milan Meštrov) during the expedition of Lukina jama. These leeches have a caterpillar like moving by stretching-contracting body. Their body bearing projections look like small legs (most probably auxiliary respiratory organs - branchia). Sket *et al.* (2001) re-described the same species and added some internal characters, and the proposed that this species is belonging to the erpobdillid leeched. Moreover, after DNA analysis, the genus name Erpobdella were fixed by Oceguera-Figueroa *et al.* (2005) and the genus taxon of this species were corrected.

The Morphometric study of the present specimens were fit with that of Kerovec *et al.* (1999) as well as Sket *et al.* (2001), and the investigated body parts were have same morphologic and morphometric characters.

Latter, *E. mestrovi* was found in a few deepest caves of Mt. Velebit in Slovacka jama, Olimp and Velebita. Some undescribed species, including erpobdellid leeches, occur in a number cave of China and the US (Sket and Trontelj, 2008).

According to Mhaisen (2019), 10 leech species were recorded in Iraq including Kurdistan Region before the present work, the first occurrence of leeches was represented as *Piscicola* sp. by (Herzog, 1969); then records continued and arranged alphabetically as, *Acipenserobdella volgensis* on *Carasobarbus luteus* and *Cyprinion macrostomum* (Al-Salmany, 2015); *Cystibranchus mammillatus* on *Mastacembelus mastacembelus* (Bashê, 2008); *Cystibranchus mastacemeli* on *Luciobarbus kersin* (as Barbus kersin) (Al-Jawda et al., 2000) and *Mastacembelus mastacembelus* (as *Mastacembelus simach*) (Rahemo , 1989; 1996); *Cystibranchus* sp. on *Mastacembelus mastacembelus* (as *Mastacembelus simach*) (Rahemo, 1989); *Dina lineata* (Ali and Jaweir, 2013) ; *Dina punctata* (Bilal *et al*., 2017); *Erpobdella octulata* (Ahmed, 2009); *Fadejewobdella quinqueannulata* (Ali, 2010); *Haemopis sanguisuga* (Ahmed, 2009); *Hemiclepsis marginata* on *Cyprinus carpio*, *Luciobarbus xanthopterus* (as *Barbus xanthopterus*), *Mesopotamichthys sharpeyi* (as *Barbus sharpeyi*) (Khalifa, 1985; 1989) and *Planiliza abu* (as *Liza abu*) (Mhaisen *et al*., 1993) and *Piscicola geometra* on *Arabibarbus grypus* (as *Barbus grypus*) (Al-Jawda *et al*., 2000), *Leuciscus vorax* (as *Aspius vorax*) (Mhaisen *et al*., 1997) and *Luciobarbus esocinus* (as *Barbus esocinus*) (Adday *et al*., 1999) and *Piscicola* sp. on *Arabibarbus grypus* (as *Barbus grypus*) (Shamsuddin *et al*., 1971), *Luciobarbus esocinus* (as *Barbus esocinus*) (Ali, 1989), *Luciobarbus pectoralis* (as *Barbus schejch*) (Herzog, 1969), *Luciobarbus xanthopterus* (as *Barbus xanthopterus*) (Shamsuddin *et al*., 1971).

Since no previous reports of the *E. mestrovi*, the present occurrence of this leech can be regards as a first in Iraq and all middle-east since no previous reports clearing it is presence in this part of the world.

CONCLUSIONS

First presences of the cave leech (Erpobdella mestrovi) is a main conclusion of the present morphological and molecular investigations for leeches in Iraq and can regard as a 12th species of Iraqi leech fauna. There is no any report for this leech (Erpobdella mestrovi) in the Middle East at all. Hence, Zalm stream in Sulaimani Province, Kurdistan Region, Iraq regard as a new habitat for this leech in the world.

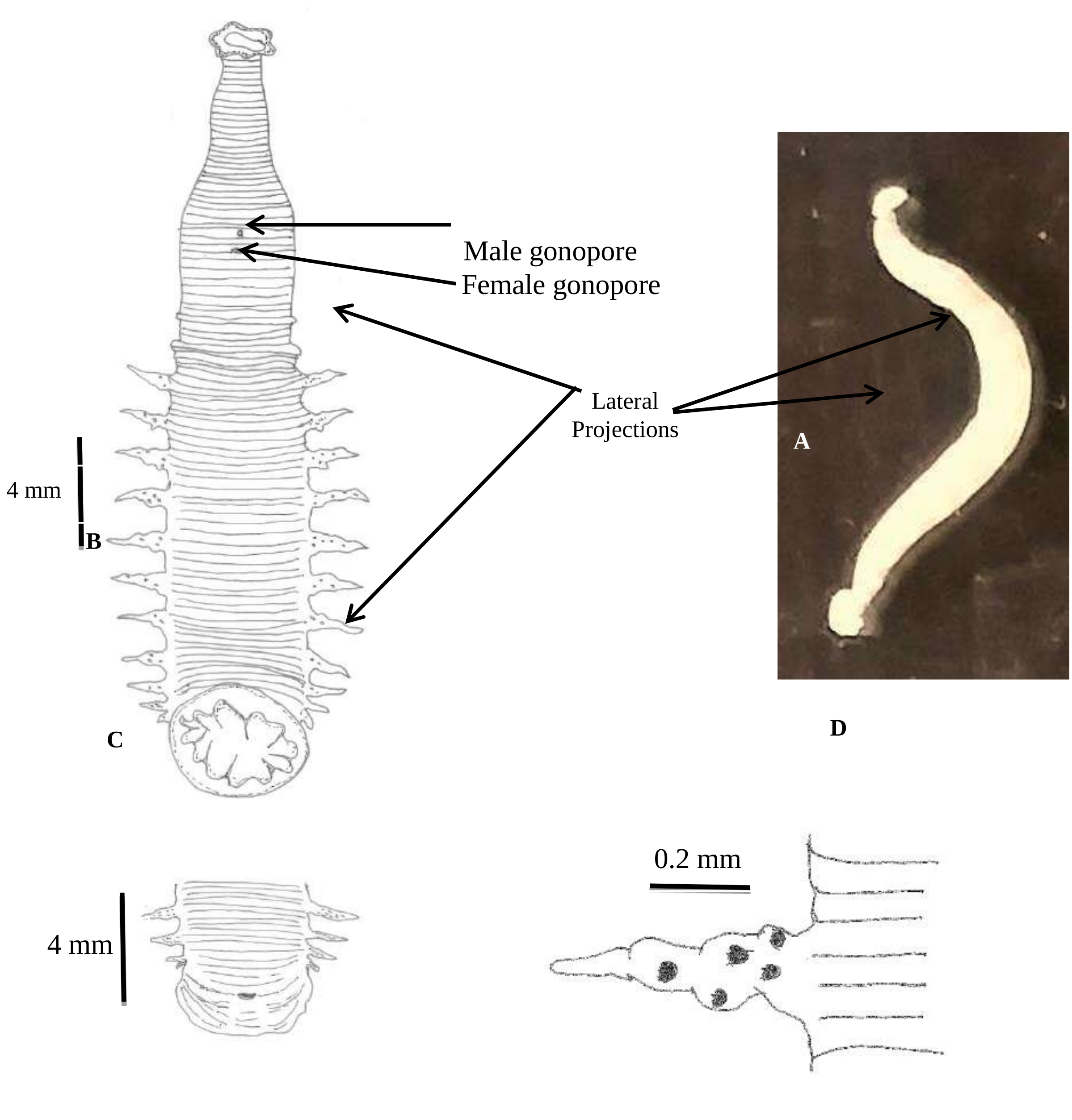

Figure 1: *Erpobdella mestrovi.*

A- Photograph of the fixed specimen whole body (2 X).

B- Lucida drawings, dorsal view.

C- Lucida drawings, dorsal view.

D- Lucida drawings of the lateral projection.

```
Score           Expect  Identities      Gaps        Strand
857 bits(464)   0.0     485/495(98%)    2/495(0%)   Plus/Minus

Query  1    ATTGTTATTTTTCGTCACCACCTCCCTGAGTTAGGAGTGGGTAATTTGCGCGCCTGCTGC  60
            |||||||||||||||||| |||||||||||||||||||||||||||||||||||||||||
Sbjct  518  ATTGTTATTTTTCGTCACTACCTCCCTGAGTTAGGAGTGGGTAATTTGCGCGCCTGCTGC  459

Query  61   CTTCCTTGGATGTGGTAGCCGTTTCTCATGCTCCCTCTCCGGAATCGAACCCTGATTCCC  120
            ||||||||||||||||||||||||||||||||||||||||||||||||||||||||||||
Sbjct  458  CTTCCTTGGATGTGGTAGCCGTTTCTCATGCTCCCTCTCCGGAATCGAACCCTGATTCCC  399

Query  121  CGTTACCCGTTACGACCATGGTAGGCATGTCGCGTACCATCGAAAGTTGATAGGGCACAC  180
            ||||||||||||||||||||||||||||||||||||||||||||||||||||||||||||
Sbjct  398  CGTTACCCGTTACGACCATGGTAGGCATGTCGCGTACCATCGAAAGTTGATAGGGCACAC  339

Query  181  ACTTGAAAGATCCGTCGCCGGCTCGAGGCCGTGCGATCAGCTCGAAGTTATCCAGAGTCA  240
            ||||||||||||||||||||||||||||||||||||||||||||||||||||||||||||
Sbjct  338  ACTTGAAAGATCCGTCGCCGGCTCGAGGCCGTGCGATCAGCTCGAAGTTATCCAGAGTCA  279

Query  241  CCATCGTTTACGGACCTACTCCCGGCCGAGACCGGGAGCGGTTAACGCCCGATTAGTTTT  300
            |||||||| ||||||| || ||| ||||||||||||||| ||| | |||||||| |||||
Sbjct  278  CCATCGTT-ACGGACCGACGCCCAGCCGAGACCGGGAGCCGTTGATGCCCGATTGGTTTT  220

Query  301  GATCTAATAAACGCGCTCTTCCCCTCGCGGGTCGGAGCTTGTCTGCATGTATTAGCTCTA  360
            ||||||||||||||||||||||||||||||||||||||||||||||||||||||||||||
Sbjct  219  GATCTAATAAACGCGCTCTTCCCCTCGCGGGTCGGAGCTTGTCTGCATGTATTAGCTCTA  160

Query  361  GAATTACCACAGTTATCCAAGTAGGGATTGTACGATCTAAGAAATCATGGGTGGCCTAAT  420
            ||||||||||||||||||||||||||||||||||||||||||||||||||||||||||||
Sbjct  159  GAATTACCACAGTTATCCAAGTAGGGATTGTACGATCTAAGAAATCATGGGTGGCCTAAT  100

Query  421  GAGCCATTCGCAGCTTTA-CCGTGTTAAGGTTTGTGCTTAGACATGCATGGCTTAATCTT  479
            |||||||||||||||||| |||||||||||||||||||||||||||||||||||||||||
Sbjct  99   GAGCCATTCGCAGCTTTAACCGTGTTAAGGTTTGTGCTTAGACATGCATGGCTTAATCTT  40

Query  480  TGAGACAAGCATATG  494
            |||||||||||||||
Sbjct  39   TGAGACAAGCATATG  25
```

Figure 3: Pair wise alignment of 18S rDNA sequence of *Croatobranchus mestrovi* Query is the study or sample sequence and Sbjct is the GenBank sequence.

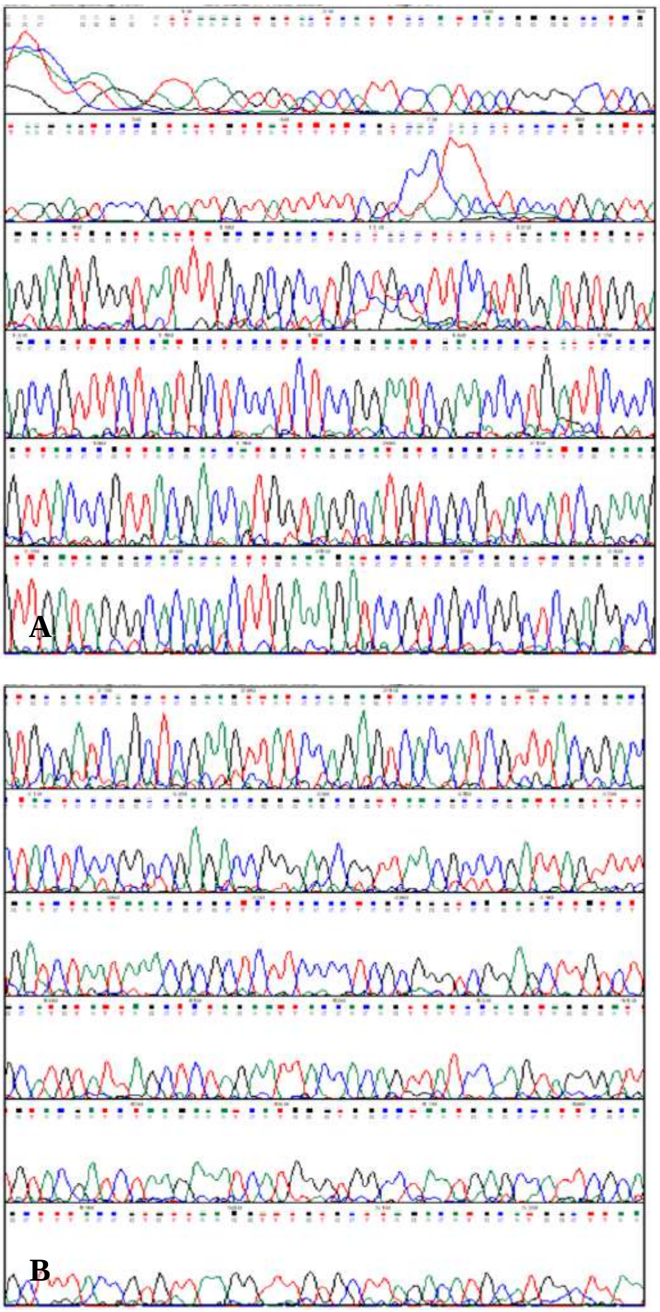

Figure 2: The sequencing result of 18S rDNA of *Erpobdella mestrovi*.

References

ADDAY, T.K.; BALASEM, A.N.; MHAISEN, F.T. & AL-KHATEEB, G.H. (1999). A second survey of fish parasites from Tigris river at Al-Zaafaraniya, south of Baghdad. *Ibn Al-Haitham J. Pure Appl. Sci.,* 12(1): 22-31.

AHMED, S. T. (2009). *Biological studies on leeches in Erbil and its suburbs*. A PhD dissertation/ Biology Dept./ College of Science- Salahaddin Univ.- Erbil. 113pp.

ALI, B.A.-R. (1989). *Studies on parasites of some freshwater fishes from Greater Zab- Iski-Kalak.* M. Sc. Thesis, Coll. Sci., Univ. Salahadden: 120pp. (In Arabic).

ALI, L. A. & JAWEIR, H. J. (2013). First record of *Dina lineata* (Hirudinea: Erpobdellidae) in Greater Zab river Kurdistan region-Iraq. *J. Univ. Zakho*, 1(A): 1: 207-209.

ALI, L. A. (2010). First record of *Fadejewobdella quinqueannulata* (Hirudinea: Erpobdellidae) in Greater Zab River-Iraq. *Zanko J.*, 22 (2): 47-50.

AL-JAWDA, J. M.; BALASEM, A. N.; MHAISEN, F. T. & AL-KHATEEB, G.H. (2000). Parasitic fauna of fishes from Tigris river at Salah Al-Deen province, Iraq. *Iraqi J. Biol. Sci*., 19 & 20: 16-24.

AL-SALMANY, S. O. K. (2015). *Parasitic infections of some fish species from Euphrates River at Al-Qaim city, Al-Anbar province.* M. Sc. Thesis Department of Biology College of Science University of Tikrit. 193 pp. (In Arabic)

BASHÊ, S. K. R. (2008). *The parasitic fauna of spiny eel Mastacembelus mastacembelus (Banks and Solanser, 1794) from Greater Zab River-Kuristan region-Iraq.* M. Sc. Thesis, Sci. Edu. Coll., Univ. Salahaddin: 62pp.

BELY, A. E. & WEISBLAT, D. A. (2006). Lessons from leeches: a call for DNA barcoding in the lab. *Evolution & Development*, 8, 491–501.

BILAL, S. J.; ALI., A. A.; ABDULLAH, L. Y.; KHAILANY, R. A.; DHAHIR, S. F. & ABDULLAH, S. M.-A. (2017). First Record of Leech *Dina Punctata* (Annelida: Erpobdellidae) from Lesser Zab River in Northern Iraq: Morphological and Molecular Investigation. *Jordan Journal of Biological Sciences*, 10 (2): 69 – 72.

BORDA, E. & SIDDALL, M. E. (2004). Review of the evolution of life history strategies and phytogeny of the Hirudinida (Annelida: Oligochaeta). *Lauterbornia* 52: 5-25, D-86424 D inkelscherben.

BRINKHURST, R. O. (1999): Lumbriculids, branchiobdellidans and leeches: an overview of recent progress in phylogenetic research on clitellates.- *Hydrobiologia,* 406: 281-290, Dordrecht

CULVER, D.; PIPAN, C.; & TANJA, T. (2009). *The biology of caves and other subterranean habitats.* New York: Oxford University Press. 456-523 pp. ISBN 9780199219933. OCLC 248538645.

HERZOG, P. H. (1969). Untersuch-ungen über die parasiten der süBwasserfische des Irak. *Arch. Fischereiwiss.*, 20(2/3): 132-147.

HOLT, P. C. (1989): Comments on the classification of the Clitellata. *Hydrobiologia*, 180: 1-5, Dordrecht.

KEROVEC, M.; KUČINIĆ, M. & JALŽIC, B. (1999). *Croatobranchus mestrovi* sp. n. -predstavnik nove endemske podzemne vrste pijavica. *Spelolog* 44/45, 35–36. (In Slovakian)

KHALIFA, K. A. (1985). Leeches on freshwater farmed fishes in Iraq. *J. Wild. Dis.*, 21(3): 312-313.

KHALIFA, K.A. (1989). Incidence of parasitic infestation of fishes in Iraq. Pak. Vet. J., 9(2): 66-69.

MHAISEN, F. T. (1993). A review on the parasites and diseases in fishes of ponds and farms of Iraq. Iraqi J. Vet. Scs., 6(2): 20-27. (In Arabic).

MHAISEN, F. T. (2019). *Index-catalogue of parasites and disease agents of fishes of Iraq*, 24 pp. (Unpublished data)

MHAISEN, F. T.; AL-KHATEEB, G. H.; BALASEM, A. N. & MUTAR, A. J. (1997). *On a collection of some fish parasites from Euphrates River, Anbar province, Iraq. Babylon.* Univ. J., Pure. Appl. Sci., 2(3): 267-272.

MHAISEN, F.T. (1993). Fish parasites of Neinava province: A review and check- lists. *Iraqi J. Vet. Med.,* 17: 110-125.

MOLLARET, I; JAMIESON, B. G. & JUSTINE, J. (2000). Phylogeny of the Monopisthocotylea and Polyopisthocotylea (Platyhelminthes) inferred from 28S rDNA sequences. *Int. J. Parasitol*, 30: 171–85.

NEUBERT, E. & NESEMANN, H. F. (1995). A new species of Batracobdella (Hirudinea, Glossiphoniidae) from Turkey. Zoology in the Middle East, 11(1):109-111. DOI: 10.1080/09397140.1995.10637679.

OCEGUERA-FIGUEROA, A.; LEO´N-RE`GAGNON, V. & SIDDALL, M. E. (2005). Phylogeny and revision of Erpobdelliformes (Annelida, Arhynchobdellidae) from Mexico based on nuclear and mitochondrial gene sequences. Revista Mexicana de Biodiversidad, 76, 191–198.

RAHEMO, Z. I. F. (1989). *Cystibranchus mastacembeli* (Annelida: Hirudinea) from the Iraqi freshwater spinyback, *Mastacembelus simach* (Wabaun, 1792). *Riv. Parasitol.*, 6 (50) No. 1: 121-126.

RAHEMO, Z. I. F. (1996). Parasites of the Iraqi spinyback *Mastacembelus simach* (Walbaum, 1792). *Iraqi J. Biol. Sci.,* 15: 42-52.

SHAMSUDDIN, M.; NADER, I.A. & AL-AZZAWI, M. J. (1971). Parasites of common fishes from Iraq with special reference to larval form of *Contracaecum* (Nematoda: Heterocheilidae). *Bull. Biol. Res. Centre, Baghdad*, 5: 66-78.

SKET, B. & TRONTELJ, P. (2008). Global diversity of leeches (Hirudinea) in freshwater. *Hydrobiologia*, 595: 129-137.

SKET, B.; DOVC, P.; JALŽIĆ, B. & TRONTELJ, P. (2001). Cave leech (Hirudinea, Erpobdellidae) from Croatia with unique morphological features. *Zoologica Scripta*, 30(3):223 – 229. DOI: 10.1046/j.1463-6409.2001.00065.

t activity of black and black mate tea polyphenols determined by ferrous tartrate and Folin–Ciocalteu methods. *Food chemistry,* 99**,** 835-841.

ZANCO Journal of Pure and Applied Sciences
The official scientific journal of Salahaddin University-Erbil
https://zancojournals.su.edu.krd/index.php/JPAS

ISSN (print):2218-0230**, ISSN (online):** 2412-3986**, DOI: http://dx.doi.org/10.21271/zjpas**

RESEARCH PAPER

Rampancy of Antinematicidal Resistance Among Gastrointestinal Nematodes in Kurdish Goat Breeds

Kareem Khoshnow Hama* , Fikry Ali Qadir *

***Department of Biology, College of Science, Salahaddin University- Erbil, Kurdistan Region of Iraq**

A B S T R A C T:

The current study was designed to determine the emergence of resistance among gastrointestinal roundworms of native goats against renowned synthetic antinematicidals such as fenbendazole, avermectin and levamisole. To meet the survey requirements, six commercial goat farms, located in Sothern and Western Erbil province-Kurdistan region of Iraq, were chosen after performing qualitative parasitological assays. The study was executed from September to end of November, 2019. From each farm, 30 adult goats were haphazardly divided into two groups, a group (n=15) for treatment and other group (n=15) served as control. The faecal egg count reduction test (FECRT) and egg hatch assay (EHA) have disclosed emergence of resistance against fenbendazole. According to RESO Computer Program, the estimated FECR% in farms 1 and 2 were 70.72 and 79.55, whilst the lower confidence intervals 95% were 63 and 73.8 respectively. The LC_{50} value of fenbendazole after conducting EHA, calculated through probit analysis, was estimated to be 2.11 μg ml^{-1} (range 1.47-2.34). Regarding avermectin, the computed FECR% in farms 3 and 4 were 93.92 and 92.98, while the lower confidence intervals 95% were 92.91 and 90.7 respectively, which signified the presence of suspicion about prevalence of resistance against avermectin. For levamisole, the calculated FECR% in farms 5 and 6 were 95.99 and 96.38, whilst the lower confidence intervals 95% were 95.1 and 95.7 respectively. Consequently, the parasitic nematodes were susceptible to this synthetic chemotherapeutic in the region.

KEY WORDS: Indigenous caprine, Alimentary tract nematodes, Synthetic dewormers, Antinematicidal resistance, Erbil province
DOI: http://dx.doi.org/10.21271/ZJPAS.32.4.12
ZJPAS (2020) , 32(4);98-107 .

1.INTRODUCTION

Indisputably, infestation with gastrointestinal (GI) nematodes is deemed one of the most rampant parasitosis threatening small ruminant resources in the world particularly the Southern Hemisphere (Kaplan and Vidyashankar, 2012) and even European countries (Blake and Coles, 2007; Furgasa *et al.*, 2018). For decades, livestock raisers have relied greatly on synthetic dewormers to cure nematodiasis in ovine and caprine (Taylor *et al.*, 2007; Hamad *et al.*, 2018). ailments have been mitigated; but on the other hand, development of antinematicidal resistance (AR) was the consequence of this practice (Gilleard, 2006).

On a particular flock of small ruminants, AR can arise in one species of GI nematodes against numerous synthetic antinematicidals or in numerous species of alimentary tract roundworms towards one type of dewormer (Chartier *et al.*, 1998). In tropical and sub-tropical zones, where AR is historically of considerable worry since last five decades, comprehensive surveys and studies have revealed that the dilemma is serious and obviously associated with recurrent deworming, widespread of *Haemonchus contortus* (a trichostrongylid helminth dwelling abomasa of sheep and goats) and the existing kind of pasture management (Waller, 1995; Kalkal *et al.*, 2019).

* **Corresponding Author:**
Kareem Khoshnow Hamad
E-mail: kk_hamad@yahoo.com
Article History:
Received: 18/01/2020
Accepted: 15/02/2020
Published: 08/09 /2020

The emergence and rampancy of AR seem to differ geographically according to the existing climatological conditions, species of parasitic roundworms and deworming policy followed in the area. Having said, the rate of emergence of antinematicidal-resistant individuals has commonly been slower in moderate regions in the European countries as compared to other warm geographical zones in the Southern Hemisphere (Jabbar *et al*., 2006). In Kurdistan region, the performed studies on AR in GI nematodes of sheep and goats are very rare and the limited surveys that have been done were related to ovine nematodes (Ahmed *et al.*, 2015; Ahmed *et al.*, 2019). Hence, this comprehensive survey was encompassed the likely emergence of resistance against renowned synthetic chemotherapeutics (broad-spectrum anthelmintics) including fenbendazole, avermectin and levamisole by GI nematodes of native goats in some districts of Kurdistan region.

2. Materials and Methods

2.1. Goat farms

Six private goat flocks were chosen from the files of the local veterinarians in September- end of November 2019. The farms that underwent this survey were located in Southern (Kandinawa district) and Western (Shamamic district) Erbil province-Iraq. The size of herd, expressed as adult does (females of goats) merely, ranged from 40 to 50 on each goat farm.

2.2. Procedure

The routine procedure to diagnose AR in parasitic nematodes was that adopted by the World Association for the Advancement of the Veterinary Parasitology (W.A.A.V.P) (Coles *et al*., 1992). None the trialed goats had been deparasited with any antinematicidal therapeutic agent for at least two months before pursuing the survey. On each of the 6 goat ranches, 30 goats, more than 1 year old, were chosen, clinically examined by the researcher (Veterinary Doctor), and arbitrarily allocated into two groups (n=15). A group was selected as untreated control and other one represented as a treatment group. The experimental animals (farm 1 and 2) were drenched fenbendazole orally by a drench gun at 10 mg/kg BW (double dose). Avermectin injected subcutaneously at 0.4 mg/kg BW (double dose) to animals in farm 3 and 4, whilst levamisole was administered orally at 12 mg/kg BW (1.5 dose) to animals in farm 5 and 6. Dewormer doses were calculated according to the heaviest animal of each group. The reason behind giving high doses to goats is back to the difference in bioavailability and potency of aforesaid synthetic drugs between ovine and caprine (Bogan *et al*., 1987; Sangster *et al*., 1991).

2.3. Preliminary tests to determine natural infections with GI nematodes

●*Faecal examination*

Qualitative and quantitative parasitological techniques were carried out to diagnose natural infestations with different GI nematodes and during performing other steps of the survey (Coles *et al*., 1992; Iqbal *et al*., 2006; Radostits *et al.*, 2007).

●*Coproculture*

Coprocultures were executed to determine the contribution of different GI nematodes in whole natural parasite infections following MAAF (1986). Faecal specimens, collected directly from the rectum, from each group of experimental animals were pooled and cultured in plastic containers. Amphotericin B (5 μg g^{-1}) was added to prevent fungal contaminations. The cultures were incubated for seven days at 27±1ºC. Then, the nematode larvae (L_3) were collected using Baermann apparatus.

●*Baermann technique*

This approach was conducted to collect the larvae (L_3) of GI nematodes from the coproculture. Approximately 15g of the incubated faeces were wrapped up in medical gauze and put in the Baermann apparatus funnel. Warm water was added to induce larval motility toward the end of collecting tube. The “Baermann” was left overnight and a small volume of water was collected and poured in a plastic container. Then the water specimen transferred to a petridish, Lugol’s iodine was added (Iqbal *et al*., 2006) and finally, larvae were recognized following MAFF (1986).

2.4. Studies on antinematicidal resistance

●*Fecal egg count reduction test (in vivo assay)*

The experimental animals (n=15) in group 1 were given fenbendazole at a dose mentioned previously; whereas group 2 served as infected untreated control (n=15) in each goat farm (two farms). Eggs per gram of faeces (EPG) were counted in control group and in fenbendazole group (group 1) after 10-14 days of treatment.

Faecal specimens were collected individually once from all the goats and applied for faecal egg counting employing Whitlock Universal Egg Counting Slide (provided by JA Whitlock & Company, PO Box 51, EASTWOOD NSW 2122 AUSTRALIA). The following formula was used to calculate EPG:

EPG= Total eggs in chamber 1, 2 and 3/3 x 50 (dilution factor)

The mean EPG for the treatment group was determined and compared with that of the control group. For this purpose, Faecal egg count reduction percentage (FECR %) was calculated utilizing the undermentioned formula:

FECR % = [1- (mean EPG treatment/mean EPG control)] x100

Having said, the same aforementioned process was applied for detection of resistance against avermectin (two farms) and levamisole (two farms). The dewormers used in this survey were obtained from a local veterinary clinic. Moreover, RESO computer program (CSIRO Animal Health Research Laboratory, Private Bag 1, Parkville, Vic. 3052, Australia) was exploited to calculate the FECR data including arithmetic mean, variance of counts, FECR% and 95% confidence interval. According to Coles *et al*. (1992), resistance is rooted if (**i**) the FECR% is less than 95% (**ii**) the lower limit of 95% confidence interval is less than 90% (**iii**) If just one of the two norms is met, resistance is suspected. On the other hand, Gill (1996) has suggested that any negative values obtained from FECR% and lower limit confidence interval are equal to zero, interpreting that the resistance is extensively rampant and has reached the catastrophic level.

●Egg hatch assay (*in vitro* test)

This approach was conducted in accordance with the protocol that was adopted by World Association for the Advancement of Veterinary Parasitology (W.A.A.V.P) to detect resistance against benzimidazole family members (Coles *et al*., 1992). This *in vitro* technique was carried out for benzimidazole merely because other synthetic drugs are not ovicidal. On the other hand, egg hatch assay (EHA) provides an enhanced quantitative estimation of AR levels as compared to FECRT (Martin *et al*., 1989). Faecal specimens from each farm (farms 1 and 2) were transported anaerobically to the laboratory to perform EHA. In brief, eggs were collected from pooled faecal samples on day 10-14 post-deworming, suspended in distilled water and counted. Fenbendazole was dissolved in 0.3% Dimethylsulfoxide (DMSO) and mother solution was prepared as 50 µg ml^{-1}. The stock solution was serially diluted (0.0244-50 µg ml^{-1} in a multiwell plate. The control well received only 1 ml solvent (0.3% DMSO). One ml (approximately 150 eggs ml^{-1}) of egg suspension was added to each well comprising the control well. Plate was incubated at 27°C ±1 for 48 hours and 70% relative humidity. After incubation, two drops of Lugol's iodine was added. At least 100 of the unhatched eggs (dead and embryonated) and hatched larvae were counted to calculate the hatching inhibition percentage (Coles *et al*., 1992). The following formula was used for assessment of hatching inhibition (%):

Hatching inhibition (%) = P test/ P total x100

P test: number of unhatched or embryonated eggs.

P total: number of unhatched or embryonated eggs + Larvae (L_1).

LC_{50} values were calculated for the eggs by probit analysis. Eggs with an LC_{50} value in excess of 0.1 µg ml^{-1} were reckoned as an indicative of antinematicidal (fenbendazole) resistance as suggested by Coles *et al*. (1992).

2.5. Statistical analysis

The diagnosis of resistance in deparasiting groups (after 10-14 days of deworming with fenbendazole, avermectin and levamisole) was scrutinized by RESO computer program after counting EPG of each animal in treatment and control groups. The level of resistance rampancy was assessed via estimation of FECR% and calculating lower limit of confidence interval using the above program.

The data collected from EHA for various concentrations of fenbendazole to evaluate its ovicidal activity against nematode eggs, one way ANOVA was applied utilizing Graph Pad Prizm (version 7). Tukey, as multiple comparison test, was utilized to compare among doses. All procured data were expressed as Mean±SE. For calculation of LC_{50} (µg ml^{-1}) at 95% confidence interval for preventing 50% of egg hatching, probit analysis of LC_{50} value on the EHA was applied.

3. Results

3.1. Involvement of gastrointestinal nematode species in infestations

The parasitic nematodes, naturally infecting goats, such as *Nematodirus*, *Trichuris* and *Marshallagia* larvae (L_3) were recognized post conduction of qualitative, quantitative, coproculture and Baermann parasitological techniques (Soulsby, 1982; MAAF, 1986; Iqbal *et al*., 2006) before and after deparasiting experimental goats in six farms (tables 1, 2 and 3).

3.2. Detection of fenbendazole resistance

3.2.1. Faecal egg count reduction test (*in vivo* test)

The data procured from EPG, FECRT, RESO Computer Program, after treatment of tentative animals with fenbendazole, had revealed that AR is rampant in the region. Details of the obtained data are exhibited in table 4.

3.2.2. Egg hatch assay (*in vitro* test)

The LC_{50} of fenbendazole was estimated to be 2.11 µg ml^{-1} (range 1.47-2.34), which was in excess to 0.1 µg ml^{-1} suggesting emergence of resistance among aforesaid GI nematodes (Coles *et al*., 1992). Correlation between impacts of different concentrations of fenbendazole and hatching inhibition (%) through conducting EHA is shown in figure 1.

3.3. Detection of avermectin resistance

The data collected from EPG, FECRT, RESO Computer Program, after deworming of tentative animals with avermectin, had shown that AR was not prevalent in the area. Details of the procured data are displayed in table 5.

3.4. Detection of levamisole resistance

The data obtained from EPG, FECRT, RESO Computer Program, after treatment of tentative animals with levamisole, had revealed that AR was not spread in the study zone. Details of the collected data are demonstrated in table 6.

Table 1 Pre-deparasiting (0 day) and post-deparasiting (10-14 days) percentage of nematode larvae (L_3) in the experimental goats chosen for detection of resistance against fenbendazole based on pooled faecal specimens collected from farm 1 and 2

Farms/groups	*Nematodirus*%	*Trichuris*%	*Marshallagia*%
Pre-deparasiting L_3 (%) of *Nematodirus*, *Trichuris* and *Marshallagia*			
Farm 1 (Kandinawa district)			
Fenbendazole group	39	31	30
Control group	36	27	37
Farm 2 (Shamamic district)			
Fenbendazole group	35	33	32
Control group	36	35	29
Post-deparasiting L_3 (%) of *Nematodirus*, *Trichuris* and *Marshallagia*			
Farm 1 (Kandinawa district)			
Fenbendazole group	40	33	27
Control group	38	32	30
Farm 2 (Shamamic district)			
Fenbendazole group	34	35	31
Control group	35	33	32

Table 2 Pre-deparasiting (0 day) and post-deparasiting (10-14 days) percentage of nematode larvae (L_3) in the experimental goats chosen for detection of resistance against avermectin based on pooled faecal specimens collected from farm 3 and 4

Farms/groups	*Nematodirus*%	*Trichuris*%	*Marshallagia*%
Pre-deparasiting L_3 (%) of *Nematodirus*, *Trichuris* and *Marshallagia*			
Farm 3 (Kandinawa district)			
Avermectin group	38	33	29
Control group	36	34	30
Farm 4 (Shamamic district)			
Avermectin group	37	35	28
Control group	35	33	32
Post-deparasiting L_3 (%) of *Nematodirus*, *Trichuris* and *Marshallagia*			
Farm 3 (Kandinawa district)			
Avermectin group	slightly obtained	slightly obtained	slightly obtained
Control group	37	32	31
Farm 4 (Shamamic district)			
Avermectin group	slightly obtained	slightly obtained	slightly obtained
Control group	34	32	34

Table 3 Pre-deparasiting (0 day) and post-deparasiting (10-14 days) percentage of nematode larvae (L_3) in the experimental goats chosen for detection of resistance against levamisole based on pooled faecal specimens collected from farm 5 and 6

Farms/groups	*Nematodirus*%	*Trichuris*%	*Marshallagia*%
Pre-deparasiting L_3 (%) of *Nematodirus*, *Trichuris* and *Marshallagia*			
Farm 5 (Kandinawa district)			
Levamisole group	36	34	30
Control group	39	35	26
Farm 6 (Shamamic district)			
Levamisole group	38	33	29
Control group	36	33	31
Post-deparasiting L_3 (%) of *Nematodirus*, *Trichuris* and *Marshallagia*			
Farm 5 (Kandinawa district)			
Levamisole group	poorly obtained	poorly obtained	poorly obtained

Control group	40	32	28
Farm 6 (Shamamic district)			
Levamisole group	poorly obtained	poorly obtained	poorly obtained
Control group	35	34	31

Table 4 Status of resistance among *Nematodirus*, *Trichuris* and *Marshallagia* populations on day 10-14 post-deparasiting with fenbendazole based on RESO program

Farm/groups	Mean EPG ±SE	Confidence interval 95% Lower	FECR%	Rampancy of resistance
Farm 1 (Kandinawa)				
Fenbendazole group	204.27±19.95	63.00	70.72	Resistant
Control group	697.67±50.67	-	-	-
Farm 2 (Shamamic)				
Fenbendazole group	164.27±17.65	73.8	79.55	Resistant
Control group	803.07±58.33	-	-	-

EPG: Egg per gram of faeces
FECR%: Faecal egg count reduction percentage

Table 5 Status of resistance among *Nematodirus*, *Trichuris* and *Marshallagia* populations on day 10-14 post-deparasiting with avermectin based on RESO program

Farm/groups	Mean EPG ±SE	Confidence interval 95% Lower	FECR%	Rampancy of resistance
Farm 3 (Kandinawa)				
Avermectin group	46.67±5.05	92.91	93.92	Suspected
Control group	768.07±51.15	-	-	-
Farm 4 (Shamamic)				
Avermectin group	48.87±5.80	90.7	92.98	Suspected
Control group	696.07±45.34	-	-	-

EPG: Egg per gram of faeces
FECR%: Faecal egg count reduction percentage

Table 6 Status of resistance among *Nematodirus*, *Trichuris* and *Marshallagia* populations on day 10-14 post-deparasiting with levamisole based on RESO program

Farm/groups	Mean EPG ±SE	Confidence interval 95% Lower	FECR%	Rampancy of resistance
Farm 5 (Kandinawa)				
Levamisole group	26.33±2.21	95.1	95.99	Susceptible
Control group	656.80±38.00	-	-	-
Farm 6 (Shamamic)				
Levamisole group	25.40±1.51	95.7	96.38	Susceptible
Control group	702.47±41.24	-	-	-

EPG: Egg per gram of faeces
FECR%: Faecal egg count reduction percentage

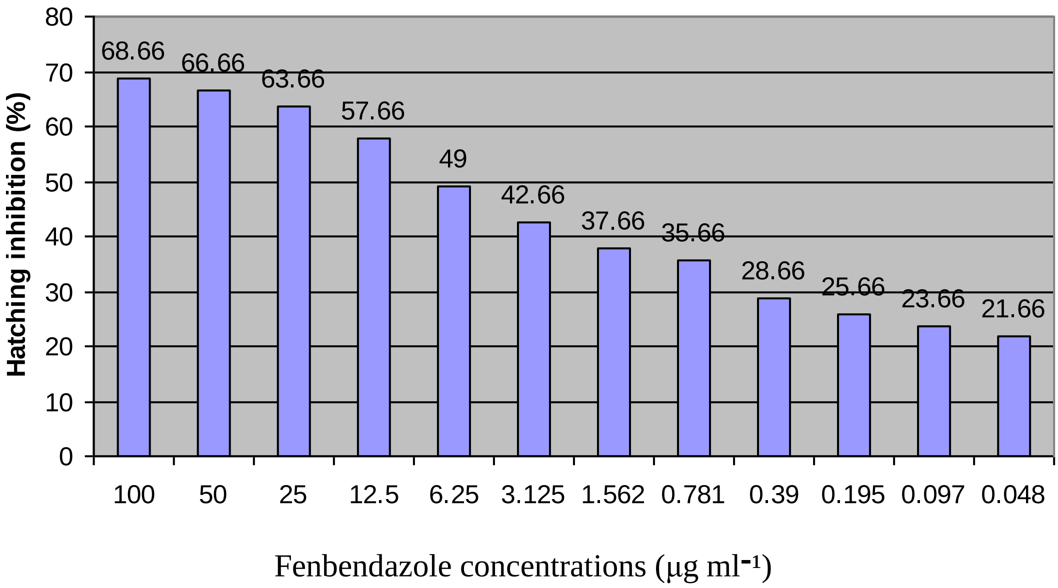

Figure 1 Correlation between the effects of different concentrations of fenbendazole and hatching inhibition (%)

4. Discussion

Undoubtedly, AR is counted a key bottleneck to control small ruminant GI nematodes and escalating concern for human nematodes owing to the wide use of antinematicidals, particularly in the under-developed nations (Geary, 2012; Furgasa *et al*., 2018). Actually, this study is reckoned a first attempt to detect AR in goats in Kurdistan region; however, few surveys have been carried out to diagnose AR in sheep (Ahmed *et al.*, 2015; Ahmed *et al.*, 2019). After treatment of experimental goats in farms 1 and 2 with fenbendazole, coprocultures produced sufficient individuals of nematodes L_3 (table 1). The FECR values in farms 1 and 2 were 70.72% and 79.55% respectively, while lower limit values of confidence intervals 95% in farms 1 and 2 were 63% and 73.8% respectively (table 4). Additionally, the LC_{50} value was 2.11 µg ml^{-1} (range 1.47-2.34) after performing EHA with fenbendazole (it has ovicidal activity as well) (figure 1). Definitely, the previous data are strong indications for the prevalence of resistance among GI roundworms (Coles *et al.*, 1992) of goats on the trialed farms. In light of the current results, fenbendazole resistance is deemed multi-specific, which means emerging AR in one flock in numerous genera of parasitic roundworms including *Nematodirus*, *Trichuris* and *Marshallagi*a. On the other hand, in tropical, sub-tropical and North American countries, fenbendazole resistance in small ruminants is often associated with *Haemonchus contortus* (Falzon *et al.*, 2013; Hamad *et al.*, 2014; Kalkal *et al*., 2019). It is imperative to draw attention to some possible factors responsible in developing fenbendazole resistance in under-developed territories including our region which comprise insufficient dose, frequent annual use, bad quality of the dewormer, storage conditions, deparasiting animals with the same drug 3-4 times annually, and improper drenching procedure (Hoekstra *et al.*, 1997; Afaq, 2003; Saeed, 2007; Furgasa *et al*., 2018). Probably, among the aforementioned factors, recurrent yearly employment of the same drug, which causes selective pressure on the parasite, conduces to occurrence of mutation (loss of dewormer binding) at ß-tubulin isotype 1 (dewormer target) in parasitic nematodes (Beech and Silvestre, 2010). Moreover, according to the veterinarian files in the study sites and experience of the first author (Veterinary clinician since last century), usually local Kurdish shepherds prefer to drench their livestock with fenbendazole and its counterparts of the benzimidazole family recurrently as compared to other dewormer families. Consequently, this practice has led to emergence and rampancy of resistance (Hamad, 2012) in the region.

Avermectin and its counterparts were commercialized in 1980 and introduced to the therapy recipe in Kurdistan region slowly in 1991, so for many years, local farmers have not been adapted to use it because this drug was new for them at that time. On the other hand, the route of administration of this dewormer is injection subcutaneously, so livestock raisers try to avoid it (local veterinarian file). Hence, use of avermectin is less than fenbendazole and its counterparts. Post-therapy of goats with avermectin in farms 3 and 4, coprocultures yielded slight numbers of nematodes L_3 (table 2). Furthermore, the FECR values in farms 3 and 4 were 93.92% and 92.98% respectively, whilst the lower limit values of confidence intervals 95% in farms 3 and 4 were 92.91% and 92.7% respectively (table 5). Consequently, and according to Coles *et al.* (1992), the resistance is suspected against avermectin in farms 3 and 4.

Levamisole, as a cholinergic agonist working at nicotinic acetylcholine receptors on the surface of the roundworm muscle cells and at the neuromuscular junction, has no antitrematicidal, anticesticidal and ovicidal activity (Taylor *et al.*, 2007). In most areas of the world including Kurdistan region, levamisole is being used against the lung worm, *Dictyocaulus filaria* of small ruminants and it has a low safe margin (Radostits *et al*., 2007; Besier *et al*., 2016). Thus, its employment by livestock raisers is too rare as compared to fenbendazole and its counterparts. After drenching the remedial dose of levamisole to tentative goats in farms 5 and 6, coprocultures produced poor numbers of nematodes L_3 (table 3). Besides, the FECR values in farms 5 and 6 were 95.99% and 96.38% respectively, whilst the lower limit values of confidence intervals 95% in farms 5 and 6 were 95.1% and 95.7% respectively (table 6). Accordingly, and pursuant to Coles *et al.* (1992), the parasitic worms were susceptible and no resistance was detected against levamisole in farms 5 and 6. In this regard, Coles *et al.* (1995) have mentioned that the resistance will develop if annual drench exceeded two times. Having said, the usual annual use of this dewormer is only two times, one in autumn and other one in spring (local veterinarian record).

5. Conclusions

In the light of results of the present original study pertaining Kurdish goat breeds in our region, it has been concluded that prevailing GI nematodes; *Nematodirus*, *Trichuris* and *Marshallagi*a are resistant to fenbendazole, whilst the resistance is suspected to avermectin. On the other hand, the abovesaid parasites are susceptible to levamisole. Farmers in the study area often prefer fenbendazole and its counterparts in drenching their livestock on other drugs such as avermectin and levamisole which belong to different families. Having said, the livestock raisers drench goats (the amount of drugs should be double as compared to sheep) the dose rate of sheep, which in turn, could lead to emergence of resistance especially against fenbendazole and its counterparts.

Acknowledgements

The authors are very grateful for the collaborations of the local veterinarians regarding access to their files related to treatment protocols against nematodiasis. We have to thank livestock owners for their sincere cooperation as well.

Conflict of interest

The authors of this research article attest that there is no any conflict of interest with other authors concerning this manuscript.

6. References

Afaq, M., 2003. Parasite control practices and anthelmintic resistance against gastrointestinal nematodes of sheep. *PhD thesis, Department of Veterinary Parasitology, University of Agriculture, Faisalabad, Pakistan*.

Ahmed, C.N., Hamad, K.K. and Qadir, F.A., 2019. *Haemonchus contortus* as a model in assessing activity of *Citrullus colocynthis* fruit extract to control benzimidazole-resistant parasitic nematodes. *ZANCO Journal of Pure and Applied Sciences*, 31, 61-70.

Ahmed, I.A., Aziz, K.J. and Abdullah, S.O., 2015. Prevalence of Gastrointestinal Nematode Parasites in Sheep and Evaluation of Some Anthelmintic Resistance in Erbil Governorate. *Basrah Journal of Veterinary Research*, 14 (1).

Beech, R. N. and Silvestre, A., 2010. Mutations associated with anthelmintic drug resistance. *Anti-infective agents in Medical Chem*istry, 9: 105-112.

Besier, R.B., Kahn, L.P., Sargison, N.D. and Van Wyk, J.A., 2016. Chapter Four- The pathophysiology, ecology and epidemiology of *Haemonchus contortus* infection in small ruminants. *Advanced Parasitology*, 143, 93-95.

Blake, N. and Coles, G., 2007. Flock cull due to anthelmintic- resistance nematodes. *Veterinary Record*, 161, 36-36.

Bogan, J., Benoit, E. and Delatour, P., 1987. Pharmacokinetics of oxfendazole in goats: a comparison with sheep. *Journal of Pharmacology and Therapy*, 10, 305-309.

Chartier, C., Pors, I., Hubert, J., Rocheteau, D., Benoit, C. and Bernard, N., 1998. Prevalence of anthelmintic resistant nematodes in sheep and goats in Western France. *Small Ruminant Research*, 29, 33-41.

Coles, G.C., Bauer, C., Borgsteede, F.H.M., Greets, S., Klei, T.R., Taylor M.A. and Waller, P.J., 1992. World Association for the Advancement of Veterinary Parasitology (W.A.A.V.P.) methods for the detection of anthelmintic resistance in nematodes of veterinary importance. *Veterinary Parasitology,* 44, 35-44.

Coles, G.C., Papadopoulos, E. and Himonas, C.A., 1995. Tubulin, resistance and worms. *Parasitology Today*, 11, 183-185.

Falzon, L.C., Menzies, P.I., Shakya, K.P., Jones-Bitton, A., Vanleeuwen, J., Avula, J., Stewart, H., Jansen, J.T., Taylor, M.A., Learmount, J. and Peregrine, A.S., 2013. Anthelmintic resistance in sheep flocks in Ontario, Canada. *Veterinary Parasitology*, 193, 150-162.

Furgasa, W., Abunna, F., Yimer, L. and Haile, G., 2018. Review on anthelmintic resistance against gastrointestinal nematodes of small ruminants: Its status and perspective in Ethiopia. *Journal of Veterinary Science and Animal Husbandry*, 6, 407-418.

Geary, T.G., 2012. Are new anthelmintics needed to eliminate human helminthiasis? *Current Opinion in Infectious Diseases*, 25, 709-717.

Gill, B.S., 1996. Anthelmintic resistance in India. *Veterinary Parasitology*, 63, 173-176.

Gilleard, J.S., 2006. Understanding anthelmintic resistance: the need for genomics and genetics. *International Journal for Parasitology*, 36, 1227-1239.

Hamad, K.K., Ahmed, S.T., Ahmed, R.K. and Koyee, K.M., 2018. Phytotherapeutics: As anticipating substitutes to synthetic drugs in combating antinematicidal-resistant gastrointestinal nematodes of small ruminants. *ZANCO Journal of Pure and Applied Sciences*, 30, 102-114.

Hamad, K.K., 2012. Efficacy of some indigenous medicinal plants to control antinematicidal-resistant Haemonchus contortus in sheep. *PhD thesis, Department of Parasitology, University of Agriculture, Faisalabad, Pakistan*.

Hamad, K.K., Iqbal, Z., Sindhu, Z.U.D., Abbas, R.Z., Khan, M.N., Muhammad, G. and Epperson, B., 2014. Combination of *Nicotiana tabacum* and *Azadirachta indica*: A novel substitute to control levamisole and ivermectin-resistant *Haemonchus contortus* in ovine. *Pakistan Veterinary Journal*, 34, 24-29.

Hoekstra, R., Visser, A., Wiley, L.J., Weiss, A.S., Sangster, N.C. and Roos, M.H., 1997. Characterisation of an acetylcholine receptor gene of *Haemonchus contortus* in relation to levamisole resistance. *Molecular and Biochemical Parasitology*, 84, 179-187.

Iqbal, Z., Sajid, M.S., Jabbar, A., Rao, Z.A. and Khan, M.N., 2006. Techniques in Parasitology. Higher Education Commission, Islamabad, Pakistan, pp 198.

Jabbar, A., Iqbal, Z., Kerboeuf, D., Muhammad, G., Khan, M.N. and Afaq, M., 2006. Anthelmintic resistance: The state of play revisited. *Life Science*, 79, 2413-2431.

Kalkal, H., Vohra, S., Singh, S., Gupta, S., Magotra, A. and Bangar, Y.C., 2019. Detection of moderate to severe anthelmintic resistance against fenbendazole in sheep and goat breeding farms, Hisar. *The Pharma Innovation Journal*, 8, 434-436.

Kaplan, R.M. and Vidyashankar, A.N., 2012. An inconvenient truth: global warming and anthelmintic resistance. *Veterinary Parasitology*, 186, 70-78.

MAAF, 1986. Manual of Veterinary Parasitological Laboratory Techniques. Technical Bulletin No. 18. Ministry of Agriculture Fisheries and Food. Her Majesty's Stationary Office, London, UK.

Martin, P.J., Anderson, N. and Jarrett, R.G., 1989. Detecting benzimidazole resistance with faecal egg count reduction tests and *in vivo* assays. *Australian Veterinary Journal*, 66, 236-240.

Radostits, O.M., Gay, C.C., Hinchcliff, K.W. and Constable, P.D., 2007. Veterinary Medicine, a text book of the diseases of cattle, horses, sheep, pigs and goats. 10th Ed., Saunders Ltd., Philadelphia, USA, pp 2065.

Saeed, M., 2007. Surveillance studies on anthelmintic resistance in some gastrointestinal nematodes of Beetal goats at livestock farms of Punjab. *Ph.D thesis, Department of Parasitology, University of Agriculture, Faisalabad, Pakistan.*

Sangster, N.C., Rickard, J.M., Hennessy, D.R., Steel, J.W. and Collins, G.H., 1991. Disposition of oxfendazole in goats and efficacy compared with sheep. *Research in Veterinary Science*, 51, 258-263.

Soulsby, E.J.L., 1982. Helminths, Arthropods and Protozoa of Domasticated Animals.7th Ed., Bailliere Tindall, London, UK, pp. 248-250, 766-770.

Taylor, M.A., Coop, R.L. and Wool, R.L., 2007. Veterinary Parasitology, 3rd Ed., Blackwell Publishing Ltd., UK.

Waller, P.J., Dash, K.M., Barger, I.A., Le Jambre, L.F. and Plant, J., 1995. Anthelmintic resistance in nematode parasites of sheep: learning from the Australian experience. *Veterinary Record*, 136, 411-413.

ZANCO Journal of Pure and Applied Sciences
The official scientific journal of Salahaddin University-Erbil
https://zancojournals.su.edu.krd/index.php/JPAS

ISSN (print):2218-0230**, ISSN (online):** 2412-3986**, DOI: http://dx.doi.org/10.21271/zjpas**

RESEARCH PAPER

Evaluating the prevalence of virulence factor gene and biofilm production in *Pseudomonas aeruginosa* isolated from different clinical samples.

Bashdar M. Hussen[1]

[1]Department of Pharmacognocy, College of Pharmacy, Hawler Medical University-Erbil, Kurdistan Region, Iraq

A B S T R A C T:
Pseudomonas aeruginosa is considered a resourceful pathogen; which has several essential virulence effectors such as exoenzyme, exotoxin and biofilm might help to it is infection. This study aimed to investigate the frequency of exoS gene, the determination of biofilm production and antimicrobial resistance among clinical samples of *P. aeruginosa*. In our study, 227 specimens of *P. aeruginosa* collected from different clinical specimens which were attending public hospitals in Erbil city. Antimicrobial resistance of samples identified by Kirby-Bauer disk diffusion method. Through PCR virulence gene exoS was studied. Biofilm production measured by both Congo Red Agar (CRA) and tissue culture plate method (TCP). Among 227 clinical samples, 40 (17.6%) were positive for *P. aeruginosa*. Imipenem was showed most effective antibiotic 95% against *P. aeruginosa*. Incidence of exoS gene was 70% within the *P. aeruginosa* isolates. Moreover, around 75% of clinical samples produced biofilm and approximately 40% of them produced strong biofilm. Our study showed that the incidence of bla exoS gene and biofilm formation, which are common virulence factors in the clinical samples, especially in burn patients, and are a severe problem in the treatment of the patient.

KEY WORDS: *Pseudomonas aeruginosa*, *Bla* exoS gene, Antibiotic resistance, Biofilm
DOI: http://dx.doi.org/10.21271/ZJPAS.32.4.13
ZJPAS (2020) , 32(4);108-113

1.INTRODUCTION :

Pseudomonas aeruginosa has developed as an important of nosocomial infection. It causes infection especially in the immunocompromised hosts as seen in the patients with severe diabetes, burns and chronic renal disease also individuals with HIV infection (Candel *et al.*, 2019, Wang *et al.*, 2019, Kang *et al.*, 2019, Azeez and Bakr, 2019).

* **Corresponding Author:**
Bashdar M. Hussen
E-mail: bashdar.hussen@hmuedu.krd
Article History:
Received: 11/01/2020
Accepted: 24/02/2020
Published: 08/09 /2020

It causes different types of infection such as septicemia, pneumonia, burn wounds, otitis and keratitis (Kang *et al*., 2019, Aka, 2015). This organism is often resistant to a large number of antibiotics and enters the blood, causing septicemia (Minasyan, 2019). The production of toxins, enzymes and also biofilm formation may contribute to its pathogenicity (Aka and Haji, 2015, Hamad, 2018, Ahmed and Salih, 2019). When a bacteria formed a biofilm, it promotes growth and survival, it becomes extremely difficult to be destroyed (Georgescu *et al*., 2016). Biofilm supports the colonization of bacteria, which is showing resistant to most antibiotics (Yin *et al*., 2019). Among bacterial pathogens, *P. aeruginosa* inherent resistance to antibiotics such as aminoglycosides, carbapenems, penicillins, quinolones and cephalosporins. Furthermore, it has been known to obtain unusual resistance genes via transformation, transduction or conjugation (Amirmozafari *et al*., 2016, Pobiega *et al*., 2015). Besides, there is a major virulence factor which was known by the type III secretion system (T3SS). It has a vital function to transfer effector proteins into the host. *Pseudomonas aeruginosa* produces irresistible proteins such as exoS and ExoU (Horna *et al*., 2019). ExoS is the main cytotoxin that is essential for colonisation, invasion and bacterial spreading during infection (Ruffin and Brochiero, 2019).

The vital virulence elements of *P. aeruginosa* is the biofilm which is leading to colonisation of microorganisms, and it plays against antimicrobial agents (Verderosa *et al*., 2019). The primary purpose behind of our study was to investigate the frequency of exoS gene, the determination of biofilm production and antimicrobial resistance among clinical samples of *P. aeruginosa* in Erbil north of Iraq.

1. MATERIALS AND METHODS

1.1.Bacterial isolates and identification test

Our samples were collected from different clinical specimens such as wounds, respiratory tract, urine, blood, burn and sputum. Each isolate was cultured by using different agars such as MacConkey agar and Blood agar then incubated at 37°C overnight. Identification was made by using biochemical tests (Jabalameli *et al*., 2012). All bacterial isolates were stored in a microtube containing tryptic soy broth with glycerol 20% and stored at −70°C until further investigation (Magalhães *et al*., 2016).

1.2.Methods:

Study population and specimens

In our study, 227 clinical samples were collected from different clinical specimens which were attending public hospitals in Erbil city from September 2017 to March 2018. Antimicrobial resistance of samples was identified. Through PCR virulence gene exoS was studied. Biofilm production was measured by both Congo Red Agar (CRA) and tissue culture plate method (TCP).

Antibiotic susceptibility tests

Antibiotic susceptibility test was used through the Kirby-Bauer disk diffusion method (Merck, Germany) agar according to the guideline of Clinical and Laboratory Standards (Magiorakos *et al*., 2012): Penicillin (P 10ug), Rifampicin (R 5ug), Bacitracin (Baci 10ug), Ciprofloxacin (Cip 5µg), Amikacin (Am 10ug), Azithromycin (Azi 10 ug), Cefotaxime (Cef 30 ug), Ceftriaxone (Cef 30ug), Meropenem (Mer 10 ug) and Imipenem (Imi 10ug).

Identification of bacterial isolates as *P. aeruginosa* by PCR:

To know the bacterial isolates as *P. aeruginosa*, all samples were checked for detection of exoS gene with specific primers as explained in Table 1.

PCR based genotyping assay

Genomic DNA was isolated from bacterial cells harvested from overnight culture according to the previously described method (Smet *et al*., 2009). The extraction kit was provided by (GeNet Bio, Korea). PCR amplification for exoS gene was performed according to the manufacturer program for amplification of target gene: initial denaturation 94°C for 5 min; one cycle and denaturation step 94°C for 30 seconds; annealing step 58°C for 30 seconds; amplification step 72°C for 30 seconds; and the final amplification step was 72°C for 5 minutes. To investigate the PCR products, 5µl of PCR product run on 1% agarose gel in trice boric acid EDTA buffer, after electrophoresis, visualised under ultraviolet transilluminator.

Table 1: Nucleotide sequences used as a primer for PCR amplification.

Name of the gene	Name of primers	Nucleotide sequences start from (5'-3')	PCR product size (bp)	Tempera ture for annealin g	Ref.
Bla exoS	*Bla* exoS forward	ATGTCAGCGG GATAT CGA AC	230	58^{O}C	(Georges cu *et al*., 2016)
	Bla exoS reverse	CAG GCG TAC ATC CTG TTC CT			

1.3.Detection of biofilm formation

Tissue culture plate method

Bacterial colonies were grown for 24hrs at 37°C in Trypticase Soy Broth (Merck Darmstadt, Germany). Then, dilution was done in TSB medium and only 150 µl of dilution transferred for sterile microtiter plates. Next, incubated for 24 hrs at 37°C without shaking, then washed by phosphate buffer saline three times. Later, 100 µl of methanol was added and incubated for 15 minutes. After removing the solution the plate was dried at room temperature.

The next step was adding crystal violet for 20 minutes, and the bound dye was released by adding acetic acid. The reading of optical density (OD) was done through ELISA reader (Biotek elx800). The assays were repeated for three times. Un-inoculated medium was used in order to determine background OD as a control.

According to the ELISA reader results, the samples were grouped into four different groups based on the reading: non-biofilm produce group (OD test <ODc), weak biofilm produce group (ODc< OD < 2× ODc), moderate biofilm produce group (2× ODc< OD < 4X ODc) and strong biofilm produce group (4× ODc< OD) (21, 22).

Congo red agar method

Bacterial suspension inoculated into a prepared solid medium (BHI) added with 5% sucrose and Congo red. It was made as a concentrated solution and sterilised by autoclave for 15 minutes at 121˚C, then added after cooling the agar to 55˚C. The agar plate was inoculated and incubated for 24-48 hours at 37˚C. The black colonies plus a dry crystalline were positives in contrast, the dark colonies without a dry crystalline were pointed as negatives, and weak producers remained as a pink. The assays were repeated for three times.

Table 2: Distribution of P. aeruginosa in different clinical samples

Results	Urine	Bronchial wash	Sputum	wound	Burn	Total	p-value
positive	7 (3.1%)	4 (1.8%)	6 (2.6%)	9 (4.0%)	14 (6.2%)	40 (17.6 %)	<0.001
Negative	113 (49.8%)	18 (7.9%)	12(5.3%)	37(16.3%)	7(3.1%)	187(82.4 %)	
Total	120 (52.9%)	22 (9.7%)	18 (7.9%)	46 (20.3 %)	21 (9.3%)	227(100.0%)	

Table 3: Screening of *P. aeruginosa* isolates for detection of biofilm formation by tissue culture plate and Congo Red Agar (CRA) methods.

Biofilm formation	Tissue culture plate	Congo red agar
Strong	14(35%)	18(45%)
Moderate	16(40%)	10(25%)
Weak	9(23%)	6(15%)
None	1 (2%)	6(15%)
Total	40	40

Table 4: PCR-based genotyping assay

PCR results	Source of samples					Total
	Urine	Bronchial wash	Sputum	wound	Burn	
Virulence gene exoS (+)	6 (15%)	2 (5%)	4 (10%)	6 (15%)	10 (25%)	28 (70%)
Virulence gene exoS (-)	1 (2.5%)	2 (5%)	2 (5%)	3 (7.5%)	4 (10%)	12 (30%)
Total	7 (17.5 %)	4 (10%)	6 (15%)	9 (22.5%)	14 (35%)	40(100.0%)

2.8. Statistical Analysis

Statistical analysis including the chi-square test with P values less than 0.05 were considered as significant. Statistical program for social sciences (SPSS V.23) was used for the analysis of the results.

2. RESULTS AND DISCUSSION

From 227 samples, 40 (17.6%) were positive for *P. aeruginosa* (Table 2). Also, the rate of isolates produced biofilms 35%, 40% respectively strong and moderate biofilms. In contrast, the ratio of weak or non- biofilm formation were about 25% (Table 3). The highest level of resistance was observed to penicillin, rifampicin, and bacitracin 100%, followed by ciprofloxacin and amikacin 92.5, 87.5% respectively, while the least resistance exhibited to imipenem 5%. Also, the level of resistance to cefotaxime and meropenem 82.5%, 75% respectively. Furthermore, the sensitivity exhibited to ciprofloxacin, azithromycin and ceftriaxone 80% (Figure 1). Figure 2 illustrated the amplification for the detection of the exoS gene. The incidence of antimicrobial resistance within the *P. aeruginosa* isolates was (70%). Moreover, it was found the highest frequency exoS gene 25% in burn infection (Table 4).

DISCUSSION:

Pseudomonas aeruginosa is an important pathogen of hospital-acquired infections, and it has resistance to a wide variety of antibiotics in clinical samples, particularly in (burn, UTI, and wound) infections (Azimi *et al*., 2016).
According to the results, the association among different clinical samples was highly significant (P<0.001). The high frequencies of *P. aeruginosa* in various clinical samples have been earlier informed (Aka and Haji, 2015).
The peak level of resistance was observed to penicillin, rifampicin, vancomycin and bacitracin 100%, and it was showed low resistance 5% to imipenem. Earlier resistant to imipenem in Erbil was stated 20% and 4% (Azeez and Bakr, 2019) followed by ciprofloxacin and amikacin 92.5%, 87.5% respectively, Similar results have been reported by (Azeez and Bakr, 2019, Azimi *et al*., 2018). Also, the level of resistance to cefotaxime and meropenem were 82.5% and 75% respectively. Furthermore, the sensitivity exhibited to azithromycin and ceftriaxone was 80%.This wide resistance showed by *P. aeruginosa* against most effective antibiotics might be related to misuse or overuse of antibiotics (Pachori *et al*., 2019).
Biofilm formation has been measured as a prime virulence factor of pathogenicity (Tharwat *et al*., 2017). The current study identified that (98%, 85%) of the isolated samples produced biofilm by TCP and CRP method respectively, this is agreed with (Jabalameli *et al*., 2012, Hamad, 2018).
The biofilm production facilitates to ascent bacterial resistant strains and eases the efficacy of antibiotic therapy (Bahador *et al*., 2019). ExoS is a major cytotoxin that is required for bacterial colonisation and invasion. In addition, it needs for bacterial dissemination during infection (Yousefi-Avarvand *et al*., 2015). Our results identified exoS gene most prevalent (70%) within the *P. aeruginosa* isolates which in agreement with other study and similar to (Bahador *et al*., 2019, Mingxiang *et al*., 2018). In Poland, Pobiega revealed a rate for exoS (92.3%) among clinical samples (Amirmozafari *et al*., 2016).

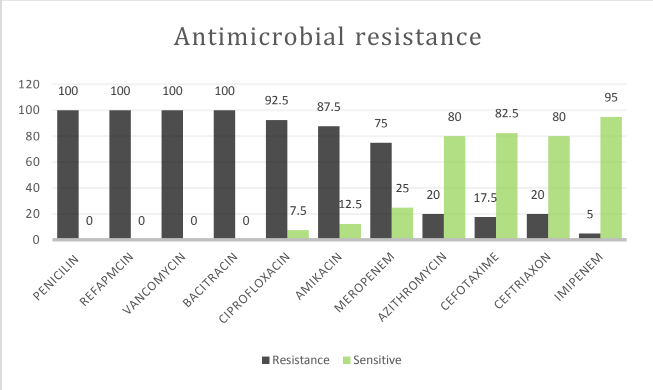

Figure 1: Antimicrobial resistance properties in *Pseudomonas aeruginosa* isolated from clinical infections.

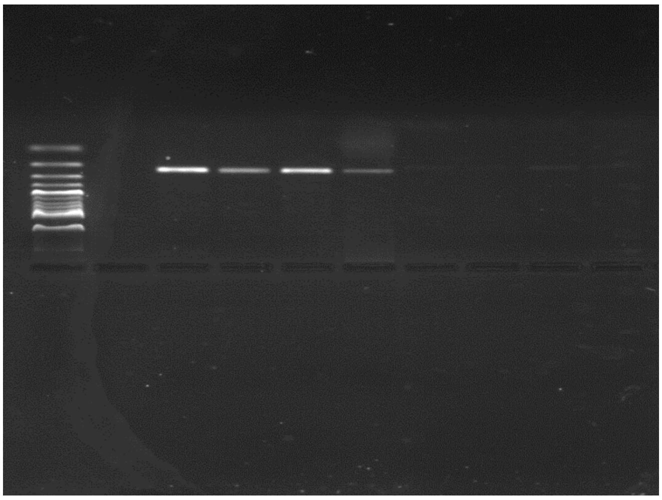

Figure 2: Gel Electrophoresis of the Polymerase Chain Reaction Products Using exoS Gene-Specific Primers. Confirmatory PCR screening analysis of the presence of exoS gene among *P. aeruginosa* clinical isolates. Lane M is DNA ladder (BioLabs); Lane 1 negative control, Lanes 2, 3, 4,5 amplified product of exo S gene (230 bp); Lane 6,7, 8, 9 Negative samples.

3. CONCLUSIONS

In conclusion, our investigation showed that the exoenzyme S is commonly disseminated among the *P. aeruginosa* samples in governmental hospitals. Moreover, a high rate of biofilm producer samples was identified in burn samples, which is a challenge in the treatment of burn patients. Additional studies are needed on other virulence factors to attain more information regarding the antibiotic resistance of *P. aeruginosa*, to find the best way to treat patients more quickly.

Acknowledgements

Thanks to Hawler Medical University sponsored this study. Thanks to the participants. Thanks to

Dr. Abbas Salihi and Dr. Fattma Ali for their cooperation.

References

AHMED, A. A. & SALIH, F. A. 2019. Quercus infectoria gall extracts reduce quorum sensing-controlled virulence factors production and biofilm formation in *Pseudomonas aeruginosa* recovered from burn wounds. *BMC Complement Altern Med,* 19**,** 177.

AKA, S. & HAJI, S. 2015. Evaluation of multi drug resistance among extended spectrum β-lactamase-producing Escherichia coli causing urinary tract infection in Erbil City. *Zanco Journal of Medical Science,* 19**,** 998-1004.

AMIRMOZAFARI, N., FALLAH MEHRABADI, J. & HABIBI, A. 2016. Association of the Exotoxin A and Exoenzyme S with Antimicrobial Resistance in *Pseudomonas aeruginosa* Strains. *Arch Iran Med,* 19**,** 353-8.

AZEEZ, B. & BAKR, K. 2019. Phenotypic and Molecular Detection of Metallo-β –Lactamase Producing Pseudomonas aeruginosa. *ZJPAS,* 31**,** 46-56.

AZIMI, A., PEYMANI, A. & POUR, P. 2018. Phenotypic and molecular detection of metallo-β-lactamase-producing *Pseudomonas aeruginosa* isolates from patients with burns in Tehran, Iran. *Revista da Sociedade Brasileira de Medicina Tropical,* 51**,** 610-615.

AZIMI, S., KAFIL, H. S., BAGHI, H. B., SHOKRIAN, S., NAJAF, K., ASGHARZADEH, M., YOUSEFI, M., SHAHRIVAR, F. & AGHAZADEH, M. 2016. Presence of exoY, exoS, exoU and exoT genes, antibiotic resistance and biofilm production among *Pseudomonas aeruginosa* isolates in Northwest Iran. *GMS Hyg Infect Control,* 11**,** Doc04.

BAHADOR, N., SHOJA, S., FARIDI, F., DOZANDEH-MOBARREZ, B., QESHMI, F. I., JAVADPOUR, S. & MOKHTARY, S. 2019. Molecular detection of virulence factors and biofilm formation in *Pseudomonas aeruginosa* obtained from different clinical specimens in Bandar Abbas. *Iran J Microbiol,* 11**,** 25-30.

CANDEL, F. J., RICO, C. M., DIAZ DE LA TORRE, I., LAGUNA, B., MARTINEZ-JORDAN, J., MEDRANO, S., ESCOBAR-PORCEL, M. C., LOPEZ-DELGADO, A., LOPEZ-GONZALEZ, L., VINUELA-PRIETO, J. M., MATESANZ, M., GONZALEZ DEL CASTILLO, J. & ARRIBI, A. 2019. Update in Infectious Diseases 2019. *Rev Esp Quimioter,* 32 Suppl 2**,** 1-9.

GEORGESCU, M., GHEORGHE, I., CURUTIU, C., LAZAR, V., BLEOTU, C. & CHIFIRIUC, M. C. 2016. Virulence and resistance features of *Pseudomonas aeruginosa* strains isolated from chronic leg ulcers. *BMC Infect Dis,* 16 Suppl 1**,** 92.

HAJI S. H. 2018. Detection of Biofilm Formation in *Pseudomonas aeruginosa* Isolates from Clinical Specimens. *ZJPAS,* 30**,** 83-89.

HORNA, G., AMARO, C., PALACIOS, A., GUERRA, H. & RUIZ, J. 2019. High frequency of the exoU+/exoS+ genotype associated with multidrug-resistant "high-risk clones" of *Pseudomonas aeruginosa* clinical isolates from Peruvian hospitals. *Sci Rep,* 9**,** 10874.

JABALAMELI, F., MIRSALEHIAN, A., KHORAMIAN, B., ALIGHOLI, M., KHORAMROOZ, S. S., ASADOLLAHI, P., TAHERIKALANI, M. & EMANEINI, M. 2012. Evaluation of biofilm production and characterization of genes encoding type III secretion system among *Pseudomonas aeruginosa* isolated from burn patients. *Burns,* 38**,** 1192-7.

KANG, D., REVTOVICH, A. V., CHEN, Q., SHAH, K. N., CANNON, C. L. & KIRIENKO, N. V. 2019. Pyoverdine-Dependent Virulence of *Pseudomonas aeruginosa* Isolates From Cystic Fibrosis Patients. *Front Microbiol,* 10**,** 2048.

MAGIORAKOS, A. P., SRINIVASAN, A., CAREY, R. B., CARMELI, Y., FALAGAS, M. E., GISKE, C. G., HARBARTH, S., HINDLER, J. F., KAHLMETER, G., OLSSON-LILJEQUIST, B., PATERSON, D. L., RICE, L. B., STELLING, J., STRUELENS, M. J., VATOPOULOS, A., WEBER, J. T. & MONNET, D. L. 2012. Multidrug-resistant, extensively drug-resistant and pandrug-resistant bacteria: an international expert proposal for interim standard definitions for acquired resistance. *Clin Microbiol Infect,* 18**,** 268-81.

MINASYAN, H. 2019. Sepsis: mechanisms of bacterial injury to the patient. *Scand J Trauma Resusc Emerg Med,* 27**,** 19.

MINGXIANG, Z., HAICHEN, W., JIAN, S., JUN, L., YONGMEI, H., QINGYA, D., QUN, Y. & WEN' EN, L. 2018. Characterization of clinical extensively drug resistant *Pseudomonas aeruginosa* from a Chinese teaching hospital. *The Journal of Infection in Developing Countries,* 12.

PACHORI, P., GOTHALWAL, R. & GANDHI, P. 2019. Emergence of antibiotic resistance *Pseudomonas aeruginosa* in intensive care unit; a critical review. *Genes Dis,* 6**,** 109-119.

POBIEGA, M., MACIAG, J., CHMIELARCZYK, A., ROMANISZYN, D., POMORSKA-WESOLOWSKA, M., ZIOLKOWSKI, G., HECZKO, P. B., BULANDA, M. & WOJKOWSKA-MACH, J. 2015. Molecular characterization of carbapenem-resistant *Pseudomonas aeruginosa* strains isolated from patients with urinary tract infections in Southern Poland. *Diagn Microbiol Infect Dis,* 83**,** 295-7.

RUFFIN, M. & BROCHIERO, E. 2019. Repair Process Impairment by *Pseudomonas aeruginosa* in Epithelial Tissues: Major Features and Potential Therapeutic Avenues. *Front Cell Infect Microbiol,* 9**,** 182.

THARWAT, N., ABOU EL-KHIER, N., EL-KAZZAZ, S., EL-GANAINY, A.-E.-R. & ELGANAINY, A. 2017. Quorum sensing-dependent virulence factors and biofilm formation of *Pseudomonas aeruginosa* isolates from retrieved orthopedic implants. *Egyptian Journal of Medical Microbiology,* 26**,** 137-143.

VERDEROSA, A. D., TOTSIKA, M. & FAIRFULL-SMITH, K. E. 2019. Bacterial Biofilm Eradication Agents: A Current Review. *Front Chem,* 7**,** 824.

WANG, T., HOU, Y. & WANG, R. 2019. A case report of community-acquired *Pseudomonas aeruginosa* pneumonia complicated with MODS in a previously healthy patient and related literature review. *BMC Infect Dis,* 19**,** 130.

YIN, W., WANG, Y., LIU, L. & HE, J. 2019. Biofilms: The Microbial "Protective Clothing" in Extreme Environments. *Int J Mol Sci*, 20.

YOUSEFI-AVARVAND, A., KHASHEI, R., SEDIGH EBRAHIM-SARAIE, H., EMAMI, A., ZOMORODIAN, K. & MOTAMEDIFAR, M. 2015. The Frequency of Exotoxin A and Exoenzymes S and U Genes Among Clinical Isolates of *Pseudomonas aeruginosa* in Shiraz, Iran. *Int J Mol Cell Med,* 4**,** 167-73.

ZANCO Journal of Pure and Applied Sciences
The official scientific journal of Salahaddin University-Erbil
https://zancojournals.su.edu.krd/index.php/JPAS

ISSN (print):2218-0230**, ISSN (online):** 2412-3986**, DOI: http://dx.doi.org/10.21271/zjpas**

RESEARCH PAPER

Stability of Palladium(II) beta-cyclodextrin nanocomposite in aqueous media and its catalytic activity in Homocoupling of Arylboronic acid

Mazin A. Othman
Department of Chemistry College of Science, Salahaddin University-Erbil, Kurdistan region-Iraq.

A B S T R A C T:

Palladium(II) beta-Cyclodextrin (Pd(II)-β-CD) nanocomposites are water-soluble compounds which can be of great importance for performing palladium-catalyzed reactions in aqueous media. The stability of water-soluble Pd(II)-β-CD nanocomposites in water were examined and was found that this nanocomposit is losing its stability in water significantly with time in the time interval of 0 to 200 minutes. In addition, the Pd(II)-β-CD nanocomposite was used as a catalyst for Aerobic homocoupling of arylboronic acid (ArBA) in water. However, the results showed that the catalytic activity of same prepared Pd(II)-β-CD nanocomposite stock solution in water for homocoupling reaction of ArBA decreases with time significantly. The Stability of the Pd(II)-β-CD nanocomposite was monitored using Ultra Violet- Visible (UV-Vis) spectroscopy. used to monitor the catalyst stability

KEY WORDS: Palladium, Cyclodextrin, nanocomposites, Catalytic activity, Homocoupling, Arylboronic acid.
DOI: http://dx.doi.org/10.21271/ZJPAS.32.4.14
ZJPAS (2020) , 32(4);114-121 .

1.INTRODUCTION

Pd(II)-β-CD nanocomposites are water-soluble materials which consists of two palladium(II) metal linked inside a beta-cyclodextin (see scheme 1) (Wei et al, 2019 , Bahareh et al., 2019, Raihana, 2016 and Kenneth, 1997). The synthesis and characterization of Pd(II)-β-CD nanocomposite was first reported by Babak Kaboudin group (Babak. et al., 2016). Also, they have developed a new protocol for homogenous catalysis of Zuzuki-Miyaura coupling reaction in neat water using Pd(II)-β-CD as an efficient nanocatalyst with high turnover frequencies.

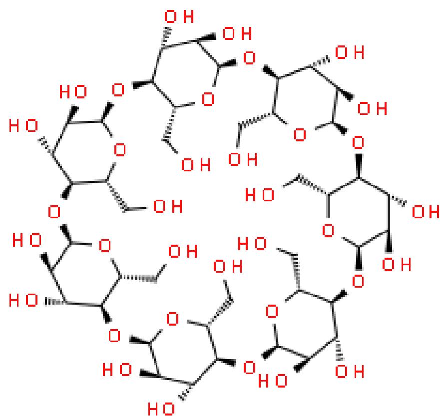

a)

* **Corresponding Author:**
Mazin A. Othman
E-mail: mazin.othman@su.edu.krd
Article History:
Received: 17/03/2020
Accepted: 21/04/2020
Published: 08/09 /2020

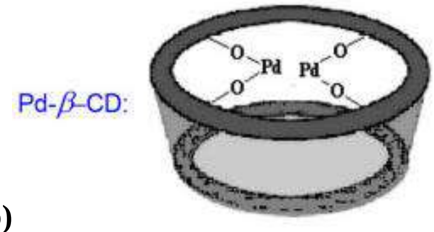

b)

Scheme 1. a) Structure of Beta cyclodextrin. b) Structure of Pd(II)-*β*-CDs (Babak Kaboudin et al., 2016)

Catalysis using palladium nanoparticles (Pd-NPs) has been widely used in many types of chemical transformations, including C-C bond-forming reactions, and in particular the Suzuki-Miyaura and Heck reactions ((Wei et al, 2019, and Yafei et al., 2017, Moreno-Manas et.al., 2003, Sawoo et al., 2009, Karimi et al., 2010, Pérez-Lorenzo, 2012 and Dell'Anna et al., 2013). Yanru Yin et al. have studied the role of poly(vinylpyrrolidone) on the synthesis four types of Pd-nanoparticles from PdCl2 and Na2PdCl2 as precursors. They have found that the nanoparticles wich have synthesized without poly(vinylpyrrolidone) have smaller sizes and can reach maximum catalytic current transfer than the ones which are synthesized in the presence of poly(vinylpyrrolidone) (Yanru et al., 2019). Additionally, highly efficient and recyclable Palladium nanoparticles decorated olyethyleneimine/Polycaprolactone PEI/PCL@PdNPs) composite Fibers have been Constructed by Electrospinning reduction methods using elexctrospun. The prepared nanocomposite was used as an efficient , stable and reusable catalyst for the reduction reaction of 4-nitrophenol and 2-nitroanlinie (Cuiru, 2019). Moreover, Palladium nanoparticles immobilized on thio modified multi walled carbon nanotubes were used as heterogeneous and rescyclable nanocatalyst for Buchwald-Hartwig C-N cross coupling reactions. The catalyst was fully characterized using different spectroscopic techniques and showed reusability for Buchwaled-Hartwig reaction for six times without change in its catalytic activity (Veisi et al., 2019). Furthermore, palladium nanoparticles are widely used in C-C coupling reactions. It has been found that in most cases of C-C coupling Pd-NPs are not the only palladium present in the reaction system, but they might lead to the formation of other active species forming "cocktail of catalysts". The active species can be formed both from Pd-NPs and/or Pd(II) complexes (Trzeciak and Augustyniak, 2019).

The applications of Pd-NPs in catalysis have been motivated by the improvements in efficiency and selectivity of Pd-NP-catalysed reactions and also by the ease of recovery and recyclability of the catalysts (Astruc et al., 2005, Asturc, 2007, Taladriz-Blanco et al., 2013 and Daniel et al., 2004). However, Aerobic homocoupling of aryboronic acids (ArBA) using different palladium nanoparticles was studied in the literature (Mazin and Niklaas, 2011 and Azzedine et al., 2017).

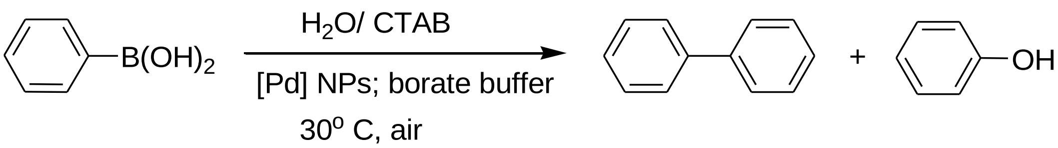

Scheme 2. Aerobic homocoupling reaction of ArBA using Pd-nanoparticles as catalyst (Mazin and Niklaas, 2011).

In this work we have studied the stability of Pd(II)-*β*-CD catalyst and its catalytic activity for the aerobic homocoupling reaction of arylboronic acid. UV-Vis spectroscopy was used to monitor the catalyst stability and reactivity in aqueous media. The Absorbance of Biphenyl formation was followed for kinetic studies.

2. MATERIALS AND METHODS

2.1. Chemicals

Arylboronic acid is purchased from Acros, K_2CO_3 is purchased from Alfa Aesar) and used as purchased without further purifications. However, Pd(II)-*β*-CD nanocomposite was provided by the Babak Kaboudin group (Babak K. et al., 2016). Distilled water was the solvent for all stock solutions.

2.2. Pd(II)-β-CD nanocomposite stability procedure

Pd(II)-β-CD nanocomposite stability was studied using Jasco UV-Vis spectrophotometer by preparing a stock solution of Pd(II)-β-CD in distilled water and follow the time-resolved absorption peak every 20 minutes from 200-800 nm.

2.3. Pd(II)-β-CD nanocomposite activity for homocoupling reaction of ArBA

The catalytic activity of Pd(II)-β-CD nanocomposites for the homocoupling reaction of ArBA in aqueous media were studied using Jasco V-650 spectrophotometer with a PAC-743R Peltier thermostatted 6-cell changer (Jasco UK Ltd., Great Dunmow, UK) at fixed maximum wave length(λmax = 250 nm) by measuring the absorbance every 5 minutes for the reaction of 0.2 M ArBA using fixed concentration of the catalyst in a cuvette.

3. Results and Discussions

3.1. Pd(II)-β-CD nanocomposite stability in water

Figure 1 shows the UV-Vis spectra of 10.0 ppm Pd(II)-β-CD nanocomposite in distilled water. The spectrum of the color less solution was measured every 20 minutes at a wavelength range of 200-800 nm.

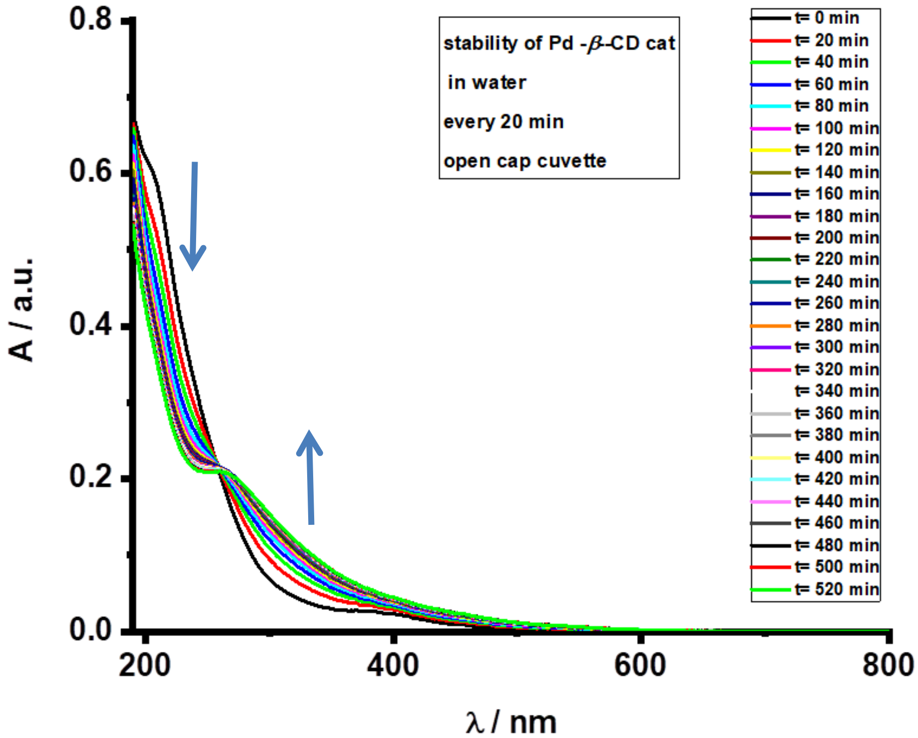

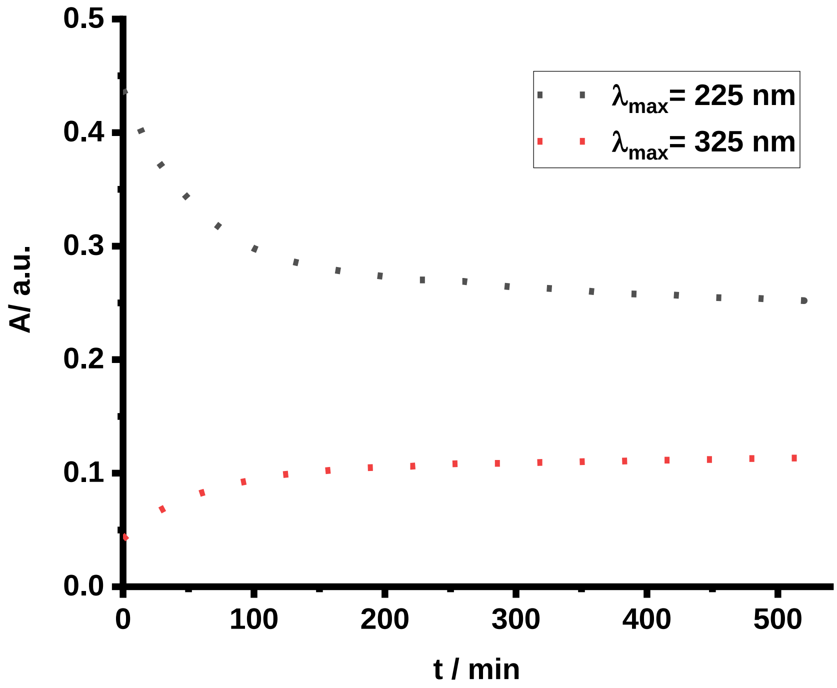

Fig. 1. a) UV-Vis Spectra of Pd(II)-β-CD nanocomposite in distilled water (20 min. is the time interval between each spectrum (see the time of each color)) b) the absorbance of Pd(II)-β-CD nanocomposite in distilled water at λmax 325 nm (red dots) and λmax 225 nm (black dots) with time.

It is clear from figure 1(a and b)) that the spectra of the catalyst solution does not stay constant, there is an increase of the peak in the range of wave length 200-250 nm (λmax 325 nm) (which we believe is the peak of Pd(II)-β-CD nanocomposite without leaching of bound Pd to the CD) and a decrease in the range 300-350 nm (λmax 325 nm) (which we believe is the peak of Pd(II)-β-CD nanocomposite leaching of bound Pd to the CD) with time which gives an indication that the structure of the catalyst dose not stay constant in water. Figure 1 (b) shows that about 200 minutes are required to reach equilibrium between Pd(II)-β-CD nanocomposite and of Pd(II)-β-CD nanocomposite leaching of bound Pd to the CD.

To explore more ^{1}H nmr was measured for the catalyst in D_2O with time as shown in figure (2)

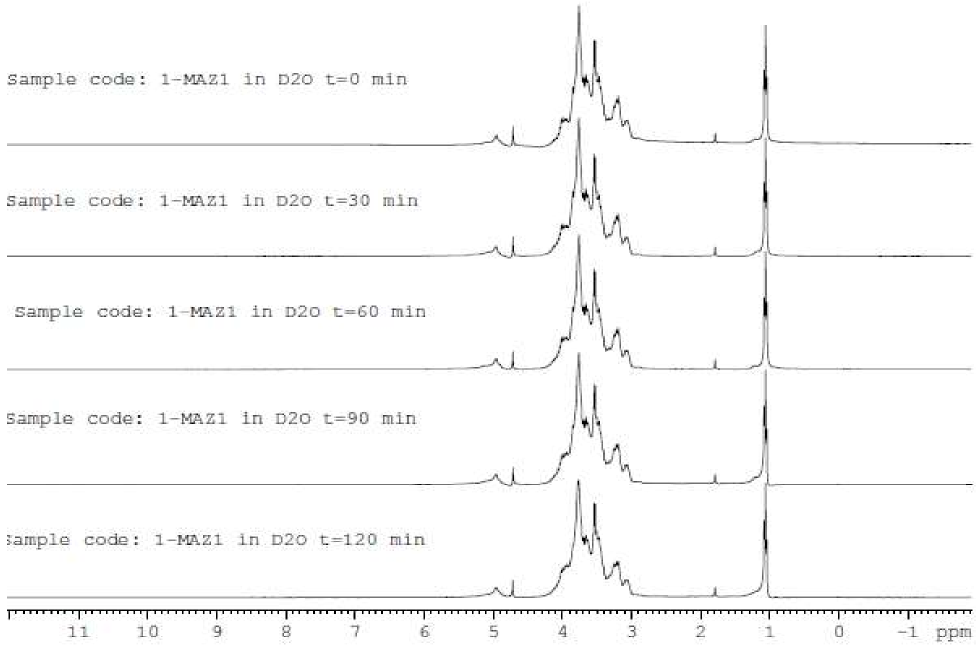

Fig. 2.Time-resolved ^{1}H nmr for Pd(II)-β-CD nanocomposite in D_2O

Figure 2 shows no changes in ^{1}H nmr peaks with time which indicates that the cyclodextrin structure does not change, this mean that Pd leach out to the solution and becomes unbound to catalyst the nanocomposite. Leaching out of some of Pd in to the solution is a common problem that some previous studies are referring to which leads to decreasing the catalytic activity of the catalyst (Azzedine et al., 2017). Also, according to Trzeciak and Augustyniak many Pd-NPs tend to form other unbound Pd species in the reaction solution which they called “Cocktail catalysts” which might be the case of changing the UV-Vis spectra of our Pd(II)-β-CD nanocomposite and no change in ^{1}H nmr spectra (Trzeciak and Augustyniak, 2019).

3.2.Homocoupling of ArBA using Pd(II)-β-CD nanocomposite

Aerobic homocoupling of ArBA in basic aqueous media using Pd(II)-β-CD nanocomposite was studied using UV-Vis spectrophotometer in an open cap cuvette using K_2CO_3 as a base.

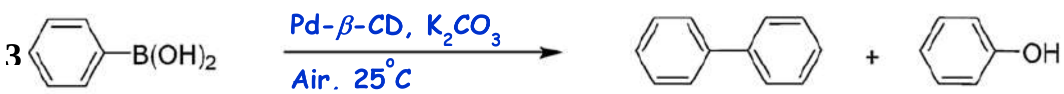

Scheme 3. Aerobic homocoupling reaction of ArBA using Pd(II)-β-CD nanocomposite in basic aqueous media. According to the literature the products of the reaction are biphenyl and phenol. (Mazin and Niklaas, 2011 and Azzedine et al., 2017)

The time-resolved absorption spectra were measured for the reaction see figure 3.

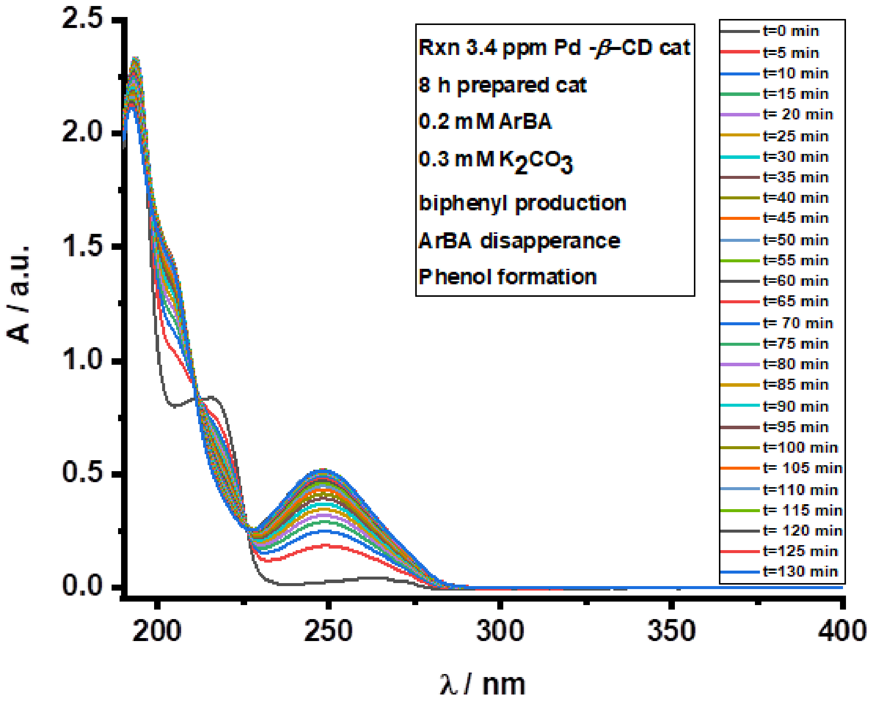

Figure 3. time-resolved absorption spectra for the aerobic homocoupling of 0.1 mM ArBA using 3 ppm Pd(II)-β-CD catalyst and 0.3 mM K_2CO_3 in distilled water. (the spec tra taken every 5 minutes).

From figure 3 we can follow the progress of the reaction with time from which we see decrease of ArBA peak (1) and an increase of biphenyl and phenol formation peaks 2 and 3 respectively. (Azzedine et al., 2017).

3.3. Pd(II)-β-CD nancomposite reactivity

The Pd(II)-β-CD nanocomposite reactivity was tested using aerobic homocoupling reaction of ArBA in aqueous media using K_2CO_3 as a base at room temperature. A 20.0 ppm of the Pd(II)-β-CD nanocomposite stock solution was prepared and used as a catalyst for the aerobic homocoupling reaction of ArBA at different time intervals of the stock solution in distilled water preparation. The reaction was monitored using UV-Vis spectroscopy and the absorbance of the biphenyl formation was measured with time at maximum wave length of 250 nm. The reaction was repeated after different period of the catalyst stock solution preparation using the same concentration of the catalyst see figure 4.

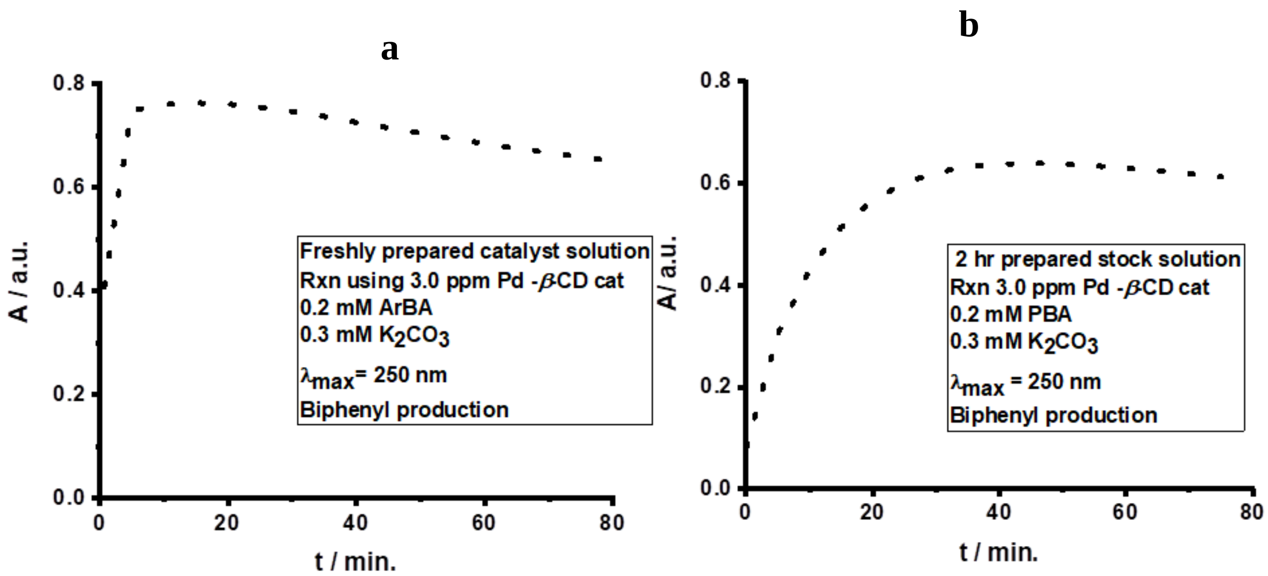

Figure 4. The absorbance of Biphenyl with time at λmax=250 nm for the aerobic homocoupling reaction of 0.2 mM ArBA using 0.3 mM K_2CO_3 and 3.0 ppm Pd(II)-β-CD nanocomposite a) fresh catalyst stock solution, b) catalyst stock solution after 2 hours preparation.

It is clear from figure 4 that the reaction rate decreases significantly when 2 hours is passing on after the catalyst stock solution preparation which indicates that the reactivity of the catalyst stock solution decreases with time. This goes in line with our result in figure 2 which shows the changing of the UV-Vis spectra of Pd(II)-β-CD nanocomposite in distilled water with time. According to our previous work on another palladium nanocomposite catalyst and other works in the literature (Azzedine et al., 2017 and Veisi et al., 2019) and our results in this work the Palladium will leach out of the catalyst solution which changes to unreactive palladium black and this will lead to the decrease of the catalyst reactivity with time.

Conclusions

In summary, the stability of Pd(II)-β-CD nanocomposites in aqueous media was followed using UV-Vis spectroscopy. The UV-Vis time-resolved absorption spectra of the Pd(II)-β-CD nanocomposite solution in distilled water showed a significant change with time which indicates that the structure of some of the Pd(II)-β-CD nanocomposite particles does not stay constant in aqueous solution due to the leach out of some of the cyclodextrin bound Pd in to the solution and becomes unbound to the cyclodextrin molecules and produce unreactive Pd black species and this process requires about 200 minutes. The reactivity of Pd(II)-β-CD nanocomposite as a catalyst for aerobic homocoupling reaction of ArBA in aqueous basic solution was decreasing with time of the catalyst stock solution preparation. These results led us to conclude that palladium will leach out of the catalyst stock solution which leads to the formation of unreactive palladium black which decreases the catalyst stock solution reactivity for the aerobic homocoupling reactions of ArBA with time.

Acknowledgment

The author extends his appreciation to chemistry department of the Institute for Advanced Studies in Basic Sciences (IASBS) in Islamic Republic of Iran, especially Babak Kboudin group for providing the fully characterized Pd(II)-β-CD nanocomposite and working in their laboratories.

References

Trzeciak, M, Augustynia W., *The* role of palladium nanoparticles in catalytic C–C cross-coupling reactions, *Coordination Chemistry Reviews* 2019, 384, 1-20.

Astruc D., Lu F. and Aranzaes R., Nanoparticles as recyclable catalysts: the frontier between homogeneous and heterogeneous catalysis, *Angewandte Chemie*, International Edition in English 2005, 44 (48), 7852-7872.

Astruc, D., Palladium nanoparticles as efficient green homogeneous and heterogeneous carbon-carbon coupling precatalysts: A unifying view. *Inorganic Chemistry*, 2007, 46, 1884–1894.

Azzedine B., Mazin O., Louis L., Soichiro M., Yoshinobu N., Syuji F., and Niklaas B., , Halide-Enhanced Catalytic Activity of Palladium Nanoparticles Comes at the Expense of Catalyst Recovery, *Catalysts*, 2017, 7(9), 280-297.

Babak K., Hadi S., Ramin M., Foad K. and Tsutomu Y., Pd(II)-β-cyclodextrin complex: Synthesis, characterization and efficient nanocatalyst for the selective Suzuki-Miyaura coupling reaction in water, *Journal of Organometallic Chemistry* 2016, 818, 195-199.

Bahareh H., Majid H., Mohammad R. Nabid, S. and Seyyed Emad H., Novel palladium nanoparticles supported on β- cyclodextrin@graphene oxide as magnetically recyclable catalyst for Suzuki–Miyaura cross- coupling reaction with two different approaches in bio- based solvents, *Applied Organometallic Chemistry* 2019, 33:e 4632-4649.

Cuiru W., Juanjuan Y., Shiqi H., Tifeng J., Zhenhua B., Jingxin Z., Lexin Z. and Qiuming P., Preparation of Palladium Nanoparticles Decorated Polyethyleneimine/ Polycaprolactone Composite Fibers Constructed by Electrospinning with Highly Efficient and Recyclable Catalytic Performances, *catalysts* 2019,9 (6), 559-574.

Maria D., Matilda M., Piero M., Antonino R., Chiara P., and Cristina L., Suzuki-Miyaura coupling under air in water promoted by polymer-supported palladium nanoparticles. *Journal of Molecular Catalysis: A Chemistry* 2013, 366, 186–194.

Karimi, B., Behzadnia, H., Farhangi, E., Jafari E. and Zamani, A., Recent Application of Polymer Supported Metal Nanoparticles in Heck, Suzuki and Sonogashira Coupling Reactions, *Current Organic Synthesis* 2010, 7, 543–567.

Kenneth A. Connors, The Stability of Cyclodextrin Complexes in Solution, *Chemical review* 1997, 97, 1325-1358.

Mazin O. and Niklaas B., Ph.D. thesis, The palladium-catalysed aerobic oxidative homocoupling reaction of arylboronic acids in aqueous micellar medium kinetic and mechanistic studies, School of Chemistry, Cardiff University, UK, 2011.

Moreno-Manas M., and Pleixats, R., Formation of Carbon−Carbon Bonds under Catalysis by Transition-Metal Nanoparticles, *Accounts of Chemical Research* 2003, 36 (8), 638-43

Pérez-Lorenzo J., Palladium nanoparticles as efficient catalysts for Suzuki cross-coupling reactions, *Physical Chemmistry Letters*, 2012, 3, 167–174

Raihana K. and Kasi P., A pyridinium modified β-cyclodextrin: an ionic supramolecular ligand for palladium acetate in C–C coupling reactions in water, *Green Chemistry*, 2016,**18**, 5518-5528

Sawoo, S., Srimani, D., Dutta, P., Lahiri, R. and Sarkar, A, Size controlled synthesis of Pd nanoparticles in water and their catalytic application in C-C coupling reactions. *Tetrahedron* 2009, 65, 4367–4374.

Taladriz-Blanco, P., Hervés, P., and Pérez-Juste, J. Supported pd-nanoparticles for carbon-carbon coupling reactions, *Topics in Catalysis* 2013, 56, 1154–1170.

Veisi H., Safarimehr P., and Hemmati S., Buchwald-Hartwig C-N cross coupling reactions catalyzed by palladium nanoparticles immobilized on thio modified-multi walled carbon nanotubes as heterogeneous and recyclable nanocatalyst, *Materials Science and Engineering: C* 2019, 96, 310-318.

Wei Z., Zi-Jian Y. and Wei D., Palladium Nanoparticles Supported on β-cyclodextrin Functionalised Poly(amido amine)s and their Application in Suzuki-Miyaura Cross-Coupling Reactions, *Journal of the Brazilian Chemical Society* 2019, 30(8), 1667-1677.

Yafei G., Jiuling L., Xiwei S., Yang L., Kai X., Yuqi L., Yubo J., Bo Y. and Rui Y., Cyclodextrin-supported palladium complex: A highly active and recoverable catalyst for Suzuki–Miyaura cross- coupling reaction in aqueous medium, *Applied Organometallic Chemistry* 2017, 31:e 3592-3607.

Yanru Y., Ning M., Jing X., Guoqiang W., Shuibo L., Hongliang L. and Peizhi G., Insights into the Role of Poly(vinylpyrrolidone) in the Synthesis of Palladium Nanoparticles and their Electrocatalytic Properties, *Langmuir* 2019, 35, 3, 787-795.

ZANCO Journal of Pure and Applied Sciences
The official scientific journal of Salahaddin University-Erbil
https://zancojournals.su.edu.krd/index.php/JPAS

ISSN (print):2218-0230**, ISSN (online):** 2412-3986**, DOI: http://dx.doi.org/10.21271/zjpas**

RESEARCH PAPER

Allelopathic Assessment by Interaction Effect of Coconut Water (*Cocos nucifera* L.), and Dipping Time on Seed Germination of Four Cereal Seeds.

Yaseen Ahmed Rasheed Goran

Department of Biology, College of Science ,Salahaddin University-Erbil, Kurdistan region-Iraq.

A B S T R A C T:

Coconut water (*Cocos nucifera* L.) is a biological and sterile liquid from coconut kernel. It contains a variety of ionic materials, sugars, amino acids, and several plant growth regulators. This work has been achieved in plant physiology research laboratory in Biology Department, College of Science at Salahaddin University/Erbil during July to December 2019. The purpose of this study is to evaluate the effect of concentration, different dipping time and the interaction between both seed germination and seedling radicle and plumule length. The effect of different concentrations (1%, 2%, 3%, and 4% v/v) of coconut water and different dipping times (5, 10, 15, and 20 seconds) on four cereal seeds germination and seedling parameters, the seedling plumule and radicle lengths, also the interaction between both treatments were studied. In this study it claims that when using different concentrations, the best one is the 3% concentration that effects on percent germination of all seeds used in this study, where the higher germination percentage was recorded. The best effective concentration on radicle and plumule elongation was in 1% and all concentrations showed significant effection. The best active dipping time was at 5 seconds and others also showed significant effection on both radicles and plumules. In the case of interaction of both treatments the more positive effective interaction was at 5 seconds in 4% concentration on radicles and plumules.

KEY WORDS: allelopathy. barley, sorghum, soft wheat, hard wheat, coconut water, dipping time.
DOI: http://dx.doi.org/10.21271/ZJPAS.32.4.15
ZJPAS (2020) , 32(4);122-134 .

1.INTRODUCTION

The term allelopathy derived from the Greek compounds *allelo-* and *-pathos* (meaning “mutual harm” or “suffering”), was first introduced by Austrian professor Hans Molisch in 1937 in the book *Der Einfluss einer Pflanze auf die andere - Allelopathie* (The Effect of Plants on Each Other) published in German. In 1971, Whittaker and Feeny published a study where they outlined allelochemicals as all chemical exchanges among organisms (Willis, 2007).

Rice (1984) expanded the definition to include all direct positive or negative influences of a plant on another plant or on micro-organisms by the release of biochemicals into the natural environment in his monograph on allelopathy. In more recent times, Botanists started to shift back to the previous definition of substances that are produced by one plant that inhibit another plant (Willis, 2007).

Coconut water (*Cocos nucifera* L.) is a biological and sterile liquid from coconut kernel. It contains a variety of ionic materials, sugars, amino acids, and several plant growth regulators. Coconut

* **Corresponding Author:**
Yaseen Ahmed Rasheed Goran
E-mail:
Article History:
Received: 27/01/2020
Accepted: 03/05/2020
Published: 08/09 /2020

water (*Cocos nucifera*) must not be mistaken with coconut milk, although some studies have used the two terms interchangeably (Kobayashi, *et al*., 1997; Sandhya and Rajamohan, 2008). Coconut water is the aqueous part of the coconut endosperm, while coconut milk is the liquid products acquired by grating the solid endosperm, with or without the addition of water (APCC, 1994). Unlike coconut water, coconut milk, is the source of coconut oil and generally is not used in plant tissue culture medium formulations (George and Sherrington, 1984; Seow and Gwee, 1997).

Coconut water is broadly used in the plant tissue culture industry. The wide-ranging use of coconut water as a growth-enhancing component in tissue culture medium formulation can be trailed back to more than 50 years ago, when first presented coconut water as a new element of the nutrient medium for callus cultures in 1941 by Van Overbeek and coworkers (Arditti, 2008). Furthermore, its nutritional role, coconut water also seems to have growth regulatory properties activity (George and Sherrington, 1984). Some of the most important and beneficial components in coconut water are cytokinins, which are a class of phytohormones (Kende and Zeevaart, 1997). In addition to many different plant-related functions, it was also discovered that some cytokinins (e.g., kinetin and *trans*-zeatin) demonstrated significant anti-thrombotic, anti-ageing, and anti-carcinogenic effects (Vermeulen *et al*., 2002; and Rattan and Clark, 1994). Other elements found in coconut water include sugar alcohols, sugars, nitrogenous compounds, lipids, amino acids, organic acids and enzymes, and they play various functional roles in plant and human systems because of their distinct chemical properties (George and Sherrington, 1984; Santos *et al*.,1996; and USDA, 2009).

Inversely, coconut water is a rich addition that naturally contains plant growth regulators such as indole 3-acetic acid (IAA). The objective work of this research was to assess the capacity of coconut water extracts containing natural IAA, on adventitious radicle development in vegetative propagation of ornamental plant canes. Five different concentrations of coconut water extracts were tested. The IAA of coconut water extract recorded the best radicle development and induction. It was discovered that the radicle expression was faster (5 weeks) using the novel method. In the standard method, the canes were disseminated by quick dip application of a commercial product containing artificial hormone IAA. It takes up to 6 weeks for the canes to develop adventitious radicles to the desired level. The study shows that adventitious plumule development, radicle development, and leaf emergence of the ornamental plant was supported by IAA of coconut water extracts (Agampodi and Jayawardena, 2009). In a study where IAA and coconut water used in different concentrations and their combination on the germination of seeds. The study revealed that the combinations of coconut water and IAA were able to hasten radicles emergence, plumule height growth and increase the number of radicles for the plant Tribulus (*Tribulus terrestris* L.), (Akhiriana *et al*., 2019).

Another study assessed if coconut water can be used as radicle setting medium in mangrove propagation *Rhizopora stylosa* in terms of number of radicles and average length of radicles generated. The results demonstrated that coconut water can be used as radicle setting hormone and can be used as alternative radicle setting medium in *Rhizopora stylosa* propagation (Ogatis, 2015).

Barley (*Hordeum vulgare* L.) wheat, both soft (*Triticum aestivum* L. cv. Adana) and hard (*T. durum* L. cv. Smito), and sorghum (*Sorghum bicolor* L.) are members of the grass family (Poaceae). They are a self-pollinating. They are important cereal crops in the world. They are of the earliest domesticated crops since the start of civilization (Dhillon *et al*., 2006).

The purpose of this study is to evaluate the effect of concentration, different dipping time and the combination of both, on seed germination percentage and seedling radicle and plumule length.

Material and Methods

This work has been achieved in plant physiology research laboratory in Biology Department, College of Science at Salahaddin University/Erbil during July to December 2019. Healthy coconut fruit (*Cocos nucifera* L.) used in this study was collected from market, Coconut water has been gotten from one fruit and kept in the refrigerator in dark bottle to be used later. Fresh white barley seeds (*Hordeum vulgare* L.), wheat seeds (*Triticum sp.*) both soft wheat (*T. aestivum* L. cv Adana) and hard wheat (*T. durum* L. cv Smito) were gotten from the agricultural research center in Kirkuk province. Sorghum seeds (*Sorghum bicolor* L.) were gotten from market. Twenty seeds, surface sterilized by rinsing for 5 seconds with 0.1% sodium hypochlorite solution, then rinsed in distilled water for each plant, prepared to be put in each of sterilized glass Petri dishes lined with 90 mm sterilized filter paper for all experiments with four Petri-dishes for each treatment as duplicates. The following experiments were conducted for this study.

Effect of dipping time on seed germination and seedlings.

Using different dipping times for each plant seeds, for short time, lasted for 5, 10, 15, and 20 seconds in fresh concentrated coconut water, rinsed with distilled water then seeds, for each plant, were placed in marked Petri dishes and 10 ml of sterilized distilled water was added to each Petri dish. Petri dishes stoppered with para-film to prevent evaporation and placed in cold incubator at 23^{o}C for 7 days. After which measurements of percent seed germination and the length of both plumule and radicle lengths, in millimeters, for each seedling was taken and recorded.

$$\%\, seed\ germination = \frac{germinated\ seeds}{sawn\ seeds} * 100$$

Effect of coconut water concentrations on seed germination and seedlings.

Using 10 ml of each 1%, 2%, 3%, and 4% concentrations (v/v) of coconut water diluted solutions and were added to 20 seed containing Petri-dishes, then stoppered with para-film to prevent evaporation and placed in cold incubator at 23^{o}C for 7 days. After which measurements of percent seed germination and the length of both plumules and radicles, in millimeters, for each seedling was taken and recorded.

Interaction effect between dipping time and different concentration on seed germination and seedling.

Here the experiment used to detect effect of the interaction of both factors on seed germination was executed by rinsing of barley, sorghum, and Wheat seeds with different times (5, 10, 15, and 20 seconds) in different coconut water concentrations (1%, 2%, 3%, and 4% v/v concentrations) and then placed in filter paper-lined Petri dishes, then adding 10 ml of distilled water, stoppered with para-film to prevent evaporation and placed in a cold incubator at 23^{o}C for 7 days. After which measurements of percent seed germination and the length of both plumules and radicles, in millimeters, for each seedling was taken and recorded.

Controls prepared by using sterilized Petri dishes lined with sterilized filter papers and 20 surface sterilized seeds for each were sawn in four replicates and 10 ml sterilized distilled water was added to be used as control instead of coconut water concentrations, stoppered with para-film to prevent evaporation and placed in cold incubator at 23^{o}C for 7 days. After germination of seeds radicle and plumule length were measured for germinated seeds. The statistical design was *Completely Randomized Factorial Design*, and using Dunkan test to show differences between means at 0.05.

Results

The effect of coconut water on seed germination

Seed germination percent of all seeds were affected whether positively or negatively by both dipping time and different concentrations of coconut water so do the interaction of both treatments.

Results showed that the percent germination of adana wheat was affected positively in different concentration of coconut water (1,2, and 3 %) while when it is deals with dipping time and interaction between both effects were slightly positive and negatively effects on seed germination percent, this is shown obviously in figure (1).

The Smito hard wheat was affected positively in 1% of coconut water concentration but there was fluctuation of slightly positive and negative effects on seed germination percent when it is dealing with other concentrations, dipping time and the interaction between them. These conclusions are obvious in figure (2).

The effect of different coconut water treatments on seed percent germination of white barley is same as the effects on Smito hard wheat seeds in that the most seed germination percent was at 1% concentration of coconut water, and this is quite obvious in figure (3).

Sorghum seeds Showed a very obvious sensitivity to coconut water treatments in all treatments whether concentration, dipping time, and their interactions. All treatments showed positive effects on seed germination with a smooth fluctuation from lower treatments to higher one. These are noticed when looking at figure (4). Where it has effects on nineteen treatments out twenty-eight with percentage between 96% up to 100% germination.

The effect of coconut water different concentrations, dipping time, and their interaction on seedling radicle length.

From the table (1) which shows the effect of coconut water different concentrations on radicles of cereals seedlings. It is easy to conclude that adana soft wheat seedlings radicles were significantly longer than control at concentrations of 1% and 3% and the other two (2% and 4%) concentrations were non-significantly shorter than control mean. While Smito hard wheat seedlings radicles were significantly elongated at 1% and 2% concentrations but the other two (3% and 4%) concentrations were non-significantly shortened. All white barley seedlings radicle means were significant longer than control seedlings radicles mean. Lastly for sorghum seedlings radicle except for the radicles at concentration 1% were shorter than control mean non-significant, all other concentrations were shortened significantly.

In the table (2) which deals with effect on different dipping times of seeds in coconut water. The table shows that Adana soft wheat radicles were significantly elongated than control at times of 5, 10, and 20 seconds while at 15 seconds was elongated non-significantly. All radicles length of Smito hard wheat were significantly longer than control radicles. The same thing happened with white barley radicles in that all dipping times affected positively on radicles length in comparison with control radicles. In sorghum seeds all dipping times, except for 15 seconds, affected positively on radicles length.

The effect of the interaction of both treatments, time and concentrations, of coconut water on the radicles length of the germinated seeds tested shown in table (3) below. The Adana soft wheat seedlings radicles length all were elongated significantly except for two, 10sec. at 1% concentration and 5sec. at 2% concentration, which were shortened non-significantly. Smito hard wheat seedlings radicles, all radicles length was significantly longer than control this means that all interactions were positively effective on radicle length. All radicles length of seedlings of white barley were positively affected with different interactions of both treatments significantly and radicles length were longer than control seedlings radicles length. But in case of sorghum seedlings radicles in all treatments were affected negatively and significantly comparing with control seedlings radicles length that means they were shorter.

The effect of coconut water different concentrations, dipping time, and their interaction on seedling plumule length.

Plumules of germinated plants shows different affect to different processing of coconut water. In table (4) different concentrations of coconut water it shows that the Adana soft wheat seedlings plumules were elongated significantly 1% concentration and decreases length significantly at concentrations 2% and 4%. The plumules of Smito hard wheat seedlings were elongated significantly at 1% and 2% concentrations. White barley seedling plumules were elongated at all concentration significantly. All concentrations of coconut water were effective positively on sorghum seedling plumules which were longer than control.

Effect of different dipping times on seedling plumules for tested cereal seeds are shown in table (5). The results show that the Adana soft wheat seedling plumules has been shortened significantly at 20 seconds dipping time and significantly elongated at 10 seconds dipping time. But the other two timings were affected non-significantly when compared with the mean of control plumule length. Seedling plumules of smito hard wheat show different responses to dipping time in that all means were significantly elongated in comparison to control seedling plumule mean. All means of white barley seedling plumules were positively affected to different dipping times in comparison with control mean plumule length. The last plant in this treatment is sorghum where its seedling plumules were significantly shorter than the mean of control plumule except at 10seconds dipping time where the mean was bigger than control length means but non-significantly.

The effect of the interaction of both treatments, dipping time and concentrations, on plumules length of seedlings differs among tested seeds. The adana soft wheat seedling plumules were divided into two parts where half of means were elongated significantly in compare with control mean, while the other half shortened or elongated non-significantly as it is obvious in table (6) below. All Smito soft wheat plumule seedlings showed positive significant differences with control mean and plumules were longer than control plumules. In white barley all means were positively significant and plumules were longer than that of control, except for the treatment with 20 seconds dipping at 1% concentration where its length was non-significant. The sorghum seedlings were divided into two groups, half were significantly shorter than the mean of control and the other half were significantly longer except for the treatment 15second dipping at 2% concentration which was non-significantly shortened.

Note that in all treatments means within a column followed with the same letters are not significantly differ from each other according to Duncan multiple range test at 5% level.

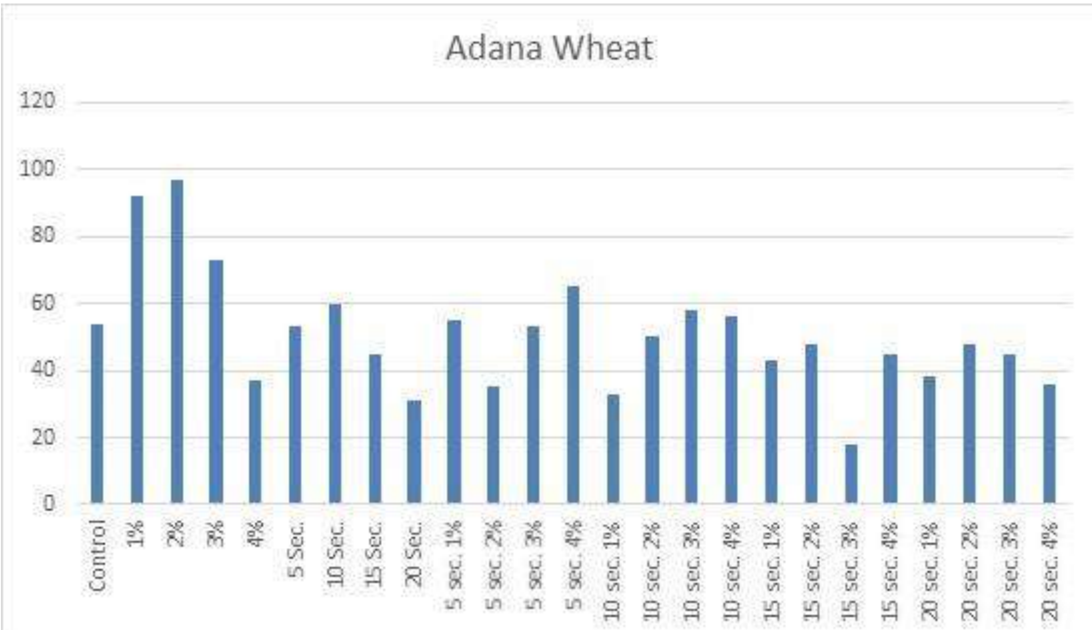

Figure 1: Effect of different treatments on Adana soft wheat seed germination percent.

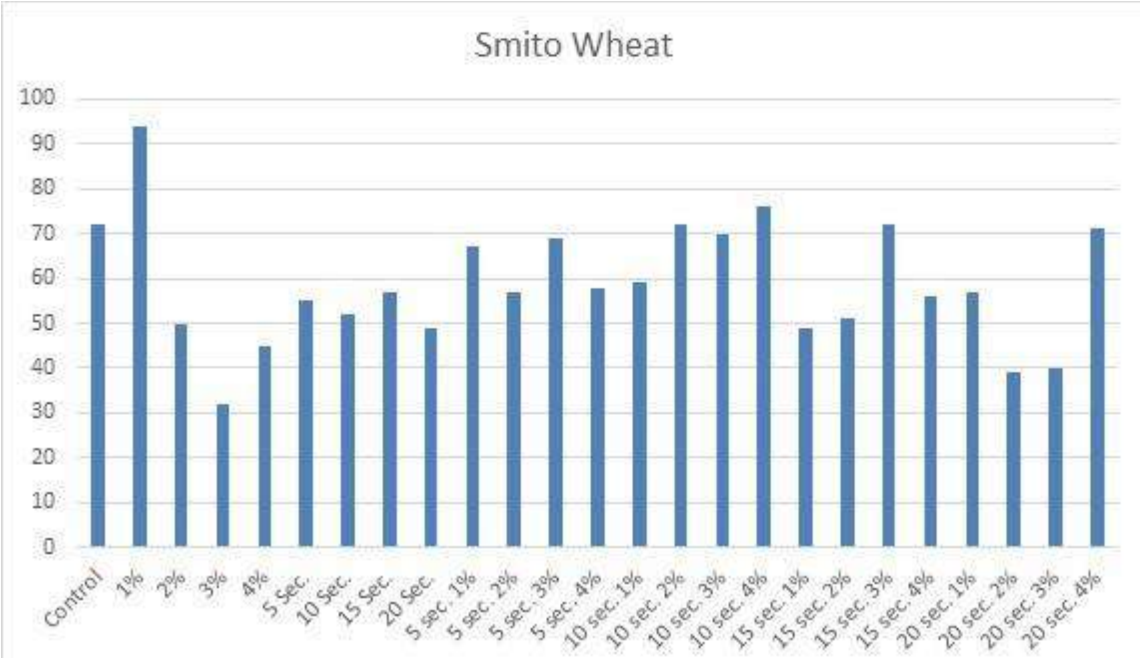

Figure 2: Effect of different treatments on Smito hard wheat seed germination percent.

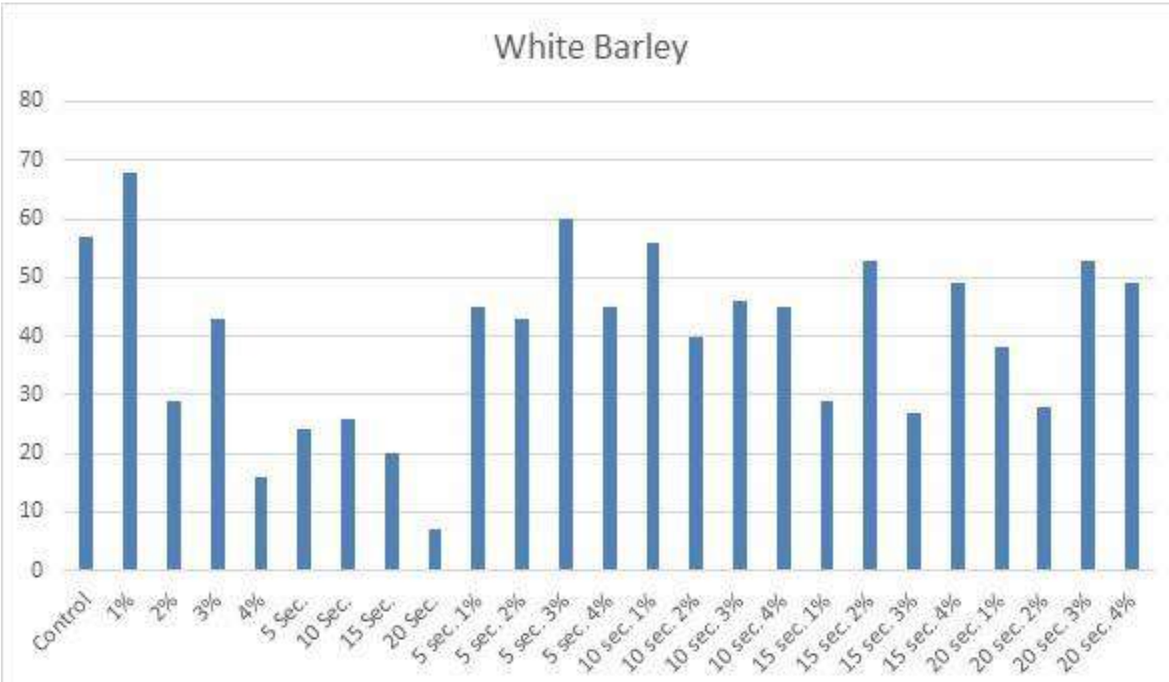

Figure 3: Effect of different treatments on white barley seed germination percent.

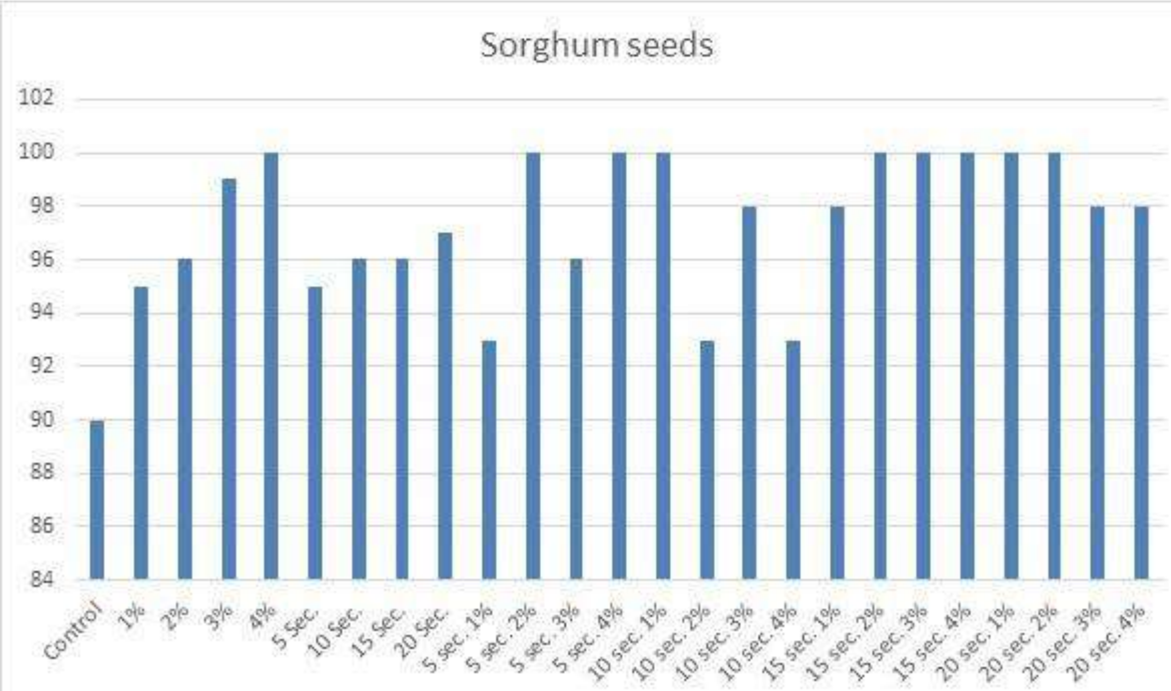

Figure 4: Effect of different treatments on sorghum seed germination percent.

Table (1) Effect of different concentrations of coconut water on radicle length of the four cereals tested seedlings.

Treatment	Adana Wheat N=22		Smito Wheat N= 37		White Barley N= 35		Sorghum N= 42	
	Radicle length (mm)		Radicle length (mm)		Radicle length (mm)		Radicle length (mm)	
	Mean	S. D.	Mean	S.D.	Mean	S.D.	Mean	S.D.
Control	10.8[a]	7.2	27.9[a]	15.1	33.3[a]	9.8	126.0[c]	183.1
1%	68.5[c]	15.6	76.4[c]	32.2	80.6[d]	13.9	91.8[c]	19.8
2%	9.9[a]	10	46.5[b]	20.4	83.7[d]	20.1	82.3[b]	27.8
3%	24.4[b]	11.7	24.9[a]	14.6	42.7[b]	15.6	83.9[b]	37.3
4%	8.5[a]	5	20.8[a]	8.3	56.9[c]	31.8	37.6[a]	23.5
Total	24.4	25.1	39.3	28.4	59.4	28	84.3	89.4

S.D. = Standard Deviation

Table (2) Effect of different dipping times in coconut water on radicle length of the four cereals tested seedlings.

Treatment	Adana Wheat N=22		Smito Wheat N= 37		White Barley N= 35		Sorghum N= 42	
	Radicle length (mm)		Radicle length (mm)		Radicle length (mm)		Radicle length (mm)	
	Mean	S. D.	Mean	S.D.	Mean	S. D.	Mean	S.D.

Control	10.8^{a}	7.2	27.9^{a}	15.1	33.3^{a}	9.8	126.0^{b}	183.1
5 Sec.	47.6^{c}	17.1	72.1^{c}	26.9	84.1^{c}	32.9	96.1^{b}	38
10 Sec.	39.1^{b}	19.4	58.3^{b}	21.8	63.0^{b}	23.7	112.0^{b}	33.8
15 Sec.	12.5^{a}	8	67.7^{c}	18.6	79.5^{c}	25.9	71.9^{a}	28.4
20 Sec.	32.3^{b}	9.3	77.9^{c}	28.3	78.1^{c}	12.5	108.4^{b}	28.5
Total	28.5	19.6	60.8	28.6	67.6	29.1	102.9	88

Table (3) Interaction effect of dipping time and concentration, of coconut water on radicle length of the four cereals tested seedlings.

Treatment		Adana Wheat N=22		Smito Wheat N= 37		White Barley N= 35		Sorghum N= 42	
		Radicle length (mm)		Radicle length (mm)		Radicle length (mm)		Radicle length (mm)	
		Mean	S.D.	Mean	S.D.	Mean	S.D.	Mean	S.D.
Control		10.8^{a}	7.2	27.9^{a}	15.1	33.3^{a}	9.8	126.0^{g}	183.1
5 sec.	1%	26.5^{c}	13.6	48.5^{d}	24.6	72.7^{f}	25.1	84.2^{f}	27.4
	2%	7.4^{a}	6.5	54.7^{e}	27.9	70.4^{e}	25.7	53.7^{c}	18.5
	3%	26.4^{c}	21	62.1^{f}	27.8	73.5^{g}	25.4	81.7^{f}	26.4
	4%	33.4^{e}	23.7	69.6^{f}	22.6	86.5^{i}	25.4	87.8^{f}	26.4
10 sec.	1%	6.9^{a}	6.1	68.3^{f}	25.5	64.5^{d}	21.5	92.7^{f}	25.5
	2%	28.4^{d}	16.6	69.8^{f}	20.4	84.1^{i}	25.2	64.0^{e}	23.1
	3%	41.8^{e}	24.4	83.4^{g}	23.3	76.1^{h}	28.7	60.0^{d}	17.7
	4%	30.1^{d}	23.8	81.8^{g}	20	88.1^{i}	26.7	33.3^{a}	8.3
15 sec.	1%	25.8^{c}	12.1	58.8^{f}	20.5	73.7^{g}	18.3	86.4^{f}	37.8
	2%	14.8^{b}	9.9	57.1^{e}	23.5	79.8^{h}	19.9	62.7^{e}	22.1
	3%	31.1^{e}	19.64	68.6^{f}	14.7	83.8^{i}	19.8	74.0^{f}	32.6
	4%	32.1^{e}	9.8	37.9^{c}	20.9	88.7^{i}	34.9	47.9^{b}	16.9
20 sec.	1%	32.1^{e}	13.2	40.8^{c}	17	61.0^{c}	17.2	76.6^{f}	22.6
	2%	14.3^{b}	6.8	30.5^{b}	19.4	85.7^{i}	18.6	46.5^{b}	16
	3%	39.0^{e}	23.1	54.3^{e}	19.6	93.8^{i}	20.2	55.8^{c}	23.5
	4%	22.1^{c}	12.3	89.9^{g}	31.4	56.6^{b}	23.4	81.2^{f}	34.3
Total		24.9	18.8	59.1	28.2	74.8	27.2	71.5	54.3

Table (4) Effect of different concentrations of coconut water on plumule length of the four cereals tested seedlings.

Treatment	Adana Wheat N=22		Smito Wheat N= 37		White Barley N= 35		Sorghum N= 42	
	Plumule length (mm)		Plumule length (mm)		Plumule length (mm)		Plumule length (mm)	
	Mean	S. D.	Mean	S.D.	Mean	S.D.	Mean	S.D.
Control	24.6[c]	7.2	21.1[a]	8.4	34.9[a]	13.8	54.8[c]	16.2
1%	55.1[d]	11	57.8[c]	27.8	100.0[d]	12.8	39.2[b]	10.4
2%	19.5[b]	15.7	38.8[b]	24.2	79.3[c]	13.8	44.5[b]	14.5
3%	25.7[c]	5.8	14.3[a]	9.3	38.7[a]	24.9	23.1[a]	19.7
4%	11.2[a]	5	13.5[a]	9.7	55.2[b]	29.1	23.7[a]	15.7
Total	27.2	17.7	29	24.6	61.8	32	37.1	19.7

Table (5) Effect of different dipping times in coconut water on plumule length of the four cereals tested seedlings.

Treatment	Adana Wheat N=22		Smito Wheat N= 37		White Barley N= 35		Sorghum N= 42	
	Plumule length (mm)		Plumule length (mm)		Plumule length (mm)		Plumule length (mm)	
	Mean	S. D.	Mean	S.D.	Mean	S. D.	Mean	S. D.
Control	24.6[b]	7.2	21.1[a]	8.4	34.9[a]	13.8	54.8[c]	16.2
5 Sec.	28.1[b]	12.2	62.1[c]	28.7	69.2[c]	30.2	43.0[a]	17.2
10 Sec.	42.2[c]	12.6	46.2[b]	15.6	63[c]	29.7	59.8[c]	14.2
15 Sec.	30.5[b]	14.9	58.2[c]	20.1	74.1[c]	25.9	48.3[b]	14.5
20 Sec.	22.0[a]	12.6	45.8[b]	27.4	59.3[b]	14.5	46.8[a]	15.6
Total	29.5	13.9	46.7	25.6	60.1	27.3	50.5	16.6

Table (6) Interaction effect of dipping time and concentration, of coconut water on plumule length of the four cereals tested seedlings.

Treatment	Adana Wheat N=22		Smito Wheat N= 37		White Barley N= 35		Sorghum N= 42	
	Plumule length (mm)		Plumule length (mm)		Plumule length (mm)		Plumule length (mm)	
	Mean	S. D.	Mean	S. D.	Mean	S. D.	Mean	S. D.

Control		24.6^{d}	7.2	21.1^{a}	8.4	34.9^{a}	13.8	54.8^{d}	16.2
5 sec.	1%	23.9^{d}	16.3	44.7^{e}	31.9	46.4^{c}	19.0	63.4^{f}	14.2
	2%	12.6^{a}	7.5	42.4^{e}	37.1	48.5^{d}	16.9	28.5^{a}	9.0
	3%	19.2^{d}	17.2	45.9^{e}	29.9	55.1^{d}	22.5	56.8^{f}	15.0
	4%	25.5^{d}	21.3	52.8^{e}	31.0	66.9^{f}	28.3	59.7^{f}	13.8
10 sec.	1%	12.1^{a}	9.1	54.5^{e}	35.0	57.9^{e}	20.2	58.3^{f}	17.1
	2%	18.1^{c}	13.3	51.4^{e}	31.8	46.8^{c}	12.8	55.9^{e}	19.4
	3%	25.0^{d}	13.9	48.4^{e}	32.7	48.2^{d}	19.1	33.3^{b}	10.3
	4%	21.3^{d}	21.3	53.0^{e}	22.6	58.2^{e}	26.0	37.7^{b}	9.4
15 sec.	1%	22.7^{d}	17.8	38.4^{d}	26.5	48.3^{d}	14.6	56.9^{f}	20.1
	2%	15.8^{b}	9.5	46.8^{e}	32.6	69.4^{f}	21.4	53.8^{d}	16.5
	3%	35.6^{e}	15.3	45.1^{e}	23.8	49.8^{d}	11.2	44.7^{c}	15.8
	4%	19.4^{d}	9.5	37.7^{d}	23.1	67.1^{f}	29.1	38.2^{b}	10.2
20 sec.	1%	16.6^{c}	9.2	30.1^{c}	27.9	35.2^{a}	19.2	62.7^{f}	11.3
	2%	19.1^{d}	10.9	26.2^{b}	19.0	54.0^{d}	19.4	46.8^{c}	10.8
	3%	26.8^{e}	18.2	40.8^{e}	22.5	53.7^{d}	11.7	30.9^{a}	12.2
	4%	29.0^{e}	15.1	54.7^{e}	25.1	37.3^{b}	16.4	58.4^{f}	21.2
Total		21.6	15.2	43.2	29.2	51.6	21.8	49.5	18.4

Discussion and conclusions

The effects of coconut water in different concentrations on plants seeds germination were in acceptance with those mentioned by other authors (Komgrit *et al*., 2011; Chan and Elevitch, 2006), where both used different concentrations (0%, 2.5%, 5%, 7.5% and 10%). The dipping time treatment has not been trialed or mentioned in any literature in any citation and this is the first time to be trialed such effect or treatment for study. The concentration affected positively on radicles and plumules length for all plants specially the 1% which their effects were the higher than others. While the dipping time showed positive effect at both 5 and 10 seconds dipping time on both radicles and plumules while other times showed different effects. The interaction between both treatments showed different affections on radicles where the radicles were affected positively and significantly in all dipping times at concentration of 4%. Plumules were more sensitive significantly positive at 4sec. in 4% concentration for adana soft wheat and so for smito hard wheat. White barley was positive and significant in 4% at the times 5 and 10 seconds, while the rest were affected in 2% concentration at 15 and 20 seconds. The sorghum seedling plumules were affected positively in 1% concentration at all dipping times except for 5 second dipping time was affected in 4% concentration. Simply these results are in agreement with the studies of (Agampodi and Jayawardena, 2009) and (Akhiriana *et al*., 2019) in that they used IAA and coconut water in different concentrations and combination of both. They noticed that adventitious plumule development and height, radicle emergence and development, and leaf emergence of the ornamental plant was supported by IAA of coconut water also they affected the seed germination.

Conclusion from results it has been that results showed concentration at 1% and dipping time with 10 seconds are the most active on enhancing radicle and plumule growth and percent germination. While the effect on interaction of both treatments were active at 15 and 20 seconds with all concentrations.

References

Agampodi,V. A. and Bimali Jayawardena (2009). Effect of coconut (*Cocos nucifera* L.) water extracts on adventitious radicle development in vegetative propagation of *Dracaena purplecompacta* L. Acta Physiologiae Plantarum 2009, Volume 31, Issue 2, pp 279-284

Akae, T., Avci, M ., Dusunceli, F.(2004). Barely; post-harvest operations. OECD (2004). Consensus document on compositional considerations for new varieties of barely (*Hordium vulgare*); key food and feed nutrients and anti- nutrient s. Report No.12 Environment Directorate, OECD, Paris.

Akhiriana E., Samanhudi K., and Yunus A. (2019). Coconut Water and IAA Effect on the InVitro Growth of Tribulus terrestris L. Acta Universitatis Agriculturae et Silviculturae Mendelianae Brunensis, 67(1): 9–18.

Arditti, J. (2008). *Micropropagation of Orchids*, 2nd ed.; Blackwell Publishing: Oxford, UK; Volume II.

Asian and Pacific Coconut Community (APCC). International Codes and Standard for Aqueous Coconut Products, 2nd draft. Standards Task Force, Asian and Pacific Coconut Community: Jakarta, Indonesia, 1994.

Chan E and Elevitch C. R ,(2006). *Cocos nusifera*(coconut) tradiotional tree 2(1).

Chandra, G.S; proudlove, MO,; baxter E. D. The structure of barely endosperm; an important determinant of malt modification. J. Sci. Food Agric., 1999, 79, 37-46.

Chang-Hung, Chou (2006). “Introduction to allelopathy”, 2006, Part 1, 1-9.

Dhillon B. S., Saxena S., Agrwal A and Tyagi R. K. (2006) Food grain crops in plant genetic resources. Narosa publishing house, New Delhi.

Ever, T; Millar, S. cereal grain structure and development: some implication for quality. J. cereal sci. 2002,36, 261 -284

Fincher, G. B.; Stone, B. A. Cell walls and their component in cereal grain technology. Adv. Cereal Sci. Technol. 1986, 8, 207-295.

Fraenkel, Gottfried S. (1959). “The raison d’Etre of secondary plant substances”, Science, 129 (3361).

Gamlath, J.; Aldred, G. P.; Panozzo, J. F. (2008). Barley (1-3; 1-4)- B-glucan and arabinoxylan content are related to kernel hardnes and water uptake. J. cereal Sci., 47, 365-371.

George, E.F.; Sherrington, P.D. (1984). Plant Propagation by Tissue Culture-Handbook and Directory of Commercial Laboratories; Exegetics Ltd: Edington, UK, 1984.

ICAR (2006) Hand book of Indian Agriculture. ICAR publication, New Delhi

Izydorczyk, M.S.; Dexter, J. E.; Desjardins, R. G.; Rossnagel, B.G.; Lagasse, S. L.; Hatcher, D. W. Roller milling condian hull-less barely; optimization of roller milling conditions and composition of mill streams. Cereal chem. 2003, 80, 637-644.

Jothi V. and Loomba S. (2013). *Cocos nusifera*; Its properties and contribution to densty; International Jornal Scientific study, volume 1. issue 3.

Kende, H.; Zeevaart. J. (1997). The five “Classical” plant hormones. *Plant Cell*, *9*, 1197–1210.

Kobayashi, H.; Morisaki, N.; Tago, Y.; Hashimoto, Y.; Iwasaki, S.; Kawachi, E.; Nagata, R.; Shudo, K. (1997). Structural identification of a major cytokinin in coconut milk as 14-O-(3-O-[β-Dgalactopyranosyl-(1-->2)-α-D-galactopyranosyl-(1-->3)-α-L-arabinofuranosyl]-4-O-(α-L-arabinofuranosyl)-β-D-galactopyranosyl)-trans-zeatin riboside. Chem. Pharm. Bull., 45, 260–264.

Komgrit I., Suhaimine C. and Sompong T. (2011). Cytokinins and coconut water promoted abnormalities in zygotic embryo culture of oil palm Songklanakarin J. Sci. Technol. 33 (6), 653-657.

Ogatis, R.A. (2015). A Comparative Evaluation of Coconut Water as Radicle Setting Medium for *Rhizopora Stylosa* Hypocotyl Propagation International Journal of Science and Research (IJSR) ISSN (Online): 2319-7064 Index Copernicus Value (2015): 78.96 | Impact Factor (2015): 6.391

Ram H. H. and Singh H. G. (2003) Crop breeding and genetics. Kalyani publication, new Delhi.

Rasmusson D. C. (1985). Barely. Crop science society of America publisher S., Madison.

Rattan, S.I.S.; Clark, B.F.C. Kinetin delays the onset of ageing characteristics in human fibroblasts. *Biochem. Biophys. Res. Commun.* 1994, *201*, 665–672.

Rice, E. L. (1984). Allelopathy, (1st Ed., November 1974 by the same editor) (2nd Ed.), Academic Press, pp. 422 p. ISBN 978-0-12-587058-0

Sandhya V.G., and Rajamohan T. (2008) Comparative evaluation of the hypolipidemic effects of coconut water and lovastatin in rats fed fat-cholesterol enriched diet. Food Chem. Toxicol., 45, 3585–3592.

Santos U., Kubo K., Ota T., Tadokoro T., and Maekawa A. (1996) Nutrient composition of coconuts water (*Cocos nucifera* L.). *Food Chem.*, *57*, 299–304.

Seow C.C., and Gwee C.N. (1997) Coconut milk: Chemistry and technology. Int. J. Food Sci. Tech., 32, 189–201.

Shewry, P. R. (1992) Barley seed storage proteins structure, synthesis, and deposition. In nitrogen metabolism of plant; pilbeam, D. J., Mengel, K., Eds.; Oxford university press; Oxford, Uk; pp 201-227.

United States Department of Agriculture (USDA). *National Nutrient Database for Standard Reference, 2008. Nuts, coconut water* [Online]. Available: http://www.nal.usda.gov/fnic/ foodcomp/cgi-bin/list_nut_edit.pl/, accessed on 9 December 2009.

Vermeulen K., Strnad M., Kryštof V., Havlicek L., Van der Aa A., Lenjou M., Njis G., Rodrigus I., Stockman B., Van Onckelen H., Van Bockstaele D.R., and Berneman Z.N. (2002). Antiproliferative effect of plant cytokinin analogues with an inhibitory activity on cyclindependent kinases. *Leukemia*, *16*, 299–305.

Willis, R. J. (2007). "The History of Allelopathy", Springer: 3, ISBN 1-4020-4092-X, retrieved 2009-08-12.

Wood P. (2007) Cereal B –Glucan in diet and health J. Cereal Sci., 46, 230 -238.

ZANCO Journal of Pure and Applied Sciences
The official scientific journal of Salahaddin University-Erbil
https://zancojournals.su.edu.krd/index.php/JPAS

ISSN (print):2218-0230**, ISSN (online):** 2412-3986**, DOI: http://dx.doi.org/10.21271/zjpas**

RESEARCH PAPER

Multivariate Models for Predicting the Maximal Diameter of the Wetted Area under Surface Drip Irrigation System

Ismael O. I smael[1], Triq H. Karim[2]

[1,2]Department of Soil and Water, College of Agricultural Engineering Science, Salahaddin University-Erbil, Kurdistan Region, Iraq

A B S T R A C T:

Water shortage has been and will continue to be a key global-scale threat to agricultural production. One approach to mitigate the intensity this problem is the efficient use of water and this necessitates introduction of high efficient irrigation systems like drip irrigation. Reliable information about the dimensions of wetted soil under drip irrigation enables designers to find out optimal emitter flow rates and spacing to offer efficient use of irrigation water. Accordingly, the current study was initiated and the main objectives were to predict the ultimate diameter of wetting area under emitters from dripper discharge and other properties of the dominant soils in Erbil plain. To achieve the above objective 24 sites were selected over the indicated plain keeping in mind covering a wide spectrum of soil properties. At each site the soil moisture distribution in horizontal and vertical directions were monitored under three drip discharges of 1.2, 2.5 and 3.5 l hr^{-1} such that each line represented a discharge level. The results indicated that among a host of input variable, emitter discharge, soil clay content and saturated hydraulic conductivity were the most influential factor affecting the maximal diameter of the wetted area (D). A linear and a nonlinear model were also derived for predicting the maximal diameter of the wetted area (D). The mean absolute percentage errors were 10.37 and 8.57 % respectively. Similarly, a linear model was proposed for predicting the wetting depth with a reasonable accuracy. Additionally, the results also confirmed that the model proposed by Schwartzman and Zur, (1986) had poor predictability for estimating D in the area under study.

KEY WORDS: Wetting Pattern, empirical models, Erbil Plain, Drip Spacing.
DOI: http://dx.doi.org/10.21271/ZJPAS.32.4.16
ZJPAS (2020) , 32(4);135-143 .

1.INTRODUCTION

Water scarcity can be considered as a threat to agricultural production on the globe. The water shortage can be mitigated by increasing irrigation efficiency through the adoption of modern technologies, such as drip irrigation, which leads to substantial water savings, releasing the saved water to other uses (Perry et al., 2017).

* **Corresponding Author:**
Ismael O. I smael
E-mail: esmahel_2008@yahoo.com
Article History:
Received: 23/12/2019
Accepted: 27/02/2020
Published: 08/09 /2020

Drip irrigation can be defined as the application of water via point or line source above or under the soil surface at small operating pressure ranging between 0.02 and 0.2 MPa and at discharge rates of 1-30 l hr^{-1}, giving rise to partial of the soil surface (Dasberg and Or, 1999). Information on moisture distribution patterns under point source trickle emitters is a pre-requisite for the design and operation of trickle irrigation systems (Subbauah and Mashru, 2013).

The distance that water spreads horizontally from a drip line and the volume of soil wetted are limiting factors that determine the spacing and number of drip lines and emitters, the frequency of irrigation, and thus the cost of irrigation (Skaggs et al., 2010).

The general objective of drip irrigation system design is to select proper layout and components to achieve suitable distribution of irrigation water throughout the field to meet the crop water requirement and deliver water efficiently (Naglič et al., 2014). Proper design and installation are essential to provide a drip irrigation system that can be managed with minimal inputs and maximum profit (Clark and Smajstrla, 1996). The dimensions of the wetting pattern are imperative in selecting the right spacing between emitters and the suitable distance between laterals (Al-Ogaidi et al., 2016). The spacing between emitters can be determined on the basis of form of wetting pattern and area which is occupied with per emitter (Neshat and Nasiri, 2012). The shape of the wetted soil volume under single drip emitter is affected by a host of factors including soil hydraulic properties, soil structure, soil texture, impermeable layers in the soil profile and anisotropy. (Gärdenäs et al., 2005, Skaggs et al., 2010).

Li et al., (2004) reported that as the time increased, the radius of saturated water entry zone becomes larger and after around 3.5 h approached to a constant size. The ultimate surface saturated wetted radius was reached faster under a higher emitter discharge. Furthermore, the findings of Abu-Awwad et al., (2017) revealed that soil surface wetted area would increase in decreasing rates as application time increased until the application rate became in equilibrium with soil infiltration rate. Roth (1974) elucidated that matric potential is dominant compared to gravitational potential in dry soils. As soil gets wetter, gravitational potential dominates the matric potential. The higher the application rate, the larger is the influence of gravity and, as a result, the smaller will be the wetted area.

Naglič et al., (2014) has shown that a number of models exist for wetting pattern prediction. The proposed models vary from relatively simple to more complex codes. They can be categorized empirical, analytical or numerical models. On the other hand, Alshammary and Salim (2016) demonstrated that several models have been developed to predict wetting front dimensions, which are important for the optimal design of drip irrigation system, using some of the variables such as emitter discharge, water application rate and soil hydraulic properties.

It is commendable to mention that the area under drip irrigation is expanding over the region under study. In this region, a wide spectrum of soils with various properties is existing. Site specific information is required on the wetting pattern and hydraulic properties of these soils. Reliable information about the dimensions of wetted soil under drip irrigation enables designers to find out optimal emitter flow rates and spacing to lessen system equipment cost and offer better soil water conditions for the most efficient use of irrigation water (Malek and Peters, 2010). Unfortunately, there is lack of information on such study in the area under study, therefore the current study was initiated to: 1) develop empirical models for predicting ultimate diameter of the wetting area of the dominant soil in Erbil plain under drip irrigation and 2) evaluate the Schwartzman and Zur (1986) model for predicting the maximum diameter for these soils under drip irrigation.

1. MATERIALS AND METHODS

2.1. Study Sites Description

The selected sites are located within the outskirts of Erbil city, mostly lying at 400 m a.m.s.l. It is bounded approximately by parallels N 36^{o} 00′ 00″ and N 36^{o} 20′ 00″ and meridians E 43^{o} 45′ 00″ and E 44^{o} 15′ 00. The study area experience Mediterranean climate type, being cold and rainy winters and hot and dry summers. Mean annual temperature amounts to about 20 ^{o}C with a maximum in July (44^{o}C) and a minimum in January (5^{o}C). Mean annual precipitation across the study ranges between about 180 and 750 mm distributed over rainy months. It has a unimodal distribution with an average value of about 400 mm. Further, the annual distribution shows a dry season lasting from June to September and a wet season from October to April.

On the basis of aridity index defined as the ratio of mean annual precipitation to potential evapotranspiration, the climate regime can be classified as semiarid (0.2 > AI < 0.5) (Unesco, 1979). There is no mountain vegetation over most of the area, even the smaller woody shrublets have been eradicated by plough, wood cutter and fuel gatherer and most of the palatable perennials have been greatly reduced or eliminated by overgrazing. It includes mostly agricultural and grazinglands, but also residential areas and marginal spots. The spring aspect of the uncultivated lands is luxuriant grasslands dominated by Poa sp and Hordium sp (Guest and Al-Rawi, 1966). According to soil taxonomy Staff (1999), the majority of the soils are categorized as: Fine Loamy, Active, Mixed, Thermic, Typic Chromoxerets. The soil textures are predominantly silty clay loam followed by silt loam and silty clay. Soil reaction is basic and organic matter content is generally low, with values of less than 2%. With no exception, all the existing soils are non-saline and calcareous. The equivalent $CaCO_3$ content ranges from about 20% to more than 40%. There are narrows strips of sandy loam to silt loam or loam along the Tigris tributaries.

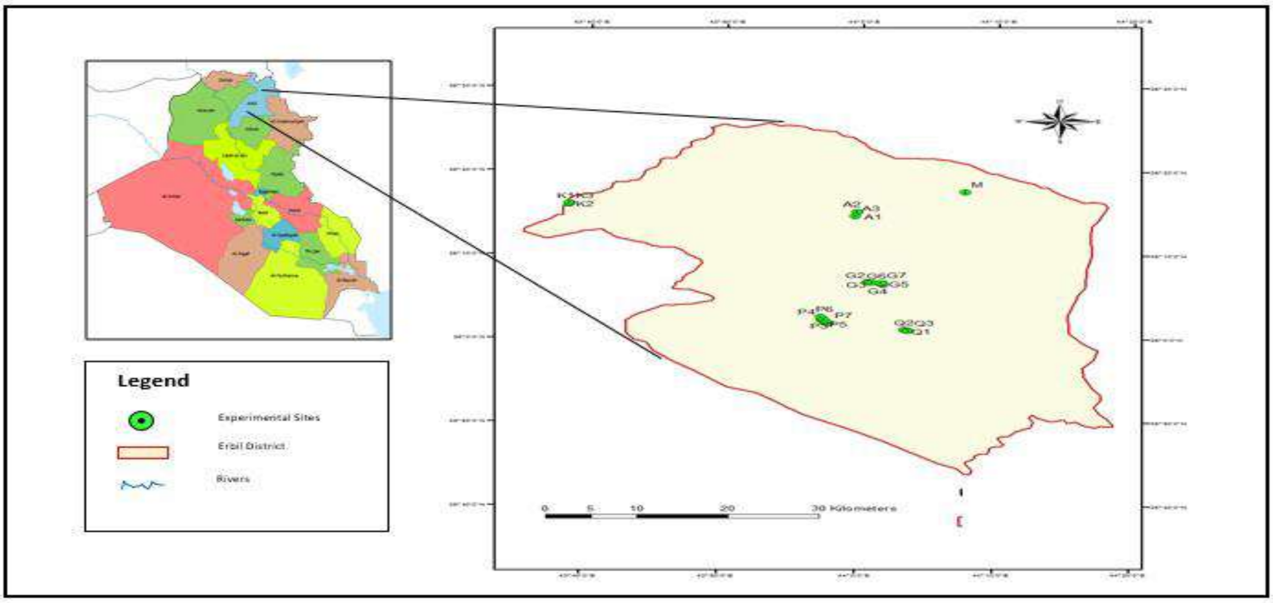

Fig. 1: The location map for the sampling and experimental sites

2.2 Field Tests

Before initiating field tests, several tours were made in the outskirts of Erbil city to select 24 sites to cover a wide spectrum of soil properties. Fig.1 shows the location map for experimental sites.

At each site, a representative bare area with negligible slope was selected. Small obstacles like stones and twigs were removed. Trampling was avoided over the location of measurements. Three laterals were installed at each site and provisions were made to install three emitters at a spacing of 2 m on each lateral. A regulating valve was installed ahead of each lateral to regulate the emitters discharge. The emitters were connected to a portable water reservoir by polyethylene tubes (main and lateral) with diameters 50 and 16 mm, respectively. The water reservoir was a cylindrical metal tank with 1000 L capacity. Three discharge rates of 1.2, 2.5 and 3.5 $l\ hr^{-1}$ were applied such that each line represented a discharge level. The three installed emitters had equal discharges of

(1.2 or 2.5 or 3.5 $l\ hr^{-1}$) and represented a unit or a replicate for a given discharge level. After operation of drip irrigation system until the wetting radius became constant by using a meter scale. The observations were taken until a steady state was reached which took a period in between 24 and 48 hours.

To monitor soil moisture distribution in horizontal and vertical directions, soil samples were also obtained on two orthogonal lines passing through the center of the wetting area at 5 positions on each line and at several depths below each position using a small auger 2 cm in diameter. The obtained samples were oven dried for measuring soil water content.

After termination of the experiment, composite disturbed soil samples were obtained from three depths (0.0-0.20; 0.20–0.4 and 0.4-0.6 m) for performing soil physical and chemical analysis. Three undisturbed soil samples were obtained from each site for measuring insitu soil bulk density by core method as outlined by (Blake and Hartge, 1986). In the meantime infiltration rate was measured at each site by using double infiltrometer according to the method outlined by (Michael, 1978). Additionally, the soil around the emitter was excavated to expose a vertical soil profile, to monitor the water distribution in the vertical direction.

2.3. Soil and Water Analyses

Particle size distribution was carried out by using both hydrometer and sieving methods according to the procedures described by (Klute, 1986). The soil bulk density was measured by core method as outlined by (Blake and Hartge, 1986).

The soil infiltration rate was measured by double ring infiltrometer method as described by (Michael, 1978). Additionally, the well water which was used as the source of irrigation was analyzed for some chemical analysis following standard procedures as outlined by (Richards, 1954) (EC =0.44 dSm^{-1}, pH= 7.51).

3.RESULTS AND DISCUSSION

3.1.General Aspects of the Soil Properties

Table 1 depicts the database of the current study. It compasses particle size distribution, soil hydraulic properties, soil bulk density, maximal diameter of wetted area and wetted depth from 24 sites surrounding Erbil city. It can be noticed from Table 1 that the database covers a wide spectrum of soil properties. For instance the clay content ranged from 4.18% at site to as high as 43.97% at site, with a mean value of 28.44%. On the other hand sand content ranged from as low as 17.7% to as high as 77.39% with an average value of 33.72%. Overall, the soil texture, ranged from loamy sand at Eski-Kalak site to clay at several sites and most of them fell in the clay loam and silty clay loam classes. Additionally, the insitu soil bulk density obtained by core method for the upper 60 cm varied between 1.17 to 1.70 Mgm^{-3} while the saturated hydraulic conductivity ranged from as low as 0.22 cm hr^{-1} to as high as 4.42 cm hr^{-1}.

It is also of note to mention that that among the study variables, the saturated hydraulic conductivity exhibited by the highest spatial variability (CV = 61.07%), followed by sand content (CV = 46.54%) and clay content (CV= 37.55%). The result is in tune in the findings of, who observed that the soil infiltration rate was characterized by a high spatial variability. It can also be noticed the remaining variables were characterized by intermediate or degree of variability.

Based on the obtained values of skewness and kurtosis, it can be that most the study variables are slightly deviated from normal distribution like saturated hydraulic conductivity (Jackson, 1958) and depth of wetting (Z), while the reverse may be true for sand (S), bulk density and the maximal diameter of the wetted area (D).

Table (1) Some statistics of the studied variables during the current study

Variable	Unit	Sample size	Minimum value	Maximum value	Range	Average Value	Standard error	Standard deviation	CV (%)	Skewness	Kurtosis
S	%	24.00	17.70	77.39	59.69	33.72	3.20	15.69	46.54	1.50	1.82
Si	%	24.00	18.42	50.00	31.58	37.83	1.69	8.30	21.93	-0.87	0.79
C	%	24.00	4.18	43.97	39.79	28.44	2.18	10.68	37.55	-0.68	-0.33
Ks	cm3 hr^{-1}	24.00	0.22	4.42	4.20	2.33	0.29	1.42	61.07	0.08	-1.42
BD	Mgm^{-3}	24.00	1.17	1.70	0.73	1.34	0.04	0.17	12.90	1.82	3.86
θi	%	24.00	3.00	12.78	9.78	6.84	0.45	2.20	32.14	1.54	3.17
D	Cm	24.00	47.00	109.00	62.00	60.21	2.52	12.33	20.48	2.84	10.67
Z	Cm	24.00	32.20	45.40	13.20	39.31	0.75	3.69	9.39	0.05	-0.75

3.2. Sensitivity Analysis

Prior to models calibration, a simple sensitivity analysis based on correlation analysis was conducted without considering interaction into account to identify non-influential variables that can be omitted from the calibration. Table 2 presents the correlation matrix using all possible cases procedure. The regressors encompassed sand (S), silt(Si), clay(C), saturated hydraulic conductivity (Jackson, 1958), bulk density (Al-Ogaidi et al., 2016), initial soil water content (θi), the maximal diameter of the wetted area (D), and the wetted depth (Z). As can be noticed in Table 2, the all correlation coefficients among the regressors were far below 0.9. This is indication of the fact the developed models with these variables will not be suffered from multicollinearity.

It also observed that the clay content offered the highest correlation coefficient with wetted diameter (r =0.547) followed by saturated hydraulic conductivity. By contrast, silt content offered the least correlation coefficient followed by initial soil water content further, the results indicated that wetted diameter was negatively correlated with each of Si, C, Ks and θ_i, while it was positively correlated with remaining variables. It was also noticed that the soil bulk density is the most initial factors affecting depth of wetted (Z). It appears from the above analysis that each of discharge, clay content and saturated hydraulic conductivity are the best candidate for predicting wetted diameter of the area under the emitters.

Table (2) Pearson's correlation matrix among the studied variables during the current study.

	S	**Si**	**C**	**Ks**	**BD**	**θi**	**D**	**Z**
S	1	-0.772**	-0.869**	-0.095	0.346	-0.347	0.435*	-0.045
Si		1	0.357	0.058	-0.188	0.121	-0.119	0.266
C			1	0.095	-0.363	0.417*	-0.547**	-0.141
Ks				1	-0.023	0.007	-0.461*	-0.137
BD					1	-0.448*	0.321	-0.473*
θi						1	-0.127	0.059
D							1	0.204
Z								1

**. Correlation is significant at the 0.01 level (2-tailed).
*. Correlation is significant at the 0.05 level (2-tailed).

3.3. Model Calibration

The results shown In Table 3 revealed than among the one-, two-, three-, four- and five-variable models M1, M2, M3, M4 and M5 offered the best performance for predicting wetted diameter (D) following all possible cases regression analysis. The selection was based on the criteria displayed in Table 3. For the sake of clarity, it can be mentioned that among the three-variable models, M3 offered the largest values for R^2, R^2adj and the lowest values of the remaining criteria. As can be noticed in Table 3 there is a steady increase in for R^2, R^2adj values and a steady decrease in Akaike information criterion (AIC) and Amemiya prediction criterion (APC) with an increase in number of regressors.

The results also indicated that there was a slight change in the value of the criteria shown in Table 3 with further increase in number of regressors above three. Additionally, stepwise linear multiple regression revealed the three variable model was based only on Q, C and Ks. On the other hand the Mallows' Cp exhibited no obvious trend.

As the variance inflation factor (VIF) is less than 10 and the tolerance (T) is more than 0.1, it means none of the five models in Table 4 has the problem of multicollinearity. In spite of higher accuracy of prediction of M4 and M5, Model 3 is proposed as a linear model for predicting wetted diameter. This decision was made to avoid the problem of overfitting. This means Model 4 and 5 may perform well for training data (the data used to develop the model), but they may not perform well for any test set out of the training data set.

To further improve the prediction of the maximal diameter of the wetted area, a multiple non-linear model (M6) was also proposed. This non-linear model took the following form:

$$D = a\,Q^b\,C^c\,Ks^d\,BD^e\,\theta_i^{\,f} \qquad (3.1)$$

Where a, b, c, d, e and f are fitting parameters. Table 5 shows the parameters of Model 3, 6 and 7.

Table (3) Results of all possible cases showing the linear models along with the included variables which scored best based on a host selection criteria

Model code	Model name	Variables	R^2	R^2adj	Selection Criteria			
					AIC	APC	MPC	SBC
M1	One –variable	Q	0.328	0.318	381.54	0.711	2.00	386.09
M2	Two-variable	Q, C	0.647	0.636	337.24	0.384	3.00	344.07
M3	Three-variable	Q, C, Ks	0.702	0.688	327.08	0.334	4.00	336.18
M4	Four Variable	Q, C, Ks, BD	0.718	0.701	325.11	0.325	5.00	336.49
M5	Five variable	Q,C, Ks, BD, θ_i	0.729	0.709	324.05	0.320	6.00	337.71

Table (4) Some multicollinearity statistics for the selected variables during the current study.

Model code	Model name	Variables	Tolerance					Variance inflation Factor				
			Q	C	Ks	BD	θ_i	Q	C	Ks	BD	θ_i
M1	One –variable	Q										
M2	Two-variable	Q, C	1.00	1.00				1.00	1.00			
M3	Three-variable	Q, C, Ks	1.00	0.99	0.99			1.00	1.01	1.01		
M4	Four Variable	Q, C, Ks, BD	1.00	0.76	0.99	0.76		1.00	0.76	0.99	0.76	
M5	Five variable	Q, C, Ks ,BD, θ_i	0.99	0.72	0.99	0.67	0.72	1.01	1.40	1.01	1.49	1.38

Table (5) Regression coefficients of the developed linear and nonlinear models for predicting maximal wetted diameter and average wetted depth from emitter discharge and some selected soil properties.

Response variable	Type of Model	Model Code	Constant	Slope or exponent				
				Emitter discharge ($cm^3\ hr^{-1}$)	Clay content (%)	Saturated Hydraulic conductivity, Ks ($cm\ hr^{-1}$)	Bulk Density, BD(Mgm^{-3})	Initial soil moisture content, θ_i(%)
Maximal wetted diameter (cm)	Multiple linear with three variables	M3	79.393	0.01	-0.871	-2.833		
	Multiple non-linear with five variables	M6	8.361	0.313	-0.216	-0.064	0.483	0.177
Average Wetted depth (cm)	Multiple linear with three variables	M7	65.096	0.002	-0.199		-17.248	

3.4. Performance of the Proposed Models

It is apparent from the above results, a linear model (Model 3) and a non- linear model (Model 6) were proposed for predicting the maximal wetted diameter under drip irrigation. Additionally, a three –variable model (M7) was proposed for predicting the depth of wetting with reasonable accuracy. The influential variables of this model are emitter discharge, clay content and bulk density.

To further investigate the degree of agreement between the observed and predicted values, the predicted values from each of M3, M6 were plotted versus the observed values of the maximal diameter of the wetted area in relation to line 1:1 (Figs. 2 and 3) As can be seen from Fig. 2 and 3 that the majority of the plotted points falls on or close to the line 1:1. It can also be noticed from Fig.2 that the slope of the regression line is close to unity. Overall, there is limited data scattering over the lower and intermediate ranges of the diameter of the wetted area.

Conversely, there is a wider scatter at the upper D value ranges. Similar trend was obtained for predicting the average depth of infiltrated water as the predicted values were plotted versus the measured values (Fig.4). Additionally, the plot of residuals of predicted D from M3 and M6 indicated that the employed data were normally distributed (Figs. 5 and 6). The same conclusion was drawn as the residual of the predicted Z values were plotted versus the observed Z values (Fig.7).

Table 6 enlists some selected efficiency criteria for evaluating the last three models. Judging from Values of mean biased error (MBE) and coefficient of residual mass (CRM), each of these models neither overpredicted nor underpredicted D and Z. It can be also observed that the mean absolute error (MAE) of prediction were 7.44, 6.12 and 2.41 for model M3, M6 and M7 respectively. Based on CV, the simulation of M3 and M6 is considered good (10% < CV < 20%), while that for Model 7 is excellent (CV < 10%). The closeness of the Willmott's index (d) suggests these models calibrated well enough to simulate D and Z.

Judging from the mean absolute percentage error (MAPE) and scheme proposed by (Lewis, 2012), M3 was categorized under potentially good class (10 %< MAPE<20%), while M6 and M7 were categorized under very potentially good class (MAPE<10%) according to the above mentioned scheme.

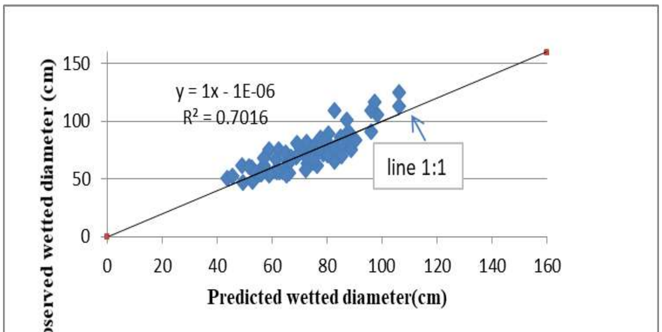

Fig.2 Plot of predicted wetted diameter from Model 3 versus observed values

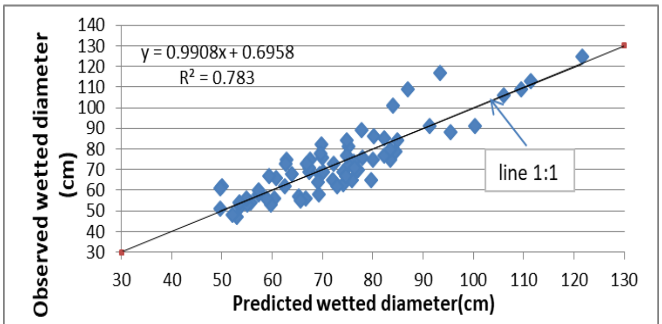

Fig. 3 Plot of predicted wetted diameter from Model 6 versus observed values

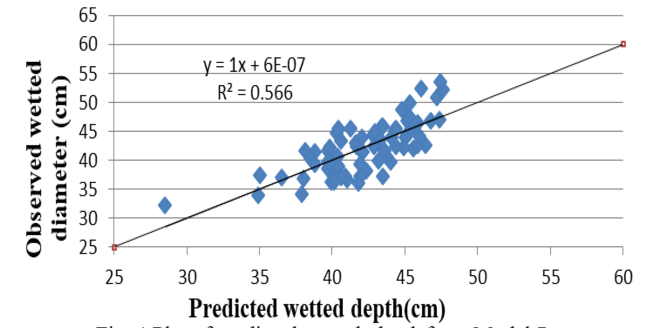

Fig. 4 Plot of predicted wetted depth from Model 7 versus observed values

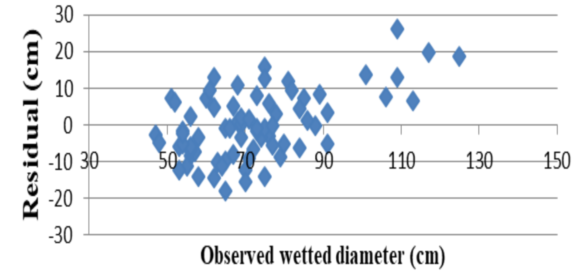

Fig.5. Plot of error prediction of wetted diameter from Model 3 versus observed values

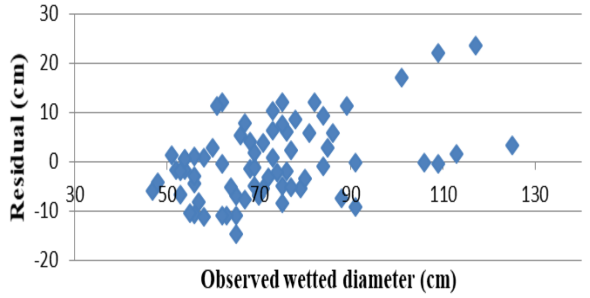

Fig.6. Plot of error prediction of wetted diameter from Model 6 versus observed values

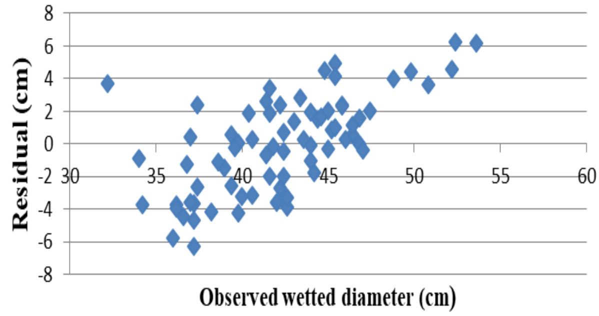

Fig.7. Plot of error prediction of wetted depth from Model 7 versus observed values

3.5. Evaluation of the Maximal Diameter of the Wetted Area from Schwartzman and Zur (1996) Model

Another trial was also made to evaluate the model proposed by (Schwartzman and Zur, 1986) to predict D from emitter discharge, wetting depth and saturated hydraulic conductivity

$$D = 1.32\left(\frac{QZ}{Ks}\right)^{0.33} \qquad (3.2)$$

Where Q= the emitter discharge ($cm^3\ hr^{-1}$), Z= wetting depth (cm) and Ks= saturated hydraulic conductivity ($cm\ hr^{-1}$).

hydraulic conductivity ($cm\ hr^{-1}$).

The results present in Fig.8 indicated that the three variables (Q, Z and Ks) explained only 40% of variation in D. There is a wide scatter of the points over the entire range of the observed D values. The mean absolute percentage of error exceeds 30%. This means this model has limited application for predicting D. It was reported that the regression models have usually restricted application outside the region where they were developed without testing their performance (Hernando and Romana, 2015). Accordingly, the two developed models (M3 and M6) are recommended for use in the area under study.

These models will be beneficial for predicting the maximal diameter of wetted area in actual practice for designing emitter spacing. This can be achieved by multiplying this parameter by a factor of 0.8 to obtain the emitter spacing (Hachem and Yaseen, 1992).

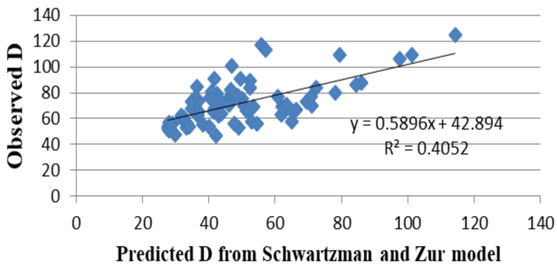

Fig. 8 Plot of observed maximal diameter of wetted area versus the predicted values from Schwartzman and Zur model.

3. CONCLUSIONS

It can be concluded from the above results that emitter discharge, clay content and saturated hydraulic conductivity are the most influential factors affecting the maximal diameter of wetted area under drip irrigation system. Furthermore, this parameter can be predicted by using linear models and its accuracy can be improved by using a non-linear model with six parameters.

These results are of vital importance in design of emitter spacing under drip irrigation. Additionally, it can be inferred from the results the maximal diameter of the wetted area cannot be predicted from Schwartzman and Zur (1986) model with a reasonable accuracy in the area under study.

References

ABU-AWWAD, A. M., AL-BAKRI, J. T. & ALFAWWAZ, M. M. 2017. Soil Surface Wetting Pattern under

Trickle Source in Arid Lands: Badia Regions. *Jordan Journal of Agricultural Sciences,* 405**,** 1-11.

AL-OGAIDI, A. A., WAYAYOK, A., ROWSHON, M. & ABDULLAH, A. F. 2016. Wetting patterns estimation under drip irrigation systems using an enhanced empirical model. *Agricultural Water Management,* 176**,** 203-213.

ALSHAMMARY, A. A. & SALIM, S. B. 2016. Measured and Predicted Wetting Patterns under Subsurface Drip Irrigation. *International Journal of Science and Engineering Investigations* 5**,** 169-176.

BLAKE, G. R. & HARTGE, K. 1986. Bulk density 1. *Methods of soil analysis: part 1—physical and mineralogical methods***,** 363-375.

CLARK, G. A. & SMAJSTRLA, A. G. 1996. Design considerations for vegetable crop drip irrigation systems. *HortTechnology,* 6**,** 155-159.

DASBERG, S. & OR, D. 1999. Practical Applications of Drip Irrigation. *Drip Irrigation.* Springer.

GÄRDENÄS, A., HOPMANS, J., HANSON, B. & ŠIMŮNEK, J. 2005. Two-dimensional modeling of nitrate leaching for various fertigation scenarios under micro-irrigation. *Agricultural water management,* 74**,** 219-242.

GUEST, E. & AL-RAWI, A. 1966. *Introduction to the Flora [of Iraq]: An Account of the Geology, Soils, Climate and Ecology of Iraq with Gazetteer, Glossary and Bibliography*, Ministry of Agriculture of the Republic of Iraq.

HACHEM, A. & YASEEN, H. 1992. Engineering of Field Irrigation Systems. *Dar Alkutub for printing and publishing. Mosul/Iraq. pp***,** 1-483.

HERNANDO, D. & ROMANA, M. G. 2015. Estimating the rainfall erosivity factor from monthly precipitation data in the Madrid Region (Spain). *Journal of Hydrology and Hydromechanics,* 63**,** 55-62.

JACKSON, M. 1958. Soil chemical analysis prentice Hall. *Inc., Englewood Cliffs, NJ,* 498.

KLUTE, A. 1986. Methods of Soil Analysis. Part 1 2nd ed. American Society of Agronomy. *Inc. Publishes, Madison, Wisconsin, USA*.

LEWIS, C. 2012. *Demand forecasting and inventory control,* WoodHead Publishing Limited., Routledge.

LI, J., ZHANG, J. & RAO, M. 2004. Wetting patterns and nitrogen distributions as affected by fertigation strategies from a surface point source. *Agricultural Water Management,* 67**,** 89-104.

MALEK, K. & PETERS, R. T. 2010. Wetting pattern models for drip irrigation: new empirical model. *Journal of Irrigation and Drainage Engineering,* 137**,** 530-536.

MICHAEL, A. M. 1978. Irrigation thepry and practice. *Vikas Press Pvt.Ltd*.

NAGLIČ, B., KECHAVARZI, C., COULON, F. & PINTAR, M. 2014. Numerical investigation of the influence of texture, surface drip emitter discharge rate and initial soil moisture condition on wetting pattern size. *Irrigation science,* 32**,** 421-436.

NESHAT, A. & NASIRI, S. 2012. Finding the optimized distance of emitters in the drip irrigation in loam-sandy soil in the Ghaeme Abad plain of Kerman, Iran. *Middle East Journal of Scientific Research,* 11**,** 426-434.

PERRY, C., STEDUTO, P. & KARAJEH, F. 2017. DOES IMPROVED IRRIGATION TECHNOLOGY SAVE WATER? : A review of the evidence. Food and Agriculture Organization of the United Nations, Cairo

RICHARDS, L. A. 1954. *Diagnosis and improvement of saline and alkali soils*, LWW.

ROTH, R. 1974. Soil moisture distribution and wetting pattern from a point source. *Proc. Second Inter'1. Drip Irrig. Cong., San Diego, CA, 1974*.

SCHWARTZMAN, M. & ZUR, B. 1986. Emitter spacing and geometry of wetted soil volume. *Journal of Irrigation and Drainage Engineering,* 112**,** 242-253.

SKAGGS, T. H., TROUT, T. J. & ROTHFUSS, Y. 2010. Drip irrigation water distribution patterns: effects of emitter rate, pulsing, and antecedent water. *Soil Science Society of America Journal,* 74**,** 1886-1896.

STAFF, S. S. 1999. Soil Survey Staff 1999, Soil Taxonomy: A basic system of soil classification for making and interpreting soil surveys, Agricultural Handbook 436, Natural Resources Conservation Service, USDA, Washington DC, USA, pp. 869. *Soil Use and management,* 17**,** 57-60.

SUBBAUAH, R. & MASHRU, H. H. 2013. Modeling for predicting soil wetting radius under point source surface trickle irrigation. *Agricultural Engineering International: CIGR Journal,* 15**,** 1-10.

UNESCO 1979. *Map of the world distribution of arid regions: explanatory note*, Unesco.

.

ZANCO Journal of Pure and Applied Sciences
The official scientific journal of Salahaddin University-Erbil
https://zancojournals.su.edu.krd/index.php/JPAS

ISSN (print):2218-0230, **ISSN (online):** 2412-3986, **DOI:** **http://dx.doi.org/10.21271/zjpas**

RESEARCH PAPER

Impact of Ascorbic acid and Potassium on Okra (*Abelmoschus esculentus*) Growth in Saline Condition

Sakar A. Saheed , Halala R. Qader

Department of Environmental science, College of Science, Salahaddin University-Erbil, Kurdistan Region, Iraq.

A B S T R A C T:

Salinity regards as one of the abiotic stress factors affect that effect the growth and development of the plant. In present investigation the combination effect of ascorbic acid and potassium has been studies on okra growth under salt stress condition. The study conducted in factorial experiment of three replications in Completely Randomized Designed replicated three times. Three levels of potassium (K) (0,200, 400 ppm) applied to the soil. Three levels of foliar application of ascorbic acid (ASA) (0, 100, 200ppm). Irrigated with three levels of NaCl (0,100,200 µS). Parameters were recorded plant height (cm), number of leaves per plant, leaf area (cm^2), water content (%), chlorophyll content, protein and proline content of leaves, mineral content; nitrogen, phosphorus, calcium, potassium, and sodium. The results elucidate that combination impact of ascorbic acid and potassium significantly the tolerance of okra plant to salinity due to an increase in height of plant, number of leaves, shoot water content, protein and proline content of leaves, and mineral contents such as nitrogen and sodium content of leaves under salt stress conditions.

KEY WORDS: Potassium; Ascorbic acid; Okra; Salt stress;
DOI: http://dx.doi.org/10.21271/ZJPAS.32.4.17
ZJPAS (2020) , 32(4);144-150 .

1. INTRODUCTION

Okra *Abelmoschus esculentus* is a herbaceous annual tall, warming season vegetables grows in all types of soil, known as lady's fingers in many countries (Singh *et al.*, 2014).Okra plant belong to malvaceae family, it's a large family many important plant belong to it. It's planting as a crop in late spring this crop takes three to four months to complete its cycle, needs well drained soil, used as fresh fruit vegetables (Tong, 2016). Okra plant is important economical vegetable known in the world, its seeds the main source of protein and oil, and use in production of oil (Gemede *et al.*, 2015).

* **Corresponding Author:**
Halalal R. Qader
E-mail: halala.qader@su.edu.krd
Article History:
Received: 23/12/2019
Accepted: 01/03/2020
Published: 08/09 /2020

Its fibrous fruit contains white seeds, which grow in warm weather and tolerant drought soil. Okra is the main source of vitamins A, B, C, minerals such as potassium, calcium, fiber, protein, carbohydrates, as well as low in cholesterol, fats and sodium chloride (Singh, 2014) (Tiwari and Ahmad, 2018).

Potassium is one the main important nutrients for plant growth beside nitrogen (Kumar *et al.*, 2006). It's play an important role in many physiological and biochemical roles in plant like; potassium increased protein production, photosynthesis, chlorophyll synthesis, formation of carbohydrates, transfer of energy, movement of stomata, resistance to stress, transport of nutrition in plant, its important in production of (ATP), and activating of several enzymes in plant processes (

Mathiyazhagan, 2015). Potassium survives the plants against salt stress, the deficient potassium level in soil led to decrease the photosynthetic process rate.(Wang *et al*, 2013). (Alrawi and Aljumail, 2018) showed that foliar application of Potassium increased plant height, leaves area. plant^{-1}, chlorophyll content and final yield. (Al.meida *et al.*, 2015) reported that potassium increased number of leaves, height and grain yields.

Ascorbic acid (Vitamin C) is one of the main antioxidant in plant; regulate many physiological processes, surviving environmental stress, controlling growth and development, (Hossain *et al.,* 2018); growth of cell wall and expansion of cell, transport function and production of other plant hormones like ethylene Pre-treatments of plants with ascorbic acid increased significantly height of plant, leaves number, and branches number, stem diameter, shoot fresh and dry weight (Aboohanah, 2016). (Al- Atrushy and Abdul-qader, 2016) showed that Ascorbic acid increased significantly all vegetative characters like leaf area dry weight of leaves, fresh weight, and also (Rashid, 2018) showed that ascorbic acid significantly increased yield in different cultivars of *Vicia faba* plants. Ascorbic acid used in pharmaceutical industry which added as antioxidants to juices and foods (Qader *et al.*, 2019).

Salt stress is a biotic stress condition due to accumulation high level of salt in soil it make difficult to plant to absorb water, and other ions which destroy the balance of water (Wang *et al.*, 2013). Salt stress due to inhibition of important nutrients like potassium which decrease germination of seed, length of shoot and root (Mittal *et al.*, 2018). As well as it effect on plant growth and development, which effect on photosynthesis, water relations, synthesis of proteins (Parida and Das, 2005). The harsh effect of salinity on plant growth makes increasing the okra tolerance to salt stress through applying potassium as soil fertilizer and ascorbic acid to the leaves an important objective of the study.

2. MATERIALS AND METHODS

2.1. Preparation of soil

Twenty seven plastic pots each pot with a diameter of 24 cm in length and 21 cm in depth, each pot loaded up with 7kg of sandy loam dried soil, the soil sieved through 2mm pore size sieves. Some physical and chemical properties of the soil were estimated (table 1). Three seeds of Okra (variety Clemson which take from college of agriculture) were sown in each pot and afterward thinned to one plant later. Fertilizers at the rate of 10kg.donm^{-1} which included urea containing %45 N, super phosphate P_2O_5 containing 45% P, added to the pots as solutions (Muhummed, 2004). Three levels of potassium(K0,K2,K3); 0,200,400 ppm applied to the soil. Three levels of foliar application of ascorbic acid (ASA0, ASA1 and ASA2); 0,100,200 ppm. Irrigated with three levels of salt (NaCl0, NaCl 1, NaCl 2);0,100,200 µS, this study done during April 20, 2019 to July 23, 2019.

Table 1: Some physical and chemical properties of the soil

Properties	value
Sand	70.10 %
Silt	24.22 %
Clay	5.68 %
Soil texture (sieve method) (Kapur and Govil, 2004)	Sandy loam
Soil moisture (Manual method) (Kapur and Govil, 2004)	3.1 %
Organic matter(Walkley and Blacks rapid titration method) (Kapur and Govil, 2004)	0.91 %
PH	7.24
$CaCO_3$ (Trimetric method)	25.7%
Electrical conductivity (ds m^{-1} at 25°C)	0.58
Total nitrogen % (kjeldahl method)	400ppm

Total phosphorus ppm(Olsen method)	118 ppm
Total potassium ppm (flame photometer)	45 ppm
Total calcium ppm (atomic absorption method)	240 ppm

2.2. Experimental parameters

2.2.1. Growth parameters

Plant height(cm).plant^{-1}, leaves number.plant^{-1}, shoot dry weight plant^{-1}, shoot water content (g.plant^{-1}): fresh weight of shoot system dried at 110 °C for 1 hours and afterward dried at 70 °C for 24 hours, in an oven. Dry weight of shoot system obtained for thirty minutes after cooled at room temperature (He et al., 2005).

2.2.2. Biochemical characters of leaves

2.2.2.1. Chlorophyll content

Chlorophyll content in leaves was estimated by chlorophyll meter by clipping the sensor on different locations on leaf surface except the veins (Padilla *et al.*, 2015).

2.2.2.2. Proline content of leaves (µg.g^{-1} fresh weight)

Proline was estimated according to the method as described by (Bates et *al.*, 1973 and Hassan, 2011)**.**

2.2.2.3. Mineral content of leaves

The total nitrogen (mg.g $^{-1}$) in dry weight of leaves was determined by kejeldahl method as described by A.O.A.C, (2010). The total phosphorus (mg.g $^{-1}$) was estimated, using spectrophotometer method as portrayed by Ryan *et al.*, (2001). The total potassium and sodium are determined by flame photometer methods as investigated by Allen (1974).

2.3. Statistical Analysis

The study conducted in factorial experiment of three treatments in complete randomized design replicated three times. Three levels pf potassium; 0,200,400 ppm applied to the soil. Three levels of foliar application of ascorbic acid; 0,100,200 ppm. Irrigated with three levels of NaCl; 0,100,200 µS. All the data were statistically analyzed using Statistical Package for Social Sciences (SPSS version 16 software). For comparison of treatment means at 5% for green house parameters and 1% levels for laboratory parameters using Duncan multiple range test (Al-Rawi and Khalafulla, 1980).

3. RESULTS AND DISCUSSION

3.1. Growth characters

Table (2) shows that soil application of potassium and foliar application of ascorbic acid under salt stress significantly ($p \leq 0.05$) increased height of plant at treatment (K_1 ASA_1 $NaCl_1$) its value (19.16) after 15 days from application, and also increased significantly number of leaves at treatment (K_2 ASA_2 $NaCl_2$) its value (2.66) after 15 days from application and at treatment (K_2 ASA_1 $NaCl_1$) its value (4.66) after 45 days from application as compared with controls (Table 3). Interaction effect of potassium and ascorbic acid significantly increased water content of shoot system at treatment (K_2 ASA_2NaCl_2) its value (3.90) as compared with their control (Figure 1). As well as there were significant difference between treatments. The results partially agreed with obtained by (Alrawi and Aljumail, 2018) and (Raza *et al*, 2013), that potassium and ascorbic acid increased vegetative growth under salt stress, and also found that ASA increased plant height, number of leaves, leaf area in okra plant under salt stress condition. Potassium responsible to cell elongation and cell division due to producing pressure in cells, accumulation of potassium in cells make osmotic stress in cells which increased plant production (Mengel and Kirkby, 2001). (Almeida *et al.*, 2015) found potassium increased the number of leaves that potassium increased transportation of nutrients, increasing photosynthesis, and also its role influence in hormonal balance in plants like axuin. ASA have roles in more processes like cell elongation, photosynthesis, resistance to environmental stresses such as salt stress .The negative and positive influence of salinity of plants rely on numerous factors like concentration, types, span of salinity and types of plants (Abdelgawad *et al.*, 2019). ASA have a good role in plant metabolism and stresses of plant (El- Bassiouny and Sadak, 2015). (Mittal *et al.*, 2018) showed that salinity because of the aggregation of ions Na^+, Cl^- which caused inhibition of uptake of main nutrients such K^+, application of ASA significantly increased plant growth, due to increasing cell division in apical meristem.

Table 2: Interaction effects of potassium (K) and Ascorbic acid (ASA) on plant height at different growth stages under saline condition

Treatment combinations	Plant height (cm) at different growth stages			
K ASA NaCl	**15 days**	**30 days**	**45 days**	**60 days**
K_0 ASA_0 $NaCl_0$	14.93 b	16.66 a	19.33a	23.96 a
K_0 ASA_1 $NaCl_1$	16.56 b	17.50 a	20.50 a	26.93 a
K_0 ASA_2 $NaCl_2$	18.50 ab	19.66 a	21.00 a	24.50 a
K_1 ASA_0 $NaCl_0$	18.16 b	20.66 a	23.00 a	25.36 a
K_1 ASA_1 $NaCl_1$	19.16 a	20.00 a	24.00 a	28.00 a
K_1 ASA_2 $NaCl_2$	18.66 ab	20.50 a	23.00 a	27.23 a
K_2 ASA_0 $NaCl_0$	16.83 b	17.93 a	20.33 a	24.45 a
K_2 ASA_1 $NaCl_1$	16.45ab	18.83 a	23.50 a	26.66 a
K_2 ASA_2 $NaCl_2$	16.50 ab	19.00 a	21.00 a	25.50 a

*Data presented as mean, the same letters mean not significantly different, while the different letters mean significant differences $p \leq 0.05$

Table 3: Interaction effects of potassium (K) and Ascorbic acid (ASA) on leaves number plant^{-1} at different growth stages under saline condition

Treatment combinations	Leaves number plant^{-1} at different growth stages			
K ASA NaCl	**15 days**	**30 days**	**45 days**	**60 days**
K_0 ASA_0 $NaCl_0$	2.00 b	2.33 a	3.33 ab	3.66 a
K_0 ASA_1 $NaCl_1$	2.00 b	2.33 a	3.66 ab	4.00 a
K_0 ASA_2 $NaCl_2$	2.33 b	2.66 a	3.33 ab	3.33 a
K_1 ASA_0 $NaCl_0$	2.33 ab	3.00 a	4.00 ab	4.00 a
K_1 ASA_1 $NaCl_1$	2.00 b	3.00 a	4.33 ab	4.66 a
K_1 ASA_2 $NaCl_2$	2.00 b	2.66 a	3.33 ab	4.00 a
K_2 ASA_0 $NaCl_0$	2.00 b	2.66 a	3.00 b	5.00 a
K_2 ASA_1 $NaCl_1$	2.00 ab	3.33 a	4.66 a	4.33 a
K_2 ASA_2 $NaCl_2$	2.66 a	2.66 a	4.33 ab	5.00 a

*Data presented as mean, the same letters mean not significantly different, while the different letters mean significant differences $p \leq 0.05$

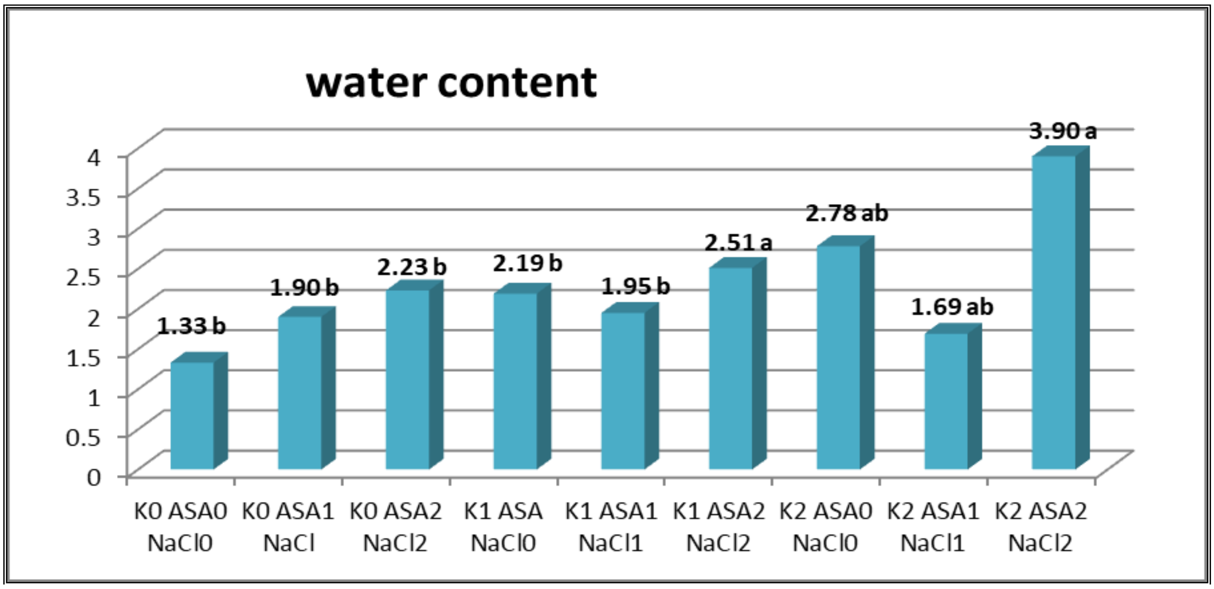

Figure 1: Interaction effects of potassium (K) and Ascorbic acid (ASA) on water content of shoot system at different growth stage under saline condition

*Data presented as mean, the same letters mean not significantly different, while the different letters mean significant differences $p \leq 0.05$

3.2. Biochemical characters

Interaction effect of potassium and foliar application of ascorbic acid increased protein content of leaves at (K_1 ASA_0 NaCl), (K_1 ASA_1 $NaCl_1$), (K_2 ASA_0 $NaCl_0$) as compared with controls, and proline content of leaves at (K_1 ASA_2 $NaCl_2$) under salt stress (table 4). Combination impact of ascorbic acid and potassium significantly ($p \leq 0.01$) increased mineral nutrients such as nitrogen at treatments (K_1 ASA_0 $NaCl_0$), (K_1 ASA_1 $NaCl_1$), and sodium content at treatment (K_2 ASA_2 $NaCl_2$) as compared with control (K_0 ASA_0 $NaCl_0$) (table 5). (Rani and Jose, 2009) reported that potassium application to okra plant significantly increased protein and nutrient uptakes such as nitrogen, phosphorus, potassium. Aboohanah (2016) mentioned that ascorbic acid increased significantly the total chlorophyll and total soluble carbohydrates, ASA provide protect cell, and cell differentiation as well as have many important function in plants antioxidant defense, regulation of photosynthesis, affected in nutritional cycle in higher plants. (Hussein and Kumar, 2014) indicated that interaction effect ascorbic acid as foliar application and salinity stress increased significantly all parameters of growth by their effects on cell division, cell enlargement in millet plant.

Table 4: Interaction effects of potassium (K) and Ascorbic acid (ASA) on chlorophyll, protein, proline content at different growth stage under saline condition

Interaction treatments K ASA NaCl	Chlorophyll at leaf sensor (chlorophyll meter)	Protein (%)	Proline($\mu g.g^{-1}$ fresh weight)
K_0 ASA_0 $NaCl_0$	32.70 ^{a}	31.11 ^{a}	8.47 ^{b}
K_0 ASA_1 $NaCl_1$	35.60 ^{a}	46.66 ^{abc}	11.52 ^{b}
$K_0$$ASA_2$ $NaCl_2$	35.90 ^{a}	29.16 ^{b}	16.10 ^{b}
K_1 ASA_0 $NaCl_0$	34.76 ^{a}	81.66 ^{ab}	11.69 ^{b}
K_1 ASA_1 $NaCl_1$	33.86 ^{a}	93.33 ^{a}	17.45 ^{ab}

$K_1ASA_2NaCl_2$	34.30 ^{a}	70.70 ^{abc}	22.30 ^{a}
K_2ASA_0 $NaCl_0$	37.30 ^{a}	32.33 ^{a}	10.16 ^{b}
K_2ASA_1 $NaCl_1$	38.2 ^{a}	70.74 ^{abc}	8.13 ^{b}
K_2ASA_2 $NaCl_2$	34.96 ^{a}	40.83 ^{bc}	15.88 ^{b}

*Data presented as mean, the same letters mean not significantly different, while the different letters mean significant differences p≤0.01

Table 5: Interaction effects of potassium (K) and Ascorbic acid (ASA) on some mineral content in leaves at different growth stage under saline condition

Treatment combination	Mineral contents ($mg.g^{-1}$)			
K ASA NaCl	**Nitrogen**	**Phosphorus**	**Potassium**	**Sodium**
K_0 ASA_0 $NaCl_0$	3.11 ^{c}	7.13 ^{a}	17.00 ^{ab}	10.29 ^{ab}
K_0 ASA_1 $NaCl_1$	4.66 ^{c}	8.11 ^{a}	19.66 ^{ab}	12.34 ^{a}
K_0ASA_2 $NaCl_2$	2.91 ^{c}	8.60 ^{a}	16.16 ^{b}	9.53 ^{b}
K_1 ASA_0 $NaCl_0$	8.16 ^{ab}	7.67 ^{a}	16.66 ^{b}	9.15 ^{b}
K_1 ASA_1 $NaCl_1$	9.33 ^{a}	8.38 ^{a}	20.50 ^{ab}	11.65 ^{b}
$K_1ASA_2NaCl_2$	7.04 ^{abc}	8.22 ^{a}	18.83 ^{ab}	10.59 ^{ab}
K_2ASA_0 $NaCl_0$	2.33 ^{c}	7.78 ^{a}	19.16 ^{ab}	12.03 ^{a}
K_2ASA_1 $NaCl_1$	7.45 ^{abc}	8.61 ^{a}	22.83 ^{a}	10.52 ^{ab}
K_2ASA_2 $NaCl_2$	4.08 ^{bc}	8.45 ^{a}	18.33 ^{ab}	14.38 ^{a}

*Data presented as mean, the same letters mean not significantly different while the different letters mean significant differences p≤0.01

4. CONCLUSIONS

The combination of soil application of potassium and foliar application of ascorbic acid has a powerful potential to increase the okra tolerance to salt stress.

5. RECOMMENDATIONS

Conducting more studies regarding ascorbic acid to improve the growth and yield components of okra and other plants, as well as further experiments could be carried under field condition to examine the positive effect of ascorbic acid and potassium on plants. More studies are suggested for alleviating negative effects of salt stress by positive effect of ascorbic acid.

REFERENCES

A.O.A.C., (2010). Determination of total nitrogen in waste water by steam distillation. Published by Association Official Agriculture Chemists, Washington, D.C., USA.

Abdelgawad, K.F.; M. M. El-Mogy; Mo I. A. Mohamed; C. Garchery and R. G. Stevens (2019). Increasing Ascorbic Acid Content and Salinity Tolerance of Cherry Tomato Plants by Suppressed Expression of the Ascorbate Oxidase Gene. Journal Agronomy. 51(9), Pp1-14.

Aboohanah, M. A. (2016). The Effect of Spraying Ascorbic and Humic acid on Growth Parameters and Yield of Okra Plant (*Abelmoschus esculentus* L . Moench.). Al-Kufa University Journal for Biology.Pp 59-68.

Al- Atrushy, S. M. M. and S. M. Abdul-Qader. (2016). Effect of potassium and ascorbic acid on growth, yield and quality of olive cv, Khadrawi. The Iraqi Journal of Agricultural Sciences – 74(6):1556-1561, 6106.

Allen, S.E. (1974). Chemical Analysis of Ecological Materials. Black well Scientific Publication Osney Mead, Oxford, 565 p.

Almeida, H.J.; M.A. Pancelli; R.M. Prado; V.S. Cavalcante; F.J.R. Cruz. (2015). Effect of potassium on nutritional status and prof peanuts in succession with sugarcane. Journal of soil science and plant nutrition. Pp1-10.

Hossain, M. A.; S. M. Bosch; P. D. Vivancos; D. Burritt. (2018). Ascorbic acid in plant growth , development, stress tolerance. Research gate.

Al-Rawi, K.M. and A.A.M. Khalafulla. (1980). Design and Analysis of Agriculture Experiments. Univ. Of Mousl. Ministry of Higher Education and Scientific Research. Mousl. Iraq. Pp488. (In Arabic).

Al-rawi, M.M. A and M.A.L. Al-jumail. (2018). Effect of foliar application with potassium and Zinc on growth, pod yield, and seed production of okra.Iraqi journal of Agricultural sciences. 49(6). 1041-1048.

Anderson. C. Home Gardening Series Okra, Agriculture and Natural Resources.

Bates, L.S.; R.P. Waldren and D. Teare. (1973). Rapid determination of free proline for water-stress studies. Plant and Soil, 39:205-207.

El-Bassiouny, H and M.SH. Sadak. (2015). Impact of foliar application of ascorbic acid and α-Tocopherol on antioxidant activity and some biochemical aspects of flax cultivars under salinity stress. Acta Biologica Colombiana, 20(2), Pp 2019-222.

Gemede, H. F. ; N. Ratta ; G. D. Haki ;A. Z. Woldegiorgis and F. Beyene. (2015). Nutritional Quality and Health Benefits of Okra (*Abelmoschus esculentus*): A Review. Journal of food. Processing and Technology. Pp6-6.

He, Y.; Y. Liu; W. Cao; M. Huai; B. Xu and B. Huang. (2005). Effect of salicylic acid on heat tolerance associated with antioxidant metabolism in Kentucky bluegrass. Am. Crop Sci. Soci., 45:988-995.

Hussein, M. M. M. and A. A. Kumar. (2014). Effects of Zinc and Ascorbic Acid Application on the Growth and Photosynthetic Pigments of Millet Plants Grown under Different Salinity. Agricultural Sciences. 05(13), 1253-1260.

Kapur, P. and S.R. Govil. (2004). Experimental plant ecology. New Delhi, india.

Kumar, A. R.; N. Kumar; M. Kavino. (2006). Role of potassium in fruit crops. (Areview). Research gate. Vol. 27, No. 4, pp 283-291.

Mathiyazhagan, K.(2015). Effect of different forms of potassium on growth and yield and fruit quality of wheat. Research gate.

Mengel. K. and E. A. Kirkby. 2001. Principles of Plant Nutrition, 5th ed. pp: 849.

Mittal, N.; S. Thakur; H. Verma and A. Kaur. (2018). Interactive effect of salinity and ascorbic acid on Brassica rapa L. plants. Global journal of bio-scinece and biotechnology.Pp, 27-29.

Muhummed, M.Q. (2004). Effect of zinc and its interaction with two auxins (IAA&NAA) on the growth and development of Pea (*Pisum sativum* L.) Var. Little Marvel. M. Sc. Thesis, College of Education, University of Salahaddin, Erbil. Iraq.

Padilla, F. M., Peña-Fleitas, M. T., Gallardo, M., and Thompson, R. B. (2015). Threshold values of canopy reflectance indices and chlorophyll meter readings for optimal nitrogen nutrition of tomato. Ann. Appl. Biol. 166, 271–285.

Parida A.K. and A.B. Das. (2005). Salt tolerance and salinity effects on plants: A review. Ecotox. Environ. Safe.; 60:324–349.

Qader, H. A.; N. A. Fakhre; S. B. Dikran and H. H. Hamad. (2019). Simultaneous Determination of Gallic Acid and Ascorbic Acid Using First Derivative Zero - Crossing Spectrophotometric Technique. Zanko journal of pure and applied sciences, 31(s4); 60-65.

Rani, B. and A.I. Jose.(2009). Studies on the dynamics of potassium and magnesium in okra (*Abelmoschus esculentus* Moench.). International Plant Nutrition Collaqium XVI. Pp, 1-7.

Rashid, S.M.S. (2018). Effect of Salicylic and Ascorbic acid on Growth, Green yield of two Broad bean Cultivars (*Vicia faba* L.). Zanko journal of pure and applied sciences, 30(5); 71-88.

Raza, S.H.; F. Shafiq; M. Chaudhary; I. Khan. (2013). Seed Invigoration with Water, Ascorbic and Salicylic Acid Stimulates Development and Biochemical Characters of Okra (*Ablemoschus esculentus*) under Normal and Saline Conditions. International Journal of Agriculture and Biology 15(3):486–492.

Ryan, J.; G. Estefon and A. Rashid. (2001). Soil and plant analysis Labrotory Manual, 2ndedition. National Agriculture Research Center (NARC). Islamabad, Pakistan.

Singh, P; V. Chauhan; B. K. Tiwari; S. S. Chauhan; S. Simon; S. Bilal; A.B. Abidi. (2014). Overview on Okra (*Abelmonoschus esculentus*) and its importance as a nutritive vegetable in the world. International journal of Pharmacy and Biological sciences. Pp 227-233.

Tiwari, B. K. and S. B. Ahmed. (2018). A n onerview on okra (*A belmoschus esculentus*) and its importance as a nutritive vegetable in the world, Research gate.pp 227-233.

Tong, P.S. Okra (*Abelmoschus esculentus*) a popular crop and vegetable. Agriculture (2014). science. Pp 39-42.

Wang, M.; Q. Zheng; Q. Shen; and S. Guo.(2013). The Critical Role of Potassium in Plant Stress Response. International journal of molecular science. Pp, 7370-7390.

ZANCO Journal of Pure and Applied Sciences
The official scientific journal of Salahaddin University-Erbil
https://zancojournals.su.edu.krd/index.php/JPAS

ISSN (print):2218-0230**, ISSN (online):** 2412-3986**, DOI:** **http://dx.doi.org/10.21271/zjpas**

RESEARCH PAPER

First Occurrence of *Plesiomonas shigelloides* Bacteria on/ in *Carassius carassius* and *Silurus triostegus* Fishes from Greater Zab River in Kurdistan Region, Iraq.

Zhakaw O. Hasan, Samir J. Bilal

Department of Fish Resource and Aquatic Animals, College of Agricultural Engineering Sciences, Salahaddin University-Erbil, Kurdistan Region, Iraq

A B S T R A C T:

The present study shows occurrence of *Plesiomonas shigelloides* bacteria from *Carassius carassius and Silurus triostegus* that collected in Greater Zab River in Aski-Kalak in Erbil from October 2018 to November 2019. Swaps were taken from lesions on the skin, fins and internal organs of the 34 fishes (14 from *C. carassius* and 20 from *S. triostegus*) and inoculated in nutrient agar, blood agar and MacConkey agar. The agar plates were incubated at 37°C for 24-48 hours. Obtained 13 isolates, the bacterial isolates identified depending on some morphological, cultural, some biochemical test and further confirmed by Vitek 2 compound system. For characterization and identification the bacterial colonies were examined and then showed Gram negative reaction and motile. Biochemical tests were done by Vitek 2 compound system and result confirming. The study showed appearance of *P. shigelloides* on the skin lesions and intestine of the examined fish. The present existence of *P. shigelloides* bacteria regarded as first record for this bacterium in Iraq on and in fishes.

KEY WORDS: Fish pathogen, *Plesiomonas shigelloides, Carassius carassius, Silurus triostegus.*
DOI: http://dx.doi.org/10.21271/ZJPAS.32.4.18
ZJPAS (2020) , 32(4);151-156 .

1.INTRODUCTION :

Bacterial diseases are the most frequent and major cause of mass death in fish worldwide. Several numbers of pathogenic bacteria have been reported that causes diseases in fish round the world (Pękala-Safińska, 2018), that responsible for economic losses in natural and cultured fishes (Khatun et al., 2011). Diseases have negative impacts on fish production due to mortality in the fish farms.

*** Corresponding Author:**
Zhakaw Othman Hasan
E-mail: zhakawothman90@gmail.com
Article History:
Received: 13/12/2019
Accepted:13/04/2020
Published:08/09/2020

Also, it can reduce reproductive performance and feed conversion efficiency leading to reducing growth and overall performance of cultured fish which it is serious economic losses due to increasing the cost thus have impact on the industry of country (Mustafa et al., 2001).

Plesiomonas shigelloides is a facultative, anaerobic, motile, Gram-negative rod aquatic bacterium recently recognized in the family Entrobacteriaceae and it is the only oxidase-positive member of this family also, as a potential human and animal pathogen of this family (Chen et al., 2013). Studies on concurrent infection with *P. shigelloides* and other microorganisms like *Vibrio* spp., *Aeromonas* spp., and *Edwardsiella tarda* (Butt et al., 1997).

Common environmental reservoirs for plesiomonads include freshwater ecosystems and estuaries and inhabitants of these aquatic environs which particularly reported from tropical and subtropical countries, different aquatic organisms, water dwelling reptiles, poikilotherms, and birds can port *P. shigelloides* (Janda et al., 2016; Behera et al., 2018).

P. shigelloides has been involved in gastrointestinal infections in human (Bodhidatta et al., 2010), and in Iraq it was isolated from drinking, bath and sewage water (Mustafa, 2015) In addition it has been shown that also causes bacteremia, pneumonia, osteomyelitis, sepsis, keratitis and meningitis (Ozdemir et al., 2010; Klatte et al., 2012).

The aim of the presnt study was to identifying the bacterial flora which has been isolated from fish in the Greater Zab River in Aski-Kalak based on morphological, cultural and biochemical characterizations, also take notice of the prevalence and intensity of this bacteria on/in fishes.

2. MATERIALS AND METHODS

A total of 34 fish specimens (from 14 *Carassius carassius* and from 20 *Silurus triostegus*) were collected from Greater Zab River by fisherman through using gill netting were fishes transported with river water as a life. The fishes identified according to Coad (2010) and Froese and Pauly (2019).

For Bacterial isolation, specimens were taken from Lesion on the skin, fins and internal organs of fishes by using sterile swabs, and streaked in nutrient agar, blood agar and MacConkey agar. The agar plates were incubated at 37°C for 24-48 hours, for characterization and identification the bacterial colonies were examined. Morphological and cultural characteristics examined such as optical characteristics shape, color, size and edge, Gram staining reaction and motility test (Thongkao and Sudjaroen, 2017). The bacterial colonies were then subjected to. Vitek 2 compound system was used for result confirming (Pincus, 2010).

3. RESULTS AND DISCUSSION

The present study was revealed existence of 13 isolates of *P. shigelloides* bacteria which isolated from lesion on the skin, fins and internal organs of *C. carassius* and *S. triostegus* with a prevalence 14.2% and 15% respectively (Table 1).

The morphological characteristic of this bacteria is non-lactic fermenting, round, yellow to pale-brown colony in MacConkey Agar. On the blood agar non hemolysis, white to gray in color and smooth round colonies. In addition it is whitish jelly like, round, flat colony on nutrient agar, colonies are oxidase positive (Fig.1). The microscopic appearance of bacterium is Gram-negative, polymorphism, round ended, non-endospore forming (Fig.2). Excellent identification was done by using vitek 2 compact system (Table 2).

In Iraq for the first time Saleh (1997) isolated six types of bacteria namely: *Aeromonas* sp., *Streptococcus* sp., *Pseudomonas* sp., *Micrococcus* sp., *Bacillus* sp. and *Alcaligenes* sp. in the skin, gills, blood, intestine, liver, kidney, spleen and muscle on *Cyprinus carpio*. Worth to mention there were other bacteria have been isolated from the fishes such as *Myxobacterium* spp. was isolated on *C. carpio* by Mohammad-Ali et al. (2000) and *Staphylococcus* sp. from skins, muscles, intestine and liver of *C. carpio* by Ali (2014). It is the first record of *P. shigelloides* from the fish in Iraq.

In Kurdistan region *Aeromonas hydrophila*, *A. sobria*, *P. shigelloides* and *A. salmonicida* were isolated from fishes (Ibrahim, 2008; Mustafa and Mustafa, 2015; Mustafa, 2016; Mustafa et al., 2019; Ibrahim, in press). The first record of *P. shigelloides* in Iraq was done by Mustafa (2015) that isolated from drinking, bath and sewage water.

P. shigelloides have been recognized as potential fish pathogens (González et al., 1999). It was isolated from diseased *Hypophthalmichthys molitrix* which associated with mortality in India (Behera et al., 2018). *P. shigelloides* pathogen has been identified as one of the main pathogen in the sturgeon’s culture in Beijing area (Wang et al., 2013). Hu et al. (2014) was isolated *P. shigelloides* from clinical cases of fishes during mass mortality of *Ctenopharyngodon idellus*, Nisha et al. (2014) was reported 100% mortality of cichlid ornamental fish by *P. shigelloides*. Also, by Liu et al. (2015) isolated *P. shigelloides* as severe pathogen of *Orechromis nilotica* cultured fish.

4. CONCLUSIONS

The present study showed first record of *P. shigelloides* as a fish pathogen in Iraq which was isolated from skin, fins and intestine lesions of *C. carassius* and *S. triostegus* with prevalence 14.2% and 15% respectively in the Greater Zab River in Aski-Kalak _ Erbil/Iraq. The recorded bacteria showed lesions in skin, fins and intestine in infected fishes.

Table 1: Showing the prevalence of *P. shigelloides* from fish hosts.

Fishes	No. of examined fishes	No. of infected fishes	Prevalence (%)	Locations
Carassius carassius	14	2	14.2	Skin, fins and intestine
Silurus triostegus	20	3	15	Skin, fins and intestine

Table 2: Biochemical details of *P. shigelloides*.

Biochemical Details																	
2	APPA	-	3	ADO	-	4	PyrA	-	5	IARL	-	7	dCEL	-	9	BGAL	+
10	H2S	-	11	BNAG	+	12	AGLTp	-	13	dGLU	+	14	GGT	-	15	OFF	+
17	BGLU	-	18	dMAL	+	19	dMAN	-	20	dMNE	-	21	BXYL	-	22	BAIap	-
23	ProA	+	26	LIP	-	27	PLE	-	29	TyrA	+	31	URE	-	32	dSOR	-
33	SAC	-	34	dTAG	-	35	dTRE	+	36	CIT	-	37	MNT	-	39	5KG	-
40	ILATK	-	41	AGLU	-	42	SUCT	+	43	NAGA	-	44	AGAL	-	45	PHOS	-
46	GlyA	-	47	ODC	+	48	LDC	+	53	IHISa	-	56	CMT	+	57	BGUR	-
58	O129R	-	59	GGAA	-	61	IMLTa	-	62	ELLM	+	64	ILATa	-			

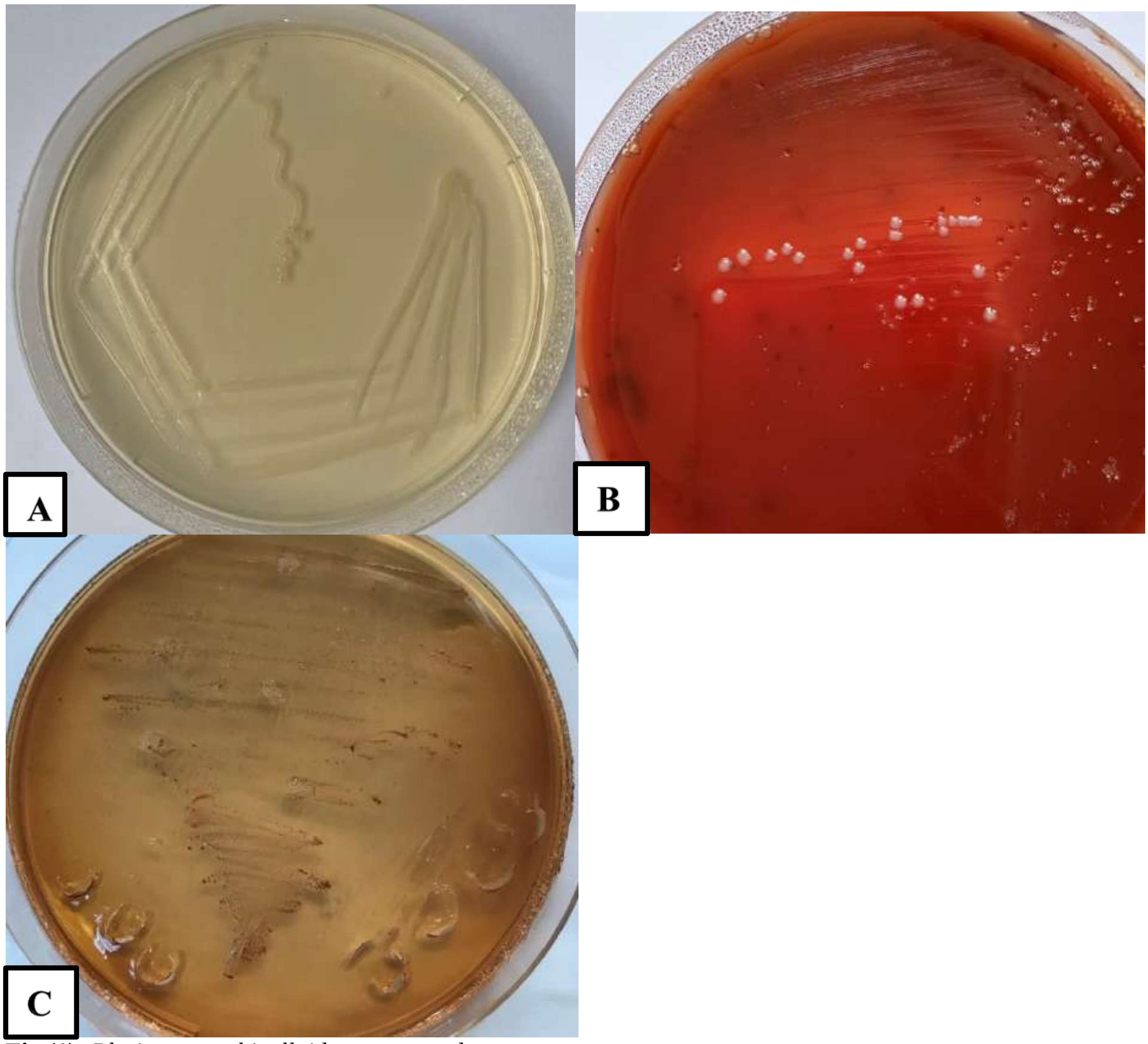

Fig (1): *Plesiomonas shigelloides* on agar cultures.
A- Colony of *Plesiomonas shigelloides* cultured on nutrient agar
B- Colony of *Plesiomonas shigelloides* cultured on blood agar
C- Colony of *Plesiomonas shigelloides* cultured on MacConkey agar

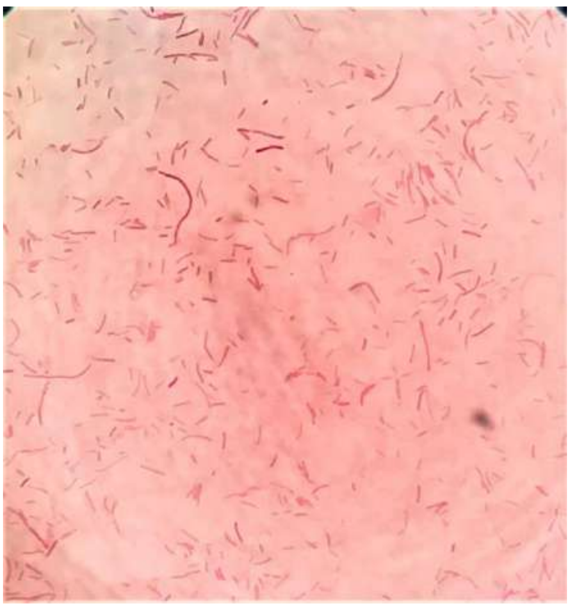

Fig (2): Photomicrograph of *Plesiomonas shigelloides* showing polymorphism of bacterial cells (1000x).

References

ALI, A.H. 2014. Isolation and identification of Staphylococcus bacteria from fish of fresh water and its antibiotics sensitivity in Mosul City. *Basrah Journal of Veterinary Research*, 1: 33-42.

BEHERA, B.K.; BERA, A.K.; PARIA, P.; DAS, A.; PARIDA, P.K.; SUMAN KUMARI, BHOWMICK, S. and DAS, B.K. 2018. Identification and pathogenicity of *Plesiomonas shigelloides* in Silver Carp. *Aquaculture*, 493: 314-318.

BUTT, A.A.; FIGUEROA, J. and MARTIN, D.H. 1997. Ocular infection caused by three unusual marine organisms. *Clinical Infectious Diseases*, 24(4): 740.

BODHIDATTA, L.; MCDANIEL, P.; SORNSAKRIN, S.; SRIJAN, A.; SERICHANTALERGS, O. and MASON, C. J. 2010. Case-control study of diarrheal disease etiology in a remote rural area in Western Thailand. *The American Journal of Tropical Medicine and Hygiene*, 83(5): 1106-1109.

CHEN, X.; CHEN, Y.; YANG, Q.; KONG, H.; YU, F.; HAN, D.; ZHENG, S.; CUI, D. and LI, L. 2013. *Plesiomonas shigelloides* infection in Southeast China. *PLoS One*, 8 (11): 1-8. e77877

COAD, B.W. 2010. *Freshwater fishes of Iraq*. Pensoft Publisher, Sofia: 275 pp+ 16 plates.

FROESE, R. and PAULY, D. 2019. "FishBase", World web electronic publication. www.fishbase.org,version (2019).

GONZÁLEZ, C.; LOPEZ-DIAZ, T.; GARCIA-LOPEZ, M.; PRIETO, M. and OTERO, A. 1999. Bacterial microflora of wild brown trout (*Salmo trutta*), wild pike (*Esox lucius*), and aquacultured rainbow trout (*Oncorhynchus mykiss*). *Journal of Food Protection*, 62(11): 1270-1277.

HU, Q.; LIN, Q.; SHI, C.; FU, X.; LI, N.; LIU, L. and WU, S. 2014. Isolation and identification of a pathogenic *Plesiomonas shigelloides* from diseased grass carp. *Wei Sheng Wu XueBao Acta Microbiologica Sinica*, 54 (2): 229-235.

JANDA, J.M.; ABBOTT, S.L.; CHRISTOPHER J. and MCIVER, C.J. 2016. *Plesiomonas shigelloides* Revisited. *Clinical Microbiology Reviews*, 29(2): 349-374. DOI: 10.1128/CMR.00103-15.

IBRAHIM, I.R.; ABDULLA, S.M.A. and KARIM, A.Y. Detection of Gene in *Aeromonas hydrophila* from Suspected Farming Fishes (*Cyprinus carpio*), Erbil Province/Iraq. *Zanco Journal of Pure and Applied Sciences* (In press).

IBRAHIM, K.S. 2008. *Pathological study of common carp (Cyprinus carpio) fish infected with Aeromonas hydrophila*. M.Sc. Thesis, Coll. Vet. Med., Univ. Duhok.

KHATUN, H.; HOSSAIN, M.D.; JAHAN, S.N. and KHANOM, D.A. 2011. Bacterial infestation in different fish at rajshahi. *Journal of Science Foundation*, 9 (1&2): 77-84.

KLATTE, J.M.; DASTJERDI, M.H.; CLARK, K.; HARRISON, C.J. and GRIGORIAN, F. 2012. Hyperacute infectious keratitis with *Plesiomonas shigelloides* following traumatic lamellar corneal laceration. *The Pediatric Infectious Disease Journal*, 31: 1200-1201.

LIU, Z.; KE, X.; LU, M.; GAO, F.; CAO, J.; ZHU, H. and WANG, M. 2015. Identification and pathological observation of a pathogenic *Plesiomonas shigelloides* strain isolated from cultured tilapia (*Oreochromis niloticus*). *Wei Sheng Wu XueBao Acta Microbiologica Sinica*, 55 (1): 96-106.

MOHAMMAD-ALI, N.R.; BALASEM, A.N. and MUSTAFA, S.R. 2000. Isolation of six bacterial species from Al-Zazfaraniya farm, South of Baghdad. *veterinarian* , 150-159.

MUSTAFA, A.; RANKADUWA, W. and CAMPBELL, P. 2001. Estimating the cost of sea lice to salmon aquaculture in eastern Canada. *Canadian Veterinary Journal*, 41: 54-56.

MUSTAFA, KH.KH. 2015. Effects of Some Medical Plants on the Growth of *Plesiomonas shigelloides* Isolated from Different Water Sources. *Duhok Journal*, 1-9.

MUSTAFA, KH. KH; MAULUD, S.Q. and PSHTEEWAN, A.H. 2019. Antimicrobial Resistance of *Aeromonas salmonicida* Isolated From Common carp (*Cyprinus carpio*)Fishes in Erbil City/ Iraq. *Baghdad science Journal*. 16(3) .DOI: http://dx.doi.org/10.21123/bsj.

MUSTAFA, KH.KH. and MUSTAFA, A.KH. 2015. Bacteriological and Molecular Study of *Aeromonas sobria* Isolated From Different Sources in Erbil

Province. *Zanco Journal of Pure and Applied Sciences*, 27(6):11-18.

MUSTAFA, S.I. 2016. *Disease agents of Cyprinus carpio from agriculture college fish farm in Erbil city- Kurdistan region*. M.Sc. Thesis, Coll. Edu., Univ. Salahaddin.

NISHA, R.G.; RAJATHI, V.; MANIKANDAN, R. and PRABHU, N.M. 2014. Isolation of *Plesiomonas shigelloides* from infected Cichlid Fishes using 16S rRNA characterization and its control with probiotic *Pseudomonas* sp. *Acta Scientiae Veterinariae*, 42: 1195.

PINCUS, D.H. 2010. Microbial identification using the biomérieux vitek® 2 system. Hazelwood, MO, USA 32.

PĘKALA-SAFIŃSKA, A. 2018. Contemporary threats of bacterial infections in freshwater fish. *Journal of Veterinary Research*, 62: 261-267.

SALEH, A.A.H. 1997. *Evaluation of bacterial content in carp (Cyprinus carpio) and their immune responseagainst Aeromonas hydrophila*. M.Sc. Thesis, Coll. Sci., Univ. Basrah.

THONGKAO, K. and SUDJAROEN, Y. 2017. Human pathogenic bacteria isolation from tilapia fishes (*Oreochromis niloticus*), a possible reservoir for zoonotic transmission. *Annals of Tropical Medicine and Public Health*, 10(6): 1563-1568.

OZDEMIR, O.; SARI, S.; TERZIOGLU, S. and ZENCIROGLU, A. 2010. *Plesiomonas shigelloides* sepsis and meningoencephalitis in a surviving neonate. *Journal of Microbiology, Immunology and Infection*, 43: 344-346.

WANG, X.; XU, L.; CAO, H.; WANG, J. and WANG, S. 2013. Identification and drug sensitivity of a *Plesiomonas shigelloides* isolated from diseased sturgeons. *Wei Sheng Wu XueBao Acta Microbiologica Sinica*, 53 (7): 723-729.

ZANCO Journal of Pure and Applied Sciences
The official scientific journal of Salahaddin University-Erbil
https://zancojournals.su.edu.krd/index.php/JPAS

ISSN (print):2218-0230**, ISSN (online):** 2412-3986**, DOI: http://dx.doi.org/10.21271/zjpas**

RESEARCH PAPER

Groundwater quality assessment of Domiz refugee camp in Duhok governorate, Kurdistan region, Iraq.

Nabaz I. Mohammed [1], Karzan A. Abduljabar [2], Honar S. Mahdi [1], Hojeen M. Abdullah [3] and Sami Youssef [1&4].

[1] Department of Recreation and Ecotourism, College of Agricultural engineering science, University of Duhok, Kurdistan Region, Iraq.
[2] Duhok Polytechnic University, Akre Technical College, Kurdistan Region, Iraq
[3] Department of Horticulture, College of Agricultural engineering science, University of Duhok, Kurdistan Region, Iraq.
[4] AMAP (botany and Modelling of Plant Architecture and vegetation), University of Montpellier / CIRAD / CNRS /INRA / IRD – AMAP, CIRAD TA A51/PS2, 34398 Montpellier Cedex 5, France.

ABSTRACT:

Groundwater is considered the fundamental source of drinking uses in Domiz refugee camp, Duhok governorate. Water quality investigation is critical component for determining water consumption. A field assessment was performed on August 2019 in order to examine the groundwater quality used for the refugees in Domiz camp. Groundwater samples were collected from 8 observation wells, 5 wells inside the camp and 3 wells outside the camp limits, and water samples investigated for basic physico-chemical parameters, major elements, as well as certain toxic metals to find out the suitability of groundwater sources for drinking purposes. The analytical out comes display high concentrations of TDS, EC, TH, SO_4, and NO_3 ions which refers to signs of contamination. Groundwater facies via piper diagram in the study area was primarily of Ca-Mg-Na-HCO_3 water type. Heavy metals show high concentration levels in some groundwater samples above drinking water permissible standard prescribed by World Health Organization. These high contents of major elements beside heavy metals in groundwater were probably due to the seepage of unprocessed waste waters from the camp. WQI method were performed to assess the current condition of groundwater samples, then the result revealed variation in water quality classes ranging from very poor to excellent water class.

KEYWORDS: Domiz camp, groundwater, water pollution, heavy metals, WQI.
DOI: http://dx.doi.org/10.21271/ZJPAS.32.4.19
ZJPAS (2020) , 32(4);157-168 .

1. INTRODUCTION

Water is considered the most significant element that profound life (Gorde and Jadhav, 2013). Groundwater resources have been utilized for industrial and domestic water supply as well as irrigation aims around the world. Though, there are several aspects influencing the quality of groundwater, such as agricultural flow out, industrial and domestic waste, geological formation, land use practices, rate of infiltration and patterns of rainfall (Federation and American Public Health Association, 2005). In the past, the demand on the fresh water has been formidable increase due to industrial acceleration and rapid population growth (Dohare *et al.*, 2014). WHO organization reported that, around 80% of human diseases are came from water (Kavitha and Elangovan, 2010). Tripathi, *et al.*, (2013) highlighted that, around 3% of the world fresh water is enough for human requirements for millions years. The water quality is declining via the pollution caused by human activities. The safest type of water sources is groundwater for both domestic and drinking purposes (Suresh and Kottureshwara, 2009).

*** Corresponding Author:**
Nabaz Ibraheem Mohammed
E-mail: nabaz.mohammed@uod.ac or nabaz_im@hotmail.com
Article History:
Received: 06 /12 /2019
Accepted: 03 /05 /2020
Published: 08 / 09/2020

Kurdistan region of Iraq display a large spatial and temporal dissimilarity in terms of water resources. The growing population, expansion of economic arrangements, and increase in internally displaced person (IDPs) and Syrian refugees certainly leads to rising request of water usage for different practices (BRHA, 2017). Groundwater resources in Iraqi Kurdistan have further more experienced of notable tension regarding the quantity of water affected by several reasons for example the global climatic changes, the regional variations of the yearly precipitation rates and unsuitable arrangement of water utilization (Trondalen, 2009; Mohammed, 2019). Hence, investigating water quality is very crucial to be accomplished so as toretain the consciousness and understanding of water resources.

Water quality index become unique and vital method aimed at the management and assessment of groundwater (Srinivas and Huggi, 2011). The soluble minerals in sedimentary rocks and soils are the main part of the soluble components in groundwater, including sulfate ions, sodium, calcium and bicarbonate, chloride, (Dohare *et al*., 2014). Weathering of the rocks for example dolomite, limestone and calcite are the common sources of the magnesium and calcium in the ground water (Marque *et al*., 2003). Greater nitrate contents in water resources may affect the health of human especially pregnant women and infants and become a source of water contamination (Bukowski *et al*., 2001). Heavy metals can also deteriorate the quality of water if they present in high concentrations. Therefore, the main aim of the current investigation is to evaluate the quality of groundwater resources that are used mainly for drinking purposes in Domiz refugee camp via using physico-chemical, major ions, heavy metals, and water quality index computing method in order to better understand and manage groundwater resources in the area of interest.

2. MATERIALS AND METHODS

2.1. Study Area:

This investigation implemented at Domiz1camp (Refugee camp of Syrian) – Duhok Governorate (Latitude: 36^{o} 78’ 29 N) and (Longitude: 42^{o} 88’ 61 E) (Figure 1) with altitude of 425m. This camp has been established 2012 in the response to the refugees’ influx from Syria especially from the North, which has turned now quickly to a residential city (Mizzouri *et al*., 2017). Refugees’ population is estimated to be around 33,000 and the total area of the camp is around 1,142,500m^2 (BRHA, 2017). The camp is located such 15 km from the south of Duhok city and 54 km from the north of Mosul city. Moreover, the average air temperature for the year 2018 – 2019 was 26°C, while rainfall amount was about 995mm fallen between October and may (Youssef *et al*., 2019). The main source of drinking and domestic purposes of Domiz camp inhabitants is from groundwater boreholes. To assess water quality of these resources, a total of eight groundwater boreholes were selected in and outside the camp which are principally used for consumption uses for the Syrian refugees in Domiz camp (Table 1).

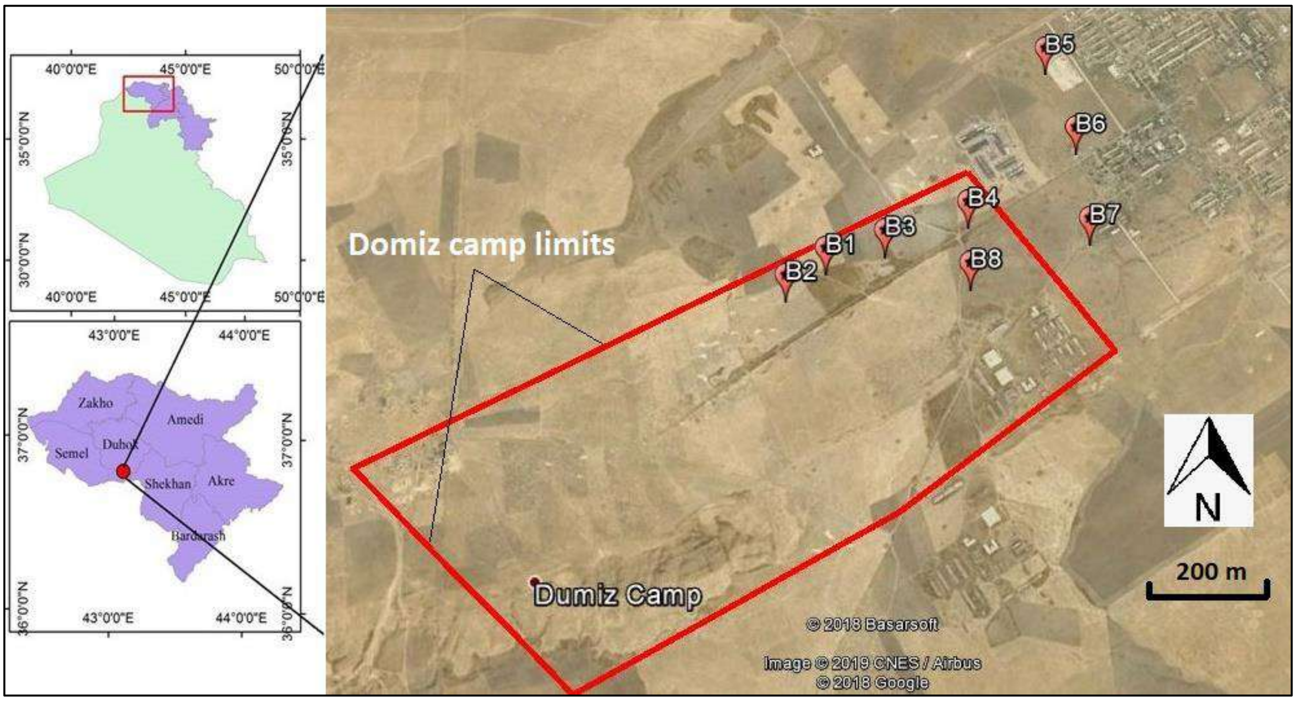

Figure 1. Study Area Map showing groundwater sampling points and Domiz camp limits (border).

Table 1. Geographical coordinates (WGS84) of the groundwater samples.

No	Sample ID		Location	Coordination	
				N	E
1	Boreholes 1	B1	Domiz 1 Refugees Camp	36° 47’ 7”	42° 52’ 53”
2	Boreholes 2	B2	Domiz 1 Refugees Camp	36° 47’ 6”	42° 52’ 45”
3	Boreholes 3	B3	Domiz 1 Refugees Camp	36° 47’ 6”	42° 52’ 1”
4	Boreholes 4	B4	Domiz 1 Refugees Camp	36° 47’ 5”	42° 52’ 14”
5	Boreholes 5	B5	Outside Domiz 1 Refugees Camp	36° 47’ 28”	42° 52’ 34”
6	Boreholes 6	B6	Outside Domiz 1 Refugees Camp	36° 47’ 8”	42° 52’ 34”
7	Boreholes 7	B7	Outside Domiz 1 Refugees Camp	36° 46’ 57”	42° 52’ 29”
8	Boreholes 8	B8	Domiz 1 Refugees Camp	36° 46’ 58”	42° 52’ 10”

2.2. Data collection and analytical methods:

Eight groundwater samples were brought from eight groundwater boreholes during August 2019 to investigate the groundwater quality for drinking purposes. The sterilized 1L polyethylene bottle was used for collected water, to avoid contamination the bottles rinsed twice with the sampled water and then saved under condition of 4^{o}C and transported to the laboratory of the Duhok Environmental Directorate for immediate analyzes. The groundwater samples examined for 24 various parameters including: turbidity (TUR), pH, electrical conductivity (EC), total dissolved solids (TDS), total alkalinity (TA), total hardness (TH), calcium (Ca), magnesium (Mg), sodium (Na), potassium (K), bicarbonate (HCO_3), sulfate (SO_4), chloride (Cl), nitrate (NO_3), chromium (Cr), manganese (Mn), iron (Fe), copper (Cu), zinc (Zn), arsenic (As), selenium (Se), silver (Ag), barium (Ba), and lead (Pb). Total dissolved solids, electrical conductivity, and pH were measured independently in the field by a transportable multi-meters (Trans ISO 9002). All other water quality parameters were analyzed in the laboratory following standard protocols. Total alkalinity and bicarbonate were determined using titration with sulfuric acid. Other chemical and heavy metals analyses were performed by spectrophotometer and flame atomic absorption spectrometer.

Water Quality Index (WQI) was computed by utilizing the Weighted Arithmetic Index technique as defined by Cude (2001) as follows:

$Qi = [(V_{actual} - V_{ideal}) / (V_{standard} - V_{ideal})] * 100$…….. (1)

Where,
Qi = Quality rating of *i* parameter for a total of *n* water quality parameters
V_{actual}: Actual value of the water quality parameter gained from laboratory analysis
V_{ideal}: Ideal value of the water quality parameter in pure water.
V_{ideal} for pH = 7, while for other parameters is equivalent to zero in pure water.
$V_{standard}$: prescribed WHO standard of the water quality parameter.

$Wi = 1/ Si$ ……… (2)

Where,
Wi = Relative (unit) weight for nth parameter
Si= Standard permissible value for *n* parameter
I = Proportionality constant.
Lastly, the total WQI was obtained by combining the quality rating with the unit weight linearly via following equation:

$WQi = \sum QiWi / \sum Wi$ ……… (3)

Where,
Qi = Quality rating
Wi = Relative weight
In this study, the WQI was measured for human drinking purposes and uses with the maximum allowable WQI for the drinking water was set as 100.

3. RESULTS AND DISCUSSION:

3.1. Physico-chemical parameters

The physico-chemical, chemical and heavy metals results of all examined groundwater boreholes are given in Table 2 and illustrated in Figure 2c. The pH measurement of water is vital since it controls many of the geochemical reactions or solubility calculations within groundwater aquifer. The pH value of current study is ranged between 7.0 and 7.6 which considered being neutral to slightly weak alkaline and measured as normal condition since in the pH of the region's groundwater categorized by alteration toward the alkaline caused mainly by geological makeup of the study site which principally comprised of limestone (Nabi, 2005). The recorded values in all boreholes were suitable for drinking uses between 6.5 – 8.5 set by WHO and Iraqi guideline (WHO, 2008). Salinity of water is specified via determining the capability of water to conduct an electrical current and is generally expressed by either electrical conductivity (EC) or total dissolved solids (TDS), which are determining the suitability of water for particular purposes. The concentration of EC varied from 663.2 µS/cm to 1183 µS/cm with an average concentration of 984.3 µS/cm, and TDS value ranged between 424.5 and 757.1 mg/l and the water is classified as high saline water (Kadhem, 2013). The allowable level of EC for consumption purposes is value less than 1500 µS/cm and no water samples surpassed this concentration, however all samples (except one sample B5) exceeded the desirable limits of TDS for drinking water value of 500 mg/l set by WHO (2008). This could be connected to availability of elevated dissolved ions, organic material from the study area, large mineral salts content from the soil dissolved minerals, and semi-arid type of climatic condition (Shekha, 2008; Al-Mezori and Harami, 2013; Shekha *et al*., 2017; Mohammed and Bamarni, 2019). The occurrence of elevated amount of dissolved solids in groundwater could change its taste. Water hardness is such a crucial parameter for domestic uses of water and is the record of how water react with the soap, for instance, hard water requests noticeably additional soap to produce lather. Water comprising hardness content lower than 60 mg/l is usually categorized as soft; 60–120 mg/l, moderately hard; 120–180 mg/l, hard; and greater than 180 mg/l is considered very hard (Mc Gowan, 2000). The results of this study show that water samples are listed as very hard water since the total hardness values vary from 240 to 476 mg/l with the average of 319.5 mg/l. High concentration of hardness in water is unwanted typically for aesthetic and economic aims (WHO, 2011). Groundwater hardness results primarily from the presence of alkaline earth metals calcium and magnesium.

Table 2. Physico-chemical, major ions and heavy metals of analyzed groundwater samples from Domiz refugee camp.

Parameters	Unites	Sample ID								AV	SD
		B1	B2	B3	B4	B5	B6	B7	B8		
TUR	NTU	0.4	0.4	0.5	0.6	0.6	0.8	0.3	0.5	0.51	0.16
pH		7.1	7	7.3	7.4	7.3	7.6	7.1	7	7.23	0.21
EC	µS/cm	905.6	1001.6	1052.1	1053.2	663.2	906.7	1183	1109.3	984.34	160.39
TDS	mg/l	579.6	641	673.4	674.1	424.5	580.3	757.1	710	630.00	102.64
TA	mg/l	322	264	214	232	222	230	384	390	282.25	73.11
TH	mg/l	296	284	296	248	240	316	476	400	319.50	79.98
Ca^{2+}	mg/l	81.6	72	57.6	57.6	40	118.4	72	67.2	70.80	22.98
Mg^{2+}	mg/l	22.4	25.4	37.1	25.4	34.2	49	72.2	56.6	40.29	17.61
Na^{+}	mg/l	50.7	70.3	84.6	88.6	40.1	67.6	75.4	77.2	69.31	16.51
K^{+}	mg/l	0.8	1.2	1.2	1.3	0.8	1.2	1.1	0.9	1.06	0.20
HCO_3^-	mg/l	392.84	322.08	261.08	283.04	270.84	280.6	468.48	475.8	344.35	89.20
SO_4^{2-}	mg/l	68.5	128.2	184.9	202	53.3	137.5	104.3	98.3	122.13	52.22
Cl^-	mg/l	60	46	56	60	38	100	26	48	54.25	21.82
NO_3^-	mg/l	24.3	21.9	25.2	25.2	26.5	30.2	34.2	24.5	26.50	3.90
Cr	mg/l	0.324	0.03	0.046	0.048	0.03	0.038	0.006	0.005	0.066	0.11
Mn	mg/l	0.311	0.004	0.002	0.003	0.002	0.003	0.005	0.001	0.041	0.11
Fe	mg/l	0.291	0.045	0.016	0.01	0.011	N.D	0.017	0.023	0.059	0.10
Cu	mg/l	0.302	0.008	0.014	0.009	0.009	0.002	N.D	N.D	0.057	0.12
Zn	mg/l	0.029	0.113	0.019	0.003	0.004	0.001	0.015	0.033	0.027	0.04
As	mg/l	0.027	0.033	0.028	0.012	0.003	0.016	0.009	N.D	0.018	0.01
Se	mg/l	0.023	N.D	0.011	N.D	N.D	N.D	0.014	N.D	0.016	0.01
Ag	mg/l	0.36	0.029	0.027	0.016	0.018	0.005	0.023	0.017	0.062	0.12
Ba	mg/l	0.391	0.076	0.045	0.035	0.055	0.037	0.082	0.081	0.100	0.12
Pb	mg/l	0.007	0.01	0.005	0.002	N.D	0.005	0.005	0.003	0.005	0.00

(NTU= Nephelometric turbidity unit, AV= average value, SD= standard deviation, N.D= Not detected)

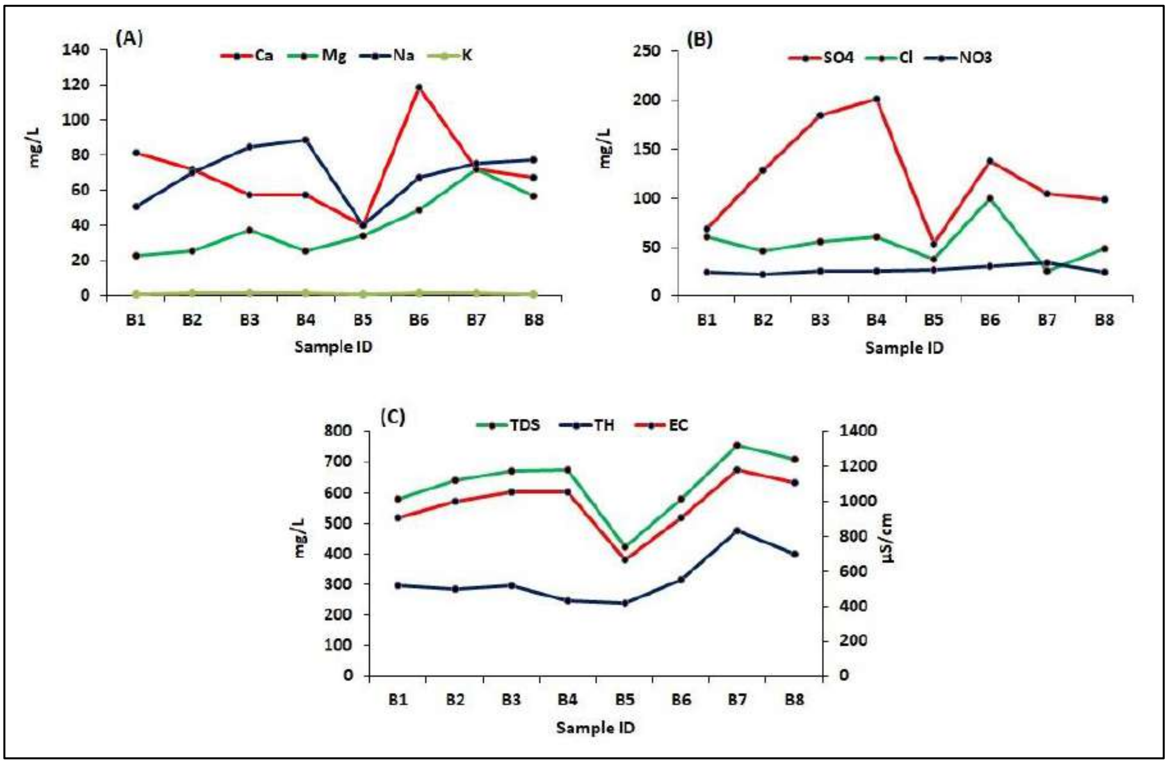

Figure 2. Physico-chemical and major ion concentration in groundwater samples.

3.2. Major ions

In all groundwater samples, no particular cation (Ca^{2+}, Mg^{2+}, Na^{+}, and K^{+}) shows a clear dominance. The major ions concentration is given in Table 2 and showed in Figure 2a and 2b. The concentration of calcium (Ca^{2+}) was fluctuated between 40 and 118.4 mg/l with the mean value of 70.8 mg/l. The magnesium contents in groundwater samples fluctuated from 22.4 to 72.2 mg/l with the mean value of 40.29 mg/l. The outcomes point out that all samples (except B5) exceeded the concentration of calcium and only two samples (B7 and B8) exceeded the concentration of magnesium for their drinking desirable limits of 50 mg/l as per Iraqi standards (MOE, 1998). High levels of $Ca^{2+}$and Mg^{2+}in water resources results in water hardness problem. The main sources of calcium and magnesium in groundwater are largely the geochemistry of the rock types. The value of sodium (Na^{+}) fluctuate from 40.1 to 88.6 mg/l with the mean value of 69.31 mg/l. The sodium contents in all groundwater samples were well below the prescribed concentration of WHO (2008) as 200 mg/l for drinking purposes. The concentration of potassium (K^{+}) were very low in groundwater samples and ranged between 0.8 and 1.3 mg/l. Parts of potassium enter clay structure and thus its concentrations get lowered in water (Kannan and Joseph, 2010).

Bicarbonate (HCO_3^{-}) was the most dominate anion measured in groundwater samples. The content of HCO_3^{-} in the investigated groundwater boreholes ranged between 261.1 and 475.8 mg/l with the mean amount of 344.3 mg/l. Entire groundwater samples contained levels that exceeded the standard concentration for drinking purposes (250 mg/l) agreed by WHO (2008). The availability of carbonate rocks like calcite and dolomite in the sediments defines the high bicarbonate contents in the aquifer (Mizzouri, 2007). Sulfate ion (SO_4^{-2}) is one of the major anions widely found in fresh water resources. The SO_4^{-2}content in groundwater samples ranged from 53.3 to 202 mg/l with the mean value of 122.1 mg/l. These were below the maximum permissible limit of 250 mg/l set by WHO (2008) for drinking purposes. Sulfate is not negatively influences the health below the standard amount for drinking purposes, never the less, it may have a laxative consequence at higher concentration, which can lead to intestinal anxiety and subsequently dehydration (WHO, 2011a). The chloride concentration in groundwater samples was fluctuated between 26 and 100 mg/l which were far lower than the acceptable limit of 200 mg/l for drinking purposes set by WHO (2008). In natural groundwater, the likely sources of chloride is the discharge of chloride-bearing minerals such as apatite, inland salinity, and the discharge of agricultural, industrial and domestic waste water (Abbasi, 1998). The nitrate (NO_3^-) content varied between 21.9 and 34.2 mg/l with the mean value of 26.5 mg/l. Despite the high concentration of nitrate in groundwater samples, none of the samples surpassed the allowable limit for drinking purposes of 50 mg/l (WHO, 2008).The wide spread use of agricultural fertilizers is considered to be a key cause of the nitrate that percolates to groundwater (Postma *et al*., 1991; Chowdary *et al*., 2005). Moreover, point sources of nitrogen for instance septic systems are revealed to consider the nitrate contamination of groundwater (Mac Quarrie *et al*., 2001). Higher nitrate content in drinking water can bring methemoglobinemia to infants and stomach cancer in adults (Lee, 1992; Wolfe and Patz, 2002).

3.3. Groundwater classification

The hydrochemical evolution of water samples could be revealed via plotting the major cations (Ca^{2+}, Mg^{2+}, Na^+, and K^+) and major anions (HCO_3^-, SO_4^{2-}, Cl^-, , NO_3^-) present in water resources. Figure 3 displays the Piper diagram which is a graphical illustration grouping water rely on the prevailing cations and anions and has extensive application to find out water facies, for the obtained data of this study (Piper, 1944). Two chemical water facies of groundwater recognized; (i) Calcium-Magnesium-Sodium-Bicarbonate facies (Ca^{2+}-Mg^{2+}-Na^+-HCO_3^-), and (ii) Calcium-Magnesium-Sodium-Bicarbonate-Sulfate facies (Ca^{2+}-Mg^{2+}-Na^+-HCO_3^--SO_4^{2-}). There is no major cation dominant in groundwater and bicarbonate by far was the most dominant anion in groundwater followed by sulfate ion. These water types could be as a consequence of the geological influences of the aquifer bed rock mainly of limestone carbonate (Mohammed and Bamarni, 2019). The geological formation of an aquifer can significantly influences the concentration of dissolved ions since the mineral-water interaction is important and hence determine the dominate ions (Panno and Hackley, 2010).

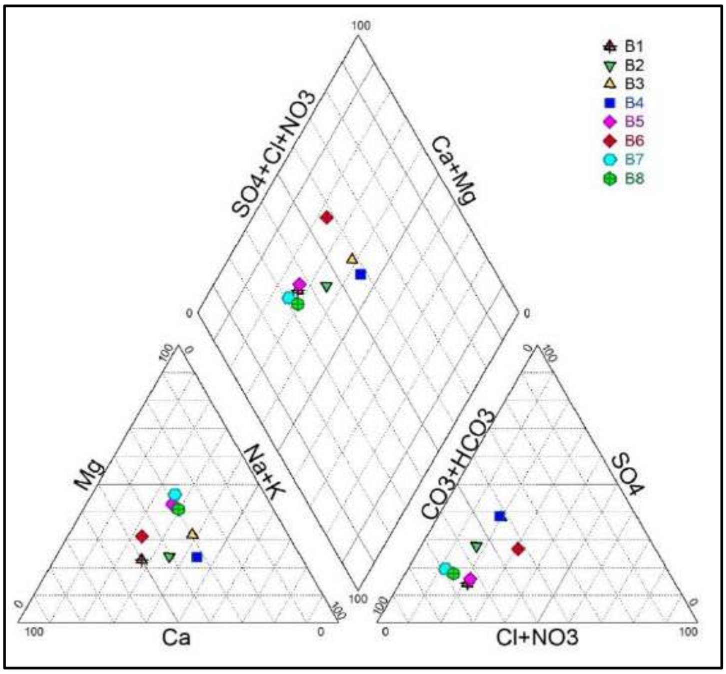

Figure 3. Piper trilinear diagram showing the groundwater chemical facies of the studied samples.

3.4. Heavy metals

The concentration, mean and standard deviation of ten dissolved heavy metals (Cr, Mn, Fe, Cu, Zn, As, Se, Ag, Ba, and Pb) in groundwater samples are presented in Table 2 and displayed in Figure 4a and 4b. The analytical results did indicate high levels of some heavy metals in few water samples. The lowest and highest concentration of Chromium (Cr) obtained from the groundwater samples at 8 different boreholes varied from 0.005 to 0.324 mg/l with the mean value of 0.066 mg/l.

The acceptable level set by WHO (2011) for Cr in water for drinking purposes is 0.05 mg/l, the lower value of Cr ions were recorded in every collected samples excluding water sample from B1 which had concentration above the WHO set, this could be mainly due to the adjacent of B1to the waste water outlet. The use of water with excessive concentration of Cr for drinking and domestic uses can cause cancer (Jarup, 2003). The concentration of Manganese (Mn) obtained from the groundwater varied from 0.001 to 0.311 mg/l with the mean value of 0.041 mg/l. The maximum allowable amount of Mn in water resources used for drinking purposes recommended by WHO is 0.4 mg/l and none of samples exceeded this limit. The results show that the maximum concentration for Mn ion was recorded in borehole B1 which was close the limit value for drinking purposes. Manganese ion is frequently detected in drinking water but is having important human health concern at lower levels (Keen and Zidenberg-Cherr, 1994). The source of Mn in groundwater may be naturally from rock and soil weathering (such as manganese carbonate and rhodonite) and anthropogenic from agricultural activities (Mohammed, 2019). The high content of manganese recorded in the water resources can cause neurological disorder; it can also stain clothes (Jarup, 2003). The minimum and maximum concentrations of Iron, Copper, and Zinc in the groundwater samples were 0.01 – 0.291 mg/l, 0.002 – 0.302 mg/l, and 0.001 – 0.113 mg/l, respectively. The WHO guideline maximum for Fe, Cu, and Zn for drinking water are 1.0, 2.0, and 4 mg/l, therefore, no water samples exceeded these levels.

The minimum and maximum concentration of Arsenic (As) obtained from the groundwater samples varying from 0.003 to 0.033 mg/l with average concentration of 0.018 mg/l. Arsenic ion was not detected in only one groundwater sample (B8). The maximum permissible limit of As in drinking water is 0.01 mg/l which is prescribed by WHO (2011). The recorded values of five boreholes (B1, B2, B3, B4, and B6) were observed to be beyond the allowable level for drinking purposes. The main sources of Arsenic in groundwater is natural from geological formation (such as arsenopyrite and arsenic sulfides) and could also be from the agricultural activities mainly pesticides and insecticides containing arsenic (Momot and Synzynys, 2005; Pirsaheb *et al*., 2015). Human exposure to high amounts of arsenic may inspire severe toxic health consequences such as gastrointestinal indications (poor appetite, vomiting, diarrhea, etc.), disruption of cardiovascular and the functions of nervous system or even death (Abernathy and Morgan, 2001). The minimum and maximum concentration of Silver (Ag) recorded from the groundwater samples ranged from 0.005 to 0.360 mg/l. The maximum allowable limit of Ag in drinking water is 0.1 mg/l set by WHO (2008). Lower concentration of Ag ion were measured in all the samples collected except for sample from B1 which had concentration to be above the maximum allowable limit set by WHO. Geological makeup could be the source of Ag in the studied groundwater samples, however, wastewater is believed to be the main source of Ag in groundwater sample of B1. The use of water with high content of Ag for drinking purposes may cause aesthetic discolorations of the skin, hair and various organs (WHO, 2003). Low concentrations of Barium (Ba) ion were detected in groundwater samples and varied from 0.035 to 0.391 mg/l which were far below the maximum permissible limit of 0.7 mg/l for drinking purposes set by WHO (2004). Lead ion (Pb) is a highly toxic metal which should normally be available in very low concentration in drinking water. The minimum and maximum concentration of Lead recorded from the groundwater samples varied from 0.002 to 0.010 mg/l. The maximum allowable limit for drinking water is 0.01 mg/l prescribed by WHO (2008), and all the water samples were below this set excluding B2 which recorded the same value.

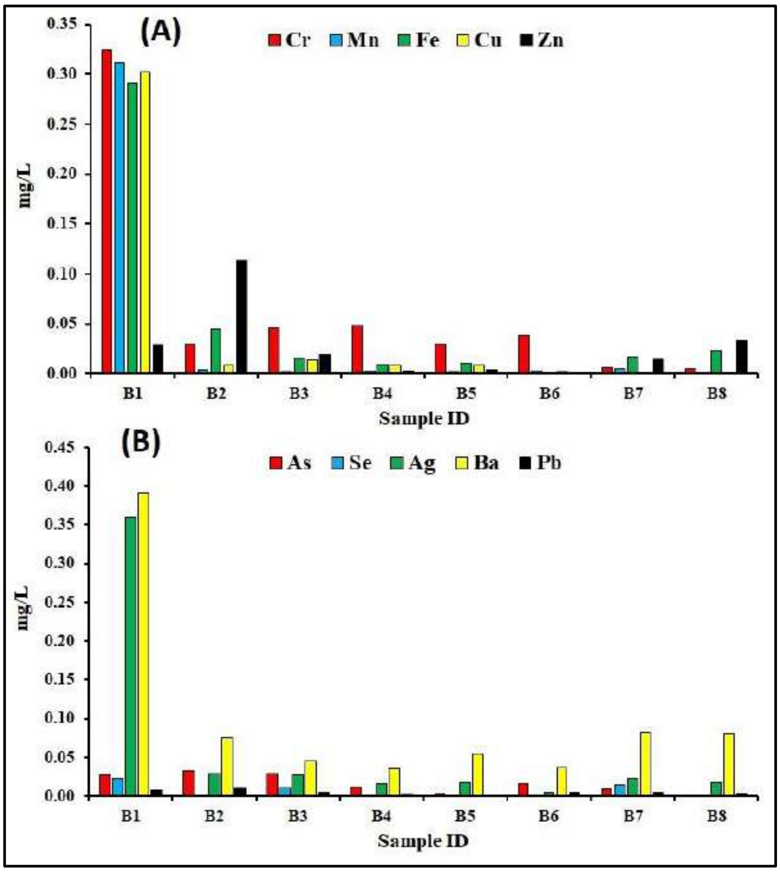

Figure 4. Concentration of the heavy metal for the groundwater samples.

3.5. Water quality index (WQI)

Water quality index is such a suitable technique for evaluating the quality of water resources as a whole (Ketata *et al*., 2011). This method decreases the great amount of data into only one meaningful number and simplifies understanding of the results. WQI is applied in water resources to identify their drinking suitability (Gibrilla *et al*., 2011; Khwakaram *et al*., 2012). Table 3 presents the results of WQI of the groundwater B1 and it was 217.3 as an example of calculation. The calculated values of WQI were classified into five sorts''as revealed in Table 4 (Ramakrishniah *et al*., 2009). The results of WQI values in the study area are demonstrated in Table 5. The computed WQI values varied from 25.43 (B8) to 217.32 (B1). Accordingly, the quality of studied groundwater samples is in the ''Excellent'' to ''Very poor water '' for drinking range. Table 4 revealed that out of eight groundwater samples, two boreholes are categorized in the ''Excellent water'' class, three as ''Good water'' class, two as ''Poor water'' class, and one as a ''Very poor water'' class. Very poor water class has been observed in the borehole B1, this may be due to anthropogenic activities surrounding the borehole mainly sewer waste water and there could be a leakage of wastewater. Thus, the results reflect the presence of anthropogenic pollution sources within the study area (Refugee camp).

Table 3: An example calculation of WQI for the groundwater sample B1.

Parameters	Actual measured values	Water quality standards	Relative weight (wi)	Quality rating (Qi)	Weighted values (Wi * Qi)
TUR	0.4	5	0.2	8	1.6
pH	7.1	8.5	0.12	6.67	0.8

EC	905.6	1000	0.001	90.56	0.09
TDS	579.6	500	0.002	115.92	0.23184
TA	322	100	0.01	322	3.22
TH	296	100	0.01	296	2.96
Ca	81.6	75	0.013	108.8	1.46
Mg	22.4	30	0.03	74.67	2.49
Na	50.7	200	0.005	25.35	0.127
SO4	68.5	250	0.004	27.4	0.109
Cl	60	250	0.004	24	0.096
NO3	24.3	50	0.02	48.6	0.972
Cr	0.324	0.05	20	648	12960
Mn	0.311	0.4	2.5	77.75	194.375
Cu	0.302	2	0.5	15.1	7.55
Zn	0.029	4	0.25	0.725	0.18125
Ag	0.36	0.1	10	360	3600
As	0.027	0.01	100	270	27000
Pb	0.007	0.01	100	70	7000
			∑Wi 233.669		**∑Wi*Qi 50776.262**

Table 4. Water Quality Index values with their status.

Water Quality Index levels	Description
<50	Excellent
50 – 100	Good water
100 – 200	Poor water
200 – 300	Very poor (bad) water
>300	Unsuitable for drinking

Table 5. Results of Water Quality Index of Domiz refugee camp groundwater for drinking water purposes.

Sample ID	WQI	Water type
B1	217.3	Very poor water
B2	190.5	Poor water
B3	150.4	Poor water
B4	68.9	Good water
B5	32.95	Excellent
B6	79.6	Good water
B7	75.07	Good water
B8	25.43	Excellent

3. CONCLUSION:

Groundwater have been evaluated in the Domiz Refugee camp for its suitability for drinking purpose. In overall, 24 different hydrochemical parameters, including physico-chemical, major elements and heavy metals, were examined from eight groundwater boreholes. The results discovered that the water was in alkaline nature and having high content of total dissolved solids above recommended set prescribed by WHO. Elevated levels of nitrate also recorded in all water samples indicating the agricultural and wastewater from sewer contamination in the area.

Moderately low levels of studied heavy metals measured in groundwater and, interestingly, elevated concentration of arsenic ion recorded in almost all samples that exceed permissible limit for drinking water. Moreover, Water Quality Index technique were used to evaluating the overall groundwater quality of the study area and the results displayed four different categories: Excellent water class; Good water class; Poor water class; and Very poor class. The water quality assessment evidently exhibited that the status of some groundwater in Domiz camp was degraded and it was also concluded that discharging of domestic effluents and other human actions were the key reasons of polluting groundwater resources predominantly boreholes B1 and B2. Nevertheless, regular seasonal observing of groundwater quality, in terms of biology, to detect variation of water quality parameters over time and to manage water resources is highly recommended.

References:

ABBASI S. A., 1998. Water Quality Sampling and Analysis. *Discovery Publishing House,* New Delhi, pp. 51.

ABERNATHY C. AND MORGAN A. 2001. Exposure and health effect. In: UN (2001). UN synthesis report on arsenic in drinking water. Geneva, Switzerland, World Health Organization. Chapter 3.

AL-MEZORI H. A. AND HARAMI K. A. 2013. Evaluation of Trace Elements in Drinking Water of Duhok province/Kurdistan region of Iraq. *International Journal of Engineering Science Invention*, 2(4), 47-56.

BRHA, 2017, Board of Relief and Humanitarian Affairs. Accessed 15 October 2019, http://www.brha-duhok.org.

BUKOWSKI, J., SOMERS, G., AND BRYANTON, J. 2001. Agricultural contamination of groundwater as a possible risk factor for growth restriction or prematurity. *Journal of occupational and environmental medicine*, 43(4), 377-383.

CHOWDARY V.M, RAO N.H. AND SARMA P.B.S, 2005. Decision support framework for assessment of non-point-source pollution of groundwater in large irrigation projects. *Agric Water Manag*, 75, 194–225.

CUDE, C. 2001. Oregon water quality index: A tool for evaluating water quality management effectiveness. *Journal of the American Water Resources Association*, 37, 125–137.

DOHARE, D., DESHPANDE, S., AND KOTIYA, A. 2014. Analysis of ground water quality parameters: a Review. *Research Journal of Engineering Sciences*, 3 (5), 26–31.

FEDERATION, W. E., AND AMERICAN PUBLIC HEALTH ASSOCIATION. 2005. Standard methods for the examination of water and wastewater. *American Public Health Association* (APHA): Washington, DC, USA.

GIBRILLA, A., BAM E. K. P., ADOMAKO D. S., GANYAGLO S., OSAE S., AKITI T. T., KEBEDE S., ACHORIBO E., AHIALEY E., AYANU G., AGYEMAN E. K., 2011. Application of water quality index (WQI) and multivariate analysis for groundwater quality assessment of the Birimian and Cape Coast Granitoid Complex: Densu River Basin of Ghana. *Water Quality Exposure Health*, 3 (2), 63-78.

GORDE S. P., AND JADHAV M. V. 2013. Assessment of water quality parameters: a review. *Journal of Engineering Research and Applications*, 3(6), 2029-2035.

JARUP L., 2003. Hazards of heavy metal contamination British Medical. *Bulletin*, 68, 167-182.

KADHEM A. J. 2013. Assessement of water quality in Tigris River-Iraq by using GIS Mapping. *Natural Resources*, 4, 441 – 448.

KANNAN N. AND JOSEPH S. 2010. Quality of Groundwater in the Shallow Aquifers of a Paddy Dominated Agricultural River Basin, Kerala, India. *International Journal of Civil and Environmental Engineering*, 2(3), 223-241.

KAVITHA R. AND ELANGOVAN K. 2010. Review article on Ground water quality characteristics at Erode district. *India), of IJES*, 1(2), 145-150.

KEEN C.L., ZIDENBERG-CHERR S. 1994. Manganese toxicity in humans and experimental animals. In: Klimis-Tavantzis DJ, editor. *Manganese in Health and Disease*. London: CRC Press; p. 193–205.

KETATA M., GUEDDARI M. AND BOUHLILA R. 2011. Use of geographical information system and water quality index to assess groundwater quality in El Khairat deep aquifer (Enfidha, Central East Tunisia). *Arabian Jour. Geosci*., 5(6), 1379–1390.

KHWAKARAM A., MAJID S. N. AND HAMA N. Y. 2012. Determination of water quality index (WQI) for Qalyasan stream in Sulaimanu city/Kurdistan region of Iraq. *International journal of plant, animal and environmental sciences*, 2 (4), 148 – 157.

LEE Y.W. 1992. Risk assessment and risk management for nitrate-contaminated groundwater supplies. Unpublished PhD dissertation. *University of Nebraska, Lincoln*, Nebraska. 136 p.

MAC QUARRIE K.T.B, SUDICKY E, AND ROBERTSON W.D, 2001. Numerical simulation of a fine-grained denitrification layer for removing septic system nitrate from shallow ground water. *J Hydrol*, 52, 29–55.

MARQUE S., JACQMIN-GADDA H., DARTIGUES J. F., AND COMMENGES D. 2003. Cardiovascular mortality and calcium and magnesium in drinking water: an ecological study in elderly people. *European journal of epidemiology*, 18(4), 305-309.

MCGOWAN W. 2000. Water processing: residential, commercial, light-industrial, 3rd ed. Lisle, IL, Water Quality Association.

MIZZOURI N. S. 2007. Identifying point sources and non-point sources of water pollution in Dohuk dam watershed. May 14-16, Taiz University, Republic of Yemen.

MIZZOURI N. S., ALGABBAN M. M., AND HASSAN H. M. 2017. Assessment of grey water disposal and different treatment options for Domiz camp in Duhok city. *Journal of University of Duhok*, 20, (1), 184-195.

MOE (Ministry of Environment) 1998. System maintenance of river and public water pollution in Iraq.

MOHAMMED N. I. 2019. Assessment of groundwater contamination with heavy metals in rural area. Case study of Barebuhar village, Duhok governorate, Kurdistan region of Iraq. *Journal of Agriculture and Veterinary Sciences*, under press.

MOHAMMED, N., AND BAMARNI K. 2019. Water Quality Monitoring of Duhok Dam (Kurdistan Region of Iraq). *ZANCO Journal of Pure and Applied Sciences*, 31(1), 7-16.

MOMOT O, SYNZYNYS B. 2005. Toxic aluminum and heavy metals in groundwater of middle Russia: health risk assessment. *International journal of environmental research and public health*, 2(2), 214-8.

NABI, Q. A. 2005. Limnological and bacteriological study in some wells within Erbil city Kurdistan region of Iraq. *MSc. Thesis* University of Salahaddin.

PANNO S. AND HACKLEY K. 2010. Geologic influences on water quality. Geology of Illinois, p.337 – 350.

PIPER A. M., 1944. A graphical procedure in the geochemical interpretation of water analyses. *Trans Amer. Geophy. Unio*., 25, 914 – 928.

PIRSAHEB M, KHAMUTIAN R, AND POURHAGHIGHAT S. 2015. Review of Heavy Metal Concentrations in Iranian Water Resources. *International Journal of Health and Life Sciences*. 1(1), 35-45.

POSTMA D., BOESEN C., KRISTIANSEN H., AND LARSEN F. 1991. Nitrate reduction in an unconfined sandy aquifer: water chemistry, reduction processes, and geochemical modeling. *Water Resour. Res.*, 27(8), 2027–45.

WOLFE A.H., AND PATZ J.A. 2002. Reactive nitrogen and human health: acute and long-term implications. *Ambio*, 31(2): 120–5.

YOUSSEF S., GALALAEY A., MAHMOOD A., MAHDI H., AND VÉLA E. 2019. Wild orchids of the

RAMAKRISHNIAH C.R., SADASHIVAIAH C. AND RANGANNA G. 2009. Assessment of Water Quality Index for the Groundwater in Tumkur Taluk. *E-Journal of Chemistry*. 6(2), 523-530.

SHEKHA Y. A., ALI L. A. AND TOMA J .J. 2017. Assessment of water quality and trophic status of Duhok lake dam. *Baghdad Science Journal*, 14 (2), 335–342.

SHEKHA Y. A. 2008. The effect of Arbel city waste water Discharge on water quality of Greater Zab river, and the risks of Irrigation. PhD. thesis,Collage of Science , university of Baghdad.

SRINIVAS P. AND HUGGI M. S. 2011. Assessment of ground water quality characteristics and water quality index (WQI) of Bidar city and its industrial area, Karnataka state, India. International Journal of Environmental Sciences, 2(2), 965-976.

SURESH T., AND KOTTURESHWARA N. M. 2009. Assessment of groundwater quality of bore wells water of Hospet taluka region, Karnataka, India. *Rasayan J Chem*, 2(1), 221-233.

TRIPATHI S., PATEL H. M., SRIVASTAVA P. K., AND BAFNA A. M. 2013. Assessment of water quality index of bore well water samples from some selected locations of South Gujarat, India. *Journal of environmental science & engineering*, 55(4), 456-465.

TRONDALEN J. M. 2009. Climate Changes, Water Security and Possible Remedies for the Middle East, United Nations Educational, Scientific and Cultural Organization.

WHO (World Health Organization), 2003. Silver in Drinking Water. Retrieved from: http://www.who.int/water_sanitation_health/dwq/chemicals/silver.pdf.

WHO (World Health Organization), 2004. Barium in Drinking Water. Retrieved from http://www.who.int/water_sanitation_health/dwq/chemicals/barium.pdf.

WHO (World Health Organization), 2008. Guidelines for Drinking Water Quality, 3rd Edition, Geneva.

WHO (World Health Organization), 2011. Hardness in Drinking-water Background document for development of WHO Guidelines for Drinking-water Quality. Geneva, Switzerland.

WHO (World Health Organization) 2011a. Guidelines for drinking-water quality, (fourth edi). Geneva: World Health Organization (WHO).

Kurdistan Region areas: a scientific window on the unexpected nature of the North-Western Zagros. La Motte-d'Aigues (FR): *Société Méditerrannéenned' Orchidologie*, 164 P. ISBN: 978-2-900082-08-9.

ZANCO Journal of Pure and Applied Sciences
The official scientific journal of Salahaddin University-Erbil
https://zancojournals.su.edu.krd/index.php/JPAS

ISSN (print):2218-0230**, ISSN (online):** 2412-3986**, DOI: http://dx.doi.org/10.21271/zjpas**

RESEARCH PAPER

Environmental Effect on Growth and Yield Parameters of Ten Kenaf Varieties (*Hibiscus cannabinus* L.) in Erbil.

Rabar Fatah Salih[1], Nawzad Ali Qader[2]

[1]Department of Field Crops, College of Agricultural Engineering Sciences, Salahaddin University-Erbil, Kurdistan Region, Iraq
[2]Department of Horticulture and Landscape Design, Bakrajo Technical Institute, Sulaimani Polytechnic University, Sulaymaniyah, Kurdistan Region, Iraq

A B S T R A C T:
Differences between growth and yield parameters of ten kenaf varieties were investigated to evaluate and determine the best variety to cultivation at Kurdistan environment. For the first time seeds of ten kenaf varieties were planted in field of Grdarasha in College of Agricultural Engineering Sciences, Salahaddin University – Erbil, Kurdistan. The experiment was arranged using four replicates in Randomized Complete Block Design. Date of flowering, plant height, stem diameter, fresh stem, fresh bast and fresh core yield were measured. Variety FH-952 had the highest value of plant height (340 cm), followed by 4383 variety (310 cm). Despite that, the highest values of other growth and yield parameters such as stem diameter, fresh stem, fresh bast and fresh core yield were recorded on HC 95 variety which was (25.1 mm, 175.0, 41.2 and 134.5) t/ha respectively. Significant results of characteristics from this current study display that, some varieties of kenaf will be selected for replanting since it noted to have high ability to adaptation with Kurdistan environment condition

KEY WORDS: Kenaf variety, Growth, Fiber yield, Environmental.
DOI: http://dx.doi.org/10.21271/ZJPAS.32.4.20
ZJPAS (2020), 32(4); 169-173.

1. INTRODUCTION:

The scientific name of kenaf is *Hibiscus cannabinus* L. native to tropical Africa which also known as one of the fast growing crops, C3 plant (three carbon compounds) (Salih *et al.*, 2014a). High biomass yield and the raised fiber content of kenaf caused to planting this crop in a wide range around the world (Hossain *et al.*, 2010). Stem and biomass yields were among the most important factors for selecting kenaf varieties as a plant material for fiber production and then using in multiple purposes (Webber and Bledsoe 2002).

Ali *et al.* (2017) reviewed that kenaf fiber can be used to make quality fine paper, lower grade papers and cordage, also used to produce rope, canvas, sacking, carpet backing, fishing nets. Also it used in industrial purposes such as interior automobile parts as door panels, headliners. Moreover, the inner part of the plant (core) can be used in animal bedding (Lips *et al.*, 2009).

Given kenaf high adaptability to all kinds of soils, it has the potential to be planted on trouble soils that have a characteristically low efficiency, and also in the soil which is poor in water-holding capacity and nutrient availability (Roslan *et al.*, 2010). These characteristics of the kenaf plant encourage researchers and farmers for choosing and planting and then using their fibers

* **Corresponding Author:**
Rabar Fatah Salih
E-mail: rabar.salih@su.edu.krd
Article History:
Received: 20/01/2020
Accepted: 17/05/2020
Published: 08/09 /2020

in wide range of applications. Additionally, climate condition of Kurdistan has a role on plant growing and productions. For example, some varieties of cotton could be grown in the cold condition in some state of Kurdistan (Salih, 2019).

The Iraqi Kurdistan Region (IKR) is located between latitudes 34°00′10″N to 37°20′33.55″N, and longitudes 42°20′25.36″E to 46°18′25″E. It covering an area of about 50,328 km², which constitutes a large portion of the whole of Iraq's territory. The IKR is characterized by a Mediterranean climate, which is cold and rainy in winter and hot and dry in summer. In general, the precipitation season starts in October to end in May with the amount of 350 in the southwestern parts to more than 1,200 mm in northern and northeastern parts. Furthermore, the mean daily temperature varies from 5°C in winter to 30°C in summer; however, this might rise to 50°C in the southern parts of the region (Gaznayee, 2020).

As kenaf was a relatively new crop in Kurdistan. The researchers want to determine the practicality of growing kenaf under local farming conditions, and the economic viability of establishing a kenaf processing enterprise for fiber and animal feed production.

1. MATERIALS AND METHODS

2.1. Location of Experiment

The experiment was conducted at Grdarasha Agriculture Research Station, Department of Field Crops, College of Agricultural Engineering Sciences, Salahaddin University – Erbil, Kurdistan.

2.2 Field Experiment

The field experiment was laid out in Randomized Complete Block Design (RCBD) with four replicates. Seeds of nine varieties with one hybrid of kenaf were planted namely; FH-952, HC 95, HC 2, 4383, 4202, V36, T15, T17, T19 and Hybrid (Table 1). All varieties were reached from Malaysia, at Institute of Tropical Forestry and Forest Production (INTROP), Universiti Putra Malaysia. Seeds were planted on 18 April, 2017 at a soil depth of 1.5 - 3.0 cm in the plot with the size of 1 m^2. The distance between plants was 5 cm and 30 cm was between rows. In this current study, no fertilizers were applied.

Several growth and yield characteristics were studied such as; day of plant flowering, and also at harvesting the following characteristics were recorded on a random sample of tree plants from each plot: Plant height (cm), Stem diameter (mm), Fresh stem yield (t/ha), Fresh bast yield (t/ha), and Fresh core yield (t/ha).

After planting seeds of three varieties which include: T15, T17 and T19 were not germinated. It might be referring to its viability.

Table 1. Number, name and country of origin of kenaf varieties were used in the present study.

Number of varieties	Name of varieties	Country of origin
1	FH-952	China
2	HC 95	Bangladesh
3	HC 2	Bangladesh
4	4383	BJRI (Bangladesh Jute Research Institute) code for origin from Sudan
5	4202	BJRI (Bangladesh Jute Research Institute) code for origin from Tanzania
6	T15	China
7	T17	China
8	T19	China
9	V36	China (Commercial production line of Malaysia)
10	Hybrid	China

2.3 Botanical Characteristics

The kenaf plants have different leaf types and flower colors. Also, the kenaf seeds are slate-black, wedge-shaped are approximately 6 mm long and 4 mm wide. Generally, kenaf has the same type of stem only may be different in color, some of them have dark red or brown stem which is affected by time of harvesting. Additionally, stem diameter also affected by cultivation practices such as fertilization, irrigation, plant density and others (Figure 1).

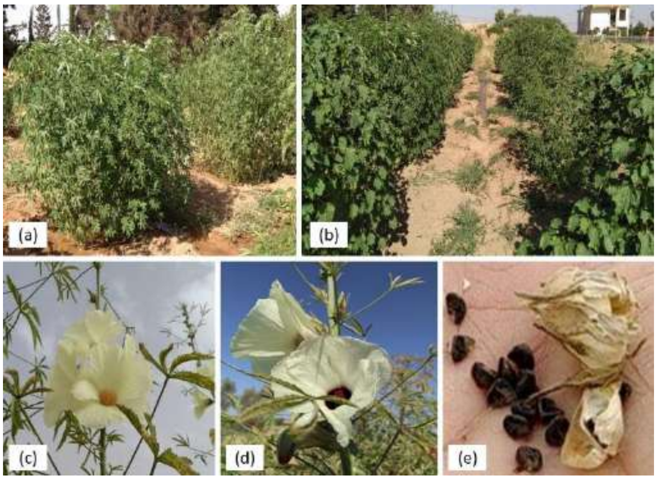

Figure 1: (a,b) different kenaf varieties; (c,d) different flowers; (e) kenaf seeds.

2.4 Data Analysis

Data of flowering, growth and yield characteristics were subjected to Analysis of Variance (ANOVA), using SPSS Statistics and mean comparison was performed by Duncan at $P \leq 0.05$

2. RESULTS AND DISCUSSION

Significant results were recorded among varieties in all parameters were studied (Table 2). As mentioned earlier kenaf plant was cultivated for the first time in Kurdistan so results from this current study will be assisted the researchers to do further research which is to establish kenaf plant as a main crop in Kurdistan since it can be used in wide range of industrial applications.

Table 2. The analysis of variance (ANOVA) for the comparison of growth and yield parameters between seven kenaf varieties.

Source of variation	Parameters	DF	Sum of Squares	Mean Square	F value	P value
Variety	DOF (d/plant)	6	2043.0	340.5	19.3	0.000
	PH (cm)	6	24185.7	4031.0	3.7	0.012
	SD (mm)	6	100.0	16.7	2.8	0.040
	FSY (t/ha)	6	24593.6	4098.9	90.4	0.000
	FBY (t/ha)	6	1077.7	179.6	17.9	0.000
	FCY (t/ha)	6	15768.0	2628.0	173.0	0.000

Significant occurs when $P \leq 0.05$, DF=Degree of freedom, DOF=Day of flowering, PH=Plant height, SD=Stem diameter, FSY=Fresh stem yield, FBY=Fresh bast yield, and FCY=Fresh core yield.

Date of flowering is one of the growth parameters was determined between varieties which is most important since it affected plant height, fiber yield and also fiber quality. The average of chemical compounds was changing during flowering, so it may be caused to improve the fiber quality and quantity. Mediavilla *et al.* (2001) reviewed that different varieties of hemp plant were recorded a similar growth pattern with a maximum of stem yield at flowering. Figure 2 shows the different results of flowering. Hybrid was flowering after 165 days, while could see the flower on V36 after 195 days of planting. It was in agreement with previous research which concluded that growth parameters were different with kenaf varieties (Salih *et al.,* 2014b).

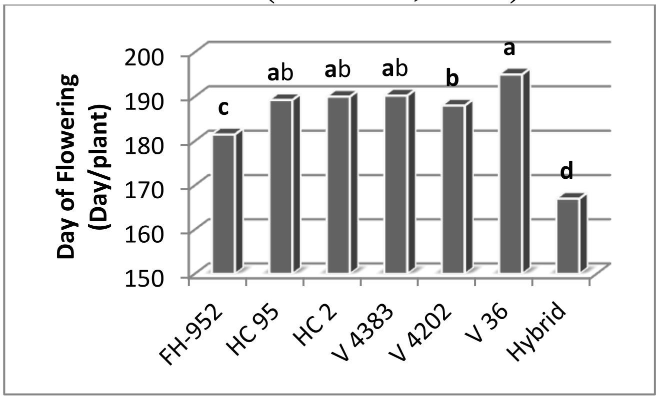

Figure 2: Day of flowering of seven kenaf varieties. Means with the same letter are not significantly different (Duncan, $P \leq 0.05$).

FH-952 variety had the highest stem compared to other varieties were studied. Its plant height was about (340 cm), while V36 had the lowest plant height (240 cm) (Figure 3). It might be caused by the varieties and its ability to adaptation with the Erbil environment. Salih *et al.* (2014b) planted seeds of two kenaf varieties (FH-952 and 4383), it was done at Universiti Putra Malaysia, 2013, so they found that kenaf plants have different growth performance. FH-952 was recorded the highest plant high.

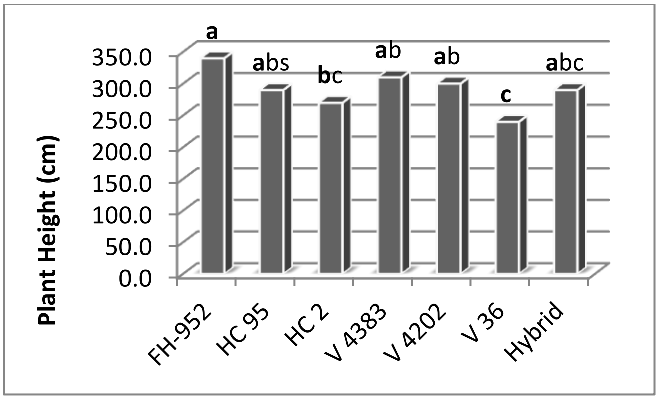

Figure 3: Comparison of plant height between seven kenaf varieties. Means with the same letter are not significantly different (Duncan, P ≤ 0.05).

The biggest stem diameter was recorded of HC95 which was by (25.1 mm), followed by FH-952 and 4383 varieties the values were about (23.7 and 23.3 mm), respectively (Figure 4). Despite that, kenaf V36 had to the smallest stem diameter which was only (18.6 mm). These results strongly supported by (Salih *et al.*, 2014b; Hossain *et al.*, 2011; and Wong *et al.*, 2008). Many factors effected stem diameter such as field management and varieties.

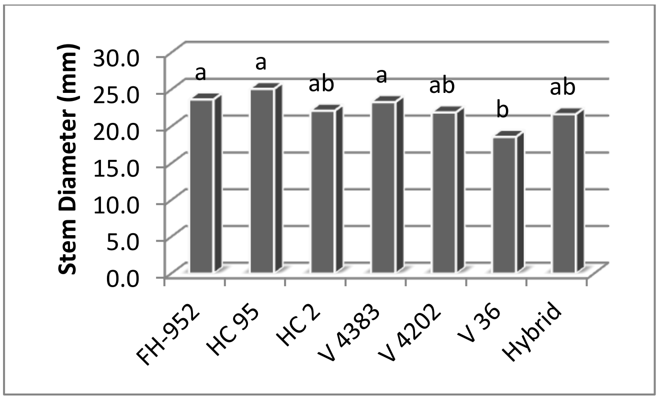

Figur 4: Comparison of stem diameter between seven kenaf varieties. Means with the same letter are not significantly different (Duncan, P ≤ 0.05).

Figures 5, 6 and 7 were showed the yields of fresh stem, fresh bast and fresh core was different according to the varieties. The maximum fresh stem yield, fresh bast and fresh core yield were recorded by (175.0, 41.2 and 134.5) t/ha respectively for HC95 variety. Conversely, V36 was recorded the minimum fresh yields (78.8, 24.9 and 53.7) t/ha respectively for all yield parameters. It was agreement with (Jie *et al.*, 2017; Salih *et al.*, 2014c; and Hossain *et al.*, 2012).

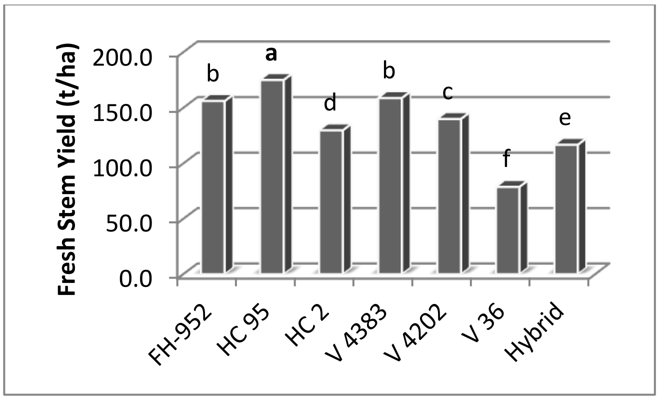

Figure 5: Comparison of fresh stem yield between seven kenaf varieties. Means with the same letter are not significantly different (Duncan, P ≤ 0.05).

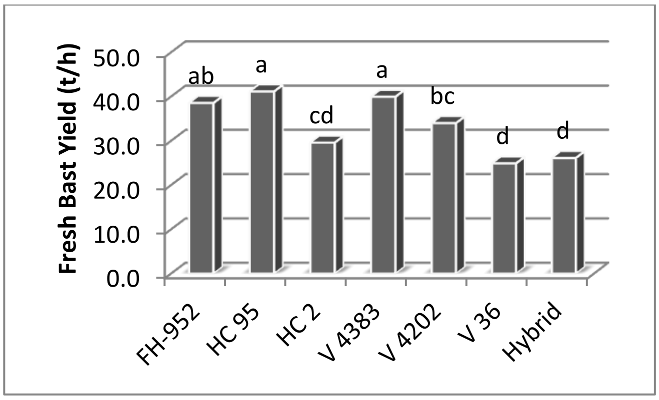

Figure 6: Comparison of fresh bast yield between seven kenaf varieties. Means with the same letter are not significantly different (Duncan, P ≤ 0.05).

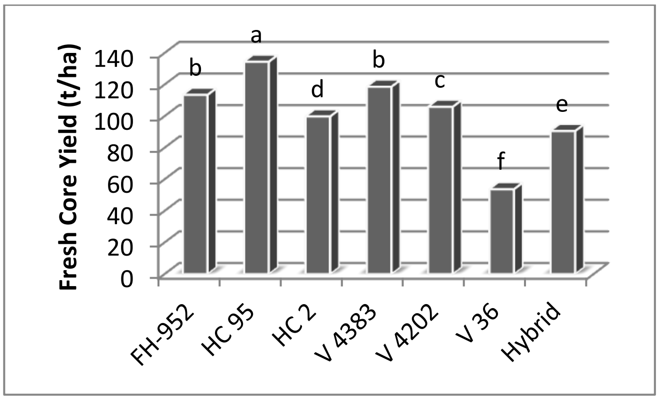

Figure 7: Comparison of fresh core yield between seven kenaf varieties. Means with the same letter are not significantly different (Duncan, P ≤ 0.05).

Highly significant results of fresh yields suggested that kenaf varieties HC95, FH-952 and 4383 can be replanted to reach on the great information about them in Kurdistan environment. On the other hand, 4202 and HC2 varieties also showed the significant results of fresh yields which was verified to its ability for adaptation in Kurdistan environment. Actually, results of these varieties less than results of HC95, FH-952 and 4383 varieties, but it may be providing the high value of fiber yield at different environmental situations. For that purpose, can say that it may be suitable with other states in Kurdistan region.

3. CONCLUSIONS

During this present study received great information about several kenaf varieties in Erbil, Kurdistan environment. The results showed that kenaf can be planted as a major crop since their fibers have potential impact to be used in industrial and as forage. Variety HC 95 had the maximum fresh stem, fresh bast and core fiber yield followed by FH-952 and 4383 varieties. As mentioned earlier, any fertilizers were not applied in this current study so believed that for the future using fertilizers may have significant effect of improving quality and quantity of fibers. On the other hand, researchers should be recommended farmers for planting this crop through Ministry of Agriculture and Water Resources.

Acknowledgements

Authors would like to thanks the all staffs at the researching filed, the Field of Grdarasha, College of Agricultural Engineering Sciences, Salahaddin University – Erbil for preparing the field and tools during the research. Also, authors want to many thanks to Institute of Tropical Forestry and Forest Production (INTROP) at Universiti Putra Malaysia and also special thanks to Mr. Baharum Zainal for providing all kenaf seeds.

Conflict of Interest (1)

The authors declare no conflict of interest.

References

ALI, M. S., GANI, M. N., & ISLAM. M. M. 2017. Efficiency of BJRI Kenaf-4 Yield Under Different Fertilizer Levels. *Ameri. J. Agric. Fores.* 5(5): 145-149.

GAZNAYEE, H. 2020. *Modeling Spatio-Temporal Pattern of Drought Severity Using Meteorological Data and Geoinformatics Techniques for the Kurdistan Region of Iraq Agriculture Science (Application of GIS and Remote Sensing in Drought).* Doctoral dissertation, Salahaddin University-Erbil.

HOSSAIN, D., MUSA, M. H., TALIB, J., & JOL. H. 2010. Effects of Nitrogen, Phosphorus and Potassium Levels on Kenaf (*Hibiscus cannabinus* L.) Growth and Photosynthesis under Nutrient Solution. *J. Agric. Sci.* 2(2): 1916-9752.

HOSSAIN, M., HANAFI, M., JOL, H., & JAMAL. T. 2011. Dry matter and nutrient partitioning of kenaf (*Hibiscus cannabinus* L.) varieties grown on sandy bris soil. *Austra. J. Cro. Sci.* 5(6): 654-659.

HOSSAIN, M. D., HANAFI, M. M., SALEH, G., FOROUGHI, M., BEHMARAM, R., & NOORI. Z. 2012. Growth, photosynthesis and biomass allocation of different kenaf (*Hibiscus cannabinus* L.) accessions grown on sandy soil. *Austra. J. Cro. Sci.* 6(3): 480-487.

JIE, B., LI D., CHEN A., LI J., HUANG S., & TANG. H. 2017. Evaluation of Nutritive Value of Seven Kenaf (*Hibiscus cannabinus* L.) Varieties Harvested Depending on Stubble Height. *Pertanika J. Trop. Agric. Sci.* 40(1): 73-86.

MEDIAVILLA, V., LEUPIN, M., & KELLER. A. 2001. Influence of the growth stage of industrial hemp on the yield formation in relation to certain fibre quality traits. *Industr. Cro. Prod.* 13(1): 49-56.

LIPS, S.J.J., INIGUEZ, D. E., HEREDIA, G. M. O. P., DEN KAMP, R. G. M., & VAN DAM. J. E. G. 2009. Water absorption characteristics of kenaf core to use as bedding material. *Ind Cro. Prod.* 29: 73-79.

ROSLAN, I., SHAMSHUDDIN. J., FAUZIAH, C. I., & ANUAR. A. R. 2010. Occurrence and properties of soils on sandy beach ridges in Kelantan-Terengganu Plains, Peninsular Malaysia. *Catena* 83: 55-63.

SALIH, R. 2019. Effect of Sowing Dates and Varieties of Cotton (*Gossypium hirsutum* L.) on Growth and Yield Parameters. *ZANCO J. Pur. Appli. Sci.* 31. (3): 64-70.

SALIH, R. F., ABDAN, K., WAYAYOK, A., RAHIM, A. A., & HASHIM. N. 2014a. Response of Nitrogen Content for Some Varieties of Kenaf Fiber (*Hibiscus cannabinus* L.) by Applying Different Levels of Potassium, Boron and Zinc. *Elsevi. Agric. Agric. Sci. Proce.* 2: 375-380.

SALIH, R. F., ABDAN, K., & WAYAYOK. A. 2014b. Growth Responses of Two Kenaf Varieties (*Hibiscus cannabinus* L.) Applied by Different Levels of Potassium, Boron and Zinc. *J. Agric. Sci.* 6: 37.

SALIH, R. F., ABDAN, K., WAYAYOK, A., & HASHIM. N. 2014c. Effect of Potassium, Boron and Zinc on Nitrogen Content in Bast and Core Fibers for two Kenaf Varieties (*Hibiscus cannabinus* L.). *Internati. J. Develop. Res.* 4: 2581-2586.

WEBBER III, C. L., & BLEDSOE. V. K. 2002. Plant maturity and kenaf yield components. *Indust. Cro. produ.* 16(2): 81-88.

WONG, C.C., MAT DAHAM, M. D., ABDUL AZIZ, A. M., & ABDULLAH. O. 2008. Kenaf germplasm introductions and assessment of their adaptability in Malaysia. *J. Trop. Agric. and Fd. Sci.* 36(1): 1-19.